

On the multi-scale analysis of land-surface mass and energy exchanges for the tropical Andean páramo of Southern Ecuador



Front cover: Landscape of the Andean tussock grasslands of Zhurucay (3765 m a.s.l.).

Back cover: Landscape of the Quinoas headwater catchment (4300 m a.s.l.).

Photos by Galo Carrillo, 2017



On the multi-scale analysis of land-surface mass and energy exchanges for the tropical Andean páramo of Southern Ecuador

kumulative Dissertation
zur
Erlangung des
DOCTORGRADES DER NATURWISSENSCHAFTEN
(Dr. rer. nat.)

dem Fachbereich Geographie
der PHILIPPS-UNIVERSITÄT MARBURG
vorgelegt von

GALO JOSÉ CARRILLO ROJAS

aus Cuenca-Ecuador

Marburg / Lahn, 2019

Vom Fachbereich Geographie
der Philipps-Universität Marburg
als Dissertation am 30.01.2019 angenommen.

Erstgutachter: Prof. Dr. Jörg Bendix
Zweitgutachter: Prof. Dr. Peter Chiffard

Weitere Mitglieder der Prüfungskommission:

Prof. Dr. Georg Miehe
Prof. Dr. Simone Strambach
Prof. Dr. Nina Farwig

Tag der mündlichen Prüfung am 24.04.2019
Hochschulkennziffer: 1180

Prolog and acknowledgments

During this long journey, structured by several stays in Germany and Ecuador, writing this thesis became an intellectual, emotional and physical challenge. Special people have travelled with me all the way, and they have encouraged me all the time. Thus, this period was one of the most precious moments I had in my life. This work represent for me, not only a phase of academic growth while enjoyed science, but also a chronological mirror, where an hesitant and doubtful student was reflected –5 years ago–, and now the same mirror reflects a researcher with further inquiries to respond. To date, this endeavor constitutes the warmest contribution I can leave to the society (academia and Ecuadorian & Andean communities), and also it is the beginning of a new campaign, in search of new questions, and new answers.

I want to thank all the people and institutions that have supported this investigation. . .

To the funding and supporting institutions of this work:

This work was funded by the "Secretaría de Educación Superior, Ciencia, Tecnología e Innovación" (SENESCYT) and the "Instituto de Fomento al Talento Humano" (IFTH) of Ecuador. I especially thank these institutions for my doctoral scholarship. Thanks to the "Departamento de Recursos Hídricos y Ciencias Ambientales" (iDRHiCA), and the "Dirección de Investigación" (DIUC) of the University of Cuenca, for the knowledge transfer, logistics and projects funding. I extend my thanks to the Authorities of the University of Cuenca, for their permanent and generous support. I am also grateful to the Deutsche Forschungsgemeinschaft (DFG) and to the Laboratory for Climatology and Remote Sensing (LCRS) of the Philipps-Universität Marburg, which supported this study in human and scientific capacities.

Prolog and acknowledgments

To my mentors and my colleagues. . .

First and foremost, I would like to thank my supervisor, Prof. Dr. Jörg Bendix, for his guidance, wise comments, fruitful conversations, extraordinary kindness and a lot of patience. His mentoring will always remain in my memory. I am equally grateful to my Ecuadorian co-supervisor, Prof. Dr. Rolando Célleri, who supported me in many ways, from the scientific discussion to the emotional advice, passing by the enjoyment of Friday's afternoon "tertulias", of course. This short quote may represent a lot of my feelings. . .

"If I have seen further, it is by standing on the shoulders of giants"

I. Newton letter to R. Hooke, 1675.

I want to express my gratitude to my co-advisors and co-authors: Brenner, Martin, Katja and Rütger, for their guidance and friendship. My warmest thanks go to my colleagues and friends of iDRHiCA: Prof. Jan Feyen, Patricio, Luis, Ana Elizabeth, Lenin, Giovanny, Wilson, Esteban, Alex, Pachy, Gina, Juan, Alicia, Xime and Diego, as well as to the technical staff for their effort during field campaigns. My heartfelt thanks are due to Mario Córdova, for the good and hard times in the technical and scientific activities. I welcome this opportunity to thank my friends of the LCRS: Birgit, Sebastian E., Sebastian A., Maik, Lukas, Boris, Paulina, Giulia and Sandro, as well as the rest of kind colleagues of this wonderful institution. Also I am grateful with the people of the ECSF. In addition, my sincere thanks go to the doctoral commission to take the time to read through this investigation and provide their valuable review.

To my beloved family. . .

This thesis is entirely dedicated to my family . . . My love for them is the main reason of my existence. I am grateful with my adored hummingbird: My wife Johanna. She has been a pillar of strength and love, and an unfailing source of encouragement, patience and support in times of happiness and affliction. I owe a debt of gratitude to my grandmother Leonor, my great-aunt Charito, and my mother Monserrath: Thanks for raising this curious child. I will greatly honor them forever. To my brother and friend Pedro, we will be always together in the ups and downs. Finally to the rest of my family and friends, who still believe in this obsessive Andean-explorer and sarcasm & humor fan.

Galo José Carrillo Rojas
January 2019.

Prolog and acknowledgments

„Das Wort Paramo, dessen ich mich oft in diesen Blättern bediene, bezeichnet in den spanischen Kolonien alle Gebirgsgegenden, welche 1800 bis 2200 Toisen (3500 bis 4290 m) über dem Meeresspiel erhaben sind und in denen ein unfreundlich rauhes, nebelreiches Klima herrscht.“...

„Der baumlosen Vegetation der Paramos geben die sparrige Verzweigung kleinblättriger, myrtenartiger Gesträuche, die Größe und Fülle der Blüten, die ewige Frische aller von feuchter Luft getränkten Organe einen eigentümlichen physiognomischen Charakter. Keine Zone der Alpenvegetation in dem gemäßigten oder kalten Erdstriche läßt sich mit der der Paramos in der tropischen Andeskette vergleichen.“

*Alexander von Humboldt
Ansichten der Natur, 1849.*

“The word Páramo, which I often employ in these pages, signifies in Spanish America all those mountainous regions which are elevated from 1800 to 2200 toises (3500 to 4290 m a.s.l.), and in which an unfriendly, rough, and foggy climate prevails.”... “The vegetation of the Páramos has a peculiar physiognomy and character; from the absence of trees, the short close branches of the small-leaved, myrtle-like shrubs, the large sized and numerous blossoms, and the perpetual freshness of the whole from the constant and abundant supply of moisture. No zone of alpine vegetation in the temperate or cold parts of the globe can well be compared with that of the

Páramos in the tropical Andes.”

*Alexander von Humboldt
Aspects of Nature, 1849.*

Summary

Studies on the atmosphere-surface exchange processes over montane regions represent a growing field. This is particular on the scope of ecohydrological investigations, which assess the estimation and prediction of water, carbon and energy fluxes, among other functional key-indicators of the biomes. Therefore, the understanding of the complexity of energy-driven processes such as actual evapotranspiration (ET_a) and carbon dioxide (CO₂) exchange is fundamental, particularly for the biodiverse tropical highlands, which are exposed to human-induced treats (e.g., global warming and land cover change). Herein, the Andean páramo region of Ecuador (3200-5000 m a.s.l.) supports vital ecosystem services, such as water supply, carbon storage and biodiversity. This biome is crucially important for the sustainability of the inter-Andean valleys' inhabitants, mainly due to its role as a massive water reservoir. Atmosphere-surface exchange processes in the páramo are largely unknown.

The aim of this thesis is to analyze the water, energy and carbon flux transfer mechanisms in páramo catchments of Southern Ecuador, by a multi-scale approach, which considers point-scale (ecosystem) and spatial-scale (catchment), through ground-level (instrumental-based) and remote sensing level (model-based). This methodology allows to quantify the accuracy of each technique, and to identify the most appropriate method according to site characteristics. This work has contemplated: (i) The analysis of the spatial dynamics of ET_a derived from satellite products (Landsat and MODIS) with a calibrated energy balance-based model (METRIC), and the evaluation with a global ET_a product (MOD16) and with ET_a obtained as water balance residual (WB); (ii) the detection and analysis of ground-level and ecosystem-scale ET_a, energy and CO₂ fluxes (through eddy covariance (EC) and micrometeorological methods), their interaction with environmental controls, and the comparison of EC ET_a with widely applied reference ET models (ET_r); and finally, (iii) the evaluation of simulated ET_a and energy fluxes obtained from a state-of-art land-surface model (CLM) parameterized to the biophysical and climate conditions of two páramo catchments. The CLM outcomes evaluation was performed with METRIC ET_a, energy fluxes observations (EC) and with WB-derived ET_a.

Summary

The findings of the first analysis reveal that spatial ETa can be successfully estimated when a proper calibration of the model parameters and a high resolution satellite product is used simultaneously. The ETa temporal dynamics from this approach showed consistent results with WB ETa. The results of the second part, demonstrate the plausibility of EC for gas and energy flux detection on this mountain ecosystem. The CO₂ budget (at different time scales) reveals the –carbon source– behavior of the páramo, which constitutes an outstanding discovery in the knowledge about this region. Mathematical functions between carbon fluxes and biophysical controls (available light and soil temperature) are also reported. The quantification of water loss in the form of ETa, and its comparison with modeled ETr, allowed for the first time, to report truthful crop coefficients for the páramo grasslands. Finally, the third analysis revealed the plausibility of CLM for ETa prediction, in spite of a poor performance of the model for the simulation of specific energy fluxes (net radiation, sensible and soil heat). The evaluation between methods, also demonstrated that METRIC ETa values are closer to the EC ETa observations, and revealed that WB ETa rendered poorly. These analyses provide insights on the methods' selection for future studies in similar locations.

The current investigation provides solid answers to unsolved questions about the dynamics of the ETa, CO₂ and energy fluxes of the páramo, and the multiscale approach adopted enhance our understanding of the ecohydrological processes of this unique Andean ecosystem.

Zusammenfassung

Studien über Austauschprozesse zwischen Landoberfläche und Atmosphäre in Gebirgsregionen stellen ein wachsendes Feld dar. Das trifft vor allem auf ökohydrologische Untersuchungen zu, die die Schätzung und Vorhersage von Wasser-, Kohlenstoff- und Energieströmen sowie andere funktionale Schlüsselindikatoren der Biome bewerten. Daher ist das Verständnis der Komplexität energiegetriebener Prozesse wie der tatsächliche Austausch von Evapotranspiration (ETa) und Kohlendioxid (CO₂) von grundlegender Bedeutung, insbesondere für das biologisch vielfältige tropische Hochland, das anthropogenen Einflüssen (z.B. globale Erwärmung und Landnutzungsänderung) stark ausgesetzt ist. Die andine Páramo-Region Ecuadors (3200-5000 m ü.d.M.) unterstützt wichtige Ökosystemdienstleistungen wie Wasserversorgung, Kohlenstoffspeicherung und Biodiversität. Dieses Biom ist für die Nachhaltigkeit der Bewohner der Andentäler von entscheidender Bedeutung, vor allem aufgrund seiner Rolle als riesiger Wasserspeicher. Die Austauschprozesse zwischen Atmosphäre und Oberfläche im Páramo sind weitgehend unbekannt.

Das Ziel dieser Arbeit ist die Analyse der Wasser-, Energie- und Kohlenstofffluss-Transfer-Mechanismen in Páramo-Einzugsgebieten im Süden Ecuadors. Dies soll durch einen Multi-Skalen-Ansatz erreicht werden, der die Punkt-Skala (Ökosystem) und die räumliche Skala (Einzugsgebiet) durch Bodenmessungen (instrumentell) und Fernerkundung(modellbasiert) berücksichtigt. Diese Methodik ermöglicht es, die Genauigkeit jeder Technik zu quantifizieren und die am besten geeignete Methode entsprechend den Eigenschaften des Standorts zu identifizieren. Diese Arbeit hat folgendes zum Ziel gehabt: (i) Die Analyse der räumlichen Dynamik von ETa, die von Satellitenprodukten (Landsat und MODIS) mit einem kalibrierten energiebilanzbasierten Modell (METRIC) abgeleitet wurde, und die Bewertung mit einem globalen ETa-Produkt (MOD16) und mit ETa, das als Wasserhaushaltsrest (WB) erhalten wurde; (ii) das Erkennen und Analysieren von bodenebenen und ökosystemaren ETa-, Energie- und CO₂-Flüssen (durch Wirbelkovarianz (EC) und mikrometeorologische Methoden), ihre Wechselwirkung mit Umweltkontrollen und der Vergleich von EC ETa mit weit verbreiteten ET-Referenzmodellen (ETr); und schließlich (iii) die Bewertung von simulierten ETa- und Energieflüssen, die aus einem hochmodernen Landoberflächen-

Zusammenfassung

modell (CLM) gewonnen wurden, das auf die biophysikalischen und klimatischen Bedingungen von zwei Páramo-Einzugsgebieten parametrisiert wurde. Die CLM-Ergebnisbewertung wurde mit metrischem ETa, Energieflussbeobachtungen (EC) und mit WB-basiertem ETa durchgeführt.

Die Ergebnisse der ersten Analyse zeigen, dass räumliches ETa erfolgreich geschätzt werden kann, wenn eine ordnungsgemäße Kalibrierung der Modellparameter und ein hochauflösendes Satellitenprodukt gleichzeitig verwendet werden. Die zeitliche ETa Dynamik aus diesem Ansatz zeigte konsistente Ergebnisse mit WB ETa. Die Ergebnisse des zweiten Teils zeigen die Plausibilität der EG für die Gas- und Energieflussdetektion in diesem Bergökosystem. Das CO₂-Budget (in verschiedenen Zeitskalen) zeigt das Verhalten des Páramo als Kohlenstoffquelle, was eine hervorragende Entdeckung im Wissen über diese Region darstellt. Mathematische Funktionen zwischen Kohlenstoffflüssen und biophysikalischen Kontrollen (verfügbare Licht- und Bodentemperatur) werden ebenfalls berichtet. Die Quantifizierung des Wasserverlustes in Form von ETa und sein Vergleich mit dem modellierten ETr ermöglichte es erstmals, wahrheitsgetreue Erntekoeffizienten für das Páramo-Grasland zu melden. Die dritte Analyse ergab, dass das CLM für die Eta-Vorhersage plausibel eingesetzt werden kann, trotz einer schlechten Leistung des Modells für die Simulation der spezifischen Energieflüsse (Netto-Strahlung, sensible und Bodenwärme). Die Bewertung zwischen den Methoden zeigte auch, dass die metrischen ETa-Werte näher an den EC ETa-Beobachtungen liegen, und zeigte, dass WB ETa schlecht abschneidet. Diese Analysen geben Aufschluss über die Auswahl der Methoden für zukünftige Studien an ähnlichen Standorten.

Die aktuelle Untersuchung liefert solide Antworten auf ungelöste Fragen zur Dynamik der ETa-, CO₂- und Energieflüsse des Páramo, und der multiskalige Ansatz verbessert unser Verständnis der ökohydrologischen Prozesse dieses einzigartigen andinen Ökosystems.

Resumen

El estudio de los procesos de intercambio superficie-atmósfera para regiones de montaña representa un campo en desarrollo. Esto está enfocado en particular, hacia investigaciones ecohidrológicas que buscan evaluar la estimación y predicción de flujos de agua, carbono y energía, en conjunto con otros indicadores funcionales clave de los biomas. Por tanto, la comprensión de la complejidad de procesos energéticamente-derivados, tales como la evapotranspiración actual (ETa) y el intercambio de dióxido de carbono (CO_2) es fundamental, particularmente para las biodiversas tierras altas tropicales, que se encuentran expuestas a amenazas inducidas por el ser humano (p. ej. El calentamiento global y cambios de la cobertura del suelo). La región de páramo andino del Ecuador (3200-5000 m s.n.m.) soporta servicios ecosistémicos vitales, tales como la provisión de agua, el almacenamiento de carbono y biodiversidad. Este bioma es crucialmente importante para la sostenibilidad de los habitantes de los valles interandinos, debido sobre todo, a su rol como una enorme reserva de agua. Los procesos de intercambio superficie-atmósfera del páramo se encuentran desconocidos ampliamente.

El objetivo de esta tesis, es el analizar los mecanismos de transporte de flujos de agua, energía y carbono en cuencas de páramo del sur del Ecuador, por medio de un enfoque multiescalar, que considera escala puntual (ecosistema) y escala espacial (cuenca), tanto a nivel del suelo (instrumental) como a nivel de sensores remotos (modelado). Esta metodología permite cuantificar la precisión de cada técnica, e identificar el método más apropiado de acuerdo con las características del sitio. Este trabajo ha contemplado: (i) El análisis de la dinámica espacial de la ETa derivada de productos satelitales (Landsat y MODIS) y de un modelo de balance de energía calibrado (METRIC); y su evaluación tanto con un producto ETa global (MOD16), como con ETa obtenida como residual de balance hidrológico (WB); (ii) la detección y análisis de flujos de ETa, energía y CO_2 a nivel del suelo y escala de ecosistema (por medio de técnica de covarianza de remolinos EC y métodos micrometeorológicos), sus interacciones con variables ambientales de control, y la comparación de ETa derivada de EC con ET derivada de modelos de referencia (ETr) ampliamente usados; y finalmente, (iii) la evaluación de flujos simulados de ETa y energía que se han obtenido

Resumen

de un modelo suelo-superficie de última generación (CLM), mismo que ha sido parametrizado para las condiciones biofísicas y climáticas de dos cuencas de páramo. La evaluación de las salidas del modelo CLM ha sido desarrollada con ETa de METRIC, observaciones de flujos de energía (de EC) y con ETa derivada de WB.

Los hallazgos del primer análisis, revelan que la ETa espacial puede ser satisfactoriamente estimada, cuando una calibración apropiada de los parámetros del modelo y un producto satelital de alta resolución, son usados simultáneamente. La dinámica temporal de la ETa derivada de este método ha mostrado resultados consistentes con ETa de WB. Los resultados de la segunda parte, demuestran la factibilidad de EC para la detección de flujos gaseosos y de energía en este ecosistema de montaña. El balance de CO₂ (a diferentes escalas temporales) revela el comportamiento como –fuente de carbono atmosférico– del páramo, lo que constituye un descubrimiento excepcional para el conocimiento sobre esta región. Se reportan también funciones matemáticas que relacionan los flujos de carbono y variables de control biofísicas (luz disponible y temperatura del suelo). La cuantificación de la pérdida de agua en forma de ETa y su comparación con ETr modelada, permite por vez primera, reportar coeficientes de cultivo veraces para los pajonales de páramo. Finalmente, el tercer análisis reveló la factibilidad de CLM para la predicción de ETa, a pesar de mostrar un desempeño pobre de este modelo para la simulación de flujos de energía específicos (radiación neta, calor sensible y calor del suelo). La evaluación entre métodos, también demuestra que la ETa derivada de METRIC es cercana a las observaciones de ETa de EC, y revela que la ETa obtenida de WB es pobremente representada. Estos análisis proveen una perspectiva para la selección de métodos, en estudios futuros sobre localidades similares.

La presente investigación provee sólidas respuestas a interrogantes no resueltas acerca de la dinámica de flujos de ETa, CO₂ y energía de los páramos, y el enfoque multiescalar que se ha adoptado, mejora nuestra comprensión sobre los procesos ecohidrológicos de este singular ecosistema andino.

Table of contents

Prolog and acknowledgments	i
Summary	v
Zusammenfassung	vii
Resumen	ix
List of Figures	xviii
List of Tables	xix
List of abbreviations	xxi
List of symbols	xxiii
1 Introduction	1
1.1 Motivation	4
1.2 Aims and hypotheses	6
1.3 Thesis outline	7
References	7
2 Conceptual design	15
2.1 Selected Andean páramo catchments of southern Ecuador - A general overview . .	15
2.2 Remote sensing approaches for spatial evapotranspiration assessment in the Andes	18
2.3 The energy, evapotranspiration and carbon dioxide detection method at páramo ecosystem-scale	19
2.4 The atmosphere-surface modeling of mass and energy fluxes and their evaluation approaches for the páramo catchments	21

Table of contents

2.5	Conception and technical preparation of the working packages	22
	References	27
3	Dynamic mapping of evapotranspiration using an energy balance-based model over an Andean páramo catchment of Southern Ecuador	31
3.1	Introduction	33
3.2	Materials and Methods	35
3.2.1	Study Area	35
3.2.2	Weather and stream flow-gage stations	36
3.2.3	Landsat and MODIS imagery	38
3.2.4	Pre-processing of the images	39
3.2.5	METRIC model implementation	40
3.2.5.1	METRIC Landsat-based implementation (METRIC _L)	41
3.2.5.2	METRIC MODIS-based implementation (METRIC _M)	42
3.2.6	Analysis of the METRIC _L and METRIC _M retrievals	43
3.2.7	Comparison of METRIC retrievals with MOD16 product	44
3.2.8	Validation of METRIC retrievals with ET from water balance	44
3.3	Results and Discussion	45
3.3.1	Reference evapotranspiration fraction (ET _{rf}) and crop coefficient (K _c)	45
3.3.2	24-hour ET maps	46
3.3.3	Monthly ET retrievals and comparison with MOD16 ET	47
3.3.4	Validation with ET from Water Balance	53
3.4	Concluding Remarks	55
	Supplementary material	58
	References	59
4	Net ecosystem exchange and evapotranspiration over the páramo of Southern Ecuador	69
4.1	Introduction	71
4.2	Materials and methods	73
4.2.1	Study site characteristics	73
4.2.2	Experimental setup	76
4.2.3	Data preprocessing, QA/QC and instrumental corrections	77

4.2.4	Advection-affected fluxes removal, gap filling and uncertainty analysis . . .	78
4.2.5	Energy balance and footprint analyses	79
4.2.6	Flux calculations and CO ₂ light / temperature-response parameterization . .	80
4.2.7	The study period in context of longer-term observations	81
4.2.8	Evapotranspiration and Kc	81
4.3	Results and Discussion	82
4.3.1	EBC and energy flux densities	82
4.3.2	NEE measurements and partition-derived carbon fluxes (GPP, Reco)	84
4.3.3	NEE / GPP light-response and carbon exchange models	90
4.3.4	CO ₂ fluxes versus climatic / biophysical controls	91
4.3.5	The study period in comparison to longer-term environmental observations	93
4.3.6	Evapotranspiration	93
4.4	Concluding Remarks	99
	Supplementary material	102
	References	108
5	Atmosphere-surface fluxes modeling for the highland páramo catchments of Ecuador	119
5.1	Introduction	121
5.2	Materials and methods	124
5.2.1	Characteristics of the catchments	124
5.2.2	Available data and instrumentation	125
5.2.3	CESM-CLM model adjustment for both catchments	126
5.2.4	Remote-sensing based ETa: METRIC model implementation for both catchments	128
5.2.5	Energy and ETa flux observations: EC and micrometeorological techniques (Zhurucay)	128
5.2.6	ETa estimated with the water balance for both catchments	129
5.2.7	Assessment and comparative analyses of CLM derived energy and ETa fluxes	130
5.3	Results and discussion	131
5.3.1	Assessment of energy and ETa CLM fluxes for Zhurucay	131
5.3.2	Representativeness of catchment-scale and footprint-scale ETa _(METRIC) areal estimates	136

Table of contents

5.3.3	Evaluation of CLM modeled ETa and remote sensing-based ETa versus ground-level ETa observations in both catchments	138
5.4	Concluding remarks and future directions	143
	Supplementary material	146
	References	149
6	Conclusions and Outlook	157
6.1	Conclusions	157
6.2	Outlook	160
	Erklärung	163
	Curriculum vitae	164

List of Figures

1.1	Distribution of the páramo Ecoregion in South America. Map based on the Ecoregions2017 ^{©Resolve} dataset (available at https://ecoregions2017.appspot.com). Country boundaries and main cities in the nearby of páramo areas are included.	5
1.2	Thesis outline scheme. The aims of the study are tagged in the core chapters (3 to 5).	8
2.1	Páramo catchments of southern Ecuador (Quinoas and Zhurucay). Headwater catchment areas with >80% of tussock grassland cover are depicted in red color.	16
2.2	Conceptual workflow from WP1 to WP3	24
3.1	Study area and the Quinoas catchment.	37
3.2	Views of the Quinoas catchment: (A) Tussock grass and wetlands, upper valley; (B) Polylepis forests/water body, upper valley; (C) Pinus and evergreen native forest, mid valley; and (D) Evergreen vegetation, low valley. (Photos by Andrés Abril, October 2015).	38
3.3	Quinoas Automatic Weather Stations Climographs (Jan 2013 - Dec 2014).	40
3.4	Reference ET fraction (ET _{rf}) for METRIC _L and METRIC _M for the vegetated testing plots in the study area (Median, minimum and maximum).	45
3.5	METRIC _L ET Map for the 19/10/2013 (cloud free day).	47
3.6	METRIC _L , METRIC _M and MOD16 ET map comparison for May 2013 (a1, b1, c1); November 2013 (a2, b2, c2) and May 2014 (a3, b3, c3).	49
3.7	Modeled and observed radiation for 2013 - 2014 (hourly means of the three AWSs) and Earth declination angle.	50
3.8	Monthly comparison of METRIC _L , METRIC _M , MOD16 ET in the testing plots. Statistical values of R ² , MBE and RMSE for the METRIC retrievals are shown, as well as the average rainfall from the AWSs. Error bars show SD.	52

List of Figures

3.9 Aggregated Precipitation, Runoff and residual ET in comparison with METRIC_L, METRIC_M and MOD16 ET. Noticeable runoff increments are highlighted in red color. 53

3.10 METRIC_L and METRIC_M algorithms flowchart (adapted from Allen et al. (2007) and Trezza et al. (2013)). 58

4.1 Study Area: A) Satellite image of the location of the páramo ecosystem (Google Earth Pro, 2016), B) Landscape image of the Zhurucay Ecohydrological Observatory and the EC tower, and C) View of the main biome in the fetch (tussock grasslands). 74

4.2 EBC for the study site: (a) EBC with an Rn Surface-Normal correction (b) EBC with uncorrected Rn (direct observation). No gap-filled data were used. 83

4.3 Hourly energy flux densities on cloud-free days for (3a) a less humid / high radiation month (August 2016) and (3b) a wet / low radiation month (January 2017), with error bars. 83

4.4 Half-hourly NEE fingerprint (a) and daily aggregated NEE, GPP and Reco fluxes (b) for the study period. The hourly standard deviation of NEE is shown as bars. . . 85

4.5 Nonlinear fit of diurnal GPP versus PPFD (a) and average diurnal NEE versus PPFD (b) with 95% confidence bands (thin lines). 90

4.6 Spearman’s correlograms for NEP, GPP, Reco, PPFD, soil water content and soil temperature. Days with positive and negative NEP are analyzed independently. Correlations with p-value > 0.05 are cross-marked. 92

4.7 Long-term analyses: (a) Temperature and rainfall series for: El Labrado AWS, Zhurucay AWS (including the 2-year EC measurements), NEE, GPP and Reco, (b) Historical monthly SPEI, and (c) MODIS GPP observations versus EC-based GPP estimations. 94

4.8 Comparison of hourly ET_a and ET_r based on scatterplots with linear fitting and an example of ET curves for 4 days in August 2016 (a) and of daily ET notched boxplots (95% confidence interval) (b). 95

4.9 Water Balance (P-ET_a) at monthly scales. 99

4.10 Monthly climograph for the Zhurucay Ecohydrological Observatory (January 2012 to December 2017) 102

4.11 6-year annual and monthly wind charts (2012-2017) for the Zhurucay Ecohydro-
 logical Observatory. 103

4.12 Cospectra binned by frequency for T, CO₂ and H₂O for wet and less humid months. 104

4.13 2D-Footprint climatology for stable and unstable stratification with wind season-
 ality. The centered black cross denotes the location of the EC tower. Footprint
 isolines (in red color) represent the percentage of R_c at intervals of 10% for 10 to
 90%. A background DEM (gray area; 3 m resolution) is also shown. 106

4.14 Nighttime CO₂ fluxes versus friction velocity for the complete period (without
 normalization of the dataset to a specific temperature). 107

4.15 Daily carbon fluxes (GPP, NEP and Reco) against soil temperature, soil humidity
 and rainfall for the full period). 108

4.16 ET_a (eddy tower), rainfall, VPD and net radiation for the full period. 108

5.1 Location of the study catchments in Southern Ecuador (páramo-headwater catch-
 ments are red lines). 125

5.2 CLM and EC diurnal cycle of fluxes for a less humid and a wet month (9-clear sky
 day sample averaged) with error bars. Mean values of R_n, H, LE and G for the
 sample and full month are shown along climate variables. 131

5.3 Daily-scale CLM modeled and observed energy and ET_a fluxes for Zhurucay. The
 bisector line is depicted as a dotted line. 133

5.4 Analysis of the four components of R_n: Daily course for R_n, R_{Sin}, R_{Sout}, R_{Lin} and
 R_{Lout} on two clear sky and two cloudy consecutive days. Hourly-step scatterplots
 for the 22-month period of CLM-derived and EC-observed values. 135

5.5 Zhurucay ET_{a(METRIC)} maps for a 16-month period (March 2016 to June 2017),
 wet sub-period (5-month: March, April, May, June and October 2016) and less
 humid sub-period (5-month: July, August, September, November and December
 2016). The EC footprint boundaries (80% of source flux area) for each period are
 drawn in red lines. Spatial ET_a statistics are provided. 137

5.6 Taylor diagrams for ET_{a(CLM)} and ET_{a(METRIC)} vs. the best available ET_a ob-
 servation method for each site. Zhurucay diagram also includes the ET_{a(WB)}
 estimation for comparison purposes. Statistics of normalized SD (concentric lines
 from zero), normalized RMSE (concentric lines from the reference method) and
 Pearson correlation (radial lines) are illustrated. 139

List of Figures

5.7 Monthly aggregated $ETa_{(CLM)}$, $ETa_{(METRIC)}$, $ETa_{(EC)}$ and $ETa_{(WB)}$ for both catchments. P, Q and ΔS are also included. 140

5.8 Inter-annual $ETa_{(CLM)}$, $ETa_{(METRIC)}$, $ETa_{(EC)}$ and $ETa_{(WB)}$ boxplots (monthly averaged). Monthly mean of precipitation (with SD) is also depicted. Some ETa boxplots with limited monthly coverage include the number of available months below. 142

5.9 6-year Zhurucay and Quinoas (Toreadora AWS) Climographs (January 2012 to December 2017). 148

5.10 Temporal variability of simulated SWC (CLM: 0.062 m and 0.118 m depth) versus Observed SWC (0.100 m depth) at daily frequency for both catchments (16-month period). Scatterplots for the available date are also depicted. 149

List of Tables

3.1	Location of weather and stream flow-gage stations, and typical vegetation cover in the surrounding area.	37
3.2	List of sensors used in the study.	39
3.3	Landsat and MODIS imagery for the study area.	41
3.4	METRIC _L & METRIC _M ET average daily values (mm day ⁻¹) according to site type.	48
3.5	Comparison of METRIC _L , METRIC _M and MOD16 retrievals with ET from water balance in the micro catchments (Annual and monthly scale). For micro catchments locations refer to Fig. 3.1	54
4.1	Instrumentation used in the experiment.	77
4.2	Flux quality flags. Flag 2 data were discarded for analysis purposes.	78
4.3	Monthly and annual NEE, GPP and Reco fluxes.	86
4.4	Comparison of Zhurucay annual C budgets (average) to other tropical, mid-high elevation, and high-latitude (tundra) grasslands around the globe (EC experiments only).	89
4.5	Daily, monthly and annual ET estimates with standard deviations, and crop coefficients (Kc) for the FAO56 and ASCE ETr models.	96
4.6	Annual and daily ETa comparisons among alpine grasslands around the globe.	98
5.1	Modification to CLM parameters for each catchment	127
5.2	Modeled and observed ETa and hydrological balances for the 16-month period.	141
5.3	Instrumentation used in the experiment.	146
5.4	Landsat imagery used in ETa mapping (METRIC)	147

List of abbreviations

a.s.l.	Above sea level
ASCE-ERWI	American Society of Civil Engineers - Environmental and Water Resources Institute
ASTER GDEM 2	Advanced Spaceborne Thermal Emission and Reflection Radiometer Global Digital Elevation Model 2
AWS	Automatic Weather Station
CLM	Community Land Model
DEM	Digital elevation model
EB	Energy Balance
EC	Eddy Covariance technique
ENSO	El Niño Southern Oscillation
ETM+	Enhanced Thematic Mapper Plus
FAO	Food and Agriculture Organization
FFP	Flux Footprint Prediction
FLUXNET	Global network of flux (micrometeorological) tower sites
IDW	Inverse Distance Weighted interpolation
IRGA	Non-dispersive Infrared Gas Analyzer
Landsat	Land Remote Sensing Satellite
ETM+	Enhanced Thematic Mapper Plus
LSM	Land-Surface Model
LULC	Land Use and Land Cover
METRIC	Mapping EvapoTranspiration at high Resolution with Internalized Calibration model

List of abbreviations

MDS	Marginal Distribution Sampling
MOD	MODIS Terra products
MODIS	Moderate-resolution Imaging Spectroradiometer
NCAR	National Center for Atmospheric Research
PFT	Plant Functional Types
QA/QC	Quality Assessments and Controls
QEO	Quinoas Ecohydrological Observatory
RS	Remote Sensing
SEBAL	Surface Energy Balance Algorithm for Land
SOM	Soil Organic Matter
SPEI	Standardized Precipitation Evapotranspiration Index
TOA	Top of Atmosphere
TKE	Turbulent Kinetic Energy
UNESCO	United Nations Educational, Scientific and Cultural Organization
USGS	United States Geological Survey
WB	Water Balance
ZEO	Zhurucay Ecohydrological Observatory

List of symbols

δ	Earth declination angle
ΔS	Change in soil water storage
ε_0	Broad-band surface emissivity
λ	Latent heat of vaporization of water
C	Carbon
CO ₂	Carbon Dioxide
dT	Near surface temperature difference
ET	Evapotranspiration
ETa	Actual evapotranspiration
ETr	Reference evapotranspiration (FAO56 or ASCE method)
ETrf	Reference Evapotranspiration fraction (crop coefficient at reference alfalfa basis)
F _{max}	Maximum Fractional Saturated Area
G	Soil heat flux
GPP	Gross Primary Productivity
H	Sensible heat flux
Kc	Crop coefficient
Kratio	Conversion value for ETrf f to Kc
Kt	Sky clearness index
L	Monin-Obukhov Length
LAI	Leaf Area Index
LE	Latent heat flux

MBE	Mean bias error
NDVI	Normalized Difference Vegetation Index
NEE	Net Ecosystem Exchange
NEP	Net Ecosystem Production
OMD	Organic Matter Density
P	Precipitation o Rainfall
PPFD	Photosynthetic Photon Flux Density
Q	Runoff (catchment discharge)
r_{ah}	Aerodynamic resistance to heat transfer
Ra	Extraterrestrial solar radiation
Reco	Ecosystem Respiration
RH	Relative humidity
RMSE	Root mean square error
Rn	Net radiation
R_{Lin}	Incoming longwave radiation
R_{Lout}	Outgoing longwave radiation
Rs	Incoming solar radiation at ground level (measured)
R_{Sin}	Incoming solar radiation (measured or modeled)
R_{Sout}	Outgoing shortwave radiation
SAVI	Soil Adjusted Vegetation Index
SD	Standard deviation
SOC	Soil Organic Matter Content
SWC	Soil Water Content
Tair	Air temperature
Ts	Surface temperature
Tsoil	Soil temperature
u^*	Friction velocity
VPD	Vapor Pressure Deficit

1 Introduction

The conservation of biodiverse terrestrial ecosystems (Myers et al., 2000) to human-induced threats, such as land cover change and global warming, must begin with a full understanding of the ecohydrological and biogeo-physical / chemical functioning of the biomes. Of particular interest to ecological studies are the worldwide grasslands, which occupy a leading place in the list of vegetated areas of the Earth surface (26% according to Foley et al. (2011)). South America possess immense areas of grasslands, most of them located in the lowlands of the Cerrado savannas (Brazil), the Gran Chaco (Paraguay, Bolivia and Argentina) and the Pampas and eastern Patagonian steppes (Argentina and Chile). These locations hold a large diversity of herbaceous species (Dixon et al., 2014; Paruelo et al., 2007) and their ecosystem functioning is, in some way, well documented in the literature. However, a number of grasslands located in the highland Andes still remain understudied, such as the Northern Andean Páramo (Venezuela, Colombia, Ecuador and Perú), the Jalca and Puna (Perú, Bolivia and Argentina) and the Southern Andean steppes (Argentina and Chile). Main difficulties to investigate these ecosystems rely on their remote location and harsh environmental conditions, which is worsened due to an insufficient deployment of scientific equipment (a generalized issue in south hemisphere tropical regions) (Aparecido et al., 2018; Córdova et al., 2015; Wohl et al., 2012). The role of these biomes is essential for providing ecosystem services (e.g., water supply, carbon storage and biodiversity) (Herzog et al., 2011; Josse et al., 2009; Oliveras et al., 2014; Peyre et al., 2018), similarly to other highland regions of the northern hemisphere (e.g., the Tibetan Plateau meadows or the Southern Rocky Mountains) (Pepin et al., 2015). Moreover, some of these montane regions are of high importance as biodiverse hotspots, with the tropical Andes the globally second-hottest one (Myers et al., 2000).

The cool and humid Neotropical grasslands of the Northern Andean cordillera, known as páramo, provide vital ecosystem services, such as fresh water for the dense-populated inter-Andean valleys, agroindustry and power hydro-generation (Buytaert et al., 2006a; Célleri and Feyen, 2009; Llambí et al., 2012) and hold a massive carbon pool (Bertzky et al., 2010; Hribljan et al., 2016). The knowledge on hydrological processes, land-surface transfer of water, energy and carbon fluxes, and

1 Introduction

atmosphere boundary-layer dynamics remain understudied for this region. To date, the main obstacles to explore the aforementioned processes have been: (i) the scarcity of hydro-meteorological instrumentation (Córdova et al., 2015; Ochoa-Tocachi et al., 2018), (ii) the lack of instrumental-based detection of evapotranspiration (ET), soil-atmosphere energy components, and carbon dioxide (CO₂) (Carrillo-Rojas et al., 2016, 2019), and (iii) the absence of site-specific implementation of land-surface exchange models.

The total terrestrial ET is approximately 60% of the total terrestrial precipitation amount (Oki and Kanae, 2006). ET is at the heart of our understanding, a key-indicator of water depletion on natural and disturbed ecosystems, which plays a fundamental (and still-poorly understood) role in hydrological processes. ET also constitutes a key-variable in the study of the biomes' response to human-induced alterations (such as land cover / climate change). Thus, the knowledge on the ET dynamics is crucially important for tropical headwater regions. A search of the literature shows very few studies of point or catchment-scale ET conducted in the páramo, most of them limited to modeled ET (Buytaert et al., 2006b; Córdova et al., 2013, 2015; Iñiguez et al., 2016; Mosquera et al., 2015). However, the instrumental-based survey of water vapor losses (i.e., actual evapotranspiration (ET_a)) has not been assessed until now. Considering that ET_a is hardly assessable in space with field measurements, its area-wide estimation via remote sensing-based methods arises as an alternative way for research or water resource-management of páramo catchments. Remotely sensed approaches use multi-scale resolution and multi-date temporal coverage of satellite imagery (e.g., MODIS, Landsat or similar products), along with the application of energy balance (EB) or vegetation index (VI)-based algorithms to derive areal ET_a (Allen et al., 2011; Irmak, 2011; Kalma et al., 2008; Karimi and Bastiaanssen, 2014; Li et al., 2012; Liou and Kar, 2014; Moore, 2004; Mu et al., 2013; Verstraeten et al., 2008). In spite of the growing development of these methods for the application on croplands or lowland-biomes, their implementation and improvement for highland and complex terrain sites is deficient today.

One of the greatest challenges to analyze the ET_a, energy and CO₂ flux exchanges in the páramo has been attributed to the lack of sophisticated micrometeorological techniques (Carrillo-Rojas et al., 2019), such as the Eddy Covariance (EC) method (Aubinet et al., 2012). This methodology has been widely implemented for ecosystem-scale flux detection in numerous biomes around the globe, with trustworthy results (Burba, 2013). Besides ET_a, the atmosphere-vegetation-soil CO₂ exchange, in the form of Net Ecosystem Exchange (NEE) has never been tested with EC in a páramo site. This situation limited the understanding of the carbon uptake / release processes in this biome (CO₂ release = +NEE, and CO₂ uptake = -NEE). Despite to the efforts of some researchers in modeling

(or measuring) related carbon fluxes, such as the Gross Primary Productivity (GPP) (Minaya et al., 2016) or Ecosystem Respiration (Reco) (McKnight et al., 2017; Sánchez et al., 2017), the absence of long term NEE measurements constituted the major obstacle to clearly define the sink / source behavior of the páramo. Such studies have generalized that this biome mainly acts as a CO₂ sink, based exclusively on carbon flux observations over –peatlands– (wetlands) areas of páramo sites. However, a crucial (and unsolved) question relies on the diurnal / nocturnal CO₂ exchange from the grasslands land cover (areal extent >70%) considering the climate variability in these harsh locations. The NEE, GPP and Reco responses to environmental drivers (e.g., light availability and soil humidity and temperature) still remain unexplored. On the other hand, the quantification of the soil-atmosphere energy components of net radiation (Rn), sensible heat (H), latent heat (LE) and soil heat flux (G), their balance and diurnal course are also unknown for the páramo, where the cold, cloudy and humid conditions significantly differ to other alpine environments.

ETa can also be approximated at a catchment-scale as the residual of the water balance closure (WB) in monthly and annual time steps with relative accuracy. Combined, the remote sensing approach for ETa, the ecosystem-scale observations of ETa, energy and CO₂ and the WB catchment-scale ETa, make them valuable resources for the evaluation of simulated fluxes from Land Surface Models (LSM) (Bonan, 2016). These complex algorithms have been under fast evolution in the recent decades (Fatichi et al., 2016) for global or regional-scale fluxes forecasting (sometimes coupled to earth-climate models). LSMs have also been applied to simulate biogeochemical and ecohydrological processes in neotropical mountains (Göttlicher et al., 2011; Marthews et al., 2012; Minaya et al., 2016; Silva et al., 2012; van de Weg et al., 2014). However, no LSM have ever been implemented for the ET and energy fluxes estimation in the Andean páramo. Certainly, this fact has been associated to a knowledge transfer lacking, computational limitations (in the region), a lack of ground-level meteorological data (needed for climate forcing), and to the inexistence of flux measurements (or reliable estimations) to validate the LSM's retrievals.

In summary, the current knowledge deficits shine out: (i) The unknown spatial-scale dynamics of ETa for the páramo region which might be obtained through an energy balance approach and remote sensing imagery; (ii) the to date unknown ecosystem-scale behavior of ETa, CO₂ and energy fluxes which might be obtained via instrumental detection, and their interactions with climatic drivers, and (iii) the not yet tested suitability of LSMs in simulating / prediction of ETa and energy fluxes, which might be evaluated with spatial and ground-level observations.

1.1 Motivation

The work of [Dinerstein et al. \(2017\)](#) reports an improved spatial classification of the world biomes which is based in the renowned classification of [Olson et al. \(2001\)](#), known as the Terrestrial Ecoregions of the World (TEOW). The study spatially-delimits 846 Ecoregions of the globe in the Ecoregions2017^{©Resolve} map. To date, this is one of the most accurate resources to quantify the extent of páramo regions in South America. For the Andes, the Ecoregions of Santa Marta (Colombia, 1 239 km²), the Northern Andean páramo (Ecuador, Colombia and Venezuela, 30 086 km²), Cordillera Central (Perú and Ecuador, 12 102 km²) and Cordillera de Mérida (Venezuela, 2 798 km²) contemplate most of the páramo biome of the globe (46 225 km² approx.). Small páramo sites of Central America (~170 km², according to [Hofstede et al. \(2014\)](#)) are not considered in the TEOW or Ecoregions2017^{©Resolve}. Figure 1.1 illustrates the spatial distribution of the ecosystem in the continent.

The reader can easily observe the proximity of some important human-settlements (main and huge cities such as the capitals Quito and Bogotá) to the páramo areas. The development of these communities has been related to the abundant water supply and other ecosystem services that historically provide these grasslands. [Dinerstein et al. \(2017\)](#) also analyzed the governmental protection initiatives of each Ecoregion. Herein, Santa Martha, The Northern Andean páramo, Cordillera Central and Cordillera de Mérida have the 88%, 80%, 36% and 13% of their respectively extents considered as World's Protected Areas (International Union for Conservation of Nature - IUCN, categories I-VI). A deepest analysis was assessed by [Bax and Francesconi \(2019\)](#). Unfortunately most of these initiatives are robustness-limited in their conservation strategies. Furthermore, the work of [Peyre et al. \(2018\)](#) exposes the biodiversity distribution of the páramo in the Andes, and explains the phyto-regionalization of the biome, considering altitudinal ranges and biogeographical classification. This study highlights the fragility of this biodiverse ecosystem. A general concern is raising in the Andean (and the international) scientific community in relation to the future management of the páramo. This interest is not only restricted to the future effects of the land cover change or global warming, but also to existing threats, such as mining activities ([Pérez-Escobar et al., 2018](#); [Pinel et al., 2018](#)), ancestral practices of grass burning ([Horn and Kappelle, 2009](#)), agricultural expansion and deforestation ([Wigmore and Gao, 2014](#)), or recreational tourism ([Tejedor Garavito et al., 2012](#); [Verano Jiménez and Villamizar González, 2017](#)).

Considering the importance of these grasslands in terms of extent and supply of ecosystem services (along other facts stated in the introduction paragraphs), an in-depth investigation of land-

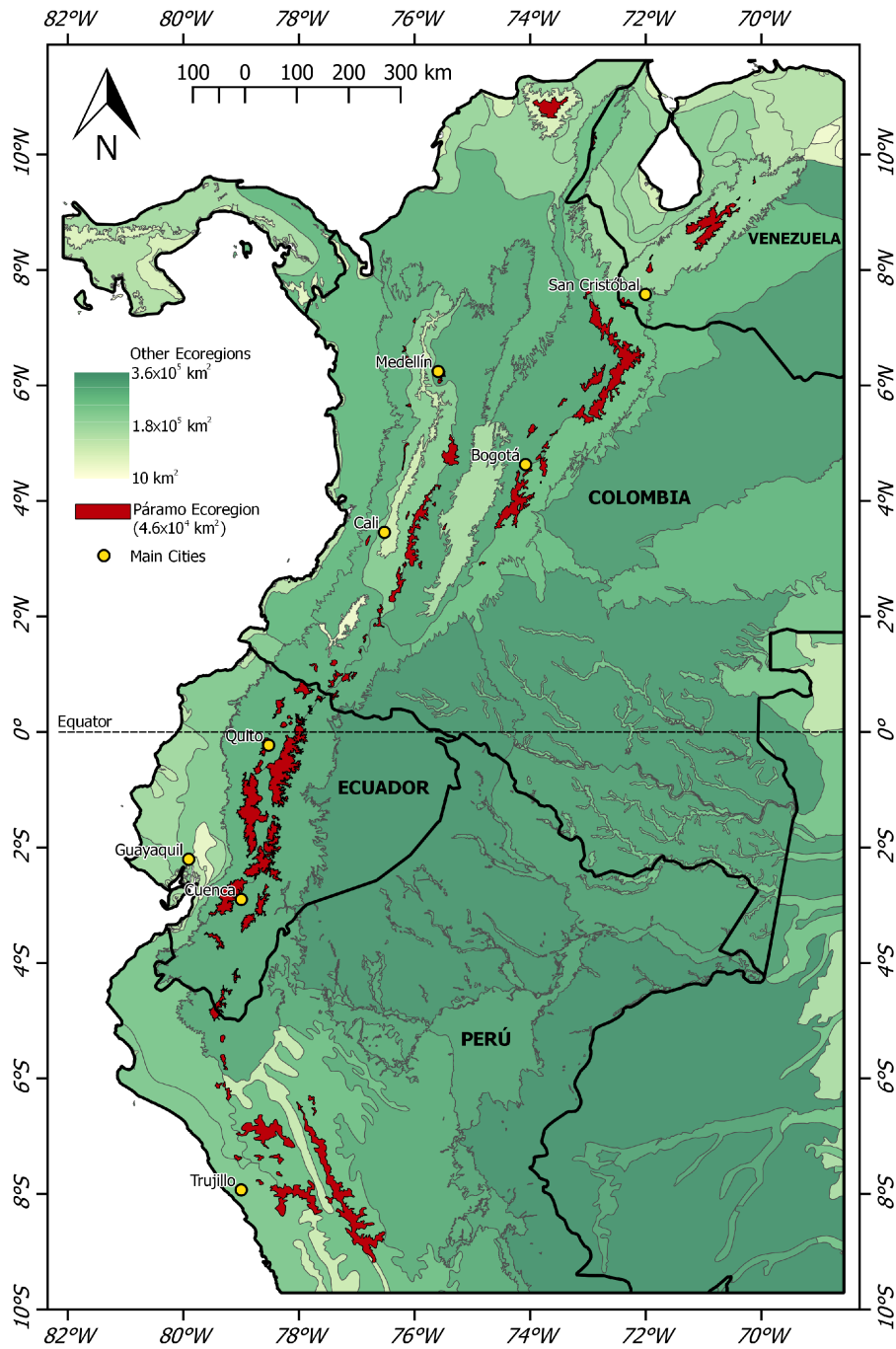


Figure 1.1: Distribution of the páramo Ecoregion in South America. Map based on the Ecoregions2017^{©Resolve} dataset (available at <https://ecoregions2017.appspot.com>). Country boundaries and main cities in the nearby of páramo areas are included.

1 Introduction

surface mass and energy exchange processes for the Northern Andean páramo is evidently needed. Moreover, it is strongly demanded due to the potential impacts that the land use / cover change (Crespo et al., 2010; Ross et al., 2017; Wigmore and Gao, 2014) and climate change (Bradley, 2006; Vuille et al., 2018, 2015) will have on the tropical Andean region in coming decades.

The fragile páramo landscapes of Southern Ecuador (which are clearly exposed to the aforementioned threats) have motivated me to conduct this pioneer investigation over two very representative catchments inside the UNESCO World Biosphere Reserve of the Cajas Massif (UNESCO, 2013). This Ecuadorian protected area of 9766 km² in size hosts more than 838 000 inhabitants in the lowland valleys, and their survival strongly depends on water supply of the surrounding páramo catchments. The research has been performed through the multidisciplinary consortium of German and Ecuadorian universities of the "Platform for Biodiversity and Ecosystem Monitoring and Research in South Ecuador" (DFG-PAK823-825). The Philipps-Universität Marburg (Germany) provided the research framework, funding support and knowledge transfer through the PAK823-825 - Subproject C6 (2014-17) and the University of Cuenca (Ecuador) provided the funding, logistics and facilities through the projects: "Meteorological cycles and evapotranspiration along an elevational gradient in the Cajas National Park" (2013-17) and "Comparative study of actual evapotranspiration methods for the humid soils of an Andean páramo microcatchment" (2015-18).

1.2 Aims and hypotheses

The general aim of the study is to unveil the ET_a, energy and carbon fluxes dynamics in the Andean páramo via the multi-scale estimation of land-surface mass and energy exchanges, by the application of remote sensing-based methods and ground level-based techniques, along with the evaluation of LSM modeled fluxes.

The specific aims are:

- (A1) To assess the quality of spatial ET_a estimates, retrieved from an energy-balance based model (site-specific calibrated) and remote sensing products (Landsat and MODIS) and to compare to an operationally and globally available VI-derived ET_a product (MOD16) for the environmental conditions and terrain characteristics of a páramo catchment.

- (A2) To describe the land-surface water vapor, CO₂ and energy exchange processes via gas / energy flux micrometeorological detection, and to define their relationship with the páramo's biophysical and climatic drivers of light availability, soil temperature and soil humidity.
- (A3) To predict ETa and energy fluxes by the parameterization of the LSM (Community Land Model, CLM 4.0), and to evaluate the outputs with the spatial remote sensing-based ETa and with the ground-level observations of ETa and energy fluxes, considering the instrumentation availability in two páramo catchments.

To assess the aforementioned objectives, the following hypotheses will be tested:

- H1. The accuracy of spatial-scale ETa estimation depends on: a) the site-specific calibration of the model, and b) the resolution of the satellite product used in the implementation of energy balance-based algorithms for the ETa calculation.
- H2. The CO₂ and ETa flux measurements at ecosystem-scale determine that: a) the páramo grasslands act as a CO₂ sink as other studies suggest, and b) the modeled reference ETr is approximated to the measured ETa, and this water loss is lower than 60% of the total precipitation amount.
- H3. The LSM CLM 4.0 is suitable for the prediction of ETa and surface energy fluxes in the páramo ecosystem for single-point simulations.

1.3 Thesis outline

A scheme of the present work is shown in Fig 1.2. The thesis begins with a general introduction and importance of the study for both the scientific and the Andean region communities. Then, an explanation of the applied methods for multi-scale land-surface mass and energy exchange for the target area páramo is provided, as well as the development of working packages in order to test the hypotheses proposed in section 1.2.

The thesis consists of three manuscripts. Two of them are currently published (Chapter 3 and 4), while the third is under review. These manuscripts are entirely presented in the core Chapters 3, 4 and 5, and constitute significant contributions to the knowledge on the páramo region. Chapter 6 summarizes the main findings of the research, providing answers to the hypotheses proposed in section 1.2, and finally presents a brief outlook for future investigations.

1 Introduction

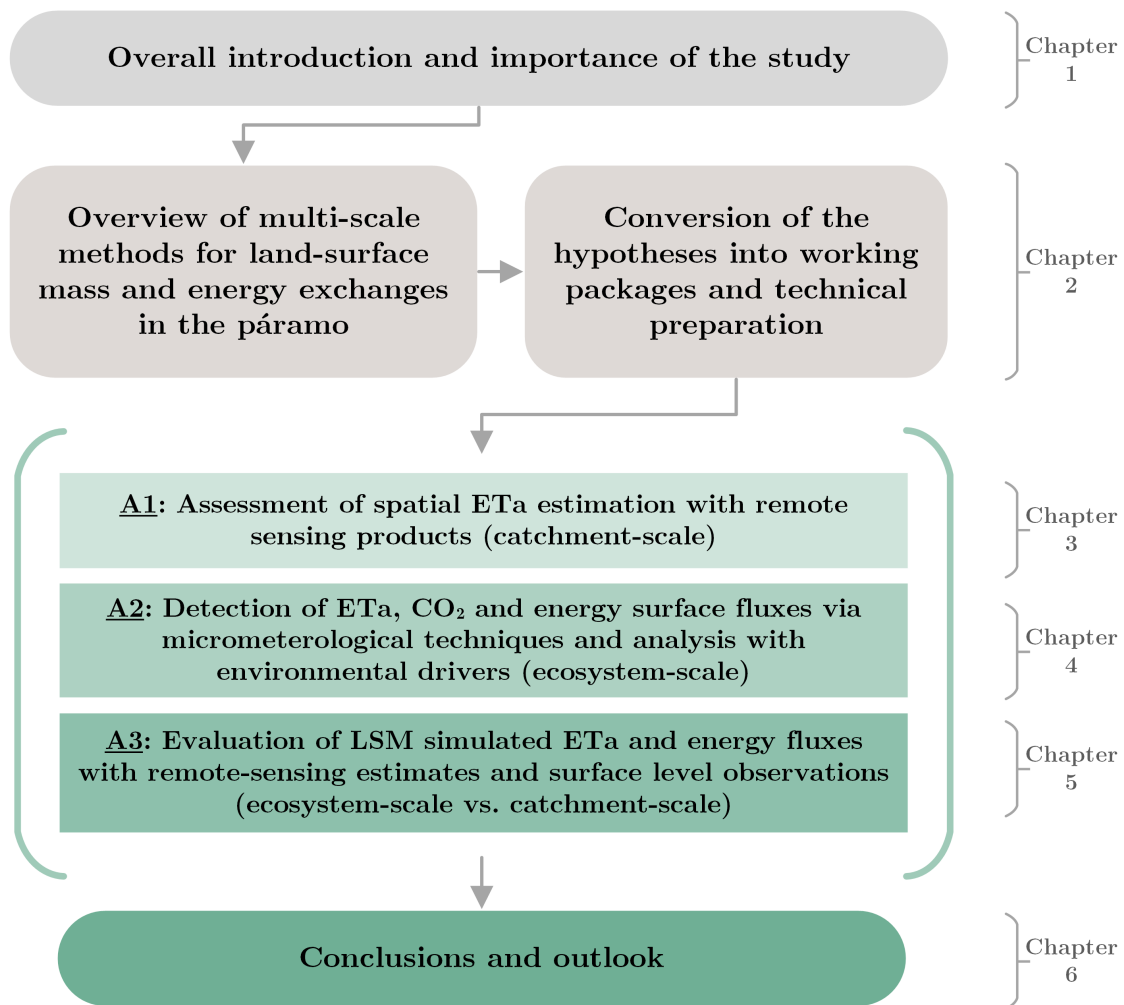


Figure 1.2: Thesis outline scheme. The aims of the study are tagged in the core chapters (3 to 5).

References

- Allen, R. G., Pereira, L. S., Howell, T. a., and Jensen, M. E. (2011). Evapotranspiration information reporting: I. Factors governing measurement accuracy. *Agricultural Water Management*, 98(6):899–920.
- Aparecido, L. M. T., Teodoro, G. S., Mosquera, G., Brum, M., Barros, F. d. V., Pompeu, P. V., Rodas, M., Lazo, P., Müller, C. S., Mulligan, M., Asbjornsen, H., Moore, G. W., and Oliveira, R. S. (2018). Ecohydrological drivers of Neotropical vegetation in montane ecosystems. *Ecohydrology*, page e1932.
- Aubinet, M., Vesala, T., and Papale, D. (2012). *Eddy Covariance: A Practical Guide to Measurement and Data Analysis*. Springer Netherlands, Dordrecht.
- Bax, V. and Francesconi, W. (2019). Conservation gaps and priorities in the Tropical Andes biodiversity hotspot:

- Implications for the expansion of protected areas. *Journal of Environmental Management*, 232(November 2018):387–396.
- Bertzky, M., Ravillous, M., Araujo-Navas, A., Kapos, V., Carrión, D., Chiu, M., and Dickson, B. (2010). Carbon, biodiversity and ecosystem services: Exploring co-benefits. page 20.
- Bonan, G. (2016). Terrestrial Ecosystems and Earth System Models. In *Ecological Climatology*, chapter 25, pages 453–473. Cambridge University Press, New York, US, 3rd edition.
- Bradley, R. S. (2006). CLIMATE CHANGE: Threats to Water Supplies in the Tropical Andes. *Science*, 312(5781):1755–1756.
- Burba, G. (2013). *Eddy Covariance Method-for Scientific, Industrial, Agricultural, and Regulatory Applications*. LI-COR Biosciences, Lincoln, Nebraska, USA.
- Buytaert, W., Célleri, R., De Bièvre, B., Cisneros, F., Wyseure, G., Deckers, J., and Hofstede, R. (2006a). Human impact on the hydrology of the Andean páramos. *Earth-Science Reviews*, 79(1-2):53–72.
- Buytaert, W., Deckers, J., and Wyseure, G. (2006b). Description and classification of nonallophanic Andosols in south Ecuadorian alpine grasslands (páramo). *Geomorphology*, 73(3-4):207–221.
- Carrillo-Rojas, G., Silva, B., Córdova, M., Célleri, R., and Bendix, J. (2016). Dynamic Mapping of Evapotranspiration Using an Energy Balance-Based Model over an Andean Páramo Catchment of Southern Ecuador. *Remote Sensing*, 8(2):160.
- Carrillo-Rojas, G., Silva, B., Rollenbeck, R., Célleri, R., and Bendix, J. (2019). The breathing of the Andean highlands: Net ecosystem exchange and evapotranspiration over the páramo of southern Ecuador. *Agricultural and Forest Meteorology*, 265:30–47.
- Célleri, R. and Feyen, J. (2009). The Hydrology of Tropical Andean Ecosystems: Importance, Knowledge Status, and Perspectives. *Mountain Research and Development*, 29(4):350–355.
- Córdova, M., Carrillo-Rojas, G., and Célleri, R. (2013). Errores en la estimacion de la evapotranspiracion de referencia de una zona de paramo andino debido al uso de datos mensuales, diarios y horarios. *Aqua-LAC*, 5(2):14–22.
- Córdova, M., Carrillo-Rojas, G., Crespo, P., Wilcox, B., and Célleri, R. (2015). Evaluation of the Penman-Monteith (FAO 56 PM) Method for Calculating Reference Evapotranspiration Using Limited Data. *Mountain Research and Development*, 35(3):230–239.
- Crespo, P., Célleri, R., Buytaert, W., Feyen, J., Iñiguez, V., Borja, P., and De Bièvre, B. (2010). Land use change impacts on the hydrology of wet Andean páramo ecosystems. In *Proceedings of the Workshop Status and Perspectives of Hydrology in Small Basins, held at Goslar-Hahnenklee, Germany, 30 March to 2 April 2009*, number APRIL, page 6, Germany. IAHS Publ. 336.
- Dinerstein, E., Olson, D., Joshi, A., Vynne, C., Burgess, N. D., Wikramanayake, E., Hahn, N., Palminteri, S., Hedao, P., Noss, R., Hansen, M., Locke, H., Ellis, E. C., Jones, B., Barber, C. V., Hayes, R., Kormos, C., Martin, V., Crist, E., Sechrest, W., Price, L., Baillie, J. E. M., Weeden, D., Suckling, K., Davis, C., Sizer, N., Moore, R., Thau, D.,

1 Introduction

- Birch, T., Potapov, P., Turubanova, S., Tyukavina, A., de Souza, N., Pinteá, L., Brito, J. C., Llewellyn, O. A., Miller, A. G., Patzelt, A., Ghazanfar, S. A., Timberlake, J., Klöser, H., Shennan-Farpón, Y., Kindt, R., Lillesø, J.-P. B., van Breugel, P., Graudal, L., Voge, M., Al-Shammari, K. F., and Saleem, M. (2017). An Ecoregion-Based Approach to Protecting Half the Terrestrial Realm. *BioScience*, 67(6):534–545.
- Dixon, A. P., Faber-Langendoen, D., Josse, C., Morrison, J., and Loucks, C. J. (2014). Distribution mapping of world grassland types. *Journal of Biogeography*, 41(11):2003–2019.
- Fatichi, S., Pappas, C., and Ivanov, V. Y. (2016). Modeling plant-water interactions: an ecohydrological overview from the cell to the global scale. *Wiley Interdisciplinary Reviews: Water*, 3(3):327–368.
- Foley, J. A., Ramankutty, N., Brauman, K. A., Cassidy, E. S., Gerber, J. S., Johnston, M., Mueller, N. D., O’Connell, C., Ray, D. K., West, P. C., Balzer, C., Bennett, E. M., Carpenter, S. R., Hill, J., Monfreda, C., Polasky, S., Rockström, J., Sheehan, J., Siebert, S., Tilman, D., and Zaks, D. P. M. (2011). Solutions for a cultivated planet. *Nature*, 478(7369):337–342.
- Göttlicher, D., Albert, J., Nauss, T., and Bendix, J. (2011). Optical properties of selected plants from a tropical mountain ecosystem - Traits for plant functional types to parametrize a land surface model. *Ecological Modelling*, 222(3):493–502.
- Herzog, S. K., Martínez, R., Jørgensen, P. M., and Tiessen, H. (2011). *Climate Change and Biodiversity in the Tropical Andes*. Inter-American Institute for Global Change Research (IAI) and Scientific Committee on Problems of the Environment (SCOPE).
- Hofstede, R., Calles, J., López, V. V., Polanco, R., Torres, F., Ulloa, J., Vásquez, A., and Cerra, M. (2014). *Los páramos Andinos Qué Sabemos. Estado de conocimiento sobre el impacto del cambio climático en el ecosistema páramo*. UICN, Quito, Ecuador.
- Horn, S. P. and Kappelle, M. (2009). Fire in the páramo ecosystems of Central and South America. In Mark A. Cochrane, editor, *Tropical Fire Ecology*, volume 25, chapter 18, pages 505–539. Springer Praxis Books, Berlin, Heidelberg.
- Hribljan, J. A., Suárez, E., Heckman, K. A., Lilleskov, E. A., and Chimner, R. A. (2016). Peatland carbon stocks and accumulation rates in the Ecuadorian páramo. *Wetlands Ecology and Management*, 24(2):113–127.
- Iñiguez, V., Morales, O., Cisneros, F., Bauwens, W., and Wyseure, G. (2016). Analysis of the drought recovery of Andosols on southern Ecuadorian Andean páramos. *Hydrology and Earth System Sciences*, 20(6):2421–2435.
- Irmak, A. (2011). *Evapotranspiration-Remote Sensing and Modeling*. InTech, Rijeka, Croatia.
- Josse, C., Cuesta, F., Navarro, G., Barrena, V., Cabrera, E., Chacón-Moreno, E., Ferreira, W., Peralvo, M., Saito, J., and Tovar, A. (2009). *Ecosistemas de los Andes del Norte y Centro. Bolivia, Colombia, Ecuador, Perú y Venezuela*.
- Kalma, J. D., McVicar, T. R., and McCabe, M. F. (2008). Estimating land surface evaporation: A review of methods using remotely sensed surface temperature data. *Surveys in Geophysics*, 29(4-5):421–469.
- Karimi, P. and Bastiaanssen, W. G. M. (2014). Spatial evapotranspiration, rainfall and land use data in water accounting

- Part 1: Review of the accuracy of the remote sensing data. *Hydrology and Earth System Sciences Discussions*, 11(1):1073–1123.
- Li, Z., Zheng, F.-L., and Liu, W.-Z. (2012). Spatiotemporal characteristics of reference evapotranspiration during 1961-2009 and its projected changes during 2011-2099 on the Loess Plateau of China. *Agricultural and Forest Meteorology*, 154-155:147–155.
- Liou, Y. A. and Kar, S. K. (2014). Evapotranspiration estimation with remote sensing and various surface energy balance algorithms-a review. *Energies*, 7(5):2821–2849.
- Llambí, L. D., Soto-W, A., Célleri, R., Bièvre, B. D., Ochoa, B., and Borja, P. (2012). *Ecología, hidrología y suelos de páramos*. Number 1. CONDENSAN, Ecuador.
- Marthews, T. R., Malhi, Y., and Iwata, H. (2012). Calculating downward longwave radiation under clear and cloudy conditions over a tropical lowland forest site: An evaluation of model schemes for hourly data. *Theoretical and Applied Climatology*, 107(3-4):461–477.
- McKnight, J. Y., Harden, C. P., and Schaeffer, S. M. (2017). Soil CO₂ flux trends with differences in soil moisture among four types of land use in an Ecuadorian páramo landscape. *Physical Geography*, 38(1):51–61.
- Minaya, V. V., Corzo, G. A., Solomatine, D. P., and Mynett, A. E. (2016). Data-driven techniques for modelling the gross primary production of the páramo vegetation using climate data: Application in the Ecuadorian Andean region. *Ecological Informatics*.
- Moore, R. D. (2004). Introduction to salt dilution gauging for streamflow measurement: Part 1. *Streamline Watershed Management Bulletin*, 7(4):20–23.
- Mosquera, G. M., Lazo, P. X., Célleri, R., Wilcox, B. P., and Crespo, P. (2015). Runoff from tropical alpine grasslands increases with areal extent of wetlands. *CATENA*, 125(FEBRUARY):120–128.
- Mu, Q., Zhao, M., and Running, S. W. (2013). MODIS Global Terrestrial Evapotranspiration (ET) Product (MOD16A2/A3) - ATBD Collection 5. page 66.
- Myers, N., Mittermeier, R. A., Mittermeier, C. G., da Fonseca, G. A. B., and Kent, J. (2000). Biodiversity hotspots for conservation priorities. *Nature*, 403(6772):853–858.
- Ochoa-Tocachi, B. F., Buytaert, W., Antiporta, J., Acosta, L., Bardales, J. D., Célleri, R., Crespo, P., Fuentes, P., Gil-Ríos, J., Gualpa, M., Llerena, C., Olaya, D., Pardo, P., Rojas, G., Villacís, M., Villazón, M., Viñas, P., and De Bièvre, B. (2018). High-resolution hydrometeorological data from a network of headwater catchments in the tropical Andes. *Scientific Data*, 5(July):180080.
- Oki, T. and Kanae, S. (2006). Global Hydrological Cycles and World Water Resources. *Science*, 313(5790):1068–1072.
- Oliveras, I., Girardin, C., Doughty, C. E., Cahuana, N., Arenas, C. E., Oliver, V., Huaraca Huarasca, W., and Malhi, Y. (2014). Andean grasslands are as productive as tropical montane cloud forests. *Environmental Research Letters*, 9(11):115011.
- Olson, D. M., Dinerstein, E., Wikramanayake, E. D., Burgess, N. D., Powell, G. V. N., Underwood, E. C., D'amico,

1 Introduction

- J. A., Itoua, I., Strand, H. E., Morrison, J. C., Loucks, C. J., Allnutt, T. F., Ricketts, T. H., Kura, Y., Lamoreux, J. F., Wettengel, W. W., Hedao, P., and Kassem, K. R. (2001). Terrestrial Ecoregions of the World: A New Map of Life on Earth. *BioScience*, 51(11):933.
- Paruelo, J. M., Jobbágy, E. G., Oesterheld, M., Golluscio, R. A., and Aguiar, M. R. (2007). The Grasslands and Steppes of Patagonia and the Río de la Plata Plains. In Veblen, T. T., Young, K. R., and Orme, A. R., editors, *The Physical Geography of South America*, chapter 14, pages 232–248. Oxford University Press, New York, US, 1 edition.
- Pepin, N., Bradley, R. S., Diaz, H. F., Baraer, M., Caceres, E. B., Forsythe, N., Fowler, H., Greenwood, G., Hashmi, M. Z., Liu, X. D., Miller, J. R., Ning, L., Ohmura, A., Palazzi, E., Rangwala, I., Schöner, W., Severskiy, I., Shahgedanova, M., Wang, M. B., Williamson, S. N., and Yang, D. Q. (2015). Elevation-dependent warming in mountain regions of the world. *Nature Climate Change*, 5(5):424–430.
- Pérez-Escobar, O. A., Cámara-Leret, R., Antonelli, A., Bateman, R., Bellot, S., Chomicki, G., Cleef, A., Diazgranados, M., Dodsworth, S., Jaramillo, C., Madriñan, S., Olivares, I., Zuluaga, A., and Bernal, R. (2018). Mining threatens Colombian ecosystems. *Science*, 359(6383):1475.1–1475.
- Peyre, G., Balslev, H., and Font, X. (2018). Phytoregionalisation of the Andean páramo. *PeerJ*, 6:e4786.
- Pinel, S. L., López Rodríguez, F., Morocho Cuenca, R., Astudillo Aguillar, D., and Merriman, D. (2018). Scaling down or scaling up? Local actor decisions and the feasibility of decentralized environmental governance: a case of Páramo wetlands in Southern Ecuador. *Scottish Geographical Journal*, 134(1-2):45–70.
- Ross, C., Fildes, S., and Millington, A. (2017). Land-Use and Land-Cover Change in the Páramo of South-Central Ecuador, 1979-2014. *Land*, 6(3):46.
- Sánchez, M. E., Chimner, R. A., Hribljan, J. A., Lilleskov, E. A., and Suárez, E. (2017). Carbon dioxide and methane fluxes in grazed and undisturbed mountain peatlands in the Ecuadorian Andes. *Mires and Peat*, 19(October):1–18.
- Silva, B., Roos, K., Voss, I., König, N., Rollenbeck, R., Scheibe, R., Beck, E., and Bendix, J. (2012). Simulating canopy photosynthesis for two competing species of an anthropogenic grassland community in the Andes of southern Ecuador. *Ecological Modelling*, 239:14–26.
- Tejedor Garavito, N., Álvarez, E., Arango Caro, S., Araujo Murakami, A., Blundo, C., Boza Espinoza, T. E., La Torre Cuadros, M. A., Gaviria, J., Gutiérrez, N., Jørgensen, P. M., León, B., López Camacho, R., Malizia, L., Millán, B., Moraes, M., Pacheco, S., Rey Benayas, J. M., Reynel, C., Timaná de la Flor, M., Ulloa Ulloa, C., Vacas Cruz, O., and Newton, A. C. (2012). Evaluación del estado de conservación de los bosques montanos en los Andes tropicales. *Revista Ecosistemas*, 21(1-2):148–166.
- UNESCO (2013). Cajas Massif Biosphere Reserve. <http://www.unesco.org/new/en/natural-sciences/environment/ecological-sciences/biosphere-reserves/latin-america-and-the-caribbean/ecuador/macizo-del-cajas/>. Last checked on 2018-11-18.
- van de Weg, M. J., Meir, P., Williams, M., Girardin, C., Malhi, Y., Silva-Espejo, J., and Grace, J. (2014). Gross Primary Productivity of a High Elevation Tropical Montane Cloud Forest. *Ecosystems*, 17(5):751–764.
- Verano Jiménez, A. and Villamizar González, A. (2017). Lineamientos agroecológicos para el desarrollo del agroeco-

- turismo en páramos. *Turismo y Sociedad*, 21:253.
- Verstraeten, W. W., Veroustraete, F., and Feyen, J. (2008). Assessment of Evapotranspiration and Soil Moisture Content Across Different Scales of Observation. *Sensors*, 8(1):70–117.
- Vuille, M., Carey, M., Huggel, C., Buytaert, W., Rabatel, A., Jacobsen, D., Soruco, A., Villacis, M., Yarleque, C., Elison Timm, O., Condom, T., Salzmann, N., and Sicart, J.-E. (2018). Rapid decline of snow and ice in the tropical Andes - Impacts, uncertainties and challenges ahead. *Earth-Science Reviews*, 176(September 2017):195–213.
- Vuille, M., Franquist, E., Garreaud, R., Lavado Casimiro, W. S., and Cáceres, B. (2015). Impact of the global warming hiatus on Andean temperature. *Journal of Geophysical Research: Atmospheres*, 120(9):3745–3757.
- Wigmore, O. and Gao, J. (2014). Spatiotemporal dynamics of a páramo ecosystem in the northern Ecuadorian Andes 1988-2007. *Journal of Mountain Science*, 11(3):708–716.
- Wohl, E., Barros, A., and Brunzell, N. (2012). The hydrology of the humid tropics. *Nature Climate Change*, 2(9):655–662.

2 Conceptual design

The present chapter provides a brief methodological review of the current advances in the research of land-surface mass and energy exchanges for mountainous regions, and their applicability for the Andean páramo. The review permitted to structure the thesis framework into working packages in order to answer the hypotheses proposed in the section 1.2. Section 2.1 presents a general overview of the Andean páramo sites selected for analysis. Section 2.2 provides a review of the remote-sensing methods currently used for spatial-scale estimation of ETa, particularly for steep terrain and harsh environmental conditions. Section 2.3, explains the micrometeorological techniques used here to analyze the energy, water vapor and CO₂ flux exchanges; and their interactions with climate and soil conditions. This section is crucially important, because of its pioneer implementation in the Andean highlands region of South America. Section 2.4 explains the methodological overview for the parameterization and evaluation of the state-of-art LSM CLM 4.0 in the páramo ecosystem, for the simulation of mass and energy fluxes. The final section (2.5) of this chapter provides a brief explanation of the design and technical preparation of the working packages.

2.1 Selected Andean páramo catchments of southern Ecuador - A general overview

The Quinoas Ecohydrological Observatory (QEO) and the Zhurucay Ecohydrological Observatory (ZEO) are representative páramo catchments of the Andean highlands of southern Ecuador and the Northern Andean páramo ecoregion in terms of climate, soil and vegetation. These headwater catchments are located in the western Andean cordillera (Cajas Massif Biosphere), and supply abundant water for human consumption, agro industrial activities, and hydropower generation (Céleri and Feyen, 2009). QEO is exposed to the east and ZEO to the west mountainside of the Andes, where the mountainous *Divortium Aquarum* separates the headwater contribution to the Amazonian and Pacific sides respectively. The full extent of QEO and ZEO develops in a mountain

2 Conceptual design

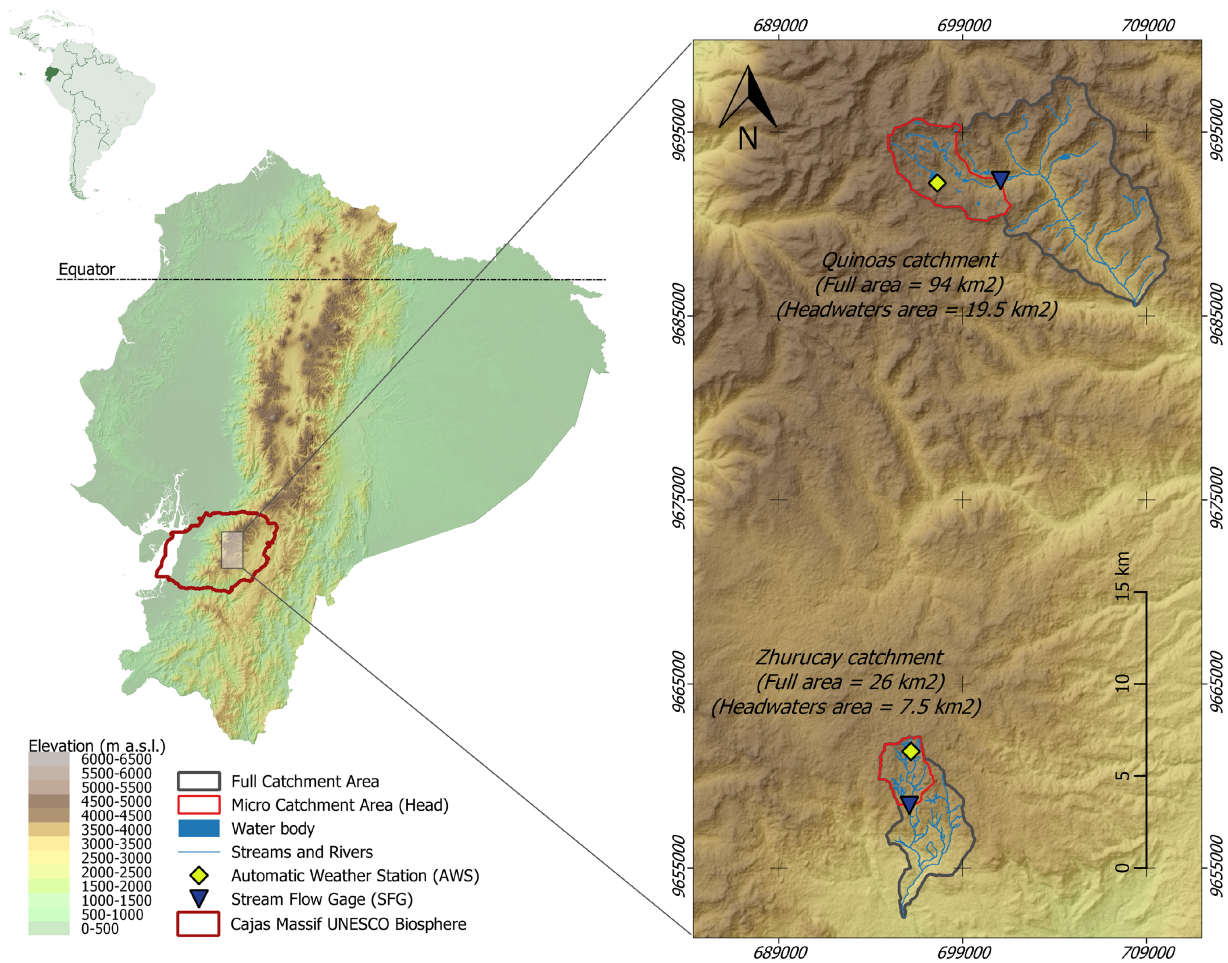


Figure 2.1: Páramo catchments of southern Ecuador (Quinoas and Zhurucay). Headwater catchment areas with >80% of tussock grassland cover are depicted in red color.

gradient from the sub páramo (3000 ~ 3500 m), the mid páramo (3500 ~ 4200 m) to the super páramo (4200 ~ 5000 m) (Llambí et al., 2012; Peyre et al., 2018). The present study is focused on the headwater catchment areas (mid and super páramo region); where QEO ranges from 3610 to 4390 m a.s.l. (area = 19.5 km², slope = 0 ~ 45%) and ZEO ranges from 3500 to 3900 m a.s.l. (area = 7.5 km², slope = 0 ~ 20%). Figure 2.1 illustrates the location of these catchments.

The geology of the sites is characterized by compacted deposits of volcanic rock originated by glacial activity (U-shaped glacial landforms). As it was stated by Mosquera et al. (2015), Andosols are the dominant soil type in these sites (80% of the landscape, especially in the hill slopes), while Histosols (wetlands) cover the remaining area (20% of relative flat areas). These non-allophanic, humic and acidic soils possess a high organic matter content (SOM), where the organometallic

2.1 Selected Andean páramo catchments of southern Ecuador - A general overview

complex formation and low redox potential development are responsible for the noticeable SOM accumulation ($> 0.64 \text{ kg}_{(SOM)} \text{ kg}_{soil}^{-1}$) (Buytaert et al., 2006). QEO and ZEO soils share quite similar characteristics, such as (i) a top soil dark Ah horizon between 0.20 to 0.70 m, with a thin soil C horizon over solid bedrock, (ii) a very high content of organic matter of 30 ~ 40%, (iii) low bulk density levels ($0.45 \sim 0.14 \text{ Mg m}^{-3}$), and (iv) a high field capacity of ($\sim 74\%$). A small portion of the QEO landscape is occupied by small water bodies ($< 5\%$ of the area).

The main canopy in both locations is constituted by tussock grasses of *Calamagrostis Intermedia* (J. Presl) Steud., (height of 30 and 80 cm). This alpine C3 grass is found to cover more than 80% of the headwater landscape, however other C3 (*Festuca* sp.) and rare C4 grass species have been reported as well (Boom et al., 2001). The coexistent vegetation includes, cushion plants ($< 10\%$) mainly on the wetlands (e.g., *Azorella* sp., *Gentiana* sp., *Plantago* sp., *Valeriana* sp., and *Xenophyllum humile* sp.), some forest patches of *Polylepis* sp. and *Gynoxys* sp. (5%), and sparse shrubs, (e.g., *Weinmannia* sp. and *Buddleia* sp.). Most of this native vegetation is perennial due to the slight climate seasonality. The sub páramo part of the full catchments (especially in QEO) are mostly covered by other grasses and upper Andean forests, while some areas have been afforested with *Pinus Patula* sp.

The climate of QEO is mainly influenced by the continental air masses from the Amazon basin, while ZEO is influenced by the Pacific regime, and in some degree by air masses from the Amazonian side. Seasonal rainfall is influenced by the passage of the Inter Tropical Convergence Zone (ITCZ) over the region. Both páramo sites are characterized by a lack of thermal seasonality, steady low temperatures and high humidity, and by convective and orographic cloud formations (Bendix et al., 2006; Emck, 2007). Sea surface temperature anomalies, such as the El Niño Southern Oscillation (ENSO), do not have a significant influence on the climate of this areas (Vuille et al., 2000). For both catchments, the rainfall regime is bimodal (Célleri et al., 2007), with a mean annual rain depth of $1076 \pm 102 \text{ mm year}^{-1}$ (QEO) and $1210 \pm 101 \text{ mm year}^{-1}$ (ZEO). This bimodal seasonality is similar to other páramo ecosystems (Célleri et al., 2007). Rainfall prevails in the afternoon, and near 30% the precipitation is drizzle (Padrón et al., 2015) with small contributions of fog. A summary of a 6-year climatology indicates respectively for QEO and ZEO: (i) daily mean temperatures of 5.4° C (max. = 13° C , min. = 0.9° C) and 6.1° C (max. = 14.2° C , min. = 0.4° C); (ii) average relative humidity of 90% and 94%; (iii) mean wind speeds of 2.3 m s^{-1} and 3.7 m s^{-1} ; and (iii) total incoming solar radiation of $4629 \text{ MJ m}^{-2} \text{ year}^{-1}$ and $4942 \text{ MJ m}^{-2} \text{ year}^{-1}$. For more details of the ecohydrological and edaphic characteristics of QEO and ZEO, the reader can refer to other interesting studies recently conducted on these catchments (Correa et al.,

2018, 2017; Mosquera et al., 2016a, 2015, 2016b; Muñoz et al., 2016; Ochoa-Sánchez et al., 2018; Orellana-Alvear et al., 2017; Pesántez et al., 2018).

2.2 Remote sensing approaches for spatial evapotranspiration assessment in the Andes

As this author stated in the introduction chapter, spatial scale ETa estimates are assessable through remote sensing-based approaches. Two methods are widely used for such processing of satellite imagery: EB and VI based. The first, mainly uses the thermal infrared spectral bands combined with surface level meteorological observations as inputs; the ETa is calculated as a residual of the EB equation:

$$LE = R_N - G - H \quad (Wm^{-2}) \quad (2.1)$$

where, the latent heat flux, LE, can be expressed as ETa by dividing it by the latent heat of vaporization of water. R_N is the net radiation, G is the soil heat flux, and H is the sensible heat flux. The second approach is based on VI and mainly uses the red and near infrared spectral bands of satellite imagery for the calculation of a crop coefficient (K_c) which can be multiplied to reference evapotranspiration areal values (ET_r) to retrieve ETa. This is the case of the Revised Remote Sensing Penman Monteith model (RS-ET) (Mu et al., 2007, 2011) which deliver regional and global ET maps (MOD16 product, 1 km of resolution, 8-day frequency). However, in both cases, specific considerations have to be taken for mountainous terrain applications, such as the Andean highlands of the páramo.

The EB-based METRIC model (Mapping Evapotranspiration at High Resolution with Internalized Calibration) (Allen et al., 2007) among similar EB models (such as SEBAL (Bastiaanssen, 1998), SEBS (Su, 2002) or sim-ReSET (Sun et al., 2009)) have been widely applied for ETa estimation at mid or high resolution (with multispectral / thermal imagery, such as Landsat products, 30 m of resolution, 16-day pass frequency) or at regional scales (MODIS-Terra product, 500 m of resolution, 1-day pass frequency). METRIC proved suitable for ETa estimation in complex and inhomogeneous terrain when specific adjustments are made to the incoming energy estimation for slope and aspect terrain effects, to the wind speed and surface roughness increments according to topography variations (Allen et al., 2013, 2008; Kjaersgaard et al., 2010) and also to the total daily radiation estimation for inclined surfaces (Allen et al., 2006).

2.3 The energy, evapotranspiration and carbon dioxide detection method at páramo ecosystem-scale

In addition, METRIC includes a calibration procedure using inverse modeling at extreme climatic conditions where the H fluxes are calibrated to wet and dry anchor pixels in the image. The METRIC product is a map of reference ET fraction ET_{rf} (of K_c equivalent) which can be multiplied to spatially-interpolated ET_r maps to obtain daily spatial ET_a , similarly to the VI based-approaches. A continuous dataset of ET_{rf} can be obtained through temporal interpolation of individual ET_{rf} scenes; this dataset allows to obtain monthly, seasonal or yearly ET_a aggregations. A flowchart of the METRIC structure and implementation procedure is illustrated in Chapter 3 Figure 3.10.

The predominant cloudy conditions of the Neotropical páramo constrain the generation of dense and (in some cases) a continuous ET_{rf} dataset. In addition, the cloudy conditions cannot be captured by the incoming radiation sub model embedded in METRIC, and also some corrections for modeled atmospheric transmissivity can result insufficient to account for cloudiness variability. In the present investigation the author has selected a study period with the maximum density of cloud free scenes, and a mosaicking filling process has been applied for the partially cloudy images. ET_a from the METRIC methodology has been retrieved at two different resolutions (Landsat and MODIS) and the results have been compared to the VI-based ET product (MOD16).

The validation of satellite-derived ET_a products can be assessed with ET_a derived from WB at catchment-scale. This widely applied approach infers ET_a from hydrological balance as the difference between total precipitation (P) and discharge (Q) and water storage (ΔS), (see Eq. 2.2):

$$ET_a = P - Q \pm \Delta S \quad (2.2)$$

This is possible because no evidence of groundwater contribution to Q has been demonstrated in páramo studies of southern Ecuador (Buytaert et al., 2006; Crespo et al., 2011). A great advantage of WB-derived ET_a relies on the low costs and easiness of implementation, maintenance and monitoring. The combination of remote sensing and WB methods for ET_a has been applied in the full extent QEO catchment (Chapter 3) and the head ZEO catchment (Chapter 5).

2.3 The energy, evapotranspiration and carbon dioxide detection method at páramo ecosystem-scale

Detection of land-surface fluxes on natural environments has shown a remarkable development in the last decades. Herein, sophisticated measurement techniques based on infrared light attenuation for gas detection, are currently used for CO_2 , water vapor, methane and other atmospheric elements

2 Conceptual design

at different scales (i.e., ecosystem level with EC, soil or plant level with static flux chamber, or leaf level via porometry). Of particular interest at ecosystem level, is the EC method, which has proved as a worldwide standard technique for the survey of land-surface exchange processes over natural or disturbed biomes (Aubinet et al., 2012; Baldocchi, 2003; Burba, 2013).

The main advantage of the EC technique relies on a continuous measurement of energy (LE and H), CO₂, water vapor (ET) and other fluxes at a higher frequency (5 ~ 20 Hz) retrieving representative information from larger ecosystem areas. This is possible with a 3D sonic anemometer, which estimates the vertical upward or downward directions of gas and water vapor concentrations (and also temperature and humidity). The general principle of EC measurements is the covariance between the concentration of interest and the vertical wind speed (Burba, 2013). From the point of view of temporal scale, the EC technique allows one to understand the diurnal / nocturnal cycle and seasonal variation of fluxes and their interactions with climatic drivers.

However, the implementation of EC experiments over complex terrain and heterogeneous canopies can be challenging, mainly due to uncertainties associated to nighttime advection effects (Galvagno et al., 2017; Novick et al., 2014) and the impact of underlying sloped surface to the incoming / outgoing energy estimates (Wohlfahrt et al., 2016). In such cases, corrections for (i) topographical inhomogeneities (Hiller et al., 2008), (ii) detection of flux sources and exclusion of noisy contributions (e.g., source footprint and low-turbulence flux filtering) (Aubinet et al., 2012; Kljun et al., 2015) and (iii) other validation approaches, such as the energy balance closure analysis (Foken, 2008), have to be considered to confirm the reliability of EC flux results.

The EC method permits to determine the net CO₂ flux exchange from the ecosystem to the atmosphere (Net Ecosystem Exchange, NEE) where the CO₂ release = +NEE, and CO₂ uptake = -NEE. This functional indicator helps to define the source / sink nature of a biome, and also permits the modeling of Gross Primary Productivity (GPP) and Ecosystem Respiration (Reco) of the biome, through nighttime partitioning approaches (Lasslop et al., 2010). The interactions of these variables with climate drivers (i.e., soil temperature and moisture, and light availability) also allows one to understand the behavior of the NEE or productivity in normal, drought or water excess environmental conditions. In addition, the direct measurements of ET_a provide insights of the real water losses of the ecosystem, such as the ratio of ET_a and total precipitation. Moreover, the measured ET can be compared with standard crop model-based estimations of evaporation losses, such as the grass-based ETr (Allen et al., 1998) or alfalfa-based ETr (ASCE-ERWI, 2001). These models has been widely used in many ecohydrological studies and water-management reports of the Andean páramo. Here, the estimation of K_c, which is the ratio between ET_a / ETr have never

2.4 The atmosphere-surface modeling of mass and energy fluxes and their evaluation approaches for the páramo catchments

been parameterized to the páramo ecosystem. Neither the key NEE and ETa functional indicators have been properly measured, or even compared to other similar ecosystems such as, high-altitude alpine grasslands or high-latitude tundra, until now.

2.4 The atmosphere-surface modeling of mass and energy fluxes and their evaluation approaches for the páramo catchments

The use of LSMs for atmosphere-surface modeling of carbon, water and energy fluxes has taken importance in recent times, demonstrating plausibility in the prediction of such ecosystem variables. One of the factors for their success, relies in the possibility to run a LSM as an independent module or coupled with earth-climate models. In addition, the performance of these models can be improved by forcing site-specific climate datasets (i.e., ground-level meteorological information) and site-specific surface characteristics (i.e., edaphic properties associated to the soil profile and physio-morphological parameters of the vegetation) in replacement of the default inputs generally embedded in the LSM. In some algorithms the vegetation is not represented as biomes, but instead as Plant Functional Types (PFTs), which are physical and phenological characteristics of the plants (e.g. optical and morphological properties, carbon allocation, etc.) and vegetation structure (e.g., Leaf Area Index (LAI), canopy height, etc.) (Bonan et al., 2002).

The global climate model Community Earth System Model (CESM 1.1.2) (Hurrell et al., 2013) includes the land surface component Community Land Model version 4.0 (CLM 4.0) (Lawrence et al., 2011; Oleson et al., 2010). The CLM 4.0 grid cell structure possess three nested hierarchical levels: land unit, snow / soil column, and PFT. Each sub grid level of land units can hold a different number of columns, and each column can hold different PFTs. The CLM 4.0 land unit types are: vegetated, wetland, glacier, lake and urban; these types can also be divided in classes (i.e., vegetated: natural / managed). On the other hand, each land unit type (and classes) can have its own column level representing the vertical soil and snow properties. Soil column is represented by 15 layers and snow can hold up to five layers. The last sub grid level is PFT, where 16 classes of vegetation phenotypes can coexist in the column (bare soil is also considered); the broad categories of PFT contemplate needle-leaf and broad-leaf tree (evergreen and deciduous for tropical, temperate and boreal regions), C3 and C4 grass, crops and base soil types. More details on the CLM grid structure is given by Oleson et al. (2010).

2 Conceptual design

CLM 4.0 adopts the same principle of energy balance of Eq. 2.1 for the estimation of energy fluxes, and its biogeophysical configuration / mode is capable to predict the exchange of energy, water, and momentum between surface and atmosphere. The present investigation used this mode for two representative páramo catchments of southern Ecuador, considering a 6-year atmospheric forcing dataset (solar radiation, temperature and humidity of the air, atmospheric pressure, wind speed and rainfall), site-tailored properties of the soil column (texture, color and organic matter content), and the PFT that mostly matches the phenotype of the tussock grasses (C3 arctic grass) in both catchments. A modification of default PFT in terms of the structure of the vegetation (e.g., LAI, canopy heights) was done, mainly due to the lack of specific physio-morphological characteristics of these grasslands which permit a deep customization of the PFT. An evaluation of CLM-based energy and ET fluxes against remote sense-based and ground-level observed fluxes has never been performed earlier, covering a multi-scale analysis of land-surface mass and energy exchange for the Andean páramo of Ecuador.

2.5 Conception and technical preparation of the working packages

In the present investigation, the author has developed three specific working packages which have been organized into a methodological workflow in order to fulfill the aims proposed in section 1.2, and to provide an answer to each hypothesis. The fulfillment of the first and second aim was needed to complete the third aim, and also to cover the multiscale analyses of the aforementioned variables in a successful way. Thus, for the evaluation of the proposed hypotheses of section 1.2, the author presents the following working packages:

- WP1.** Analysis of remote sensing-derived and catchment-scale ETa estimations for the páramo, by the implementation of an EB-model (METRIC) with two (low and a mid-resolution) satellite products, the comparison of such ETa outputs with a VI-based ETa product (MOD16), and the overall validation with WB-derived ETa observations.
- WP2.** Analysis of the ecosystem-scale energy, ETa and CO₂ surface-atmosphere flux exchanges of a páramo site, by micrometeorological techniques (EC), the fluxes interactions with environmental drivers, and the comparison of measured ETa values to modeled ETr estimates.

2.5 Conception and technical preparation of the working packages

- WP3.** Analysis of simulated ETa and energy fluxes on two páramo catchments by the implementation of the CESM CLM 4.0 with site-specific parameterization, the multiscale evaluation of predicted CLM ETa retrievals with METRIC, WB and EC ETa values, and the CLM simulated energy fluxes with EC observations.

Figure 2.2 illustrates the conceptual workflow from WP1 to WP3 for the present investigation.

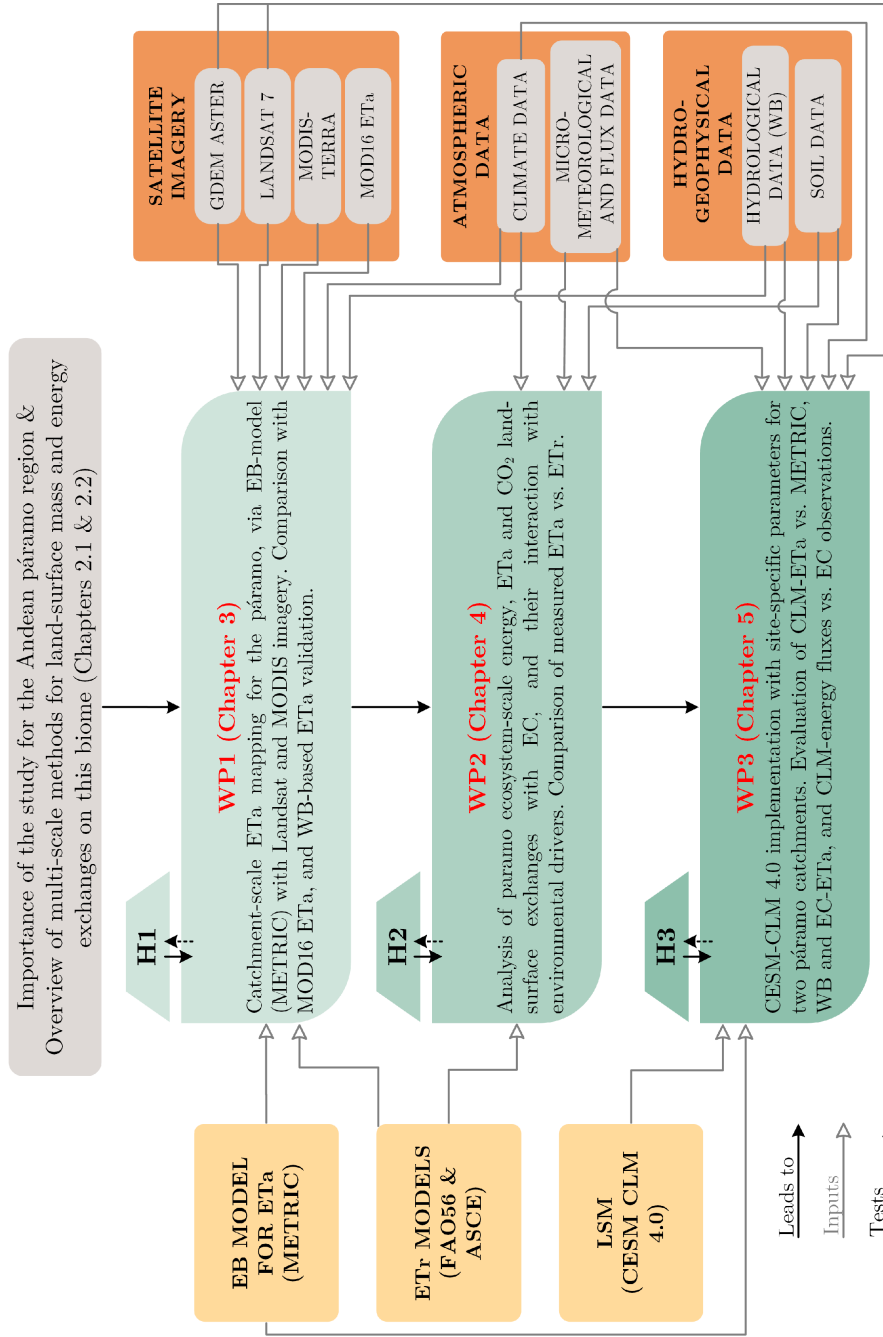


Figure 2.2: Conceptual workflow from WP1 to WP3

2.5 Conception and technical preparation of the working packages

The technical implementation of the working packages is summarized as follows:

The **WP1** determined the spatio-temporal dynamics of ETa for the full-extent catchment and head-catchment of the QEO. To test the dependency of the imagery resolution level on the accuracy of spatial-scale ETa estimations, the METRIC model was implemented with 6 Landsat 7 ETM+ and 9 MODIS-Terra scenes and ground-level meteorological data from three AWSs between 2013 ~ 2014.

The model was parameterized with the following adjustments for terrain characteristics of the QEO: (i) Corrections to Landsat 7 SLC-off banding effect and cloud contamination on raw imagery were done firstly; (ii) the GDEM ASTER v2 digital elevation model was used in calculation of incoming shortwave radiation (slope and aspect terrain adjustments); (iii) LAI was derived with the soil-adjusted vegetation index (SAVI) and a site-specific adjustment of the soil-brightness dependent factor (L); (iv) the surface temperature and G flux were corrected to local temperature lapse rate; (v) H flux was calculated with roughness length values (obtained with a land use and land cover map (LULC)) along with corrections to wind speed for mountainous topography; (vi) LE was retrieved as residual of the EB, and then converted into instantaneous ETrf and ETa; (vii) finally, daily and monthly ETa was calculated considering a correction for daily solar radiation variability for complex terrain. For ETa mapping with MODIS-Terra imagery the same procedure as Landsat was taken, but it required a specific calibration of the ETrf estimates through the Normalized Difference Vegetation Index (NDVI) of the páramo.

Spatial ETa estimates were analyzed across 4 different land covers: Tussock grasslands (6 testing plots - head catchment), *Polylepis* sp. forest patches (4 plots - mid and high catchment), *Pinus* sp. forest patches (4 plots - low catchment), and 9 water bodies (3 lakes - head catchment). Then, an intra-annual comparison of METRIC-derived ETa from Landsat and MODIS was conducted including the resampled MOD16 ETa monthly product (imagery from May 2013 ~ July 2014). The validation of all spatial ETa estimates was performed with ETa from WB in the full and head-catchment scales. Finally, the conversion of the METRIC ETrf in the equivalent Kc was done for comparison purposes with other Kc values reported in regional and global studies.

The **WP2** assessed the determination of the ground-level exchange of energy, ETa and CO₂ fluxes between surface and the atmosphere. To test the ecosystem-scale exchange of such variables, the implementation of micrometeorological techniques was adopted. The first eddy covariance system of the high Andes is a 3.6 m EC tower which was installed in the páramo grasslands of the ZEO from March 2016 until February 2018 surveying fluxes from a 1.6 ha representative area of this ecosystem. Micrometeorological sensors for the measurement of Rn, Photosynthetic Photon Flux

2 Conceptual design

Density (PPFD), and temperature / relative humidity of the air were setup in the tower. In addition three heat flux plates with soil moisture / temperature sensors were buried at 5 cm depth in the surrounding area. Fast fluxes data were collected at 20Hz and temporal aggregated to 30 min after quality assessments and controls (QA/QC), and slow data (climate and soil) were collected at 5 min of resolution. During the processing of raw data, site-specific corrections were considered: (i) a planar fit adjustment for the site topography, (ii) cospectral-based filtering of anomalous data, and (iii) time lag compensation of fluxes as a function of air humidity. Afterwards, the data gaps and those affected due to nocturnal advection fluxes were removed, then gap filled and an uncertainty analysis was carried on.

An assessment of the EB and diurnal cycle of energy flux densities were performed in order to analyze the thermodynamics of the páramo. This work was fundamental to completely understand the energy dynamics which were fulfilled in [WP1](#). Also, the footprint prediction of the spatial flux sources was done. For carbon fluxes the NEE was calculated and it was partitioned into its main components of GPP and Reco. Daily, monthly and annual balances were estimated. The correlations between carbon fluxes (NEE, GPP and Reco) with light and temperature / moisture of soil were established, and the parameterization of site-specific equations for CO₂ response to these environmental variables was done. Moreover, in order to put the 2-year period of flux observation in the longer-term context of the páramo climate, a 54-year period of meteorological data was used to detect anomalies in precipitation and temperature, with the support of a drought / water excess index (Standardized Precipitation Evapotranspiration Index, SPEI). Carbon fluxes evaluation ended with a comparative analysis of local observations with those reported from similar ecosystems in the world.

ETa measurements had the same QA/QC treatment as NEE. To test the EC-based ETa representativeness in comparison to modeled ETr, it was aggregated at daily, monthly and annual scales and evaluated with ETr derived from FAO56 PM and ASCE-ERWI models; in a similar way to the [WP1](#), but at a point-scale. Subsequently, Kc values were calculated from ETa / ETr ratio, and contrasted with other Kc values reported in the literature. Finally the ETa / P ratio was estimated to detect WB anomalies (i.e., water deficits).

The [WP3](#) assessed the implementation of CESM CLM 4.0 on the head catchments of QEO (the less instrumental monitored basin) and ZEO (the more equipped basin). Catchment-specific parameterization of CLM mainly modified the surface inputs in two aspects: (i) soil column: texture (clay, sand and silt contents), organic matter content, soil color and Maximum Fractional Saturated Area (Fmax), and (ii) vegetation: C3 arctic grass PFT selection with unaltered composition in

optical and phenological functioning, but specific changes in the vegetation structure (LAI, canopy height and bottom and percentage of land cover). CLM was setup with single-point simulation mode and a 6-year climate dataset were used to force the model and to the previous spin-up process. To test the reliability of predicted energy and ETa fluxes, the same experimental setup used in WP1 and WP2 was applied to evaluate the LSM outcomes. CLM energy fluxes (Rn, H, LE and G) were correlated with micrometeorological / flux observations from EC, along with the diurnal cycle analysis of fluxes for representative days of the time series. Then, catchment-scale areal estimates from ETa maps (METRIC Landsat 7) were compared with their correspondent area of EC footprint contribution of fluxes. This analysis favors the understanding of differences between catchment and ecosystem-scales ETa estimations. An evaluation of predicted CLM ETa retrievals versus METRIC, WB and EC-ETa values was conducted via goodness-of-fit assessment and monthly aggregated balances. A 16-month period (March 2016 to June 2017) was used for such purpose (where continuous datasets of modeled and observed ETa existed simultaneously in both catchments). Finally, an interannual evaluation of monthly ETa averages for the full period of CLM simulation (6 years) versus the ETa derived from the other methods was conducted (where available ETa existed in the time series). The results of this work package enlighten the knowledge about the ETa methods applicability for the páramo, and provides a clear overview of the differences between less and high monitored catchments in this Andean territories.

The establishment of physio-morphological characteristics for the tussock grasses (based on in-situ phenological and biochemical measurements) is mandatory for successful simulations of carbon fluxes. Therefore, CLM-based carbon predictions were not included in the WP3 due to a lack of instrumental-based observation of the aforementioned parameters.

References

- Allen, R. G., Burnett, B., Kramber, W., Huntington, J., Kjaersgaard, J., Kilic, A., Kelly, C., and Trezza, R. (2013). Automated calibration of the METRIC-Landsat evapotranspiration process. *Journal of the American Water Resources Association*, 49(3):563–576.
- Allen, R. G., Kjaersgaard, J. H., and Garcia, M. (2008). Fine-tuning Components of Inverse-calibrated, Thermal-based Remote Sensing Models for Evapotranspiration. *Pecora 17 - The Future of Land Imaging... Going Operational*.
- Allen, R. G., Pereira, L. S. L., Raes, D., Smith, M., and Others (1998). Crop evapotranspiration-Guidelines for computing crop water requirements-FAO Irrigation and drainage paper 56. *FAO, Rome*, 300(56):D05109.

2 Conceptual design

- Allen, R. G., Tasumi, M., and Trezza, R. (2007). Satellite-Based Energy Balance for Mapping Evapotranspiration with Internalized Calibration (METRIC)-Model. *Journal of Irrigation and Drainage Engineering*, 133(4):380–394.
- Allen, R. G., Trezza, R., and Tasumi, M. (2006). Analytical integrated functions for daily solar radiation on slopes. *Handbook of Environmental Chemistry, Volume 5: Water Pollution*, 139(1-2):55–73.
- ASCE-ERWI (2001). ASCE's Standardized Reference Evapotranspiration Equation. In *Watershed Management and Operations Management 2000*, pages 1–11, Reston, VA. American Society of Civil Engineers.
- Aubinet, M., Vesala, T., and Papale, D. (2012). *Eddy Covariance: A Practical Guide to Measurement and Data Analysis*. Springer Netherlands, Dordrecht.
- Baldocchi, D. D. (2003). Assessing the eddy covariance technique for evaluating carbon dioxide exchange rates of ecosystems: past, present and future. *Global Change Biology*, 9(4):479–492.
- Bastiaanssen, W. G. M. (1998). *Remote Sensing in Water Resources Management : The State of the Art*. International Water Management Institute, Colombo, Sri Lanka.
- Bendix, J., Homeier, J., Cueva Ortiz, E., Emck, P., Breckle, S. W., Richter, M., and Beck, E. (2006). Seasonality of weather and tree phenology in a tropical evergreen mountain rain forest. *International Journal of Biometeorology*, 50(6):370–384.
- Bonan, G. B., Levis, S., Kergoat, L., and Oleson, K. W. (2002). Landscapes as patches of plant functional types: An integrating concept for climate and ecosystem models. *Global Biogeochemical Cycles*, 16(2):5–1–5–23.
- Boom, A., Mora, G., Cleef, A., and Hooghiemstra, H. (2001). High altitude C4 grasslands in the northern Andes: relicts from glacial conditions? *Review of Palaeobotany and Palynology*, 115(3-4):147–160.
- Burba, G. (2013). *Eddy Covariance Method-for Scientific, Industrial, Agricultural, and Regulatory Applications*. LI-COR Biosciences, Lincoln, Nebraska, USA.
- Buytaert, W., Célleri, R., De Bièvre, B., Cisneros, F., Wyseure, G., Deckers, J., and Hofstede, R. (2006). Human impact on the hydrology of the Andean páramos. *Earth-Science Reviews*, 79(1-2):53–72.
- Célleri, R. and Feyen, J. (2009). The Hydrology of Tropical Andean Ecosystems: Importance, Knowledge Status, and Perspectives. *Mountain Research and Development*, 29(4):350–355.
- Célleri, R., Willems, P., Buytaert, W., and Feyen, J. (2007). Space-time rainfall variability in the Paute basin, Ecuadorian Andes. *Hydrological Processes*, 21(24):3316–3327.
- Correa, A., Breuer, L., Crespo, P., Célleri, R., Feyen, J., Birkel, C., Silva, C., and Windhorst, D. (2018). Spatially distributed hydro-chemical data with temporally high-resolution is needed to adequately assess the hydrological functioning of headwater catchments. *Science of The Total Environment*, In press.
- Correa, A., Windhorst, D., Tetzlaff, D., Crespo, P., Célleri, R., Feyen, J., and Breuer, L. (2017). Temporal dynamics in dominant runoff sources and flow paths in the Andean Páramo. *Water Resources Research*, 53(7):5998–6017.
- Crespo, P. J., Feyen, J., Buytaert, W., Bücker, A., Breuer, L., Frede, H.-G., and Ramírez, M. (2011). Identifying controls of the rainfall-runoff response of small catchments in the tropical Andes (Ecuador). *Journal of Hydrology*,

- 407(1-4):164–174.
- Emck, P. (2007). *A Climatology of South Ecuador-With special focus on the Major Andean Ridge as Atlantic-Pacific Climate Divide*. Phd thesis, Friedrich Alexander-Universität, Erlangen-Nürnberg, Germany.
- Foken, T. (2008). The energy balance closure problem: An overview. *Ecological Applications*, 18(6):1351–1367.
- Galvagno, M., Wohlfahrt, G., Cremonese, E., Filippa, G., Migliavacca, M., Mora di Cella, U., and van Gorsel, E. (2017). Contribution of advection to nighttime ecosystem respiration at a mountain grassland in complex terrain. *Agricultural and Forest Meteorology*, 237-238:270–281.
- Hiller, R., Zeeman, M. J., and Eugster, W. (2008). Eddy-Covariance Flux Measurements in the Complex Terrain of an Alpine Valley in Switzerland. *Boundary-Layer Meteorology*, 127(3):449–467.
- Hurrell, J. W., Holland, M. M., Gent, P. R., Ghan, S., Kay, J. E., Kushner, P. J., Lamarque, J.-F., Large, W. G., Lawrence, D., Lindsay, K., Lipscomb, W. H., Long, M. C., Mahowald, N., Marsh, D. R., Neale, R. B., Rasch, P., Vavrus, S., Vertenstein, M., Bader, D., Collins, W. D., Hack, J. J., Kiehl, J., and Marshall, S. (2013). The Community Earth System Model: A Framework for Collaborative Research. *Bulletin of the American Meteorological Society*, 94(9):1339–1360.
- Kjaersgaard, J. H., Allen, R. G., Trezza, R., and Olivieria, A. (2010). Refining components of satellite based surface energy balance models for forests and steep terrain. In *The 3rd USGS Modeling Conference*.
- Kljun, N., Calanca, P., Rotach, M. W., and Schmid, H. P. (2015). A simple two-dimensional parameterisation for Flux Footprint Prediction (FFP). *Geoscientific Model Development*, 8(11):3695–3713.
- Lasslop, G., Reichstein, M., Papale, D., Richardson, A. D., Arneeth, A., Barr, A., Stoy, P., and Wohlfahrt, G. (2010). Separation of net ecosystem exchange into assimilation and respiration using a light response curve approach: critical issues and global evaluation. *Global Change Biology*, 16(1):187–208.
- Lawrence, D. M., Oleson, K. W., Flanner, M. G., Thornton, P. E., Swenson, S. C., Lawrence, P. J., Zeng, X., Yang, Z.-L., Levis, S., Sakaguchi, K., Bonan, G. B., and Slater, A. G. (2011). Parameterization improvements and functional and structural advances in Version 4 of the Community Land Model. *Journal of Advances in Modeling Earth Systems*, 3(1):1–27.
- Llambí, L. D., Soto-W, A., Célleri, R., Bièvre, B. D., Ochoa, B., and Borja, P. (2012). *Ecología, hidrología y suelos de páramos*. Number 1. CONDENSAN, Ecuador.
- Mosquera, G. M., Célleri, R., Lazo, P. X., Vaché, K. B., Perakis, S. S., and Crespo, P. (2016a). Combined use of isotopic and hydrometric data to conceptualize ecohydrological processes in a high-elevation tropical ecosystem. *Hydrological Processes*, 30(17):2930–2947.
- Mosquera, G. M., Lazo, P. X., Célleri, R., Wilcox, B. P., and Crespo, P. (2015). Runoff from tropical alpine grasslands increases with areal extent of wetlands. *CATENA*, 125(FEBRUARY):120–128.
- Mosquera, G. M., Segura, C., Vaché, K. B., Windhorst, D., Breuer, L., and Crespo, P. (2016b). Insights into the water mean transit time in a high-elevation tropical ecosystem. *Hydrology and Earth System Sciences*, 20(7):2987–3004.

2 Conceptual design

- Mu, Q., Heinsch, F. A., Zhao, M., and Running, S. W. (2007). Development of a global evapotranspiration algorithm based on MODIS and global meteorology data. *Remote Sensing of Environment*, 111(4):519–536.
- Mu, Q., Zhao, M., and Running, S. W. (2011). Improvements to a MODIS global terrestrial evapotranspiration algorithm. *Remote Sensing of Environment*, 115(8):1781–1800.
- Muñoz, P., Célleri, R., and Feyen, J. (2016). Effect of the Resolution of Tipping-Bucket Rain Gauge and Calculation Method on Rainfall Intensities in an Andean Mountain Gradient. *Water*, 8(11):534.
- Novick, K., Brantley, S., Miniati, C. F., Walker, J., and Vose, J. (2014). Inferring the contribution of advection to total ecosystem scalar fluxes over a tall forest in complex terrain. *Agricultural and Forest Meteorology*, 185:1–13.
- Ochoa-Sánchez, A., Crespo, P., and Célleri, R. (2018). Quantification of rainfall interception in the high Andean tussock grasslands. *Ecohydrology*, (October 2017):e1946.
- Oleson, K. W., Lawrence, D. M., B, G., Flanner, M. G., Kluzek, E., J, P., Levis, S., Swenson, S. C., Thornton, E., Feddema, J., Heald, C. L., Lamarque, J.-f., Niu, G.-y., Qian, T., Running, S., Sakaguchi, K., Yang, L., Zeng, X., Zeng, X., and Decker, M. (2010). Technical Description of version 4.0 of the Community Land Model (CLM). NCAR/TN-478+STR.
- Orellana-Alvear, J., Célleri, R., Rollenbeck, R., and Bendix, J. (2017). Analysis of Rain Types and Their Z-R Relationships at Different Locations in the High Andes of Southern Ecuador. *Journal of Applied Meteorology and Climatology*, 56(11):3065–3080.
- Padrón, R. S., Wilcox, B. P., Crespo, P., and Célleri, R. (2015). Rainfall in the Andean Páramo: New Insights from High-Resolution Monitoring in Southern Ecuador. *Journal of Hydrometeorology*, 16(3):985–996.
- Pesántez, J., Mosquera, G. M., Crespo, P., Breuer, L., and Windhorst, D. (2018). Effect of land cover and hydro-meteorological controls on soil water DOC concentrations in a high-elevation tropical environment. *Hydrological Processes*, 32(17):2624–2635.
- Peyre, G., Balslev, H., and Font, X. (2018). Phytoregionalisation of the Andean páramo. *PeerJ*, 6:e4786.
- Su, Z. (2002). The Surface Energy Balance System (SEBS) for estimation of turbulent heat fluxes. *Hydrology and Earth System Sciences Discussions*, 6(1):85–100.
- Sun, Z., Wang, Q., Matsushita, B., Fukushima, T., Ouyang, Z., and Watanabe, M. (2009). Development of a simple remote sensing evapotranspiration model (Sim-ReSET): algorithm and model test. *Journal of Hydrology*, 376(3):476–485.
- Vuille, M., Bradley, R. S., and Keimig, F. (2000). Climate Variability in the Andes of Ecuador and Its Relation to Tropical Pacific and Atlantic Sea Surface Temperature Anomalies. *Journal of Climate*, 13(14):2520–2535.
- Wohlfahrt, G., Hammerle, A., Niedrist, G., Scholz, K., Tomelleri, E., and Zhao, P. (2016). On the energy balance closure and net radiation in complex terrain. *Agricultural and Forest Meteorology*, 226-227:37–49.

3 Dynamic mapping of evapotranspiration using an energy balance-based model over an Andean páramo catchment of Southern Ecuador

This chapter is published in *Remote Sensing (MDPI)*, 8(2), 160, 2016.

Received: 09 December 2015

Accepted: 14 February 2016

First published online: 19 February 2016

DOI: <https://doi.org/10.3390/rs8020160>

Reprinted under the Creative Commons license.

Dynamic mapping of evapotranspiration using an energy balance-based model over an Andean páramo catchment of Southern Ecuador

Galo Carrillo-Rojas^{1,2}, Brenner Silva¹, Mario Córdova², Rolando Célleri² and Jörg Bendix¹

¹ Laboratory for Climatology and Remote Sensing (LCRS), Faculty of Geography, Philipps-Universität Marburg, Deutschhausstr. 12, Marburg 35032, Germany

² Departamento de Recursos Hídricos y Ciencias Ambientales (iDRHiCA), Facultad de Ciencias Químicas y Facultad de Ciencias Agropecuarias, Universidad de Cuenca, Cuenca EC010207, Ecuador

Abstract: Understanding of evapotranspiration (ET) processes over Andean mountain environments is crucial, particularly due to the importance of these regions to deliver water-related ecosystem services. In this context, the detection of spatio-temporal changes in ET remains poorly investigated for specific Andean ecosystems like the páramo. To overcome this lack of knowledge, we implemented the energy-balance model METRIC with Landsat 7 ETM+ and MODIS-Terra imagery for a páramo catchment. The implementation contemplated adjustments for complex terrain in order to obtain daily, monthly and annual ET maps (between 2013 and 2014). In addition, we compared our results with the global ET product MOD16. Finally, a rigorous validation

of the outputs was conducted with residual ET from water balance. ET retrievals from METRIC (Landsat-based) showed good agreement with the validation-related ET at monthly and annual steps (mean bias error $< 8 \text{ mm month}^{-1}$ and annual deviation $< 17\%$). However, METRIC (MODIS-based) outputs and the MOD16 product revealed unsuitable for our study due to its low spatial resolution. At last, the plausibility of METRIC to obtain spatial ET retrievals using higher resolution satellite data is demonstrated, which constitutes the first contribution to the understanding of spatially-explicit ET over an alpine catchment in the neo-tropical Andes.

Keywords evapotranspiration; Ecuador; Andes; páramo; tropical mountains; METRIC; remote sensing; Landsat; MODIS

3.1 Introduction

The importance to investigate the hydrological responses of tropical mountains to climate change scenarios (Diaz et al., 2003; Krishnaswamy et al., 2014; Mora et al., 2014; Pepin et al., 2015; Vuille et al., 2015) and also to the influence of land cover changes (Balthazar et al., 2015; Crespo et al., 2010; Mosquera et al., 2015; Thies et al., 2014) lies in the imperative conservation of water resources and the tropical mountain environment. One of the main hydrological response variables is evapotranspiration (ET). This water depletion key-indicator plays a fundamental and still-poorly understood role in water regulation processes, particularly in highland areas. Therefore, accurate area-wide estimates of ET over mountain environments are crucial for the sustainable management of water resources and conservation of pristine ecosystems like the páramo, a high and humid neo-tropical alpine grasslands in the Andean cordillera of South America (Llambí et al., 2012).

Only a few studies of reference ET at point scale have been conducted in this ecosystem (Córdova et al., 2013, 2015), considering that ET is hardly assessable in space with field measurements. To overcome this problem, remote sensing-based models for spatial ET estimation are under evolution with important improvements in accuracy levels reported during the last decade (Allen et al., 2011; Courault et al., 2005; Gowda et al., 2008; Irmak, 2011; Kalma et al., 2008; Karimi and Bastiaanssen, 2014; Kustas and Norman, 1996; Li et al., 2009; Liou and Kar, 2014; Moran and

3 Dynamic mapping of evapotranspiration

Jackson, 1991; Verstraeten et al., 2008) using diverse approaches. The METRIC approach (Mapping EvapoTranspiration at high Resolution with Internalized Calibration) developed by Allen et al. (Allen et al., 2007b) is a state-of-the-art model for mapping actual ET using satellite imagery with thermal infrared band. METRIC and its predecessor SEBAL (Bastiaanssen, 1998) are similar to other energy balance-based models such as the Two-Source Energy Balance (TSEB) model (Norman et al., 1995), Surface Energy Balance System (SEBS) model (Su, 2002), Simple Remote Sensing EvapoTranspiration (sim-ReSET) model (Sun et al., 2009), Two-Source Model (TSM) (Kustas and Norman, 1999) and the Atmosphere Land Exchange Inverse (ALEXI) model (Anderson et al., 1997). These approaches can deliver representative ET at landscape (Landsat or similar mid-high resolution products) or regional (MODIS) scales.

The METRIC model has been applied in several locations worldwide, especially in croplands to estimate the seasonal and spatial variability of ET at different spatial scales and time resolutions (Allen et al., 2011, 2007b; Carrasco-Benavides et al., 2014; Hankerson et al., 2012; Morton et al., 2013; Pôças et al., 2014; Trezza et al., 2013). New studies reveal a good performance of the model when applied over river basins and riparian vegetation (Allen et al., 2007a; Kamble et al., 2013; Kjaersgaard et al., 2011; Singh et al., 2012), but only very few implementations have been conducted over complex terrain (Allen et al., 2012, 2013; Pôças et al., 2013; Senay et al., 2011). Nevertheless, applications of energy balance-based algorithms over mountainous areas have been reported in recent studies with promising results (Dastorani and Poormohammadi, 2012; Jassas et al., 2015; Kiptala et al., 2013; Li et al., 2013; Liu et al., 2008; Mkhwanazi, 2014). Unlike the most common applications of these type of models in flat cropland areas, a modification of the algorithms is needed for irregular terrain. This encompasses the adjustment of the incoming energy estimates for slope and aspect terrain effects, and also adjustments that account for wind speed and surface roughness increments according to topography variations (Allen et al., 2008; Hansen, 1993; Kjaersgaard et al., 2010). In addition, a correction of the total daily radiation for inclined surfaces needs to be accounted for in the model (see Allen et al. (2006)).

An alternative approach to retrieve ET from satellite data is the use of vegetation indices (VI) and its derivatives (Glenn et al., 2011; Guerschman et al., 2009; Mu et al., 2007, 2011; Murray et al., 2009; Zhang et al., 2009). Of particular interest is the Revised Remote Sensing Penman Monteith model (RS-ET) (Mu et al., 2007, 2011). This model was developed for regional and global ET mapping (MOD16 product) and uses the Enhanced Vegetation Index (EVI), the albedo, the Leaf Area Index (LAI), the land cover type and climate data from reanalysis. Some VI models are highly promising due to the ease of implementation over large vegetated areas (Glenn et al., 2010). The

comparison of energy-balance and vegetation-index models against ground-based measurements and water balance-ET responses is needed to assess site-specific ET estimates (Velpuri et al., 2013). This has been tested in several studies with interesting results (Karimi and Bastiaanssen, 2014; Liou and Kar, 2014; Vinukollu et al., 2011).

In summary, ET retrievals remain challenging for the Andean mountains. To our knowledge, no study has so far focused on the spatio-temporal determination of ET in páramo ecosystems of South America with remotely sensed data. Moreover, although the validation of remote sensing-based ET through the residual ET derived from water balance is a convenient method (Karimi and Bastiaanssen, 2014), it has never been applied to an Andean catchment before.

Thus, the aims of the present study are (1) to retrieve daily and monthly ET maps by application of the METRIC model adapted to the páramo conditions at two different resolutions (Landsat and MODIS), (2) to compare the Landsat and MODIS METRIC ET retrievals to a VI model-based ET product (MOD16), and (3) to validate the remote sensing-based ET outputs with ET obtained as the residual of the water balance of the catchment in monthly and annual time steps. For our case, the METRIC implementation to landscape and regional scales will permit to assess which product is more accurate.

3.2 Materials and Methods

3.2.1 Study Area

Our study area is a páramo catchment exposed to the east mountainside of the Andes (2800 to 4250 m a.s.l.) in southern Ecuador (Josse et al., 2009). Climate of this region is mainly influenced by the continental air masses (moisture-laden) from the Amazon basin, to a lesser degree by the Inter Tropical Convergence Zone (ITCZ) fluctuations, and in a few cases by dry cool air masses from the West (Humboldt current influence). Consequently, steady low temperatures and a prevalent convective and orographic cloud formation occur (Bendix et al., 2006; Emck, 2007; Hastenrath, 1981). Although the Amazonian air masses tend to lose a high percentage of humidity due to condensation over the eastern lower flanks of the cordillera, annual precipitation totals between 800 and 1500 mm are common in the Andean highlands (Vuille et al., 2000). Hence, the páramo ecosystems have a surplus of water, constantly nourished by rainfall events and drizzle, as well as a slight fog interception (Bendix et al., 2008).

In this region, the Quinoas catchment (94.1 km²) plays a significant role as an headwater

3 Dynamic mapping of evapotranspiration

catchment inside of the Cajas Massif, a UNESCO World Biosphere Reserve (UNESCO, 2013). This catchment is located in the Paute river, a tributary of the Santiago river, which in turn is part of the Amazon basin. In the inter-Andean basin (Beck et al., 2008) below the páramo, more than 580.000 inhabitants benefit from the water supply from Quinoas and other neighboring catchments. Besides human consumption, agriculture, industrial activities, and hydropower generation are supported by this abundant resource (Céleri and Feyen, 2009). The catchment is mostly shaped by glacial landforms with slopes that usually range from 0 to 45%. Predominant soil types according to the FAO soil classification system are andosols and histosols (WRB-IUSS, 2014), with a very high content of organic matter (30% and 60% respectively) and a field capacity that ranges between 0.39 0.90 cm³ cm⁻³ (mean = 0.64) (Aucapiña and Marín, 2014; Crespo et al., 2011; Quichimbo et al., 2012). Wetlands and small lakes are important elements in the highlands.

Prevailing vegetation is tussock grass (*Calamagrostis* sp. and *Festuca* sp.) which covers more than 70% of the territory and coexist with cushion plants patches (e.g. *Plantago* sp., *Valeriana* sp. and *Gentiana* sp.), small forest patches of *Polylepis* sp. and *Gynoxys* sp. (< 5%), and low shrubs like *Weinmannia* sp., *Buddlea* sp. among others (Crespo et al., 2007; Sklenar and Jørgensen, 1999). Mid and low valley areas of the catchment (< 3000 m a.s.l.) are covered by sub-páramo (dominated by shrubs and grasses), upper Andean forest, and grasslands with some areas afforested with *Pinus Patula* sp. (25%). Andean tussock grasses and most of the native vegetation are perennial due to the slight seasonality (Buytaert et al., 2006a; Luteyn and Churchill, 1999; Mark, 1969). Figure 3.1 shows the location of the study area including topographic information, and Figure 3.2 shows predominant vegetation types in the catchment.

3.2.2 Weather and stream flow-gage stations

Three automatic weather stations (AWSs) and two stream flow-gage stations were installed in the catchment (details are in Figure 3.1 and Table 3.1).

Meteorological and stream flow-gage data were collected every 5 minutes during 2013 and 2014 with a quality assessment (Zahumensky et al., 2004). Stream flow-gage datasets were available from July 2013 to June 2014. Table 3.2 and Figure 3.3 describe the deployed sensors and the meteorological data.

According to Figure 3.3 there is no significant temperature seasonality. However considerable changes occur in the diurnal course. The average variability of the diurnal temperature range is 8.7° C (average daily Tmax = 17.8° and Tmin = 1.8°) for all AWSs sites. Wind speed varies seasonally,

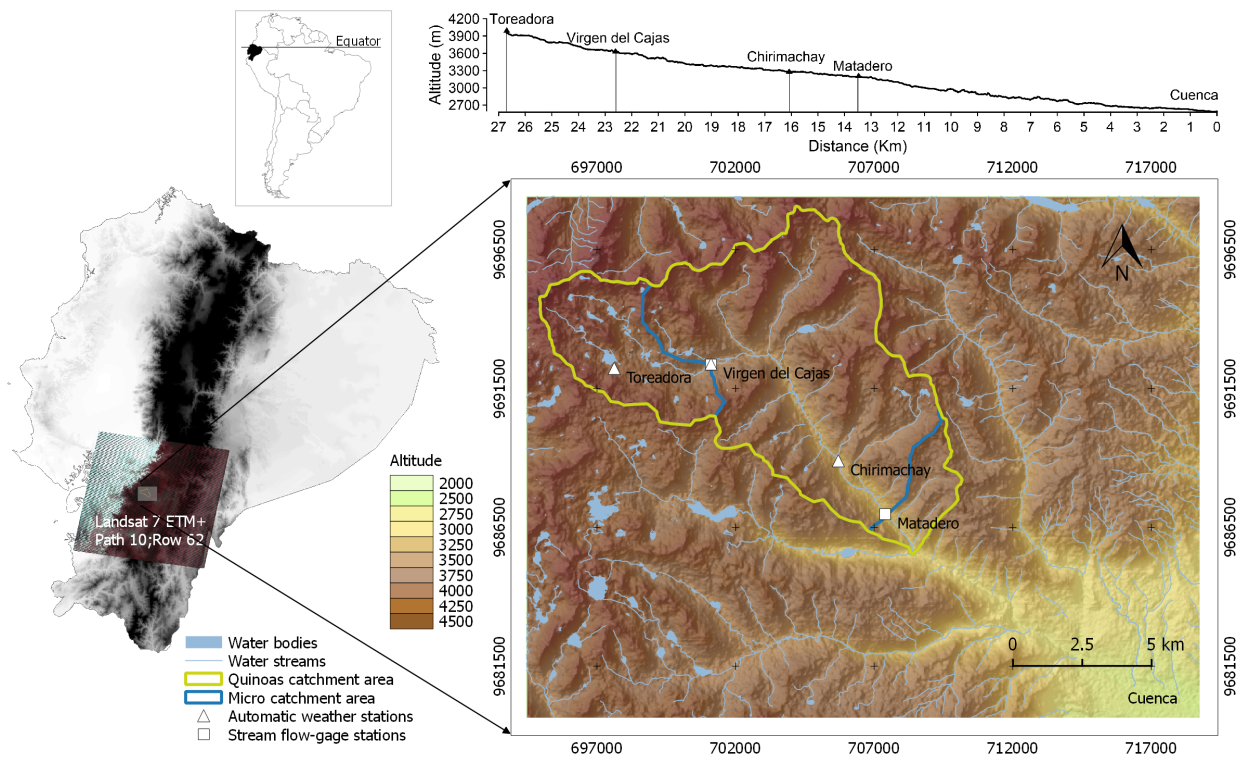


Figure 3.1: Study area and the Quinoas catchment.

Table 3.1: Location of weather and stream flow-gage stations, and typical vegetation cover in the surrounding area.

Station	Latitude & Longitude (UTM)	Elevation (m a.s.l.)	Vegetation Type - Approx. Height
Toreadora ¹	9692227.1; 697618.7	3955	Tussock Grass ("Pajonal") (0.40 m)
Virgen del Cajas ^{1,2}	9692382.2; 701110.7	3626	Mixed High Grass (0.40 m)/Low Grass (0.15 m)
Chirimachay ¹	9688895.5; 705703.9	3298	Mixed: High Grass (0.40 m)/Native Subalpine & Forest (8 m)
Matadero ²	9686975.5; 707391.7	3209	Mixed: High Grass (0.40 m)/ Native Subalpine & Forest (> 8 m)

¹ AWSs.

² Stream flow-gage station.

with mean daily values of 3.0, 2.0 and 1.9 m s⁻¹ from June to September, and 1.9, 1.5 and 1.6 m s⁻¹ for the rest of the year for Toreadora, Virgen del Cajas, and Chirimachay respectively. Likewise,

3 Dynamic mapping of evapotranspiration



Figure 3.2: Views of the Quinoas catchment: (A) Tussock grass and wetlands, upper valley; (B) Polylepis forests/water body, upper valley; (C) Pinus and evergreen native forest, mid valley; and (D) Evergreen vegetation, low valley. (Photos by Andrés Abril, October 2015).

daily total solar radiation also shows a light seasonal pattern, with average values of 13.9, 13.8 and 13.8 MJ m⁻² day⁻¹ from November to December, and 11.3, 11.3 and 9.7 MJ m⁻² day⁻¹ for the rest of the year. Increased radiation in November leads to a decrease in relative humidity. In the same way, rainfall can be characterized by a bimodal pattern with a peak between March and May, and another in October. The same rainfall regimes for the study area and for the inter-Andean basin were also reported by Célieri et al. (2007).

3.2.3 Landsat and MODIS imagery

For the period April 2013 to December 2014 six Landsat 7 ETM+ SLC-off (scan line corrector off) scenes (30 m resolution) were obtained from the USGS Earth Explorer. Nine cloud-free MODIS-Terra images (Level 1, 500 m resolution) were acquired from the Land Processes Distributed Active

Table 3.2: List of sensors used in the study.

Variable	Sensors	Unit	Accuracy	Time Resolution
Air Temperature/ Relative Humidity ^{1,2}	Campbell CS-215 + radiation shield	°C/ %RH	±0.3°C/ ±2%RH	5 min
Wind Speed and Direction ¹	Met-One 034B Wind set	m s ⁻¹	±0.11 m s ⁻¹	5 min
Pressure ^{1,2}	Vaisala PTB110 Barometer	hPa	± hPa	5 min
Solar Radiation ¹	Campbell CS300 Pyranometer	W m ⁻²	±5% daily total	5 min
Rainfall ¹	Texas TE525MM rain gage	mm	±1%	5 min
Water Level ²	Campbell SR50A-L Sonic Ranging Sensor	m	±0.025 m	5 min

¹ At AWSs: Toreadora, Virgen del Cajas and Chirimachay.

² At stream flow-gage stations: Virgen del Cajas and Matadero.

Archive Center (LP DAAC). MODIS-Terra data was selected considering sensor view angles < 20° in order to avoid pixel deformation (Trezza et al., 2013). Finally, monthly MOD16 Evapotranspiration data (1000 m resolution) were taken from The Numerical Terradynamic Simulation Group (NTSG-University of Montana). Although optical satellite imagery is normally contaminated by frequent cloud cover over the Andes of Ecuador, especially in the southern Cordillera, all images used were hardly affected by clouds (Table 3.3).

3.2.4 Pre-processing of the images

First, a radiometric correction for the Landsat and MODIS images was applied using the method recommended by Allen et al. (2007b) and Tasumi et al. (2008). The typical Landsat 7 SLC-off banding effect affected less than 2.3% of the image cover for our study area (due to its location in the center of the images with path/row = 10/62). Nonetheless, a gap filling correction was done to correct this problem using a focal analysis technique (USGS, 2017). Finally, a mosaicking filling process was applied for the partially cloudy images. The latest was conducted using the FMASK algorithm for cloud & shadow detection (Zhu and Woodcock, 2012), as well as a time-weighted interpolation technique recommended by Kjaersgaard et al. (2012). This process is explained in detail in the supplementary information of this paper. For the topographic correction in METRIC we used the GDEM ASTER v2 digital elevation model (DEM) (30 m resolution) which was obtained from the NASA Land Processes Distributed Active Archive Center (LP DAAC, 2011; Tachikawa

3 Dynamic mapping of evapotranspiration

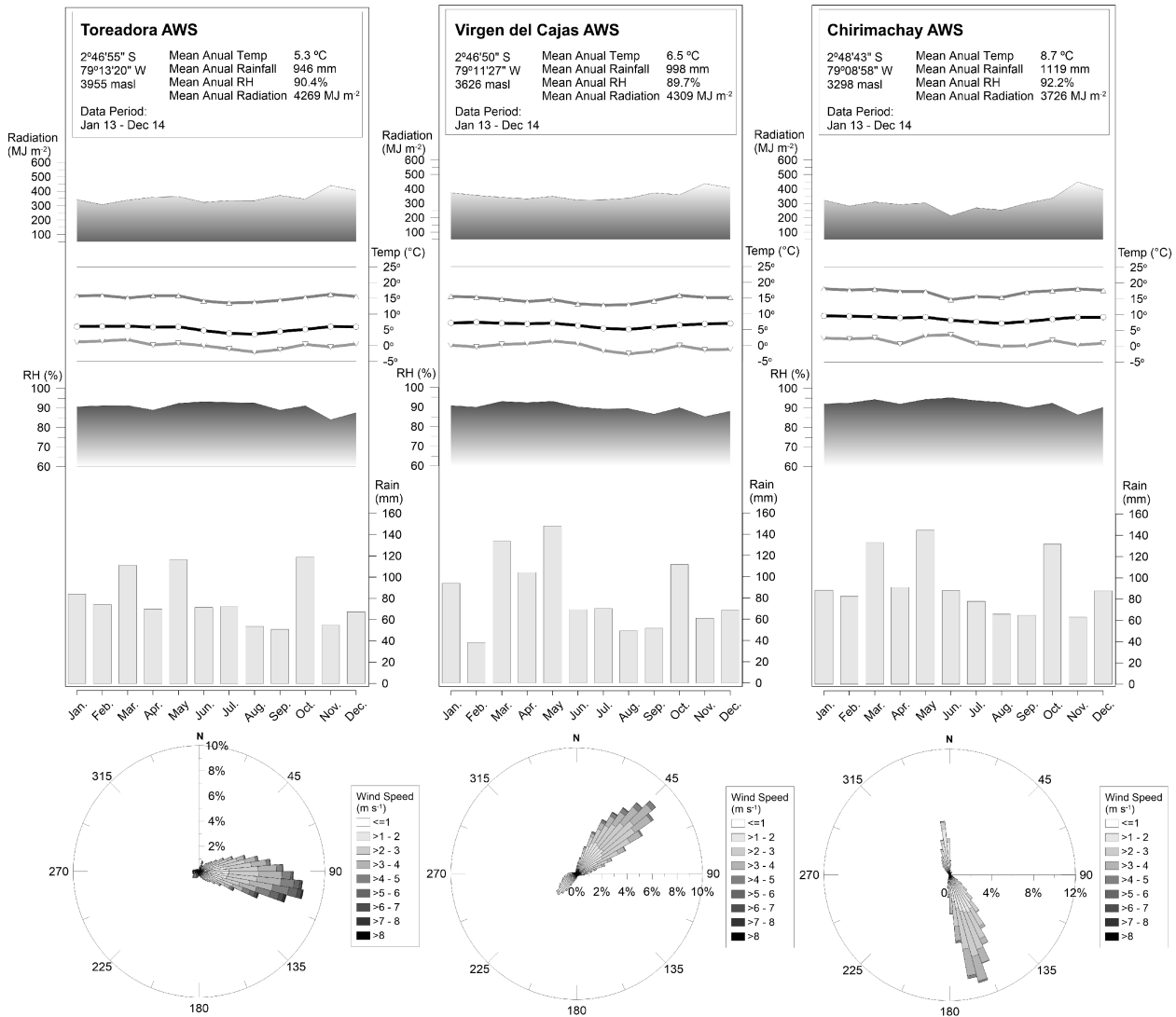


Figure 3.3: Quinoas Automatic Weather Stations Climographs (Jan 2013 - Dec 2014).

et al., 2011). For the development of surface roughness maps, a land use / land cover map (LULC) was obtained from the Geoportal database of the Ministerio del Ambiente del Ecuador (Ministerio del Ambiente del Ecuador, 2018).

3.2.5 METRIC model implementation

METRIC delivers the instantaneous latent heat flux on a pixel-by-pixel basis as a residual of the subtraction of the soil and sensible heat fluxes from the available net radiation. METRIC includes

Table 3.3: Landsat and MODIS imagery for the study area.

Landsat 7 ETM+ SLC-Off Scene ID	Date	Path/Row	% Cloud & cloud-shadow over the Quinoas study area *
LE70100622013116EDC00	26/04/2013	10 / 62	0.0
LE70100622013180EDC00	26/06/2013	10 / 62	<9.4
LE70100622013292EDC00	19/10/2013	10 / 62	<12.1
LE70100622014087EDC00	28/03/2014	10 / 62	<9.5
LE70100622014183EDC00	02/07/2014	10 / 62	<12.5
LE70100622014215EDC00	03/08/2014	10 / 62	<38.0
MODIS-Terra Scene ID	Date	Tile Covering	% Cloud & cloud-shadow over the Quinoas study area *
MOD02HKM.A2013118.1530	28/04/2013	H10/V9	<5.0
MOD02HKM.A2013242.1555	30/08/2013	H10/V9	<3.0
MOD02HKM.A2013265.1600	22/09/2013	H10/V9	<30.0
MOD02HKM.A2013313.1600	09/11/2013	H10/V9	<8.0
MOD02HKM.A2014021.1555	21/01/2014	H10/V9	<35.5
MOD02HKM.A2014087.1540	28/03/2014	H10/V9	<30.9
MOD02HKM.A2014233.1530	21/08/2014	H10/V9	<20.0
MOD02HKM.A2014249.1530	06/09/2014	H10/V9	<5.0
MOD02HKM.A2014348.1600	14/12/2014	H10/V9	<2.5
MOD16 Global ET product	Date	Tile Covering	
MOD16A2.A2 monthly imagery	January 2013 to	H10/V9	
...	December 2014		

* Identified before the mosaicking procedure.

a calibration procedure using inverse modeling at extreme climatic conditions where sensible heat fluxes are calibrated to wet and dry anchor pixels (Allen et al., 2007b). Figure S1 in the supplementary information of this paper shows the implementation flowchart of the METRIC model with Landsat and MODIS imagery, hereinafter called $METRIC_L$ and $METRIC_M$ respectively. We used ERDAS ImagineTM and R software to implement the model.

3.2.5.1 METRIC Landsat-based implementation ($METRIC_L$)

A detailed flowchart of the METRIC model is provided in Figure 3.10 of the supplementary material section and is based on the equations given by Allen et al. (2007b). The latter also included specific calibrations of the model implementation for Landsat imagery considered the following:

- (i) The incoming shortwave radiation was calculated considering terrain slope and aspect corrections for our location (Allen et al., 2007b; Duffie and Beckman, 2013).
- (ii) The albedo was calculated according to Tasumi et al. (2008).

3 Dynamic mapping of evapotranspiration

(iii) The emissivities were computed using the approach of [Tasumi \(2003\)](#).

(iv) LAI was derived from [Bastiaanssen \(1998\)](#) and computed using the soil-adjusted vegetation index (SAVI) with a local calibration of the soil-brightness dependent factor (L) ([Huete, 1988](#)).

(v) The surface temperature was estimated according ([Markham and Barker, 1986](#); [Wukelic et al., 1989](#)).

(vi) Soil heat flux was calculated using the approach of [Bastiaanssen et al. \(2000\)](#); [Cuenca et al. \(2013\)](#).

(vii) Sensible heat flux was calculated according [Allen et al. \(2007b\)](#) where the roughness length values were assigned using a land use and land cover map (LULC) and specific values for the biome of the páramo ([Brutsaert, 1982](#); [Hansen, 1993](#); [Ministerio del Ambiente del Ecuador, 2018](#); [Yang and Friedl, 2003](#)).

(viii) We implemented the method recommended by [Allen et al. \(2008\)](#) for an adjustment of roughness length, a correction of wind speed for mountainous effects, and a specific calibration of the temperature lapse rate for each image.

(ix) Once radiation, soil and sensible fluxes were calculated, we obtained latent heat as the residual of the balance and subsequently the instantaneous ET ([Allen et al., 2007b](#)), then converted it to a daily basis using the approach recommended by ([Allen et al., 2007b](#); [ASCE-ERWI, 2001](#)).

(x) Cloud contaminated pixels were previously assessed according ([Allen et al., 2007a,b](#); [Irmak et al., 2012](#); [Kjaersgaard et al., 2012](#); [Zhu and Woodcock, 2012](#)).

(xi) Finally, ET on a daily basis was obtained applying a correction for solar radiation variability over sloping terrain ([Allen et al., 2006](#)) and monthly ET was calculated according [Kjaersgaard et al. \(2011\)](#).

3.2.5.2 METRIC MODIS-based implementation (METRIC_M)

METRIC_M implementation follows the same method as with Landsat imagery, except for modifications in specific intermediate components and the use of a linear correlation of the Reference Evapotranspiration Fraction (ET_{rf}) and the Normalized Difference Vegetation Index (NDVI) to assist in the selection process of the cold and hot pixels in accordance with the methodology of [Trezza et al. \(2013\)](#). The input imagery products we used were MOD02HKM v5 (calibrated radiances), MOD11_L2 v5 (land surface temperature), MOD03 (geolocation fields) and MOD35 (cloud mask). To obtain net radiation we used the same methodology than METRIC_L with the following exceptions: Albedo for MODIS_M was calculated by integrating the at-surface reflectances from

bands 1 to 7 of the MOD02 product (Tasumi et al., 2008), surface temperature was obtained from the MODIS surface temperature product MOD11_L2, to obtain LAI we applied the relationship between LAI-NDVI for different biomes described in the MODIS LAI backup method (Knyazikhin et al., 1999), for our study we calculated a linear relationship between the ET_{rf} and NDVI (previously obtained in the $METRIC_L$ implementation) and aggregated it to the MODIS scale. According to a similar statistical approach by Allen et al. (2013) we selected the 20% of coldest pixels from a NDVI population with the 20% highest values to obtain a local site calibrated relationship as shown in Equation 3.1.

$$\begin{aligned} ET_{rf} &= 0.804 * NDVI + 0.289; & \text{for } NDVI < 0.75 \\ ET_{rf} &= 1.05; & \text{for } NDVI \geq 0.75 \end{aligned} \quad (3.1)$$

In the same way that in $METRIC_L$, we selected the hot pixels considering candidates with low vegetated pixels, relative high temperature and homogeneous terrain. A similar statistical-based approach was used. Cloud masking was performed using the MOD35 (cloud mask) product from USGS (Ackerman et al., 2010), and an interpolation for cloud masked images. Finally, the calculation of daily and monthly ET was carried out in similar way than $METRIC_L$ implementation.

3.2.6 Analysis of the $METRIC_L$ and $METRIC_M$ retrievals

In order to analyze the variability of daily ET according to the predominant vegetation of the study site, we selected and classified testing plots with homogeneous land cover. The selected plots in the ET maps were classified as follows: (i) Tussock grass (6 sites in the head of the catchment), (ii) *Polylepis* sp. forest patches (4 sites in the high and mid locations), (iii) *Pinus* sp. forest plantations (4 in the lowlands) and (iv) Water bodies (3 small lakes in the uplands). The plots had at least 500 x 500 m of properly identified biome during ground truth fieldwork campaigns. *Polylepis* plots are usually neighboring water bodies, and *Pinus* plots are mostly located in steep terrain. Daily time series of the ET maps were statistically analyzed (using mean, maximum and standard deviation) from one high radiation month (November) and one typical rainy month (April) in order to compare extreme situations. In addition to this, ET_{rf} (which is equal to a crop coefficient at reference alfalfa basis according Allen et al. (2007b) retrieved $METRIC_L$ and $METRIC_M$ for the tussock grass sites were compared with literature values of grass-based crop coefficient (K_c) obtained by applying a conversion value (K_{ratio}) according to Allen et al. (1998). The method to obtain K_{ratio} is described in the supplementary information of this paper.

3.2.7 Comparison of METRIC retrievals with MOD16 product

METRIC_L and METRIC_M monthly ET retrievals were resampled (using nearest-neighbor interpolation) to a 1000 m resolution and were compared with MODIS ET (MOD16) monthly product for the May 2013 to July 2014 period. The monthly MOD16 HDF archives were processed according to [Mu et al. \(2014\)](#). We used histogram-frequency analysis and the Kolmogorov-Smirnov distribution test to compare monthly ET maps for each product.

3.2.8 Validation of METRIC retrievals with ET from water balance

ET was directly inferred from water balance as a difference between total precipitation and discharge (i.e., $ET = P - Q$) in two nested micro catchments inside the Quinoas catchment (areas 19.5 and 87.2 km² respectively, see [Fig. 3.1](#) for location). This approach was used because no evidence of groundwater contribution to discharge has been found in páramo sites of Ecuador ([Buytaert et al., 2006a](#); [Crespo et al., 2011](#)). Discharge data from the stream flow-gage stations of Virgen del Cajas and Matadero was used to calculate the runoff and runoff coefficients (i.e., Q/P) of each micro catchment. We applied the Manning equation ([Chow et al., 1988](#)) to convert water-level data into flow rates. A discharge vs. water-level analysis was conducted with constant-rate based calibrations of stream flow measurements applying salt-dilution technique ([Hongve, 1987](#); [Moore, 2004](#)). Precipitation for the area was averaged using Thiessen polygons method for the rain gauges data of the AWSs. A validation analysis of METRIC_L and METRIC_M retrievals with ET from water balance was conducted using mean bias error (MBE), root mean square error (RMSE) and percentual mean bias error (%MBE) according to equations 3.2 to 3.4:

$$MBE = \frac{1}{n} \sum_{i=1}^n (ET_{METRIC/MOD16} - ET_{WB}) \quad (3.2)$$

$$RMSE = \sqrt{\frac{1}{n} \sum_{i=1}^n (ET_{METRIC/MOD16} - ET_{WB})^2} \quad (3.3)$$

$$\%MBE = \frac{1}{n} \sum_{i=1}^n \frac{(ET_{METRIC/MOD16} - ET_{WB})}{ET_{WB}} * 100 \quad (3.4)$$

Where $ET_{METRIC/MOD16}$ is the monthly ET value of METRIC_L, METRIC_M or MOD16. ET_{WB} is the monthly value of ET from water balance. Finally, n is the number of months. In this

analysis we included the MOD16 ET product for comparative purposes against METRIC retrievals.

3.3 Results and Discussion

3.3.1 Reference evapotranspiration fraction (ET_rf) and crop coefficient (K_c)

The ET_rf values for the three vegetated covers (testing plots) are illustrated in boxplots of Figure 3.4 for the study period. We observe that METRIC_M ET_rf values were slightly higher than those obtained with Landsat. Trezza et al. (2013) reported similar values of ET_rf for Landsat retrievals, but lower values for MODIS over high vegetation in the Middle Rio Grande valley of New Mexico. The differences in the medians between both products were 0.06, 0.13 and 0.08 respectively for Tussock Grass, Polylepis and Pinus. The variation of ET_rf for the mentioned vegetation types can be attributed to the following factors: 1) Proximity of the Polylepis plots to water bodies and wetlands, and 2) MODIS thermal band (MOD11-LST, 1000 m resolution) can be compromised by neighboring effects (especially in the steep terrain of Pinus plantations). The lower ET_rf variation for Tussock grass sites was attributed by the relative surface thermal homogeneity; however for the MODIS product this variation probably was affected by the coarse resolution of its thermal band.

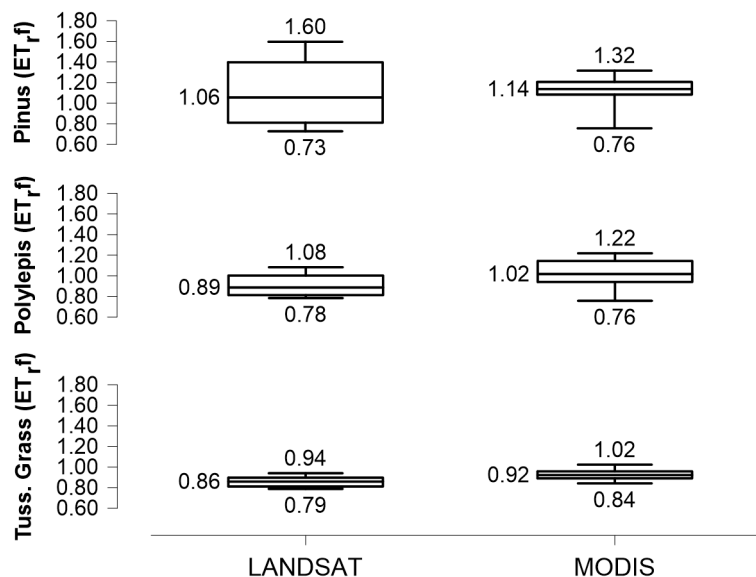


Figure 3.4: Reference ET fraction (ET_rf) for METRIC_L and METRIC_M for the vegetated testing plots in the study area (Median, minimum and maximum).

3 Dynamic mapping of evapotranspiration

In order to compare the ETrf values of the Tussock grass to other reported in similar studies, we multiplied it by the Kratio = 1.143 (calculated in an annual period). This value permitted to convert ETrf into an equivalent grass-based crop coefficient (Kc) as mentioned above. The equivalent range obtained for METRIC_L was 0.90 ~ 1.07. These values were closer to those obtained in highland irrigated meadows of northern Portugal (Kc = 0.88 ~ 0.89) (Pôças et al., 2013), and to those reported for irrigated pastures in the lowlands of Galicia (Kc = 1.05) (Cancela et al., 2006). For METRIC_M the equivalent range of Kc was 0.96 ~ 1.17. The latter retrievals were higher than Landsat values, which is probably due to the coarse resolution of the MODIS product and the heterogeneous vegetation cover within a single pixel. In addition, our results showed higher Kc than those reported by Buytaert et al. (2006b): Kc = 0.42 for tussock grass and a Kc = 0.95 for interfered areas in a field-scale study of páramo catchments. Our ETrf and thus Kc estimations were supported by the evidence of no water stress and a constant humid condition of the soil.

3.3.2 24-hour ET maps

Figure 3.5 presents an ET map for October 19, 2013 corresponding to the Landsat image of that cloud free day. The testing plots are also marked in the map.

As thermally expected, lower ET values generally occurred in the crests, while higher ET values were found in the valley. The map shows that ET consistently decreases as altitude increases. Highest values were observed over water bodies and densely vegetated areas, especially over the mountain forests and the riparian vegetation. The ET derived from the high vegetation in the northeast-faced slopes of the center valley is noticeable, particularly due to the amount of radiation in this month and aspect/declination of these slopes. As expected, land cover impacts directly on the amount of ET of the map. Daily ET statistics of METRIC_L and METRIC_M for single relative dry and humid months in the testing plots are shown in Table 3.4.

Table 3.4 shows that daily averages of METRIC_L generally increase from tussock to trees to water bodies similarly to applications of METRIC and SEBAL over riparian vegetation (Pôças et al., 2013; Trezza et al., 2013), for METRIC_M this finding is not noticeable, mainly due the lack of spatial fidelity of the model considering the heterogeneity of our study area. Both METRIC_L & METRIC_M daily results revealed differences between the relatively dry and humid months, with ET values in November 2013 higher than in April 2014 for all vegetated-sites, with exception of water bodies in METRIC_L. This was in agreement with the local climate (section 3.2.2), where increments of solar radiation cause a reduction in relative humidity and the differences between both periods

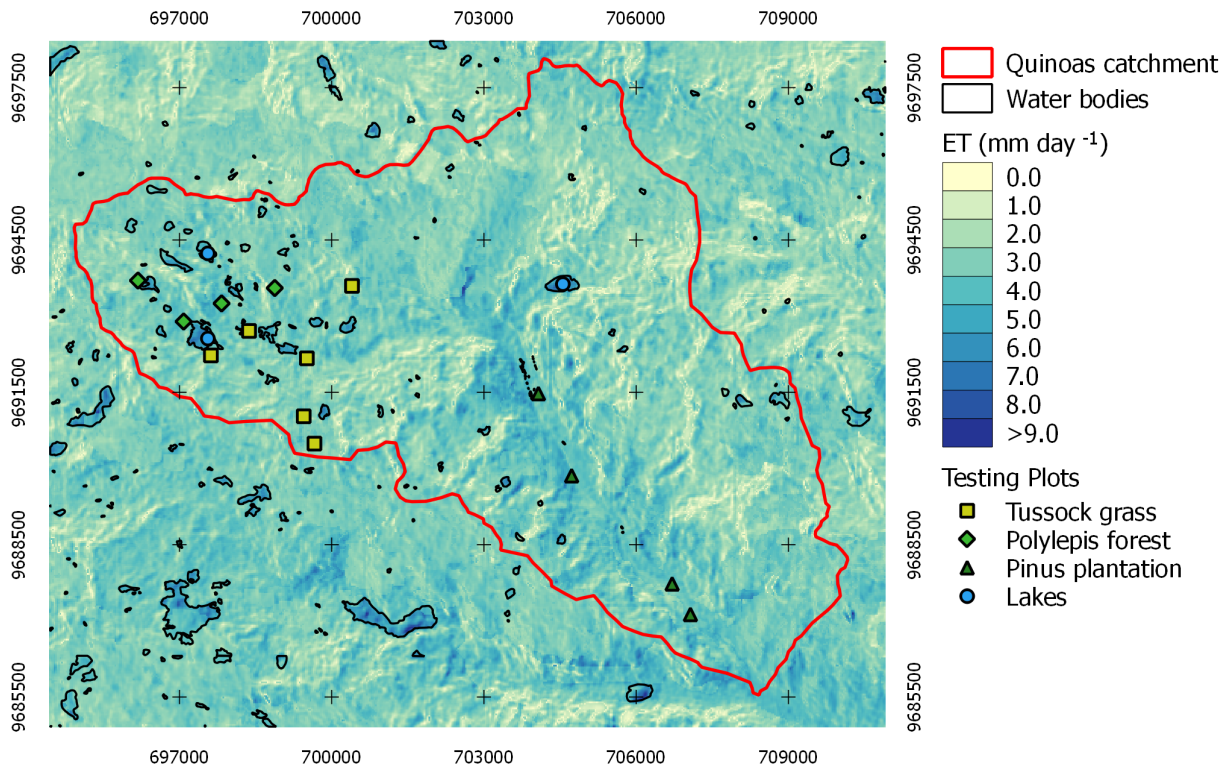


Figure 3.5: METRIC_L ET Map for the 19/10/2013 (cloud free day).

were wider for METRIC_M than that of METRIC_L. We presume this finding is associated with an increased sensitivity of the METRIC_M model when rain events occur, as previously reported by [Ruhoff et al. \(2012\)](#). Mean ET values for tussock grass are in agreement to those reported by [Pôças et al. \(2013\)](#) for grasslands in northern Portugal.

3.3.3 Monthly ET retrievals and comparison with MOD16 ET

Figure 3.6 shows the monthly METRIC_L, METRIC_M ET, and monthly MOD16 ET product comparison for May 2013 (a1, b1, c1), November 2013 (a2, b2, c2) and May 2014 (a3, b3, c3) respectively. For the METRIC outputs, changes in ET presented a corresponding pattern between wet and dry periods. METRIC_L showed lower ET (mean = 68.9 mm, SD = 23.0 mm) in the driest month, while higher values were found for METRIC_M (mean = 110.1 mm, SD = 16.5 mm) and MOD16 ET (mean = 89.9 mm, SD = 5.4 mm) for the same month. Distributions of ET values in humid months (May 2013 & May 2014) were similar between METRIC_L and METRIC_M with

3 Dynamic mapping of evapotranspiration

Table 3.4: METRIC_L & METRIC_M ET average daily values (mm day⁻¹) according to site type.

	n	November 2013 (high radiation month)			April 2014 (low radiation, rainy month)			
		Mean	Max	SD	Mean	Max	SD	Period.Diff.
ET METRIC_L (mm day⁻¹)								
Tussock grass sites	6	2.27	3.56	0.63	1.64	2.76	0.47	-0.63
<i>Polylepis</i> sp. forest sites	4	2.68	4.46	0.84	2.36	3.79	0.72	-0.32
<i>Pinus</i> sp. forest sites	4	2.83	4.37	0.85	2.44	3.83	0.72	-0.39
Water body	3	4.37	7.01	1.33	4.46	7.02	1.34	-0.09
ET METRIC_M (mm day⁻¹)								
Tussock grass sites	6	3.31	5.07	0.88	1.90	3.44	0.54	-1.41
<i>Polylepis</i> sp. forest sites	4	3.98	5.87	1.00	1.69	3.41	0.53	-2.29
<i>Pinus</i> sp. forest sites	4	3.55	4.93	0.94	1.96	2.93	0.52	-1.59
Water body	3	3.66	5.32	0.95	2.06	3.68	0.60	-1.6
METRIC Difference (means and max.) (mm day⁻¹)								
Tussock grass sites		1.04	1.51		0.26	0.68		
<i>Polylepis</i> sp. forest sites		1.3	1.41		-0.67	-0.38		
<i>Pinus</i> sp. forest sites		0.72	0.56		-0.48	-0.9		
Water body		-0.71	-1.69		-2.4	-3.34		

* Mean = mean of daily ET, Max = maximum of daily ET, SD = standard deviation in the period. Period. Diff. = Difference of the means between periods. n = 30 days for November and April.

Kolmogorov-Smirnov (KS) distances of 0.080 and 0.086 respectively. The same observation does not hold for MOD16 ET (KS value of 0.564 for the same months) which revealed that distributions between these products were different. The standard deviations were considerably higher for METRIC products than for MOD16, probably due to the capability of the model to capture the land cover and topography heterogeneity.

The noticeable difference of the METRIC retrievals in November 2013 revealed a tendency of the METRIC_M model to overestimate ET when compared with METRIC_L and MOD16 in this month. This could be attributed to the model inability to reproduce the predominant high-moisture conditions of the páramo during this relatively less wet period, and also to the errors in the estimation of net radiation due the limited capacity of the surface temperature input (MOD11_L2) to account for cloudy conditions in a high-radiation month. This has also been reported by [Ruhoff et al. \(2012\)](#) for a SEBAL implementation in Brazil. On the other hand, we observed lower values of METRIC_M for May 2013 and 2014, this indicated that the sensitivity of the model is clearly affected by rainfall and radiation seasonality (moisture and cloudiness increased). The ET variability of the complete period will be explained further (in Figure 3.8).

Additionally, ET values in May were higher on northeast-facing slopes of the center of the valley

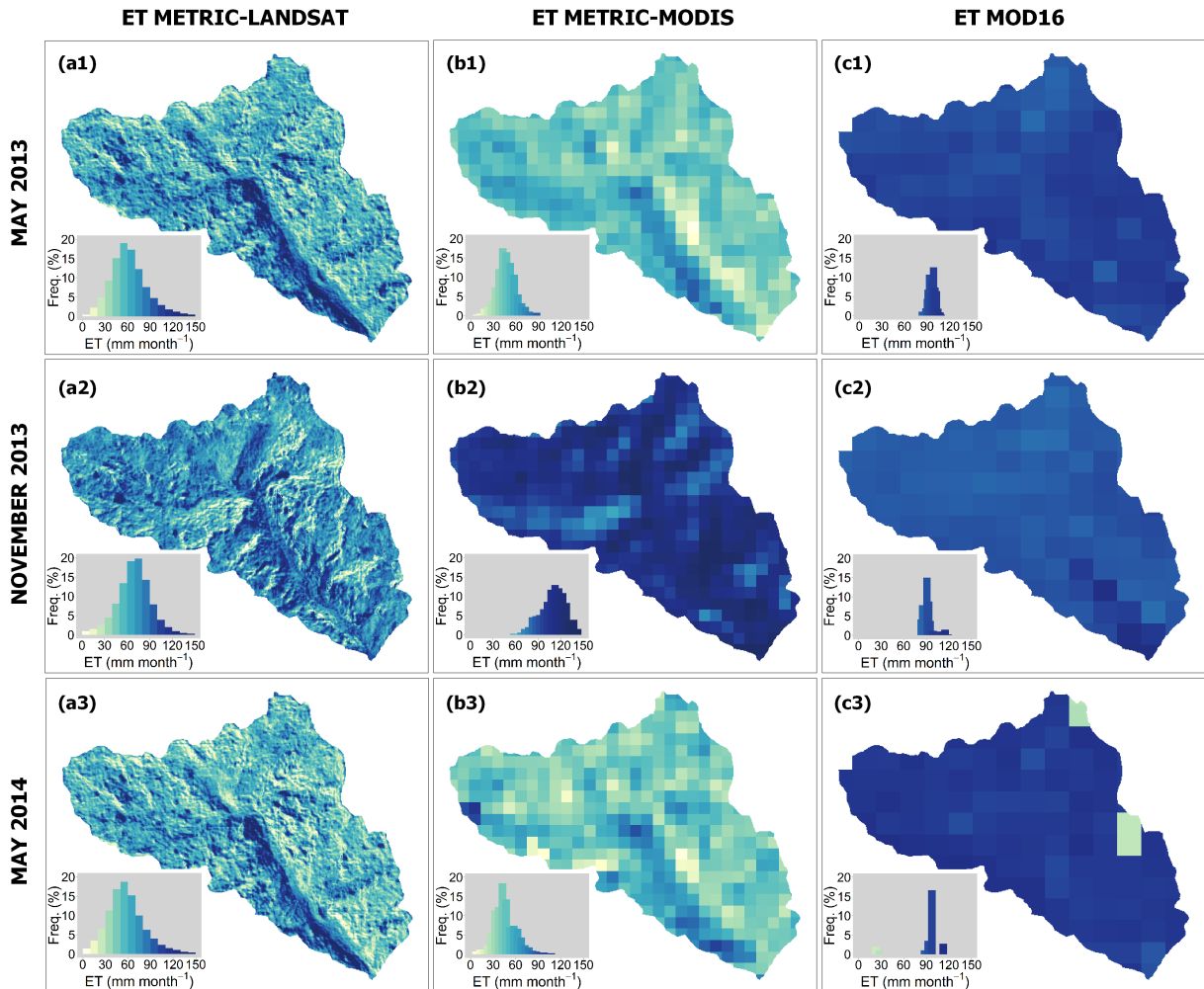


Figure 3.6: METRIC_L, METRIC_M and MOD16 ET map comparison for May 2013 (a1, b1, c1); November 2013 (a2, b2, c2) and May 2014 (a3, b3, c3).

(center of Figures 3.6.a1 & 3.6.a3). This effect is attributed to the METRIC radiation sub-model due to a combination of two factors: 1) seasonal variation of the declination of the Earth and 2) aspect angle of the area. The northeast-facing slope of this part of the valley has an aspect angle of 24.2° (considering the east-west horizontal) and an average slope of 45.2° , hence for months with a high incident angle of the sun (due June solstice) the impact is significant.

In Figure 3.7 we observe the typical oscillation in the Earth declination angle (δ). This parameter ranges for May from $+14.8^\circ$ to $+21.8^\circ$ and for November from -14.19° to -21.5° . Thus, the incident radiation increases ET over the northeast-facing slopes of the valley in the humid months. This

3 Dynamic mapping of evapotranspiration

increase is clearly reduced in November (December solstice), where the southwest-facing slope of the valley receives more radiation. The acquisition time of the Landsat imagery is around 10:30 and for MODIS between 10:30 to 11:00 (local time), when (in June) the northeast slopes are normal to the sun. In addition, the dense forest vegetation in this part of the valley strengthens this effect by increasing the NDVI. It is important to mention that mountain shadows are not accounted for in the 24h-radiation algorithm (Allen et al., 2006). In addition, Ramsay (1992) stated that east-facing slopes receive more sunlight in páramo ecosystems, mainly due to differences in rainfall on lee and windward slopes and cloudiness occurrence during the afternoon on west-facing slopes.

Figure 3.7 also reveals the marked difference between the modeled and observed radiation (the latest retrieved from the AWSs pyranometers) with an hourly time step. The Landsat and MODIS image dates used in the study are also depicted in the figure.

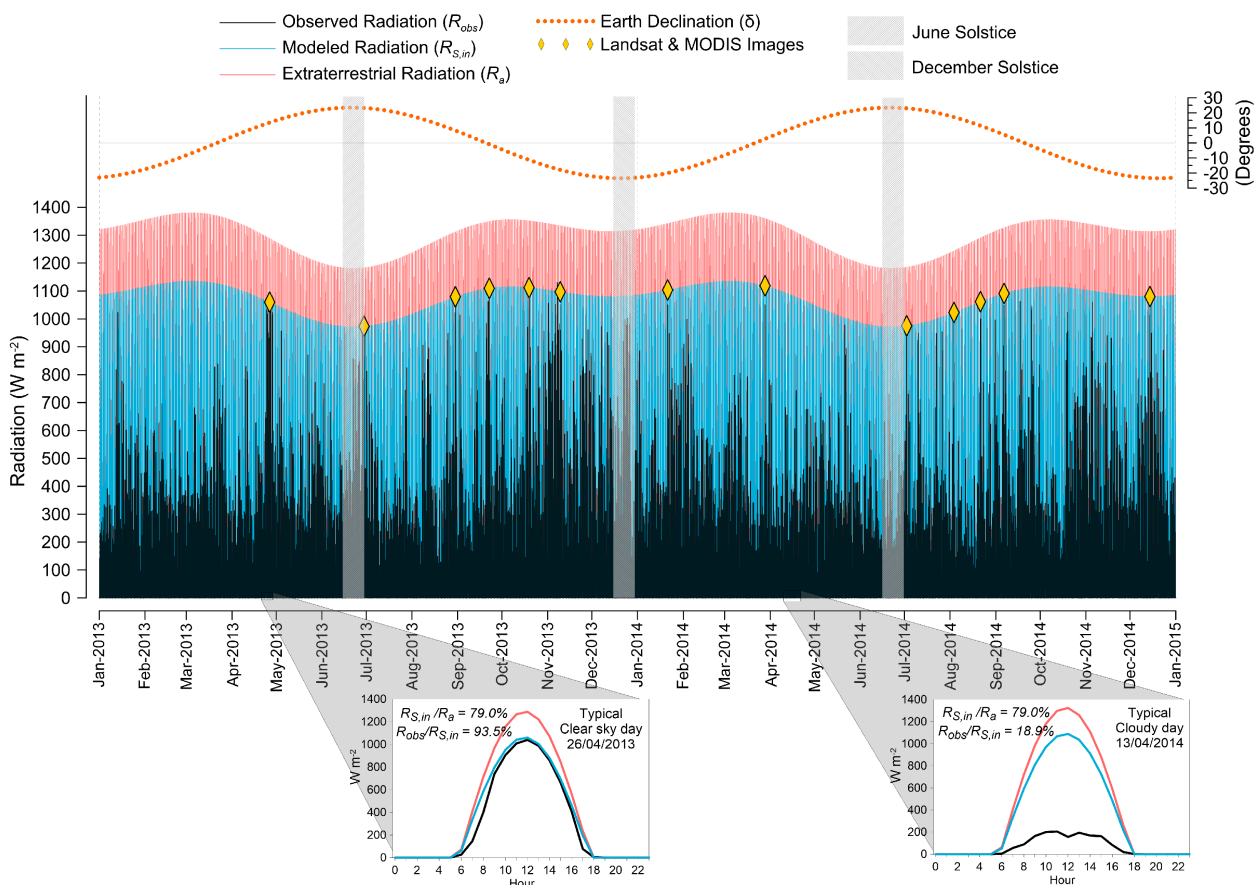


Figure 3.7: Modeled and observed radiation for 2013 - 2014 (hourly means of the three AWSs) and Earth declination angle.

The analysis of Fig. 3.7 determines: 1) The radiation sub-model was able to reduce 21% of the extraterrestrial radiation (R_a) considering clear-sky conditions. 2) The modeled radiation (RS_{in}) constantly varied according to the sun angle and elevation-related fluctuations of R_a and with the atmospheric transmissivity at cloud-free conditions. 3) When RS_{in} was compared with ground-level radiation measurements (R_{obs}) good estimations are obtained only when clear-sky conditions prevailed (difference of 6.5% of R_{obs}). Given a considerable cloudiness, the sub-model would overestimate radiation up to 81% of the R_{obs} , and this in turn would lead to an overestimation in ET. Time series of $METRIC_L$ and $METRIC_M$ retrievals were compared with MOD16 ET product and average rainfall from the AWSs; results are shown in Fig. 3.8. Statistical comparison between METRIC estimations (i.e.: Coefficient of determination R^2 , percentual mean bias %MBE, and root mean square error RMSE) are also included in the figure.

According to Figure 3.8, $METRIC_L$ and $METRIC_M$ for tussock grass showed a R^2 coefficient of 0.56. This can be attributed to the relative homogeneity of the vegetation and topographic characteristics of the plots. For the tussock grass sites (most representative vegetation cover in our area) it was noticeable an increment of ET in the last months of 2013 (Oct, Nov, and Dec) and a clear reduction in the rainy-humid season (more visible for 2014 than for 2013) with a small error for the models retrievals, however for the *Polylepis* and *Pinus* sites this finding is similar but with a great temporal variability and significant errors for all products. The above-mentioned increment in ET is attributed to the reduction of the vapor pressure deficit (due to the increment of water in the atmosphere) and to a reduction in the incoming solar energy due to the reigning cloudy conditions in these periods. Positive bias (13.7%) and lower RMSE ($12.2 \text{ mm month}^{-1}$) were observed for tussock grass sites. Nonetheless, *Polylepis* and *Pinus* sites showed lower R^2 coefficients than tussock grass (0.21 and 0.11 respectively), as well as negative bias (-11.8 and -5.4%) and higher RMSE (35.8 and $28.5 \text{ mm month}^{-1}$). This finding can be attributed to the lack of spatial fidelity of $METRIC_M$ when applied over heterogeneous vegetated areas in steep terrain.

MOD16 time series exposed an overestimation for November 2013 to June 2014, this was more evident for the tussock grass sites than the other vegetation covers. This finding reveals that MOD16 was not able to capture the diminishing of ET in this relative humid period, in contrast to METRIC retrievals. A similar behavior was seen in May 2013. The rainy and high radiation month October 2013 slightly impacted ET to all models, unlike the longest annual rainy period. Overestimation of MOD16 has already been reported for the tropics in other studies (Ferreira Junior et al., 2013; Kim et al., 2012; Ruhoff et al., 2013). We also calculated the %MBE and RMSE values for MOD16 when compared with $METRIC_L$ outputs (Tussock grass %MBE = 47.6% & RMSE = 36.0 mm

3 Dynamic mapping of evapotranspiration

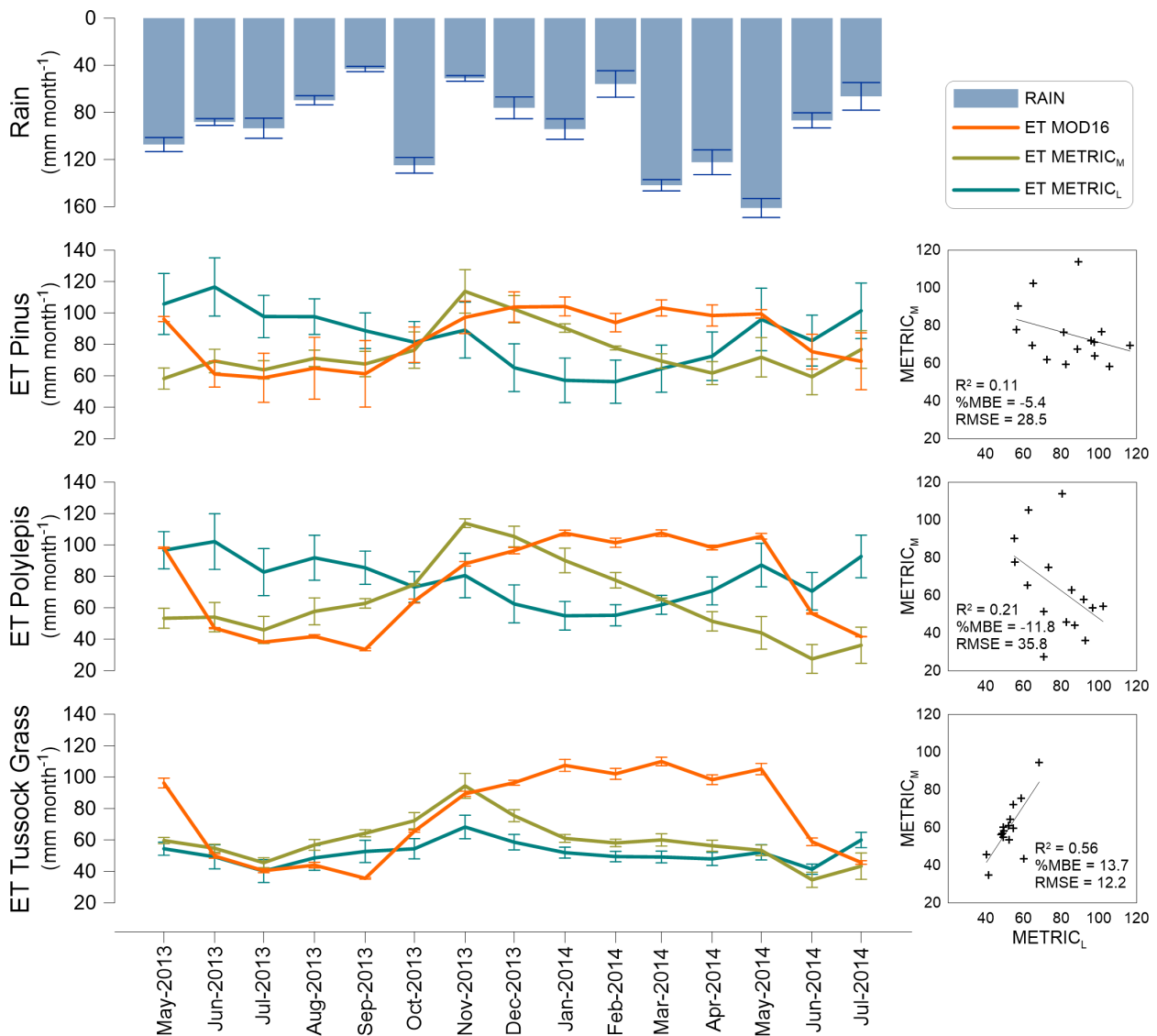


Figure 3.8: Monthly comparison of METRIC_L, METRIC_M, MOD16 ET in the testing plots. Statistical values of R², MBE and RMSE for the METRIC retrievals are shown, as well as the average rainfall from the AWSs. Error bars show SD.

month⁻¹; Polylepis %MBE = 4.5% & RMSE = 38.7 mm month⁻¹; and Pinus %MBE = 7.6% & RMSE = 31.6 mm month⁻¹). Generally, bias and RMSE for MOD16 were higher than for METRIC. However, considering that tussock grass vegetation constitutes the most extensive area in our study site (> 70%), a lack of METRIC accuracy in the forest land covers is understandable. Our results are what we expected due to the low representativeness of these land covers.

3.3.4 Validation with ET from Water Balance

The runoff coefficients corresponding to our validation micro catchments were 0.46 for the Virgen del Cajas micro catchment (head of the basin) and 0.49 for the Matadero micro catchment (whole basin) for the data-available study period. These runoff coefficients were similar to those obtained by Mosquera et al. (2015) for a small páramo catchment ($A = 7.53 \text{ km}^2$) located 35 km south of our study area, and those reported by Crespo et al. (2011) for a páramo micro catchment near the study area. Both reported studies have very similar biophysical conditions (i.e. soil type, vegetation and elevations) to the present study. The aggregated values for runoff (Q), precipitation (P) and residual ET for our study are depicted in Figure 3.9.

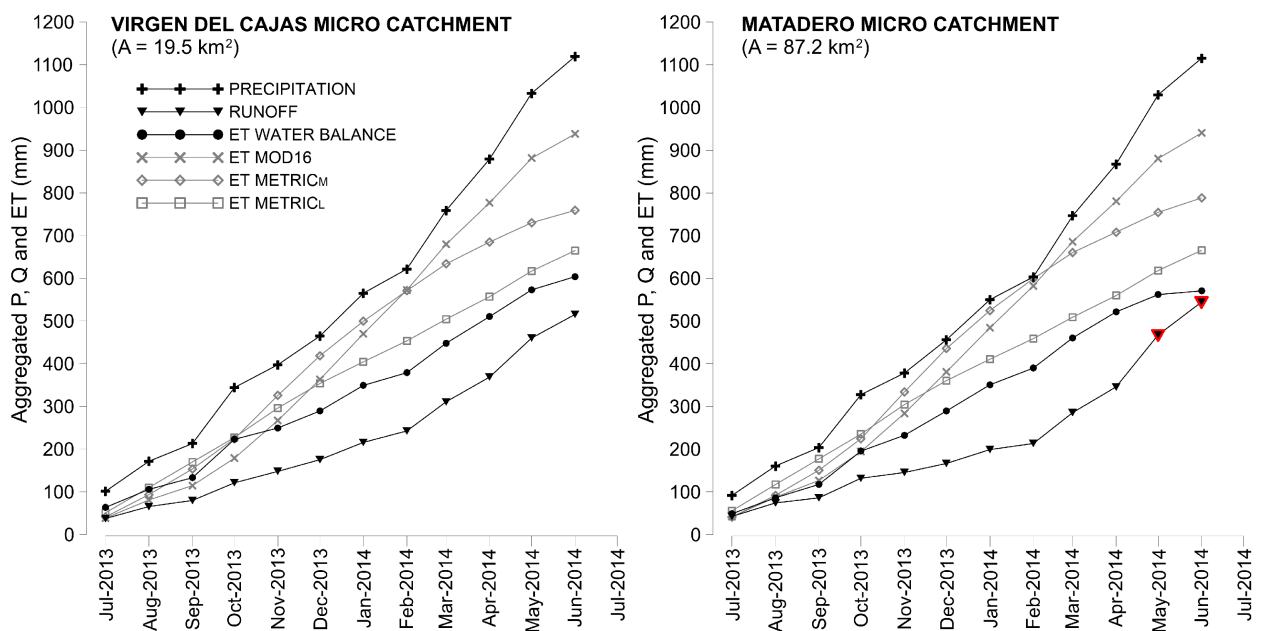


Figure 3.9: Aggregated Precipitation, Runoff and residual ET in comparison with $METRIC_L$, $METRIC_M$ and MOD16 ET. Noticeable runoff increments are highlighted in red color.

Figure 3.9 shows similar patterns for P, Q and ET for both micro catchments, although Matadero runoff shows a noticeable increment during rainy months. Mosquera et al. (2015) determined that ET from the water balance is particularly sensitive to increments in runoff of páramo, especially in lowest micro catchments (where land use change and non-native vegetation prevail), which was noticeable in May and June 2014. The validation approach demonstrated that $METRIC_L$ ET aggregated values tend to align closer to the water balance ET, while the estimates of $METRIC_M$ and MOD16 significantly overestimated it. Results of the monthly/annual statistical analysis are

3 Dynamic mapping of evapotranspiration

summarized in Table 3.5.

Table 3.5: Comparison of METRIC_L, METRIC_M and MOD16 retrievals with ET from water balance in the micro catchments (Annual and monthly scale). For micro catchments locations refer to Fig. 3.1

	Virgen del Cajas Micro catchment				Matadero Micro catchment			
	ET Water Balance	ET METRIC _L	ET METRIC _M	ET MOD16	ET Water Balance	ET METRIC _L	ET METRIC _M	ET MOD16
Annual Total (mm year ⁻¹)	603.91	664.91	759.04	937.91	570.70	665.82	788.53	940.50
Annual Error (mm year ⁻¹)		61.01	155.14	334.00		95.12	217.84	369.80
Percentual Annual Error (%)		10.10	25.69	55.31		16.67	38.17	64.80
Monthly Mean (mm month ⁻¹)	50.33	55.41	63.25	78.16	47.56	55.49	65.71	78.37
Monthly MBE (mm month ⁻¹)		5.08	12.93	27.83		7.93	18.15	30.82
Percentual Monthly MBE (%)		30.42	51.37	76.15		57.36	65.79	108.28
Monthly RMSE (mm month ⁻¹)		22.02	33.06	41.69		21.23	30.61	39.03

Results in Table 3.5 reveal that annual statistics were better for the upland smaller micro catchment (Virgen del Cajas) than for the larger micro catchment (Matadero). This might be due to the relative homogeneity of páramo vegetation above 3500 m a.s.l., in contrast to the heterogeneous vegetation and steep topography observed in the mid and low valley. RMSE was slightly lower for the larger micro catchment (Matadero). METRIC_L retrievals showed annual and monthly differences of 10 and 30% respectively for Virgen del Cajas micro catchment, and 17 and 57% respectively for Matadero micro catchment. Annual differences for METRIC_M estimates were two times higher for both micro catchments, and monthly %MBE were larger as well. MOD16 retrievals showed the most significant differences for annual and monthly time steps in both micro catchments, where annual %MBE ranges 55 ~ 65%.

Monthly RMSE values were lower for METRIC_L when compared to METRIC_M and MOD16 for both micro catchments. We found that METRIC_L annual differences ranged within the absolute errors of annual/seasonal ET, which according to Karimi and Bastiaanssen (2014) varied between 1 and 20%. In addition, Velpuri et al. (2013) reported differences of 17 and 6 mm month⁻¹ for MOD16 and Operational Simplified Surface Energy Balance (SSEBop) model, respectively in locations with elevation > 1500 m a.s.l. in the southwestern United States.

In a comparative study between water balance ET and SEBAL ET, an overestimation of 17% for

the SEBAL ET retrievals was reported for a mountainous catchment in central Iran (semi-arid and cold conditions) (Dastorani and Poormohammadi, 2012). Consequently, METRIC_L ET presented very good performance in comparison to the energy balance-based ET models reported in previous studies, in spite of the unsatisfactory performance of METRIC_M ET of our investigation. The main reason of the overestimation observed in both METRIC_L and METRIC_M ET retrievals can be attributed to the model limitation to estimate the diminished incoming radiation levels in the páramo (clearly noticeable in Figure 3.7). This was also reported by similar studies where the prevailing cloudy conditions represented a challenge when energy balance-based models were applied (Luo et al., 2015; Ruhoff et al., 2012; Seiler and Moene, 2011).

The overestimation of the incoming energy only affected the ETrf calculations, in contrast to ETr which used the ground-level radiation measurements and was obtained via the ASCE-ERWI Standardized Reference Evapotranspiration Equation ASCE-ERWI (2001). In addition, overestimation of aggregated daily or monthly ET for the páramo can be influenced by a stable daily temperature condition during long periods (more than a week) due to a decrease in relative humidity, especially in the absence of rain events (Córdova et al., 2013). For the above-mentioned reasons the use of direct measurements of solar radiation and relative humidity in the páramo is crucial for ETr calculations, which supports the findings of Córdova et al. (2015).

3.4 Concluding Remarks

Our study demonstrated that spatially-explicit ET can be estimated for tropical páramo catchments using an energy balance-based approach for two remote sensing products and with a dynamic aggregation of the time series. The latter was possible when adequate topographic corrections and specific model adaptations were properly performed, as well as a systematic hot and cold pixel selection. In this way, we found anchor pixels with sufficient temperature range for a successful application of METRIC in the páramo, which is similar to other studies conducted over non-water stressed vegetation and also in semi-arid climates (Allen et al., 2013; Trezza et al., 2013). However, model sensitivity to rainfall occurrence remains unknown and requires a deeper study in benefit of a fine adjustment of the model, similarly to Singh and Irmak (2011). This has not been investigated in the Andes, mainly due the inexistence of in site flux measurements like Bowen ratio or eddy covariance to obtain observed values of latent and sensible heat flux, and hence actual ET.

Good performance of METRIC_L retrievals has been confirmed by the validation using catchment scale runoff and precipitation data. Monthly and annual differences are around 30% and 10%

3 Dynamic mapping of evapotranspiration

respectively for $METRIC_L$, which points to a slight overestimation, as already expected based on similar studies (Dastorani and Poormohammadi, 2012; Karimi and Bastiaanssen, 2014). However this level of error is the minimum to be expected, considering that we cannot account for the uncertainty of the runoff and precipitation measurements. Nonetheless, we assume that sensitivity of the model to vegetation and terrain heterogeneity is superior to the other products, considering the finer resolution of Landsat imagery and the terrain correction approach using a mid-high resolution elevation model.

Cloud cover conditions were not captured by the incoming radiation sub model and the corrections for modeled atmospheric transmissivity were insufficient to account for the strong cloudiness variability. For $METRIC_M$, we detected a lack of accuracy causing an overestimation of ET that can be attributed to its coarse scale. This overestimation was particularly related to the thermal band of 1000 m resolution, which averaged sub-pixel heterogeneity and thus affected thermally-representative anchor pixels.

Despite the unsuitable results of $METRIC_M$, the local calibration of the ET_{rf} vs. NDVI function seems to be a feasible approach to retrieve near-real ET estimations in the páramo using MODIS imagery. In terms of water management, ET overestimation would lead to an underestimation of the runoff in the hydrological balance when data on stream flows are not available (i.e., only rainfall measurements and ET estimations available). For that reason, the local calibration of specific parameters in the model is a mandatory requirement to improve the accuracy of the ET maps, particularly when those spatial-retrievals will serve as an input in hydrological studies. In our study, we also recognized the limitations of the method under a low availability of clear-sky images. Nevertheless, the applicability of this method over perennial vegetation covers (like the páramo grasslands and native evergreen forests) using a limited amount of images has been demonstrated with plausible results. Thus, $METRIC_L$ showed high potential as a monitoring tool for the mountain páramos on an operational basis. Finally, the comparative analysis revealed that the global ET product MOD 16 rendered deficient for our study area, which emphasizes the importance of further refinement of this VI-ET model for applications in the tropical Andes.

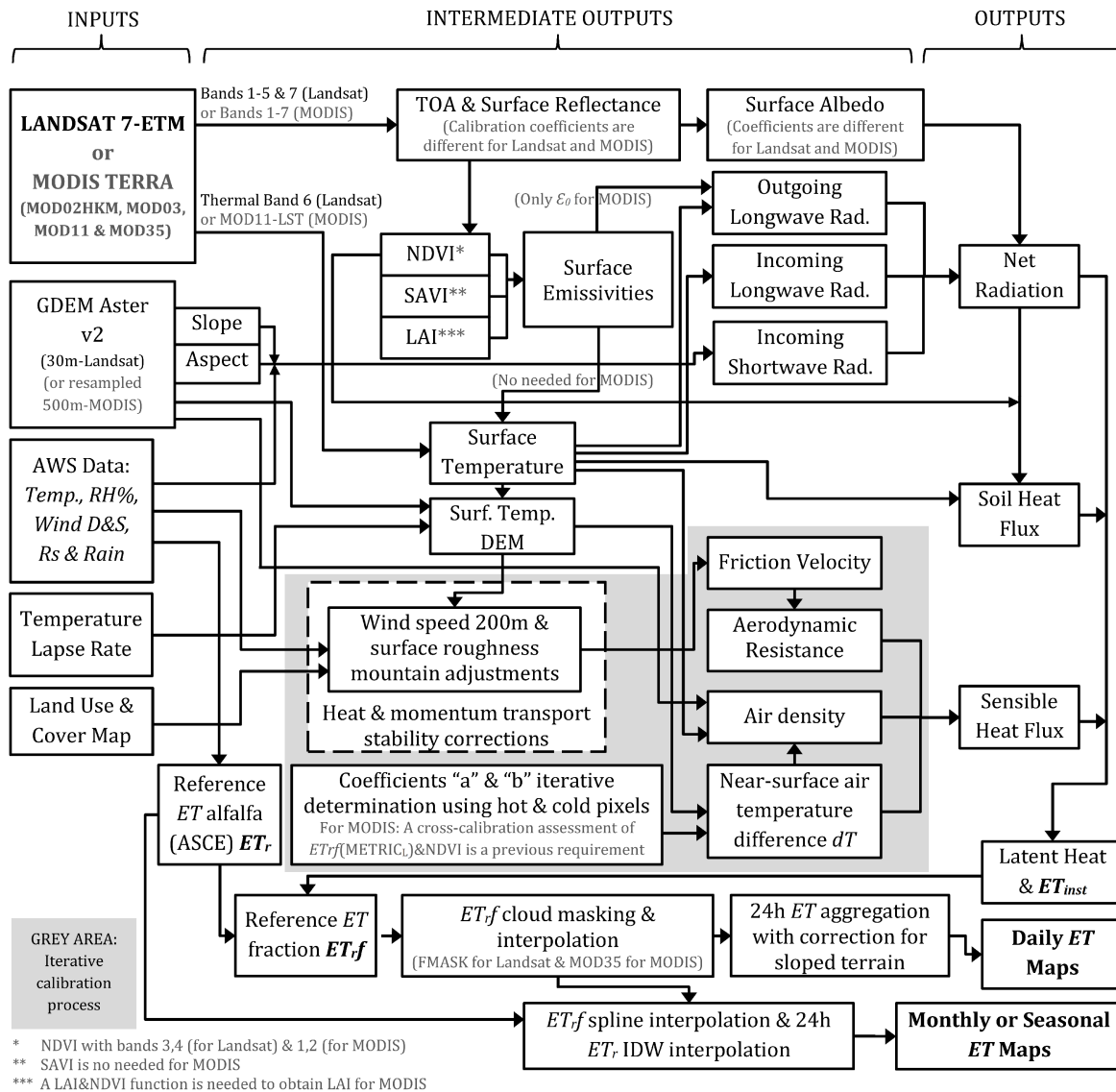
Future work should pursue a more accurate validation of daily spatial ET retrievals with field-scale measurements (eddy covariance and porometry techniques) and also the study of similar water depletion key-indicators such as water use efficiency over this singular Andean ecosystem.

Acknowledgments

The current study has been performed in the scope of two collaborating projects: The program PAK823-825 'Platform for Biodiversity and Ecosystem Monitoring and Research in South Ecuador', subproject C6 (BE1780/38-1) and the project "Meteorological cycles and evapotranspiration along an elevational gradient in the Cajas National Park". The first was funded by the German Research Foundation DFG and the latest was funded by the Research Office of the University of Cuenca (DIUC), the Municipal Company of Telecommunications, Drinking Water, Sewage and Sanitation of Cuenca (ETAPA-EP), and the Ecuadorian Secretary of Higher Education, Science, Technology and Innovation SENESCYT (PIC-11-715). We thank these institutions for their generous funding, and also to the Ministry of Environment of Ecuador (MAE) for the research permissions. The first author specially thanks SENESCYT and the Ecuadorian Government for funding his doctoral scholarship. We are grateful to Johanna Orellana for her valuable support in the model implementation; to Patricio Lazo, Giovanni Mosquera and Patricio Crespo for the stream flow data processing and their support in the water balance analysis, to Andrés Abril for the photography of the areas, and to the staff who contributed to the meteorological monitoring. We finally thank the editors and three anonymous reviewers, whose comments led to a greatly improved manuscript.

Supplementary material

METRIC_L and METRIC_M implementation flowchart



Supplementary Figure 3.10: METRIC_L and METRIC_M algorithms flowchart (adapted from Allen et al. (2007) and Trezza et al. (2013)).

The Kratio conversion factor methodology

According to the methodology of [Kjaersgaard et al. \(2011\)](#) a crop coefficient based on the alfalfa reference (in our case) can be converted to a crop coefficient with a grass reference (K_c) by multiplying it by a conversion value (K_{ratio}) which usually ranges between 1.0 to 1.3. The Equation 3.5 uses averaged climate data for the period of study and a constant value of the alfalfa crop coefficient for the mid-season stage (K_{cmid}):

$$K_{ratio} = K_{cmid} + [0.04 * (u_{AWS_{mean}} - 2) - 0.004 * (RH_{min} - 45)] * \left(\frac{h}{3}\right)^{0.3} \quad (3.5)$$

Herein $K_{cmid} = 1.20$ was obtained from tables in [Allen et al. \(1998\)](#), $u_{AWS_{mean}}$ was the daily mean value for wind speed during the study period, RH_{min} was the mean value for daily minimum relative humidity (%) during the study period, and h is the height for alfalfa reference crop ($h = 0.5$).

References

- Ackerman, S., Strabala, K., Menzel, P., Frey, R., Moeller, C., and Gumley, L. (2010). Discriminating clear-sky from cloud with MODIS algorithm theoretical basis document (MOD35). In *MODIS Cloud Mask Team, Cooperative Institute for Meteorological Satellite Studies, University of Wisconsin*.
- Allen, R. G., Kjaersgaard, J. H., and Garcia, M. (2008). Fine-tuning Components of Inverse-calibrated , Thermal-based Remote Sensing Models for Evapotranspiration. *Pecora 17 - The Future of Land Imaging... Going Operational*.
- Allen, R. G., Kjaersgaard, J. H., Trezza, R., Oliveira, A., Robison, C., and Lorite-Torres, I. (2012). Refining components of a satellite-based surface energy balance model to complex land-use systems. *IAHS-AISH publication*, pages 73–75.
- Allen, R. G., Pereira, L. S., Howell, T. a., and Jensen, M. E. (2011). Evapotranspiration information reporting: I. Factors governing measurement accuracy. *Agricultural Water Management*, 98(6):899–920.
- Allen, R. G., Pereira, L. S. L., Raes, D., Smith, M., and Others (1998). Crop evapotranspiration-Guidelines for computing crop water requirements-FAO Irrigation and drainage paper 56. *FAO, Rome*, 300(56):D05109.
- Allen, R. G., Tasumi, M., Morse, A., Trezza, R., Wright, J. L., Bastiaanssen, W., Kramber, W., Lorite, I., Robison, C. W., Morse, A., Trezza, R., Wright, J. L., Bastiaanssen, W., Kramber, W., Lorite, I., and Robison, C. W. (2007a). Satellite-Based Energy Balance for Mapping Evapotranspiration with Internalized Calibration (METRIC)-Applications. *Journal of Irrigation and Drainage Engineering*, 133(4):395–406.

3 Dynamic mapping of evapotranspiration

- Allen, R. G., Tasumi, M., and Trezza, R. (2007b). Satellite-Based Energy Balance for Mapping Evapotranspiration with Internalized Calibration (METRIC)-Model. *Journal of Irrigation and Drainage Engineering*, 133(4):380–394.
- Allen, R. G., Trezza, R., Kilic, A., Tasumi, M., and Li, H. (2013). Sensitivity of Landsat-Scale Energy Balance to Aerodynamic Variability in Mountains and Complex Terrain. *Journal of the American Water Resources Association*, 49(3):592–604.
- Allen, R. G., Trezza, R., and Tasumi, M. (2006). Analytical integrated functions for daily solar radiation on slopes. *Handbook of Environmental Chemistry, Volume 5: Water Pollution*, 139(1-2):55–73.
- Anderson, M. C., Norman, J. M., Diak, G. R., Kustas, W. P., and Mecikalski, J. R. (1997). A two-source time-integrated model for estimating surface fluxes using thermal infrared remote sensing. *Remote Sensing of Environment*, 60(2):195–216.
- ASCE-ERWI (2001). ASCE's Standardized Reference Evapotranspiration Equation. In *Watershed Management and Operations Management 2000*, pages 1–11, Reston, VA. American Society of Civil Engineers.
- Aucapiña, G. and Marín, F. (2014). *Efectos de la posición fisiográfica en las propiedades hidrofísicas de los suelos de páramo de la microcuenca del Río Zhurucay*. Graduate thesis, Universidad de Cuenca, Ecuador.
- Balthazar, V., Vanacker, V., Molina, A., and Lambin, E. F. (2015). Impacts of forest cover change on ecosystem services in high Andean mountains. *Ecological Indicators*, 48:63–75.
- Bastiaanssen, W., Davids, G., Allen, R., and Sebal, A. (2000). The SEBAL Remote Sensing tool for water consumption Remote Sensing Services for Water Resources Management. *Irrigation and Drainage*, page 6118.
- Bastiaanssen, W. G. M. (1998). *Remote Sensing in Water Resources Management : The State of the Art*. International Water Management Institute, Colombo, Sri Lanka.
- Beck, E., Makeschin, F., Haubrich, F., Richter, M., Bendix, J., and Valerezo, C. (2008). The Ecosystem (Reserva Biológica San Francisco): Geology. In Beck, E., Bendix, J., Kottke, I., Makeschin, F., Mosandl, R., editor, *Gradients in a Tropical Mountain Ecosystem of Ecuador. Ecological Studies*, volume 198, chapter The Ecosys, page 4. Springer Verlag, Berlin, Germany.
- Bendix, J., Homeier, J., Cueva Ortiz, E., Emck, P., Breckle, S. W., Richter, M., and Beck, E. (2006). Seasonality of weather and tree phenology in a tropical evergreen mountain rain forest. *International Journal of Biometeorology*, 50(6):370–384.
- Bendix, J., Rollenbeck, R., Richter, M., Fabian, P., and Emck, P. (2008). Climate. In Beck, E., Bendix, J., Kottke, I., Makeschin, F., Mosandl, R., editor, *Gradients in a Tropical Mountain Ecosystem of Ecuador. Ecological Studies*, volume 198, chapter Climate, pages 63–74. Springer Verlag, Berlin, Germany.
- Brutsaert, W. (1982). *Evaporation into the atmosphere: theory, history and applications*, volume 1. Springer Netherlands, Dordrecht.
- Buytaert, W., Célleri, R., De Bièvre, B., Cisneros, F., Wyseure, G., Deckers, J., and Hofstede, R. (2006a). Human impact on the hydrology of the Andean páramos. *Earth-Science Reviews*, 79(1-2):53–72.

- Buytaert, W., Iñiguez, V., Célleri, R., De Bièvre, B., Wyseure, G., and Deckers, J. (2006b). Analysis of the water balance of small páramo catchments in south Ecuador. In *Environmental role of wetlands in headwaters*, pages 271–281. Springer.
- Cancela, J. J., Cuesta, T. S., Neira, X. X., and Pereira, L. S. (2006). Modelling for Improved Irrigation Water Management in a Temperate Region of Northern Spain. *Biosystems Engineering*, 94(1):151–163.
- Carrasco-Benavides, M., Ortega-Farías, S., Lagos, L., Kleissl, J., Morales-Salinas, L., and Kilic, A. (2014). Parameterization of the Satellite-Based Model (METRIC) for the Estimation of Instantaneous Surface Energy Balance Components over a Drip-Irrigated Vineyard. *Remote Sensing*, 6(11):11342–11371.
- Célleri, R. and Feyen, J. (2009). The Hydrology of Tropical Andean Ecosystems: Importance, Knowledge Status, and Perspectives. *Mountain Research and Development*, 29(4):350–355.
- Célleri, R., Willems, P., Buytaert, W., and Feyen, J. (2007). Space-time rainfall variability in the Paute basin, Ecuadorian Andes. *Hydrological Processes*, 21(24):3316–3327.
- Chow, V. T., Maidment, D. R., and Mays, L. W. (1988). *Applied hydrology*.
- Córdova, M., Carrillo-Rojas, G., and Célleri, R. (2013). Errores en la estimación de la evapotranspiración de referencia de una zona de páramo andino debido al uso de datos mensuales, diarios y horarios. *Aqua-LAC*, 5(2):14–22.
- Córdova, M., Carrillo-Rojas, G., Crespo, P., Wilcox, B., and Célleri, R. (2015). Evaluation of the Penman-Monteith (FAO 56 PM) Method for Calculating Reference Evapotranspiration Using Limited Data. *Mountain Research and Development*, 35(3):230–239.
- Courault, D., Seguin, B., and Olioso, A. (2005). Review on estimation of evapotranspiration from remote sensing data: From empirical to numerical modeling approaches. *Irrigation and Drainage Systems*, 19(3-4):223–249.
- Crespo, A., Pinos, N., and Chacón, G. (2007). Determinación del Rango de Variación del índice de Vegetación con Imágenes Satélite en el Parque Nacional Cajas.
- Crespo, P., Célleri, R., Buytaert, W., Feyen, J., Iñiguez, V., Borja, P., and De Bièvre, B. (2010). Land use change impacts on the hydrology of wet Andean páramo ecosystems. In *Proceedings of the Workshop Status and Perspectives of Hydrology in Small Basins, held at Goslar-Hahnenklee, Germany, 30 March to 2 April 2009*, number APRIL, page 6, Germany. IAHS Publ. 336.
- Crespo, P. J., Feyen, J., Buytaert, W., Bücker, A., Breuer, L., Frede, H.-G., and Ramírez, M. (2011). Identifying controls of the rainfall-runoff response of small catchments in the tropical Andes (Ecuador). *Journal of Hydrology*, 407(1-4):164–174.
- Cuenca, R. H., Ciotti, S. P., and Hagimoto, Y. (2013). Application of landsat to evaluate effects of irrigation forbearance. *Remote Sensing*, 5(8):3776–3802.
- Dastorani, M. T. and Poormohammadi, S. (2012). Evaluation of water balance in a mountainous upland catchment using SEBAL approach. *Water resources management*, 26(7):2069–2080.
- Diaz, H. F., Grosjean, M., and Graumlich, L. (2003). Climate Variability and Change in High Elevation Regions: Past,

3 Dynamic mapping of evapotranspiration

- Present and Future. In *Climate Variability and Change in High Elevation Regions: Past, Present & Future*, pages 1–4. Springer.
- Duffie, J. A. and Beckman, W. A. (2013). *Solar Engineering of Thermal Processes*. Wiley Interscience, New York, second edition.
- Emck, P. (2007). *A Climatology of South Ecuador-With special focus on the Major Andean Ridge as Atlantic-Pacific Climate Divide*. Phd thesis, Friedrich Alexander-Universität, Erlangen-Nürnberg, Germany.
- Ferreira Junior, P., Sousa, A. M., Vitorino, M. I., Souza, E. B. D., and de Souza, P. J. O. P. (2013). Estimate of evapotranspiration in eastern Amazonia using SEBAL. *Revista de Ciências Agrárias - Amazon Journal of Agricultural and Environmental Sciences*, 56(1):33–39.
- Glenn, E. P., Nagler, P. L., and Huete, A. R. (2010). Vegetation index methods for estimating evapotranspiration by remote sensing. *Surveys in Geophysics*, 31(6):531–555.
- Glenn, E. P., Neale, C. M. U., Hunsaker, D. J., and Nagler, P. L. (2011). Vegetation index-based crop coefficients to estimate evapotranspiration by remote sensing in agricultural and natural ecosystems. *Hydrological Processes*, 25(26):4050–4062.
- Gowda, P. H., Chavez, J. L., Colaizzi, P. D., Evett, S. R., Howell, T. A., and Tolck, J. A. (2008). ET mapping for agricultural water management: present status and challenges. *Irrigation science*, 26(3):223–237.
- Guerschman, J. P., Van Dijk, A. I. J. M., Mattersdorf, G., Beringer, J., Hutley, L. B., Leuning, R., Pipunic, R. C., and Sherman, B. S. (2009). Scaling of potential evapotranspiration with MODIS data reproduces flux observations and catchment water balance observations across Australia. *Journal of Hydrology*, 369(1-2):107–119.
- Hankerson, B., Kjaersgaard, J., and Hay, C. (2012). Estimation of evapotranspiration from fields with and without cover crops using remote sensing and in situ methods. *Remote Sensing*, 4(12):3796–3812.
- Hansen, F. V. (1993). *Surface Roughness lengths*. U.S. Army Research Lab No. ARL-TR-61.
- Hastenrath, S. (1981). *The glaciation of the Ecuadorian Andes*. CRC Press, first edition.
- Hongve, D. (1987). A revised procedure for discharge measurement by means of the salt dilution method. *Hydrological processes*, 1(3):267–270.
- Huete, A. (1988). A soil-adjusted vegetation index (SAVI). *Remote Sensing of Environment*, 25(3):295–309.
- Irmak, A. (2011). *Evapotranspiration-Remote Sensing and Modeling*. InTech, Rijeka, Croatia.
- Irmak, A., Allen, R. G., Kjaersgaard, J., Huntington, J., Kamble, B., Trezza, R., Ratcliffe, I., Kjaersgaard, J., Huntington, J., Trezza, R., and Allen, R. G. (2012). Operational Remote Sensing of ET and Challenges. In *Evapotranspiration - Remote Sensing and Modeling*. INTECH Open Access Publisher.
- Jassas, H., Kanoua, W., and Merkel, B. (2015). Actual Evapotranspiration in the Al-Khazir Gomal Basin (Northern Iraq) Using the Surface Energy Balance Algorithm for Land (SEBAL) and Water Balance. *Geosciences*, 5(2):141–159.
- Josse, C., Cuesta, F., Navarro, G., Barrena, V., Cabrera, E., Chacón-Moreno, E., Ferreira, W., Peralvo, M., Saito, J., and

- Tovar, A. (2009). *Ecosistemas de los Andes del Norte y Centro. Bolivia, Colombia, Ecuador, Perú y Venezuela.*
- Kalma, J. D., McVicar, T. R., and McCabe, M. F. (2008). Estimating land surface evaporation: A review of methods using remotely sensed surface temperature data. *Surveys in Geophysics*, 29(4-5):421–469.
- Kamble, B., Irmak, A., Martin, D. L., Hubbard, K. G., Ratcliffe, I., Hergert, G., Narumalani, S., and Oglesby, R. J. (2013). Satellite based energy balance approach to assess riparian water use. *Evapotranspiration An Overview.*
- Karimi, P. and Bastiaanssen, W. G. M. (2014). Spatial evapotranspiration, rainfall and land use data in water accounting - Part 1: Review of the accuracy of the remote sensing data. *Hydrology and Earth System Sciences Discussions*, 11(1):1073–1123.
- Kim, H. W., Hwang, K., Mu, Q., Lee, S. O., and Choi, M. (2012). Validation of MODIS 16 global terrestrial evapotranspiration products in various climates and land cover types in Asia. *KSCE Journal of Civil Engineering*, 16(2):229–238.
- Kiptala, J. K., Mohamed, Y., Mul, M. L., Zaag, P., Van Der Zaag, P., Zaag, P., Van Der Zaag, P., Zaag, P., and Van Der Zaag, P. (2013). Mapping evapotranspiration trends using MODIS and SEBAL model in a data scarce and heterogeneous landscape in Eastern Africa. *Water Resources Research*, 49(12):8495–8510.
- Kjaersgaard, J., Allen, R., and Irmak, a. (2011). Improved methods for estimating monthly and growing season ET using METRIC applied to moderate resolution satellite imagery. *Hydrological Processes*, 25(26):4028–4036.
- Kjaersgaard, J., Richard, A., Trezza, R., Robinson, C., Oliveira, A., Dhungel, R., and Kra, E. (2012). Filling satellite image cloud gaps to create complete images of evapotranspiration. *IAHS Publication*, Remote Sen(352):102–105.
- Kjaersgaard, J. H., Allen, R. G., Trezza, R., and Olivieria, A. (2010). Refining components of satellite based surface energy balance models for forests and steep terrain. In *The 3rd USGS Modeling Conference.*
- Knyazikhin, Y., Glassy, J., Privette, J. L., Tian, Y., Lotsch, a., Zhang, Y., Wang, Y., Morisette, J. T., Votava, P., Myneni, R. B., Others, Nemani, R. R., Running, S. W. S., Knyazikhin, Y., Privette, J. L., Running, S. W. S., Nemani, R. R., Zhang, Y., Tian, Y., Wang, Y., Morisette, J. T., Glassy, J., and Votava, P. (1999). MODIS Leaf Area Index (LAI) And Fraction Of Photosynthetically Active Radiation Absorbed By Vegetation (FPAR) Product. *Modis Atbd*, Version 4.(4.0):130.
- Krishnaswamy, J., John, R., and Joseph, S. (2014). Consistent response of vegetation dynamics to recent climate change in tropical mountain regions. *Global Change Biology*, 20(1):203–215.
- Kustas, W. P. and Norman, J. M. (1996). Use of remote sensing for evapotranspiration monitoring over land surfaces. *Hydrological Sciences Journal*, 41(4):495–516.
- Kustas, W. P. and Norman, J. M. (1999). Evaluation of soil and vegetation heat flux predictions using a simple two-source model with radiometric temperatures for partial canopy cover. *Agricultural and Forest Meteorology*, 94(1):13–29.
- Li, Z., Liu, X., Ma, T., Kejia, D., Zhou, Q., Yao, B., and Niu, T. (2013). Retrieval of the surface evapotranspiration patterns in the alpine grassland-wetland ecosystem applying SEBAL model in the source region of the Yellow River,

3 Dynamic mapping of evapotranspiration

- China. *Ecological Modelling*, 270:64–75.
- Li, Z.-L., Tang, R., Wan, Z., Bi, Y., Zhou, C., Tang, B., Yan, G., and Zhang, X. (2009). A review of current methodologies for regional evapotranspiration estimation from remotely sensed data. *Sensors*, 9(5):3801–3853.
- Liou, Y. A. and Kar, S. K. (2014). Evapotranspiration estimation with remote sensing and various surface energy balance algorithms-a review. *Energies*, 7(5):2821–2849.
- Liu, C., Gao, W., Gao, Z., and Xu, S. (2008). Improvements of regional evapotranspiration model by considering topography correction. *Proceeding SPIE 7083, Remote Sensing and Modeling of Ecosystems for Sustainability*, 7083(1998):70830L.
- Llambí, L. D., Soto-W, A., Célleri, R., Bièvre, B. D., Ochoa, B., and Borja, P. (2012). *Ecología, hidrología y suelos de páramos*. Number 1. CONDENSAN, Ecuador.
- LP DAAC (2011). ASTER GDEM v2 Product. <http://gdex.cr.usgs.gov/gdex/>. Last checked on 2014-11-01.
- Luo, T., Jutla, A., and Islam, S. (2015). Evapotranspiration estimation over agricultural plains using MODIS data for all sky conditions. *International Journal of Remote Sensing*, 36(5):1235–1252.
- Luteyn, J. L. and Churchill, S. P. (1999). *Páramos: a checklist of plant diversity, geographical distribution, and botanical literature*. New York Botanical Garden Press, Bronx, NY, USA.
- Mark, A. F. (1969). Ecology of snow tussocks in the mountain grasslands of New Zealand. *Vegetatio*, 18(1-6):289–306.
- Markham, B. L. and Barker, J. L. (1986). Landsat MSS and TM post-calibration dynamic ranges, exoatmospheric reflectances and at-satellite temperatures. *EOSAT Landsat technical notes*, 1(1):3–8.
- Ministerio del Ambiente del Ecuador (2018). Mapa de Ecosistemas del Ecuador Continental. <http://mapainteractivo.ambiente.gob.ec/portal/>. Last checked on 2018-01-02.
- Mkhwanazi, M. (2014). *Developing a modified SEBAL algorithm that is responsive to advection by using limited weather data*. Phd thesis, PhD Thesis, Colorado State University, USA.
- Moore, R. D. (2004). Introduction to salt dilution gauging for streamflow measurement: Part 1. *Streamline Watershed Management Bulletin*, 7(4):20–23.
- Mora, D. E., Campozano, L., Cisneros, F., Wyseure, G., and Willems, P. (2014). Climate changes of hydrometeorological and hydrological extremes in the Paute basin, Ecuadorean Andes. *Hydrology and Earth System Sciences*, 18(2):631–648.
- Moran, M. S. and Jackson, R. D. (1991). Assessing the spatial distribution of evapotranspiration using remotely sensed inputs. *Journal of Environmental Quality*, 20(4):725–737.
- Morton, C. G., Huntington, J. L., Pohl, G. M., Allen, R. G., Mcgwire, K. C., and Bassett, S. D. (2013). Assessing Calibration Uncertainty and Automation for Estimating Evapotranspiration from Agricultural Areas Using METRIC. *Journal of the American Water Resources Association*, 49(3):549–562.
- Mosquera, G. M., Lazo, P. X., Célleri, R., Wilcox, B. P., and Crespo, P. (2015). Runoff from tropical alpine grasslands

- increases with areal extent of wetlands. *CATENA*, 125(FEBRUARY):120–128.
- Mu, Q., Heinsch, F. A., Zhao, M., and Running, S. W. (2007). Development of a global evapotranspiration algorithm based on MODIS and global meteorology data. *Remote Sensing of Environment*, 111(4):519–536.
- Mu, Q., Zhao, M., and Running, S. (2014). Brief Introduction to MODIS Evapotranspiration Data Set (MOD16). In *Water Resources Research*, number 2014, pages 1–4.
- Mu, Q., Zhao, M., and Running, S. W. (2011). Improvements to a MODIS global terrestrial evapotranspiration algorithm. *Remote Sensing of Environment*, 115(8):1781–1800.
- Murray, R. S., Nagler, P. L., Morino, K., Glenn, E. P., Murray, R. S., Osterberg, J., and Glenn, E. P. (2009). An empirical algorithm for estimating agricultural and riparian evapotranspiration using MODIS enhanced vegetation index and ground measurements of ET. I. Description of method. *Remote Sensing*, 1(4):1125–1138.
- Norman, J. M., Kustas, W. P., and Humes, K. S. (1995). Source approach for estimating soil and vegetation energy fluxes in observations of directional radiometric surface temperature. *Agricultural and Forest Meteorology*, 77(3):263–293.
- Pepin, N., Bradley, R. S., Diaz, H. F., Baraer, M., Caceres, E. B., Forsythe, N., Fowler, H., Greenwood, G., Hashmi, M. Z., Liu, X. D., Miller, J. R., Ning, L., Ohmura, A., Palazzi, E., Rangwala, I., Schöner, W., Severskiy, I., Shahgedanova, M., Wang, M. B., Williamson, S. N., and Yang, D. Q. (2015). Elevation-dependent warming in mountain regions of the world. *Nature Climate Change*, 5(5):424–430.
- Pôças, I., Cunha, M., Pereira, L. S., and Allen, R. G. (2013). Using remote sensing energy balance and evapotranspiration to characterize montane landscape vegetation with focus on grass and pasture lands. *International Journal of Applied Earth Observation and Geoinformation*, 21(1):159–172.
- Pôças, I., Paço, T. A., Cunha, M., Andrade, J. A., Silvestre, J., Sousa, A., Santos, F. L., Pereira, L. S., and Allen, R. G. (2014). Satellite-based evapotranspiration of a super-intensive olive orchard: Application of METRIC algorithms. *Biosystems Engineering*, 128:69–81.
- Quichimbo, P., Tenorio, G., Borja, P., Cárdenas, I., Crespo, P., and Célleri, R. (2012). Efectos sobre las propiedades físicas y químicas de los suelos por el cambio de la cobertura vegetal y uso del suelo: Páramo de Quimsacocha al sur del Ecuador. *Suelos Ecuatoriales*, 42(2)(2):138–153.
- Ramsay, P. M. (1992). *The Paramo Vegetation of Ecuador : the Community Ecology, Dynamics and Productivity of Tropical Grasslands in the Andes*.
- Ruhoff, A. L., Paz, A. R., Aragao, L. E. O. C., Mu, Q., Malhi, Y., Collischonn, W., Rocha, H. R., and Running, S. W. (2013). Assessment of the MODIS global evapotranspiration algorithm using eddy covariance measurements and hydrological modelling in the Rio Grande basin. *Hydrological Sciences Journal*, 58(8):1658–1676.
- Ruhoff, A. L., Paz, A. R., Collischonn, W., Aragao, L. E., Rocha, H. R., and Malhi, Y. S. (2012). A MODIS-based energy balance to estimate Evapotranspiration for clear-sky days in Brazilian tropical savannas. *Remote Sensing*, 4(3):703–725.
- Seiler, C. and Moene, A. F. (2011). Estimating actual evapotranspiration from satellite and meteorological data in

3 Dynamic mapping of evapotranspiration

- central Bolivia. *Earth Interactions*, 15(12):1–24.
- Senay, G. B., Budde, M. E., and Verdin, J. P. (2011). Enhancing the Simplified Surface Energy Balance (SSEB) approach for estimating landscape ET: Validation with the METRIC model. *Agricultural Water Management*, 98(4):606–618.
- Singh, R. K. and Irmak, A. (2011). Treatment of anchor pixels in the METRIC model for improved estimation of sensible and latent heat fluxes. *Hydrological Sciences Journal*, 56(5):895–906.
- Singh, R. K., Liu, S., Tieszen, L. L., Suyker, A. E., and Verma, S. B. (2012). Estimating seasonal evapotranspiration from temporal satellite images. *Irrigation Science*, 30(4):303–313.
- Sklenar, P. and Jørgensen, P. M. (1999). Distribution patterns of páramo plants in Ecuador. *Journal of Biogeography*, 26(4):681–691.
- Su, Z. (2002). The Surface Energy Balance System (SEBS) for estimation of turbulent heat fluxes. *Hydrology and Earth System Sciences Discussions*, 6(1):85–100.
- Sun, Z., Wang, Q., Matsushita, B., Fukushima, T., Ouyang, Z., and Watanabe, M. (2009). Development of a simple remote sensing evapotranspiration model (Sim-ReSET): algorithm and model test. *Journal of Hydrology*, 376(3):476–485.
- Tachikawa, T., Kaku, M., Iwasaki, A., Gesch, D., Oimoen, M., Zhang, Z., Danielson, J., Krieger, T., Curtis, B., Haase, J., and Others (2011). ASTER Global Digital Elevation Model Version 2-Summary of Validation Results August 31, 2011.
- Tasumi, M. (2003). *Progress in operational estimation of regional evapotranspiration using satellite imagery*. PhD thesis, University of Idaho, USA.
- Tasumi, M., Allen, R. G., and Trezza, R. (2008). At-Surface Reflectance and Albedo from Satellite for Operational Calculation of Land Surface Energy Balance. *Journal of Hydrologic Engineering*, 13(2):51–63.
- Thies, B., Meyer, H., Nauss, T., and Bendix, J. (2014). Projecting land-use and land-cover changes in a tropical mountain forest of Southern Ecuador. *Journal of Land Use Science*, 9(1):1–33.
- Trezza, R., Allen, R. G., and Tasumi, M. (2013). Estimation of actual evapotranspiration along the Middle Rio Grande of New Mexico using MODIS and landsat imagery with the METRIC model. *Remote Sensing*, 5(10):5397–5423.
- UNESCO (2013). Cajas Massif Biosphere Reserve. <http://www.unesco.org/new/en/natural-sciences/environment/ecological-sciences/biosphere-reserves/latin-america-and-the-caribbean/ecuador/macizo-del-cajas/>. Last checked on 2018-11-18.
- USGS (2017). Gap-Filling Landsat 7 SLC-off Single Scenes Using ERDAS Imagine 2014. <https://landsat.usgs.gov/gap-filling-landsat-7-slc-single-scenes-using-erdas-imagine-TM>. Last checked on 2017-12-13.
- Velpuri, N. M., Senay, G. B., Singh, R. K., Bohms, S., and Verdin, J. P. (2013). A comprehensive evaluation of two MODIS evapotranspiration products over the conterminous United States: Using point and gridded FLUXNET and water balance ET. *Remote Sensing of Environment*, 139:35–49.

- Verstraeten, W. W., Veroustraete, F., and Feyen, J. (2008). Assessment of Evapotranspiration and Soil Moisture Content Across Different Scales of Observation. *Sensors*, 8(1):70–117.
- Vinukollu, R. K., Wood, E. F., Ferguson, C. R., and Fisher, J. B. (2011). Global estimates of evapotranspiration for climate studies using multi-sensor remote sensing data: Evaluation of three process-based approaches. *Remote Sensing of Environment*, 115(3):801–823.
- Vuille, M., Bradley, R. S., and Keimig, F. (2000). Climate Variability in the Andes of Ecuador and Its Relation to Tropical Pacific and Atlantic Sea Surface Temperature Anomalies. *Journal of Climate*, 13(14):2520–2535.
- Vuille, M., Franquist, E., Garreaud, R., Lavado Casimiro, W. S., and Cáceres, B. (2015). Impact of the global warming hiatus on Andean temperature. *Journal of Geophysical Research: Atmospheres*, 120(9):3745–3757.
- Wukelic, G. E., Gibbons, D. E., Martucci, L. M., and Foote, H. P. (1989). Radiometric calibration of Landsat Thematic Mapper thermal band. *Remote sensing of environment*, 28:339–347.
- Yang, R. and Friedl, M. A. (2003). Determination of roughness lengths for heat and momentum over boreal forests. *Boundary-Layer Meteorology*, 107(3):581–603.
- Zhang, J., Hu, Y., Xiao, X., Chen, P., Han, S., Song, G., and Yu, G. (2009). Satellite-based estimation of evapotranspiration of an old-growth temperate mixed forest. *Agricultural and Forest Meteorology*, 149(6):976–984.
- Zhu, Z. and Woodcock, C. E. (2012). Object-based cloud and cloud shadow detection in Landsat imagery. *Remote Sensing of Environment*, 118:83–94.

4 Net ecosystem exchange and evapotranspiration over the páramo of Southern Ecuador

This chapter is published in *Agricultural and Forest Meteorology (Elsevier)*, 265, 30-47, 2019

Received: 16 March 2018

Accepted: 05 November 2018

First published online: 15 November 2018

DOI: <https://doi.org/10.1016/j.agrformet.2018.11.006>

Reprinted with permission from Elsevier.

The breathing of the Andean highlands: Net ecosystem exchange and evapotranspiration over the páramo of southern Ecuador

Galo Carrillo-Rojas^{1,2,3}, Brenner Silva¹, Rütger Rollenbeck¹,
Rolando Céleri^{2,3} and Jörg Bendix¹

¹ Laboratory for Climatology and Remote Sensing, Faculty of Geography, Philipps-Universität Marburg, Deutschhausstr. 12, Marburg 35032, Germany

² Departamento de Recursos Hídricos y Ciencias Ambientales, Universidad de Cuenca, Campus Balzay, Cuenca 010207, Ecuador

³ Facultad de Ciencias Químicas, and Facultad de Ingeniería, Universidad de Cuenca, Av. 12 de Abril y A. Cueva, Cuenca 010203, Ecuador

Abstract: Atmospheric carbon (CO₂) exchange, evapotranspiration (ET) processes, and their interactions with climatic drivers across tropical alpine grasslands are poorly understood. This lack of understanding is particularly evident for the páramo, the highest vegetated frontier in the northern Andes, the main source of water for inter-Andean cities, and a large carbon storage area. Studies of CO₂ and ET fluxes via the standard Eddy Covariance (EC) technique have never been applied to this region, limiting the understanding of diurnal / nocturnal exchanges and budget estimations. In this paper, we report the first EC analysis conducted on the Andean páramo (3765 m a.s.l.); this analysis measured CO₂, ET, and micrometeorological variables over two

years (2016-2018) to understand their interactions with climatic / biophysical controls. The páramo was found to be a source of CO₂ and exhibited a net positive exchange (mean = +99±30 gC m⁻² per year). The light-responses of net CO₂ exchange and the primary productivity were correlated and model-parameterized. Evapotranspiration was 635±9 mm per year (51% of the annual rainfall total), and we obtained crop coefficients for the dominant vegetation (Tussock grass) based on reference-ET models FAO56 and ASCE-ERWI (0.90 and 0.78, respectively). We also compared our results to those from other high-altitude (alpine) and high-latitude grasslands (tundra). Finally, we demonstrate that our measurement period is representative of the páramo's longer-term climate dynamics. Our investigation contributes to the body of knowledge on the land surface-atmosphere processes of the tropical Andes and supports decision-making about ecosystem services management and the preservation of this vulnerable biome.

Keywords Tropical Andes, Ecuador, Páramo, Eddy covariance, Carbon, Evapotranspiration

4.1 Introduction

The tropical Andes leads the list of worldwide biodiversity hotspots (Myers et al., 2000). Approximately 6.7% of the globe's endemic plants and 5.7% of the world's vertebrate species are observed along the mountain gradient that extends to a vast alpine ecosystem between 3200 (subpáramo) and 4500 m a.s.l. (superpáramo or subnival) (Llambí et al., 2012). This neotropical biome covers large areas of Colombia (19 330 km²), Ecuador (13 372 km²), Venezuela (2660 km²), Perú (462 km²) and Central América (Costa Rica 150 km² and Panamá 20 km²) (Hofstede et al., 2014). The páramo extends across 7% of the Ecuadorian territory (Beltrán et al., 2009; Josse et al., 2009) and is highly biodiverse (Mena-Vásquez and Hofstede, 2006). Unfortunately, less than 40% of the area is formally protected (Cuesta and De Bièvre, 2008). The climate, soils and dominant vegetation (tussock grasses) of the area significantly affect water regulations and supplies for the heavily populated inter-Andean valleys (Buytaert et al., 2006a; Céleri and Feyen, 2009; Mosquera et al., 2015). Moreover, they form a massive organic carbon (C) pool (Bertzky et al., 2010; Farley et al.,

4 Net ecosystem exchange and evapotranspiration

2004; Hribljan et al., 2016). Unfortunately, the fragile ecosystem is clearly exposed to the negative effects of climate and land-use change (Harden et al., 2013; Vuille et al., 2003). Water vapor and carbon dioxide (CO₂) dynamics at regional and landscape scales are crucial elements in determining the aforementioned effects on this pristine environment (Herzog et al., 2011; Pepin et al., 2015). Thus, an understanding of the C assimilation and carbon / water relationships in the páramo is needed owing to its ecohydrological importance (Aparecido et al., 2018), as is the case for other mountainous tundra ecosystems. Unfortunately, land-atmosphere gas exchange processes of natural grasslands in the tropics remain unexplored (Fisher et al., 2009; Grace et al., 2006), especially those of the highlands, because relevant instrumentation for these remote areas is lacking (Pepin et al., 2015).

The eddy covariance method (EC) has been proven to be a reliable technique for measuring gas and energy exchanges between land masses and the atmosphere across natural and disturbed areas (Aubinet et al., 2012; Baldocchi et al., 2001; Baldocchi, 2003; Burba, 2013). As a consequence, the EC method has been applied in over 562 active EC flux towers in the FLUXNET consortium, which covers diverse biomes (Baldocchi et al., 2001). However, EC implementation represents a challenge when nonideal conditions are present (Baldocchi, 2003); such nonideal conditions include complex terrain, in which uncertainties are related to nighttime advection effects (Galvagno et al., 2017; Novick et al., 2014) and to the incoming / outgoing energy observations that are affected by the underlying sloped surface (Wohlfahrt et al., 2016). Although its application to mountainous terrain has limitations, the EC technique allows one to obtain reliable energy, CO₂, and water vapor estimates when specific topographical corrections (Hiller et al., 2008), source analyses and data filtering (e.g., footprint modeling, low-turbulence fluxes removal) (Aubinet et al., 2012; Kljun et al., 2015) and validation approaches (e.g., energy balance closure) (Foken, 2008; Leuning et al., 2012) are properly conducted. On this basis, two major EC-derived quantities are the most important for the analysis of the C and water balance of land surfaces: (i) the Net Ecosystem Exchange (NEE) and (ii) the Actual Evapotranspiration (ET_a).

First, the NEE, which is the net CO₂ flux from the ecosystem to the atmosphere (CO₂ release = +NEE, and CO₂ uptake = -NEE), can be partitioned into Gross Primary Productivity (GPP) and Ecosystem Respiration (Reco) (Lasslop et al., 2010; Reichstein et al., 2005), which provide reliable insights into CO₂ assimilation / respiration processes. While GPP is considered to be the quantitatively most important global CO₂ flux (12 ± 8 PgC year⁻¹) (Beer et al., 2010), modeled or instrument-derived GPP estimates are rarely reported for the páramo. Limited data for this biome have been obtained only via the static flux chamber method (McKnight et al., 2017; Sánchez

et al., 2017), empirically via the aboveground-biomass estimation (Ramsay and Oxley, 2001), or by computational simulations (i.e., via biogeochemical-physiological models such as BIOME-BCG) (Minaya, 2016; Minaya et al., 2016). In spite of their limitations (Damm et al., 2010; Heinsch et al., 2006), remote sensing-based GPP estimations (i.e., MODIS GPP product (Running et al., 2004)) have not been tested or validated for the páramo. Hence, in situ evaluations of NEE and GPP and their responses to light, humidity and temperature are central to a proper understanding of ecosystem productivity under cloudy, cold and humid conditions in tropical páramos.

Second, the ETa, a functional indicator of water stress affecting native tussock grasses, is another understudied variable of these mountain grasslands (Carrillo-Rojas et al., 2016). ETa is a key component of the hydrological cycle and therefore critical for water balance analyses (Buytaert et al., 2006b; Céleri and Feyen, 2009) and for studies of land-cover change in these locations (Crespo et al., 2010). Consequently, a thorough understanding of the relationships between primary productivity and micrometeorological conditions including ETa and the crop coefficients (Kc), used to convert reference evapotranspiration (ETr) to ETa, can lead to a better understanding of model-based estimations, which are generally not parameterized to the ecosystem. Neither indicators (NEE and ETa) has been well-studied in the Andean páramo.

In this paper, we present a pioneering EC-based investigation conducted in this relevant Andean ecosystem by describing: (i) the energy, CO₂ and water vapor exchange processes for a Neotropical site in southern Ecuador; (ii) the dependency of CO₂ uptake and release processes on soil temperature, humidity and light availability, (iii) the interpretation of the shorter-term results in the context of the longer-term climate drivers, particularly drought / water excess scenarios; and finally, (iv) the relationships between the observed ETa and the modeled ETr, which help determine the Kc of tussock grass via water vapor detection (the EC technique).

4.2 Materials and methods

4.2.1 Study site characteristics

The study site is located in the Zhuruca Ecohydrological Observatory (FLUXNET EC-APr), which is positioned in the headwaters of a 7.53 km² catchment in southern Ecuador at 3765 m a.s.l. (the Northern Andean Páramo Ecoregion, according to Olson et al. (2001)). Hydrological, geochemical and landscape characteristics of the observatory have been extensively discussed in several studies (Córdova et al., 2015; Correa et al., 2016, 2017; Mosquera et al., 2016a, 2015, 2016b;

4 Net ecosystem exchange and evapotranspiration

Ochoa-Sánchez et al., 2018; Padrón et al., 2015; Quichimbo et al., 2012). Figure 4.1 shows the study location, a satellite view of the site, and the landscape features surrounding the observatory.

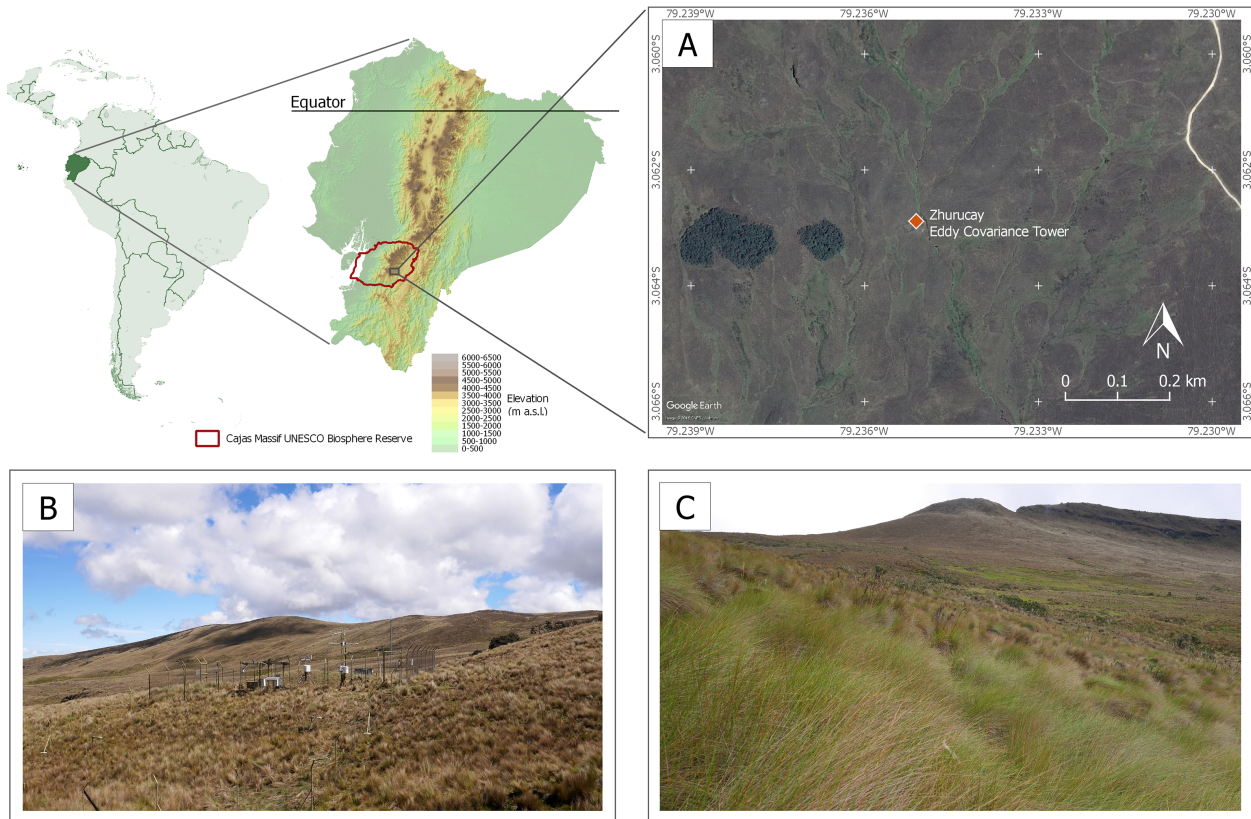


Figure 4.1: Study Area: A) Satellite image of the location of the páramo ecosystem (Google Earth Pro, 2016), B) Landscape image of the Zhurucaj Ecohydrological Observatory and the EC tower, and C) View of the main biome in the fetch (tussock grasslands).

The area studied plays a crucial role as a headwater basin within the Cajas Massif, a UNESCO World Biosphere Reserve (9766 km²); more than 838,000 inhabitants in the inter-Andean and lowland valleys benefit from its water supply (Célleri and Feyen, 2009; UNESCO, 2013). The geology of the area belongs to the Quimsacocha and Turi formations (Mosquera et al., 2015). The glacially shaped topography is characterized by slopes positioned at a 0 to 70% incline. According to the FAO soil classification system (WRB-IUSS, 2014), the prevailing soil types in the area include Andosols and Histosols (ratio 3:1-4:1), with a dark Ah horizon that originates from volcanic ash and overlies a mineral-rich C horizon (clay dominated). These non-allophanic, humic and acidic soils develop at 0.24 ~ 0.44 m for Andosols and at 0.24 ~ 0.70 m for Histosols. Local Soil Organic Matter (SOM) levels are high, ranging from 0.44 to 0.84 kg kg_{soil}⁻¹ (Aucapiña and Marín,

2014); the waterlogging, the formation of organometallic complexes (from Holocene ash deposits), and the low redox potential (a result of the high soil moisture and the wet / cold environment) are responsible for its significant accumulation (Buytaert et al., 2006b). Low bulk density levels, between 0.45 and 0.14 Mg m⁻³, and a high field capacity of the pore space, between 39 and 90% (mean = 74%), characterize the Andosols and Histosols, respectively (Mosquera et al., 2015, 2016b; Quichimbo et al., 2012). The shallow wetland soils are Histosols and are therefore always saturated.

Our study site is mainly (> 80% coverage) covered by tussock grasses of *Calamagrostis Intermedia* (J. Presl) Steud., which reach heights of between 30 and 80 cm. This native C3 grass is perennial with a ratio of aboveground biomass / necromass ranging from 0.18 to 0.75 (mean = 0.45) and with an estimated sunlit Leaf Area Index (LAI), which ranges between 2.8 and 3.4 m² m⁻² (Hofstede et al., 1995; Nagy et al., 2011). Some areas of the páramo are recurrently affected by grazing, cattle ranching and burning for pasture management (Hofstede et al., 1995; Suarez and Medina, 2001). However, there is no evidence of induced fires or grazing occurring over the past decade in our study area. Local coexistent endemic vegetation includes other grasses, such as *Festuca* sp. (< 5%), and patches of cushion plants (< 10%) that are sparsely distributed across the wetlands outside of the study fetch (e.g., *Azorella* sp., *Gentiana* sp., *Plantago* sp., *Valeriana* sp., and *Xenophyllum humile* sp.). Finally, remnant patches of small *Polylepis* sp. forests and low shrubs, such as *Weinmannia* sp. and *Buddleia* sp. (<5%), are also found outside the fetch of the observatory.

The climate of the study area is influenced by the Pacific regime and the predominant continental air masses of the Amazon Basin. Peak values in seasonal rainfall are related to the passage of the Inter Tropical Convergence Zone (ITCZ) through the region. However, as noted by Vuille et al. (2000), sea surface temperature anomalies, such as the El Niño Southern Oscillation (ENSO), do not have a significant influence on the climate at this high elevation. Páramos are also characterized by a lack of thermal seasonality, by steady low temperatures and by prevalent convective and orographic cloud formations (Bendix et al., 2006; Emck, 2007). The average annual temperature is 6.1°C (max. = 14.2° C, min. = 0.4° C), the relative air humidity is 93.6%, and the solar radiation level is 4942 MJ m⁻² per year (daily average = 13.73 MJ m⁻² per day), with a noticeable increase in the incoming energy occurring from October to December. Wind speeds follow seasonal patterns and have a monthly mean of 3.21 m s⁻¹ from October to March and 4.77 m s⁻¹ from June to September. Seasonality is more evident in the levels of precipitation, with the highest levels recorded from January to June (and October) and with an annual mean of 1210±101 mm year⁻¹. Thus, bimodal rainfall seasonality is found, similar to other páramo ecosystems (Célleri et al., 2007). Throughout the day, rainfall prevails in the afternoon and almost 30% of all local precipitation is defined as a

4 Net ecosystem exchange and evapotranspiration

drizzle, according to [Padrón et al. \(2015\)](#). Hence, our páramo site is characterized by a constant input of water delivered as rain, as is the case for other Neotropical alpine areas ([Bendix et al., 2008](#); [Janeau et al., 2015](#)). This climatological information is detailed in Figures 4.10 and 4.11 in the supplementary material, showing a monthly climograph (6 years, from Jan. 2012 to Dec. 2017) and annual / monthly wind charts for the same period.

4.2.2 Experimental setup

To understand the bioclimatic properties of the study site, we used climate data (2012 to 2017) extracted from a conventional automatic weather station (AWS) located 10 m from the EC tower. Measurements taken included the solar radiation, temperature, relative humidity, wind speed and direction, atmospheric pressure and rainfall levels. The quality assessments and controls (QA/QC) of the data were assessed according to [Rollenbeck et al. \(2016\)](#), and data gaps (7% of the total) were filled using an interpolation scheme based on information from a nearby páramo AWS within the same climatic regime (Toreadora site in Cajas National Park, 31 km north and 3995 m a.s.l., data not shown). The AWS data were also used to calculate ETr values (section 4.3.6).

Within the 2-year period (March 01, 2016 to February 28, 2018), a 3.6 m EC tower was operational over a site characterized by a gentle slope of 10° and covered by homogeneous and healthy tussock grassland. Atmospheric CO₂ and water vapor (H₂O) fluxes were measured with a LI-7200 enclosed path infrared gas analyzer (IRGA) (LI-COR, Lincoln, NE, USA) running at a constant flow of 15 l min⁻¹ delivered through a flow module. Due to the highly humid conditions of the site, an insulated and electrically heated intake tube (LI-COR 7200-050, 71.1 cm in length and 5.33 mm in internal diameter) was installed with the LI-7200. This accessory employed 5 Watts of power and proved essential for preventing condensation and improving the H₂O frequency response ([Metzger et al., 2016](#)). Furthermore, we set this intake tube tilted down at a 5° with a rain cap with a fine screen to prevent water from entering the measurement cell during storm events. In addition, we installed a 2 μm particulate filter into the tube line to prevent insect and dust contamination. We made 3D wind speed / direction and sonic temperature measurements using a GILL-WM Gill New WindMaster 3D Sonic Anemometer (Gill Instruments, Hampshire, UK). The IRGA and sonic anemometer operated at 20 Hz and data were collected from a LI-COR LI-7550 analyzer unit. Complementary micrometeorological sensors were deployed to measure the Net Radiation (Rn), the Photosynthetic Photon Flux Density (PPFD), and the air temperature / relative humidity levels. In addition, the Soil Heat Flux (G) was measured (3 m from the tower) using

three heat flux plates while measuring soil moisture / temperature levels with three water content reflectometers (with integrated thermocouples). Detailed characteristics of the aforementioned instrumentation are shown in Table 4.1. The power supply was provided by two solar panels (250 W each, SolarWorld SW250), which had a MPPT charge controller (SolarEpic Tracer4215BN) and a wind turbine generator (600 W, Windmill DB-600, with an independent MPPT controller, installed at 5 m height, outside of the EC footprint). Both systems were connected in parallel to a battery bank of 550 Ah (5 AGM batteries 12 V & 110 Ah, Power King). The EC tower operation with this hybrid power system proved crucial given the harsh and remote conditions of the study site, where incoming solar energy is often limited due cloudy conditions, but substantial wind power is available most of the time.

Table 4.1: Instrumentation used in the experiment.

	Variable	Sensors Type and Setup	Unit / Time Step	Accuracy
CO₂ and H₂O Gas Fluxes and Sensible Heat (Fast Sensors) With LI-7550 Analyzer Unit and LI-COR 7200-101 Flow Module	CO ₂ and H ₂ O gas concentration	Enclosed Path IRGA: LI-COR LI-7200 with insulated & heated intake tube at 3.6 m height	ppm and mmol mol ⁻¹ / 20 Hz	CO ₂ : Within 1% of reading H ₂ O: Within 2% of reading
	Wind Speed/Direction/ Sonic temperature	3D Sonic Anemometer: GILL-WM Gill New WindMaster at 3.6 m height	m s ⁻¹ / 20 Hz	Wind Speed <1.5%RMS, Direction <2° (at 12 m s ⁻¹) Sonic Temp. < ±0.5% @ 20°C
Complementary Micrometeorological sensors (Slow sensors) With Sutron 9210B data logger	Net Radiation	4-Component Net Radiometer: Kipp & Zonen CNR4 at 3.6 m height	W m ⁻² / 1 min	<1%
	Soil Heat Flux	Three Soil Heat Flux Plates: Hukseflux HFP01 at 5 cm soil depth	W m ⁻² / 1 min	±0.3%
	Soil Moisture and Temperature	Three Water Content Reflectometers: Stevens Hydra Probe II (each with temperature probes) at 5 cm soil depth	cm ³ cm ⁻³ / 1 min °C / 1 min	Stevens Hydra Probe II (Soil moisture ±2.0% , Soil Temp. ±0.3°C)
	Air temperature and relative humidity PPFD	Thermometer/Hygrometer: Vaisala HMP155 + Radiation Shield at 3 m height Quantum Sensor: LI-COR LI190-R at 3.6 m height	°C and %RH / 1 min μmol m ⁻² s ⁻¹	±1.7%RH (>90%RH) / ± 0.226 °C <1%
Automatic Weather Stations (AWS) (Zhurucay & Toreadora) With Campbell CR1000 data logger	Total Solar Radiation	Pyranometer: Campbell CS300 at 2 m height	W m ⁻² / 5 min	±5% daily total
	Air temperature and relative humidity	Thermometer/Hygrometer: Campbell CS-215 + Radiation Shield at 2 m height	°C and %RH / 5 min	±0.3 °C / ±2% RH
	2D Wind Speed/Direction	Anemometer: Met-One 034B Wind Set at 2 m height	m s ⁻¹ / 5 min	±0.11 m s ⁻¹
	Barometric Pressure	Barometer: Vaisala PTB110 at 1 m height	hPa / 5 min	±0.3 hPa
	Rainfall	Rain Gage: Texas TE525MM Tipping Bucket with wind shield at 1 m height	mm / 1 min	±1%

4.2.3 Data preprocessing, QA/QC and instrumental corrections

During the study period, the total loss of flux measurements was 12.7% due to power failures and instrumental errors. Therefore, levels of temporal coverage were superior to the 65% value (annual average) reported by Falge et al. (2001) for other EC sites. Available data on H₂O, CO₂ and energy

4 Net ecosystem exchange and evapotranspiration

Table 4.2: Flux quality flags. Flag 2 data were discarded for analysis purposes.

Quality Flags	Sensible Heat	Latent Heat	CO ₂ flux	H ₂ O flux
Percentage Flag 0 (High Quality)	12.70%	9.90%	13.60%	9.90%
Percentage Flag 1 (Intermediate Quality)	68.70%	65.50%	72.10%	65.50%
Percentage Flag 2 (Poor Quality)	18.60%	24.60%	14.20%	24.60%

fluxes from the IRGA and 3D anemometer were binned with an average window of 30 min and were processed using the EddyPro software (version 6.2.0, LI-COR, Lincoln, NE, USA). Here, we applied the following QA/QC: (i) diagnostic flags provided by the instruments, (ii) plausibility limits (sensors and site-related) and (iii) spike removal.

Specific corrections applied included (i) a sectorwise planar fit adjustment for sloped topography and potential canopy inhomogeneities (Wilczak et al., 2001), (ii) cospectra filtering (Mauder and Foken, 2004; Vickers and Mahrt, 1997), (iii) time lag compensations for CO₂ and water vapor (as a function of relative humidity) and (iv) a humidity dependent spectral correction using the method of (Fratini et al., 2012). An analysis of the normalized ensemble-averaged hourly cospectra is provided in the supplementary material section. QA/QC values for the half-hourly computed fluxes were determined according to Mauder and Foken (2004) using the 0,1,2 flag system, from which low quality data were removed (flag 2). Table 4.2 lists the percentages of flagged fluxes.

4.2.4 Advection-affected fluxes removal, gap filling and uncertainty analysis

Because katabatic flows (generated during calm nights with clear skies) across the slopes of the high Andes (Litt et al., 2015; Trachte et al., 2010), can lead to an underestimation of Reco levels due to the drainage of CO₂ emissions, we performed a flux removal when low turbulence and advection conditions prevailed (i.e., nocturnal katabatic and afternoon anabatic flows) (Aubinet et al., 2012). For this, data with low friction velocity (u^*) were filtered by applying the Moving Point Test for threshold detection according to Papale et al. (2006). Then, gaps identified due to data losses resulting from power failures, QA/QC filtering, and low-turbulence filtering were filled via Marginal Distribution Sampling (MDS) using the REddyProc R-package (Reichstein et al., 2005, 2017).

We estimated the uncertainty error induced by gap filling using a bootstrapping technique (resampling with replacement) and by creating a dataset of pseudoreplicates. The differences between the high and low threshold estimates (95% and 5% quantiles of the bootstrapped uncertainty

distribution) corresponded to the uncertainty level (introduced by the uncertain estimate of the u^* threshold). We also calculated the random error of the original CO_2 fluxes according to [Finkelstein and Sims \(2001\)](#) method.

To provide insights about the occurrence of nocturnal advection in our site, we included an analysis of the nocturnal turbulence (u^*) and its relationship to nocturnal C fluxes (supplementary material section). Finally, we tested the sensitivity of the NEE balance to the u^* threshold-based filtering and gap filling processes.

4.2.5 Energy balance and footprint analyses

The suitability of the flux results is also based on the Energy Balance Closure (EBC) level and our footprint analysis of the source of fluxes. EBC was conducted from R_n , G , Latent Heat (LE) and Sensible Heat (H) values and gap-filled data were excluded to avoid bias. Hence, turbulent fluxes ($H + LE$) should be approximately equal to the amount of available energy ($R_n - G$) (linear regression). For this computation, R_n was corrected by slope and aspect conditions (slope = 10° and aspect = 145° southeast) to force the surface-normal energy incoming into the system following the methodology developed by [Olmo et al. \(1999\)](#) and detailed in [Leuning et al. \(2012\)](#) and [Serrano-Ortiz et al. \(2016\)](#). We applied this correction under relatively sunny conditions using a sky clearness index (Kt) of greater than 0.7 to avoid making unnecessary corrections when diffuse-irradiance sky conditions due cloudy conditions that characterize the páramo were present. Kt values were calculated to be the ratio between the incoming shortwave radiation (R_s) (pyranometer measurements) and the modeled Extraterrestrial Radiation (R_a), following [Duffie and Beckman \(2013\)](#); the resulting Kt values were found to account for 9.4% of the R_n observations. Final G fluxes accounted for the direct measurements with the plates (G_s), plus the heat storage estimation (GST) of [Mayocchi and Bristow \(1995\)](#). Energy flux densities for relatively sunny days were analyzed as well.

A Flux Footprint Prediction (FFP) based on the method of [Kljun et al. \(2015\)](#) was conducted to estimate the spatial origins of the flux and to exclude potential flux sources of nontussock grass vegetation. The FFP demonstrated the existence of unidirectional fluxes (northeast) with minor contributions from the southwest. Here, 80% of the footprint was found within 100 ~ 130 m of the tower, covering a homogeneous grassland area of approximately 1.6 ha (97.5% of grassland cover, 0.4 ~ 0.8 m canopy height), which had a low level of topographical variability. Thus, less than 2.5% of the data were excluded after the FFP assessment. The analysis is described in detail in

the supplementary material.

4.2.6 Flux calculations and CO₂ light / temperature-response parameterization

The NEE is a crucial indicator for understanding the páramo's role as a C source / sink by aggregation over time (i.e., daily, seasonally and yearly). For a long-term analysis, the calculation of the NEE, is only achievable through continuous flux detection (the EC technique). Consequently, the NEE was divided into its main components of GPP and Reco (where: $NEE = GPP - Reco$). For this purpose, we used a regression of nighttime NEE and soil temperature (Lloyd and Taylor, 1994), in which the latter was taken as a proxy for the daily rates of Reco. Then, GPP was estimated to be the difference between NEE and Reco. Finally, negative nighttime GPP values were set to zero. Flux partitioning was conducted using the R REdDyProc package (Reichstein et al., 2017), and NEE, GPP and Reco were aggregated in daily, monthly and annual sums to explore the C budgets over different time periods.

Furthermore, we parameterized specific equations from half-hourly datasets to represent the CO₂ response to light and soil temperature, a process that is applicable to non-EC monitored sites that have only conventional meteorological measurements available. For these sites, NEE was fitted to a Mitscherlich equation form (Falge et al., 2001) in which GPP_{max} is the diurnal maximum productivity level (or max. C uptake when compared with PPFD). The model was adjusted, with days showing a minimum midday uptake of $-2 \mu\text{mol m}^{-2} \text{s}^{-1}$. The Mitscherlich formulae were used instead of the traditional Michaelis and Menten (rectangular hyperbola) models to prevent an overestimation of NEE (at light saturation) (Stoy et al., 2014). Based on the full half-hourly dataset, GPP was linearly correlated with NEE and Reco was represented by a polynomial correlation with soil temperature (T_{soil}).

By convention, the positive Net Exchange (+NEE) represents the negative Net Ecosystem Production (-NEP) according to Chapin et al. (2006). Therefore, we used NEP instead of NEE to compare the positive C assimilation in the ecosystem (sink), the GPP and the Reco against control variables such as PPFD, soil temperature and soil moisture. For this purpose, we calculated Spearman's correlations (with a *t*-test for each case) for the full period and for days with positive NEP (> +0.10) and negative NEP (< -0.10) values. Correlations with p-values > 0.05 were considered to be insignificant.

4.2.7 The study period in context of longer-term observations

To bring our shorter-term measurements in line with the longer-term climate conditions in the páramo, a 48-year climate dataset (monthly temperature and precipitation for 1964-2011) from the nearby páramo AWS El Labrado (40 km north-east and 3335 m a.s.l., data provided by the National Institute of Meteorology and Hydrology of Ecuador INAMHI) was compared with the available measurements from Zhurucay (6-year) and, in particular, with the 2-year flux monitoring data. Using this dataset, the integrated anomalies in precipitation and temperature were determined for the complete period (54 years) using the well-known Standardized Precipitation Evapotranspiration Index (SPEI) (Beguería et al., 2014; Vicente-Serrano et al., 2010). The SPEI is advantageous for describing the meteorological dryness / wetness because it combines multiscale characteristics with a sensitivity to temperature fluctuations. A 1-month-based SPEI scale served to classify the historical drought or excess water conditions of our study period. Prior to the establishment of this scale an adjustment for the páramo's specific altitudinal temperature lapse rate (according to Córdova et al. (2016)), was adopted to fit the El Labrado dataset to the elevation of Zhurucay.

Furthermore, we obtained a 19-year dataset of satellite GPP observations from the MODIS product MOD17A2H (MODIS/TERRA Gross Primary Productivity, version 6, 500 m of resolution, 8-day composite for 2000-2018, available from the Land Processes Distributed Active Archive Center (LP DAAC)) for the correspondent pixel of our EC footprint. Cloud-contaminated images (low QA/QC of the product) were excluded from the analysis prior to obtaining daily averages for each month to compare the results to our GPP estimations.

4.2.8 Evapotranspiration and Kc

The EC method produced measurements of ETa, which were derived from the air density (ρ), vertical wind speed (ω) and water vapor mixing ratio (water vapor mass divided by dry air mass = q) values, according to Equation 4.1:

$$ETa = \bar{\rho} * \overline{\omega' * q'} \quad (4.1)$$

This flux consists of transpiration, the evaporation of intercepted rain / fog and the evaporation from soil surfaces, and it is extremely useful for understanding water availability and carbon / water coupling in natural and disturbed biomes. As was done for NEE fluxes, diurnal half-hourly ETa observations affected by power failures, QA/QC filtering and low turbulence were identified and

discarded (30.7% of data), following Papale et al. (2006). Then, the gaps were filled via the MDS technique and the corresponding uncertainty was retrieved. ETa observations were aggregated at daily, monthly and annual time steps and were compared with ETr values calculated from standard (and frequently used) methods of FAO56 PM Penman-Monteith reference evapotranspiration (grass-based) (Allen et al., 1998) and ASCE-ERWI standardized reference evapotranspiration (alfalfa-based) calculation (ASCE-ERWI, 2001). Finally, the Kc values for the páramo tussock grasses were obtained from the ETa / ETr ratio for both ETr methods (considering the less humid and wet periods of the site) and were then contrasted with other Kc values reported in the literature.

4.3 Results and Discussion

4.3.1 EBC and energy flux densities

Figure 4.2 shows two EBC scenarios: (4.2a) EBC with an Rn Surface-normal correction and (4.2b) EBC with direct Rn observations (i.e., without correction). For both cases, we obtained a regression slope of 1.02, which represents an outstanding closure comparable to other tropical sites with moist environments (Cabral et al., 2015, 2010). We also observed a linear intercept of $6.5 \sim 6.9 \text{ W m}^{-2}$, a high correlation R^2 value of $0.92 \sim 0.93$, and analogous values of RMSE.

While some studies encourage the geometrically-based adjustment of Rn for EC experiments of steep terrain (Hammerle et al., 2007; Olmo et al., 1999; Wohlfahrt et al., 2016), our findings demonstrate that for our location (which has a high diffuse radiation dominance), a surface-normal correction does not significantly improve the EBC.

Figure 4.3 shows the energy flux densities for the relatively cloud-free days (average of 9 days) during a less humid / high radiation period (August 2016) and during a wet / low radiation period (January 2017). The Rn Surface-Normal corrected and Rn observed curves are shown, as are the LE, H, G and residuals of the corrected or uncorrected Rn scenarios (Res_{RnSN} and Res_{Rn}). Standard deviation bars are also shown in the figure.

During the less humid month (4.3a), the sensible heat doubled the latent heat density ($H_{mean} = 127.6 \text{ W m}^{-2}$ versus $LE_{mean} = 64.0 \text{ W m}^{-2}$). However, differences between H and LE during the wet month (4.3b) were less significant ($H_{mean} = 89.6 \text{ W m}^{-2}$ versus $LE_{mean} = 93.0 \text{ W m}^{-2}$). This can be attributed to an increase in the humidity of the environment and the soil due to higher levels of precipitation. Finally, differences in the available energy ($Rn_{SN} - G$), the turbulent flux ($H + LE$), and the residuals (Res_{RnSN}) were measured to be 10.5%, 4.7% and 30.1% higher, respectively, in

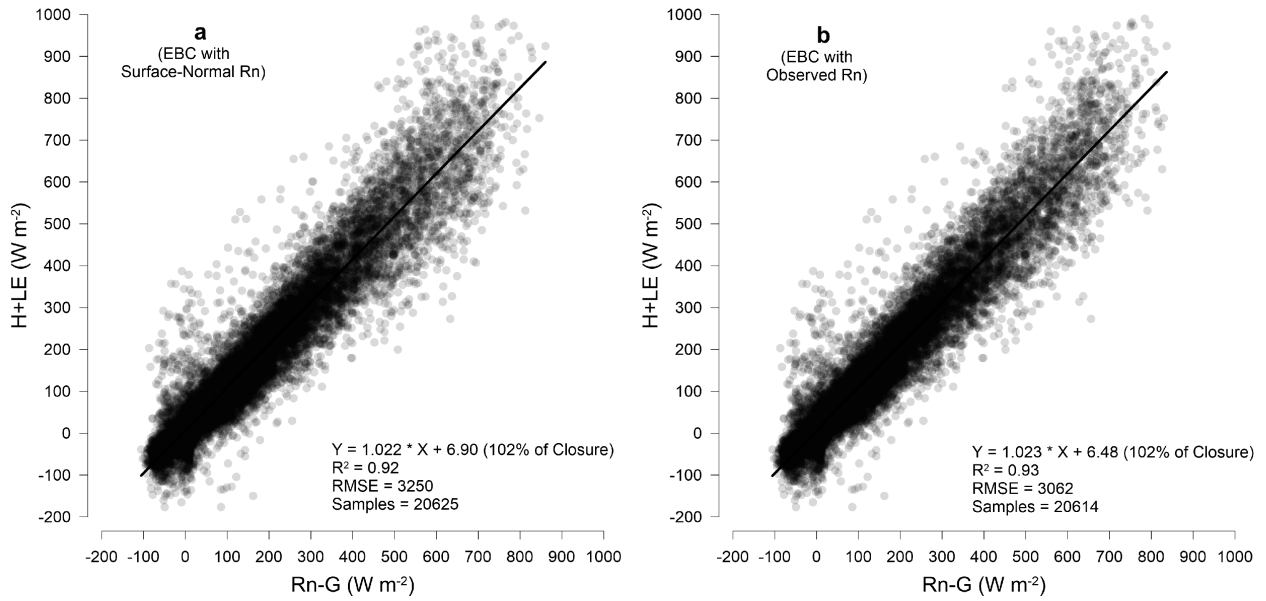


Figure 4.2: EBC for the study site: (a) EBC with an Rn Surface-Normal correction (b) EBC with uncorrected Rn (direct observation). No gap-filled data were used.

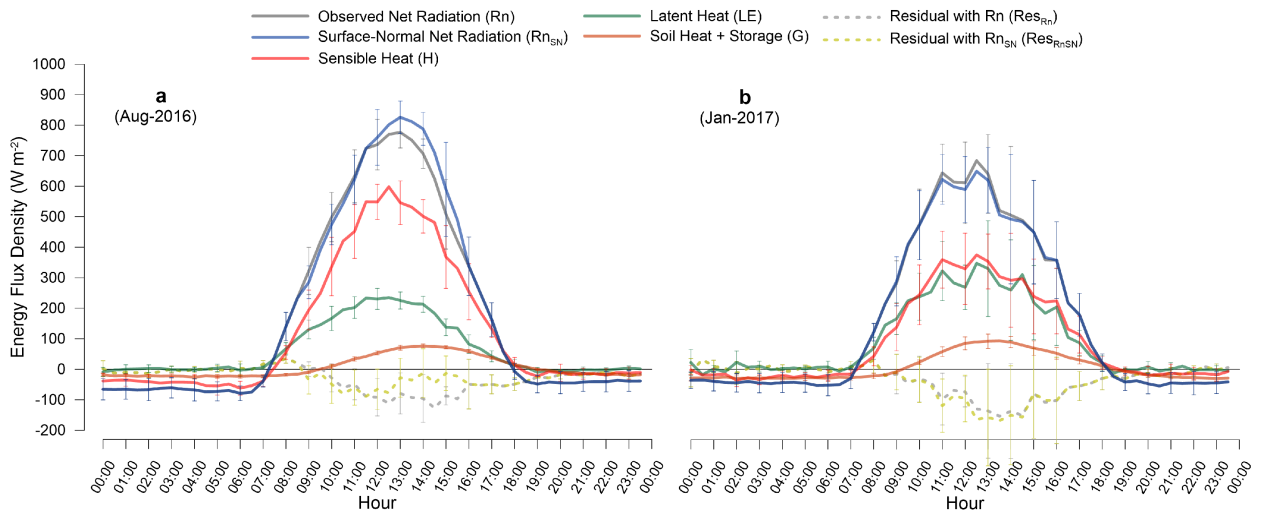


Figure 4.3: Hourly energy flux densities on cloud-free days for (3a) a less humid / high radiation month (August 2016) and (3b) a wet / low radiation month (January 2017), with error bars.

the less humid period than in the wet period. Additionally, the deviations of all of the density curves (SD) were found to be notably higher for the wet period.

The 2-year of energy fluxes analysis shows daily averages of $Rn_{SN} = 102.2 \pm 40.4 \text{ W m}^{-2}$, $H = 64.4 \pm 39.2 \text{ W m}^{-2}$, $LE = 57.7 \pm 27.3 \text{ W m}^{-2}$, and $G = 0.5 \pm 5.4 \text{ W m}^{-2}$ with residuals of (Res_{RnSN})

4 Net ecosystem exchange and evapotranspiration

= $-15.0 \pm 36.1 \text{ W m}^{-2}$. However, the diurnal partitioning of the net available energy (07:00 - 18:00) into H and LE was measured to be 55.0% and 43.5%, respectively. Therefore, a significant amount of the available energy is used for atmospheric heating.

4.3.2 NEE measurements and partition-derived carbon fluxes (GPP, Reco)

NEE ($\mu\text{mol m}^{-2} \text{ s}^{-1}$) half-hourly fluxes were obtained from the available CO_2 flux measurements (after the QA/QC process). Data affected by low turbulence and advective conditions were filtered (25.5% of NEE) (via u^* threshold-detection) and friction velocity thresholds of $u^* = 0.344$ and $u^* = 0.321$ were applied, for the first and second year, respectively. The NEE half-hourly means for the first and second year were 0.33 ± 3.86 and $0.19 \pm 3.77 \mu\text{mol m}^{-2} \text{ s}^{-1}$, respectively. The correspondent uncertainty averages were 0.02 ± 0.68 and $0.02 \pm 0.56 \mu\text{mol m}^{-2} \text{ s}^{-1}$ (6.9% and 12.6% of the induced error to the gap-filled data, respectively). Following the method of [Finkelstein and Sims \(2001\)](#), original CO_2 half-hourly fluxes had a mean of $0.07 \pm 3.97 \mu\text{mol m}^{-2} \text{ s}^{-1}$, with an average random error of $0.02 \pm 0.49 \mu\text{mol m}^{-2} \text{ s}^{-1}$ (28% of the error). These uncertainties are lower than those reported by [Baldocchi et al. \(2001\)](#) for other FLUXNET sites ($0.4 \mu\text{mol m}^{-2} \text{ s}^{-1}$). The analysis of the nighttime turbulence (u^*) and its relationship with nighttime C fluxes, presented in the supplementary material section, demonstrates that the selected u^* thresholds used in the data filtering can reduce the possibility of an underestimation of nighttime Reco.

The GPP and Reco modeled by the partitioning process developed by [Reichstein et al. \(2005\)](#) are shown in Figure 4.4. The half-hourly NEE fingerprint is shown in Figure (4.4a) and the daily aggregated NEE, GPP and Reco fluxes are shown in Figure (4.4b).

In this figure, the NEE fingerprint (4.4a) shows consistent levels of diurnal-nocturnal fluctuation from sunrise (approx. 07:10) to sunset (approx. 18:05) without intra-annual seasonality or a noticeable degree of C uptake (by the ecosystem) from 09:00 to 15:00. The C fixation process tended to decline in the late afternoon hours as was expected due to the frequent afternoon-cloudiness of the páramo, which limits photosynthesis earlier in the day than is the case under cloud-free conditions. The hourly daytime NEE mean was $-2.97 \pm 3.01 \mu\text{mol m}^{-2} \text{ s}^{-1}$ (max. = $-13.55 \mu\text{mol m}^{-2} \text{ s}^{-1}$) and the nighttime NEE mean was measured to be $+3.23 \pm 1.04 \mu\text{mol m}^{-2} \text{ s}^{-1}$ (max. = $+19.56 \mu\text{mol m}^{-2} \text{ s}^{-1}$). During a few days in June, October, November and December 2016-17, we observed higher values of C release at night, likely because these days preceded less humid periods and were followed by rain events, conditions that can promote respiration.

Daily aggregations of fluxes (4.4b) show predominantly positive NEE values with a daily mean of

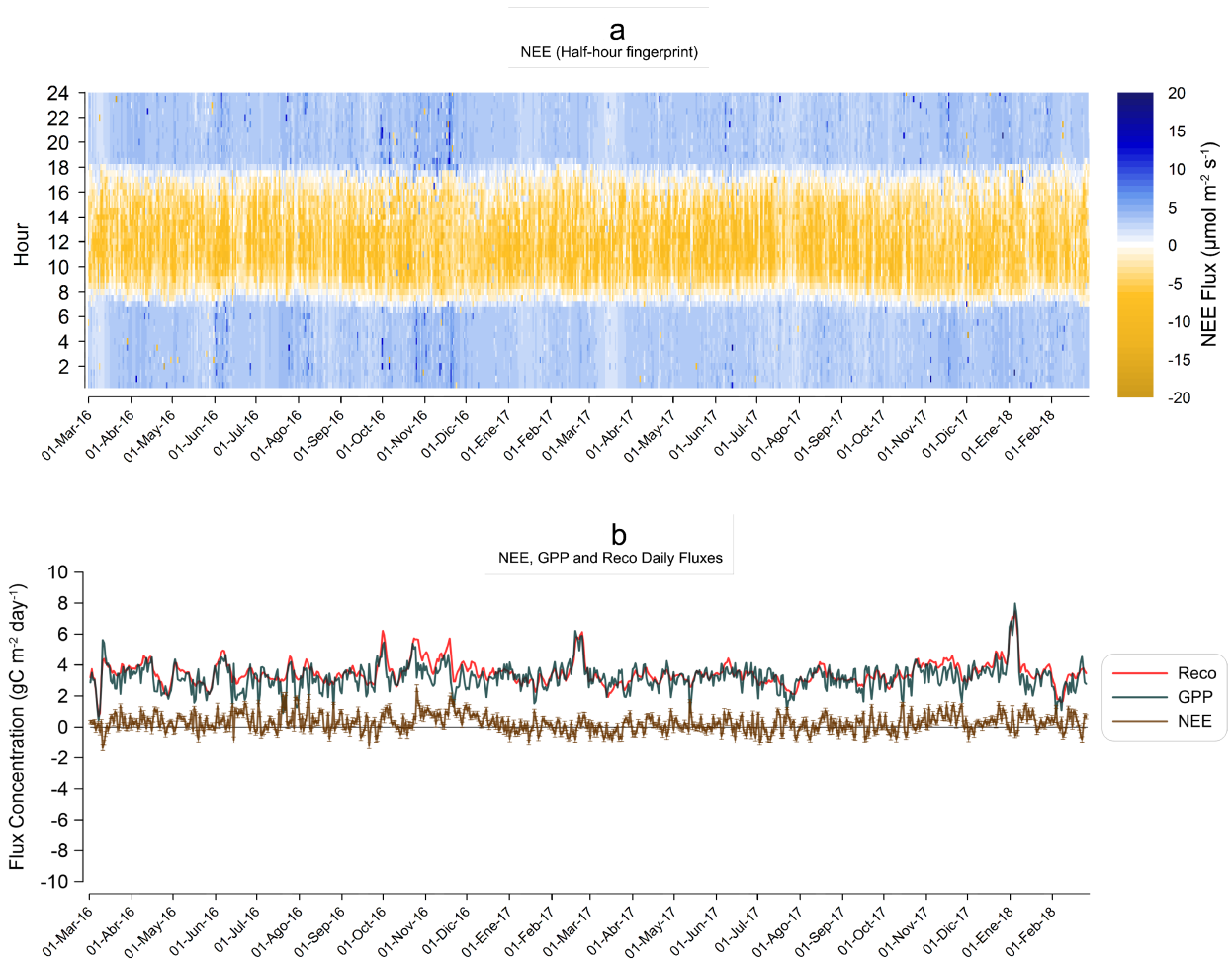


Figure 4.4: Half-hourly NEE fingerprint (a) and daily aggregated NEE, GPP and Reco fluxes (b) for the study period. The hourly standard deviation of NEE is shown as bars.

$+0.27 \pm 0.58 \text{ gC m}^{-2} \text{ day}^{-1}$, a maximum of $+2.50$ and a minimum of $-1.36 \text{ gC m}^{-2} \text{ day}^{-1}$. In total, 484 days registered positive values and 246 days registered negative NEE values, meaning that for only 34% of the time, the páramo acted as a weak C sink. On the other hand, partition-retrieved GPP values reached a mean of $3.21 \pm 0.86 \text{ gC m}^{-2} \text{ day}^{-1}$, (max. = 7.98, min. = 0.45) and the Reco mean reached $3.48 \pm 0.76 \text{ gC m}^{-2} \text{ day}^{-1}$, (max. = 7.47, min. = 0.69). Very few studies have evaluated observations (or validated model estimations) of atmospheric C flux in the páramo. For instance, [McKnight et al. \(2017\)](#) obtained a Reco flux average of $4.58 \pm 0.22 \mu\text{mol m}^{-2} \text{ s}^{-1}$ from midday measurements (between 10:00 and 14:00) by applying the soil CO_2 flux chamber technique to a similar biome (Mazar Wildlife Reserve: 3450 m a.s.l. 91 km east of Zhurucay). This Reco value is

4 Net ecosystem exchange and evapotranspiration

39% higher than our observations ($3.30 \pm 0.81 \mu\text{mol m}^{-2} \text{s}^{-1}$). [Sánchez et al. \(2017\)](#) used diurnal NEE measurements, combined with simulated nocturnal Reco and inferred GPP values, derived from a CO_2 IRGA with a custom-made transparent chamber for NEE and a sunlight block fixture to simulate dark respiration for an undisturbed peatland site (cushions and lawns over histosols) in the Cayambe-Coca National Park (4260 m a.s.l., near the active volcanic highlands of northern Ecuador). Values reported from this survey (09:00 - 16:00 during dry-days) are as follows: NEE = $-0.69 \pm 0.08 \text{ gC m}^{-2} \text{ hour}^{-1}$, Reco = $0.66 \pm 0.06 \text{ gC m}^{-2} \text{ hour}^{-1}$ and GPP = $1.35 \pm 0.12 \text{ gC m}^{-2} \text{ hour}^{-1}$. In this study, the authors noted that CO_2 losses might be higher if nighttime respiration were measured. Our corresponding daytime NEE reached $-0.18 \pm 0.09 \text{ gC m}^{-2} \text{ hour}^{-1}$, the nighttime Reco reached $0.14 \pm 0.03 \text{ gC m}^{-2} \text{ hour}^{-1}$, and the GPP (full dataset) reached $0.33 \pm 0.10 \text{ gC m}^{-2} \text{ hour}^{-1}$. Our values are clearly lower than those for the Cayambe-Coca site. It should be stressed that these studies only used daytime sampling methods in a short-term monitoring period, rather than the EC technique, which performs a continuous (diurnal / nocturnal) monitoring of fluxes, surveying the whole ecosystem ([Baldocchi, 2003](#)).

Monthly and annual aggregations of C fluxes are shown in [Table 4.3](#). We found that NEE, GPP and Reco monthly averages for the less humid period were higher than those for the wet period, especially for NEE.

Table 4.3: Monthly and annual NEE, GPP and Reco fluxes.

	NEE	GPP	Reco
Monthly Average with SD ¹ ($\text{gC m}^{-2} \text{ month}^{-1}$)	8.2 ± 7.7	97.6 ± 10.7	105.8 ± 13.9
Wet Period Average ²	6.2 ± 6.2	98.9 ± 12.5	105.1 ± 14.9
Less humid Period Average ³	11.1 ± 9.0	95.7 ± 7.9	106.8 ± 13.2
Difference Wet vs. Less humid (%)	80.80%	-3.3%	1.7%
First year Sum ($\text{gC m}^{-2} \text{ year}^{-1}$)	128.8	1175.1	1303.7
Second year Sum ($\text{gC m}^{-2} \text{ year}^{-1}$)	68.7	1166.4	1235.2

¹ SD Standard deviation.

² Wet period contemplated: January, February, March, April, May, June and October.

³ Less humid period contemplated: July, August, September, November and December.

In investigating analogous carbon-exchange studies of the Ecuadorian páramos, [Minaya et al. \(2016\)](#) retrieved monthly GPP estimations by applying the Biome-BGC model and validated the model with ground-based GPP values (derived from aboveground biomass and C stock ratios) for the Antisana Ecological Reserve (near to Cayambe-Coca). In their study, low elevation sampling areas (4000-4200 m a.s.l.) showed a modeled GPP of between 80 and 120 gC m⁻² month⁻¹ and ground-based GPP values of approximately 95 to 100 gC m⁻² month⁻¹. The latter results are similar to our estimates.

We found that our site is a source of carbon, with annual NEE budgets of +128.8 gC m⁻² year⁻¹ for the first year, +68.7 gC m⁻² year⁻¹ for the second year, and annual uncertainties (attributed to u* threshold removal and gap filling) of 4.33 gC m⁻² year⁻¹ and 3.41 gC m⁻² year⁻¹, respectively. The C balance shown in [Table 4.3](#) is sensitive to the u* threshold-based filtering and gap filling. To quantify this sensitivity we increased the u* threshold by 20% (i.e., from 0.344 to 0.413 m s⁻¹ for the first year and from 0.321 to 0.385 m s⁻¹ for the second year) and then recalculated the annual budgets of NEE. This modification increased the NEE balance by 2.64 gC m² year⁻¹ and 1.92 gC m² year⁻¹, respectively (which represents 61% and 56% of the annual aforementioned uncertainty). Therefore, it is unlikely that higher u* threshold values can affect the NEE budget beyond the uncertainty level.

Respiration clearly exceeded gross primary productivity (11% and 6%, first and second year, respectively). Consequently, the páramo behaved as a CO₂ source for this particular period. This finding can be explained by several key ecosystem characteristics: (i) páramo soils release CO₂ depending on the stability of SOM to decomposition ([Tonneijck et al., 2010](#)), but this is strongly dependent on local alpine inhibition factors (i.e., limited radiation, low temperatures, high humidity levels and mineral inputs) that not yet fully understood ([Hribljan et al., 2016](#)); (ii) heterotrophic (RecoH) and autotrophic (RecoA) respiration mechanisms have been rarely investigated for this harsh ecosystem; however, a study of the RecoH of páramo soils in Colombia ([Curiel Yuste et al., 2017](#)) reported a high sensitivity of CO₂ emissions to changes in soil temperature (unaffected by soil water saturation). Thus, given persistent diurnal-nocturnal variations in soil temperature found at our site (max. = 20.3° C, and min. = 4.8° C), the daytime RecoH rates may potentially overcome the CO₂ sequestration rates; and (iii) the photosynthesis of tussock grasses (the dominant species, which possesses a low biomass / necromass ratio) is strongly affected by the limitations of sunlight in the cloudy páramo. The phenology and water use efficiency of this plant species are still unexplored.

[Table 4.4](#) compares the annual C budgets (EC technique-based) of globally distributed tropical, mid-high elevation, and high-latitude (tundra) grasslands (with similar characteristics as the system

4 Net ecosystem exchange and evapotranspiration

studied here) to values obtained in this study.

Certainly, most undisturbed prealpine and alpine grasslands (e.g., Niwot Ridge, Qinghai-Tibetan Plateau and Monte Bondone) and to a lesser degree the Australian subalpine grasslands (Dargo) act as strong C sources. These ecosystems are, however, subject to seasonality and their water supplies are dependent on snowmelt during the winter (rainfall is also scarce). Additionally, some of these biomes share related species of mid-tall grasses (*Carex*, *Poacea* and *Eriophorum* sp.). On the other hand, arctic tundra sites (e.g., Imnavait Creek and Atqasuk) mostly act as weak C sources. Despite having a significant water surplus, these biomes have a considerable deficit of incoming solar radiation, which limits C fixation during a significant period of the year. Regardless of the mid-elevation location of the Cerrado grassland in Brazil (which has a large water supply and is closer in latitude to our site), this biome acts as a C sink, unlike the Panama pasture (Sardinilla), which serves as a strong source of CO₂. Finally, our site shows annual GPP levels as high as those of other source-type ecosystems (Monte Bondone and Sardinilla) and nearly as high as those of the Qinghai-Tibetan Plateau.

Similarly, páramo soil and vegetation can release significant CO₂ relative to other low-elevation tropical ecosystems, as is the case for boreal and arctic tundra biomes where NEP decrements are greater than GPP decrements according to latitude (releasing larger emissions relative to respiration). This behavior can remain constant over time (possibly interannually), as the seasonal variability in GPP and Reco levels for the tropics is lower than that of other biomes, as noted by [Falge et al. \(2002\)](#), given the dominant role of cloudiness in photosynthesis modulation for tropical regions as stated by [Baldocchi et al. \(2018\)](#) in a review of numerous FLUXNET sites.

Estimates of páramo soil age ranging from 6675 to 8270 years before present (B.P.) were reported by [Hribljan et al. \(2016\)](#) for grasslands of the Cayambe-Coca National Park, with historical C accumulation rates of up to 23 gC m² year⁻¹ and a soil C storage of 183 kgC m⁻². [Jantz and Behling \(2012\)](#) reported an estimate of soil age of 8428 ± 41 years B.P. for the Quimsacocha Tres-Lagunas site (2 km north of our site, with the estimate based on pollen and charcoal records). Their results indicate that cooler and humid conditions (late-Holocene 2200 years B.P.) were optimal for the soil C accumulation. However, a stronger human influence is also detected during the last 200 years B.P. In spite of the alterations in C-dynamics due to natural processes, such as volcanic activity or preindustrial-era climatic shifts, whether some páramo locations (such as our site) are experiencing recent C stock depletion (in contrast to its longer-term accumulation capacity) remains unclear. To understand these processes, a longer-term observational period of EC exchange measurements combined with of the study of soil and vegetation-level C stocks and diurnal / nocturnal fluxes is

Table 4.4: Comparison of Zhurucay annual C budgets (average) to other tropical, mid-high elevation, and high-latitude (tundra) grasslands around the globe (EC experiments only).

Location (Country)	World Ecoregion*	Elev. (m a.s.l.)	Lat. / Long.	Biome / Dominant species	Seasonality	SWC (%) or Water Table (cm)	Period	NEE (gC m ⁻² year ⁻¹)	GPP (gC m ⁻² year ⁻¹)	Reco (gC m ⁻² year ⁻¹)	Reference
Zhurucay											
Páramo (Ecuador)	Northern Andean páramo	3765	3.06 S / 79.24 W	Alpine Tundra / <i>Calamagrostis l. sp.</i> , <i>Festuca sp.</i>	No	74%	2016-2018	+98.8	1170.8	1269.5	(Present study)
Brazilian Cerrado (Brazil)	Cerrado	1060	15.55 S / 47.54 W	Wet Grassland / <i>Axonopus C. sp.</i>	No	>80%	2005-2006	-83.9	1459.3	1375.4	Meirelles et al. (2015)
Sardinilla ** (Panama)	Isthmian-Atlantic moist forests	70	9.32 N / 79.63 W	Pasture / <i>Paspalum D. sp.</i> , <i>Rhynchospora N. sp.</i>	No	~39%	2007-2009	+261.0	2345.0	2606.0	Wolf et al. (2011)
Niwot Ridge (USA)	Colorado Rockies forests	3500	40.05 N / 105.258 W	Alpine Tundra / <i>Carex R. sp.</i> , <i>Paronychia P. sp.</i>	Yes	-	2008-2012	+175.0	124.0	329.0	Knowles et al. (2015a)
Qinghai-Tibetan Plateau (China)	Southeast Tibet shrublands and meadows	3250	37.58 N / 101.33 E	Alpine Meadow / <i>Kobresia. T. sp.</i> , <i>Carex P.sp.</i>	Yes	30cm	2004-2006	+106.1	629.9	737.3	Zhao et al. (2009)
Dargo (Australia)	Australian Alps montane grasslands	1648	37.13 S / 147.17 E	Subalpine Grassland / <i>Poa Hiemata sp.</i>	Yes	-	2007-2014	+18.0	95.0	78.0	Beringer et al. (2016)
Monte Bondone (Italy)	Alps conifer and mixed forests	1563	46.02 N / 11.03 E	Subalpine Grassland / <i>Molinia C. sp.</i> , <i>Carex R. and N. sp.</i> , <i>Eriophorum V. sp.</i>	Yes	74%	2012-2014	+180.7	1191.0	1307.7	Pullens et al. (2016)
Graswang (Germany)	Western European broadleaf forests	864	47.57 N / 11.03 E	Subalpine Grassland / <i>Plantago L. sp.</i> , <i>Trifolium R. sp.</i>	Yes	~50%	2011-2014	-226.0	1518.0	1293.0	Zeeman et al. (2017)
Imnavait Creek (Alaska, USA)	Arctic tussock tundra	930	68.61 N / 149.30 W	Arctic Tussock Tundra / <i>Eriophorum V. sp.</i> , <i>Sphagnum sp.</i>	Yes	-	2013-2014	+30	-	-	Euskirchen et al. (2017)
Atkasuk (Alaska, USA)	Arctic coastal tundra	24	70.46 N / 157.40 W	Arctic Tundra / <i>Eriophorum V. sp.</i> , <i>Carex B. sp.</i> , <i>Vaccinium V. sp.</i>	Yes	-	2006	+13.6	-	-	Oechel et al. (2014)
Auchencorth Moss (Scotland)	Celtic broadleaf forests	267	55.79 N / 3.24 W	Peatland / <i>Deschampsia F. sp.</i> , <i>Eriophorum V. sp.</i>	Yes	4cm	2002-2013	-64.1	-	-	Helfter et al. (2015)

NEE, GPP and Reco are reported as annual averages. Negative NEE indicates a C sink ecosystem, Positive NEE a C source ecosystem.

* SWC = Soil Water Content.

** Retrieved from the Terrestrial Ecoregions of the World (TEOW) map (Olson et al., 2001)

** Values of Sardinilla are reported for 2008.

urgently needed.

4.3.3 NEE / GPP light-response and carbon exchange models

As photosynthesis and C fixation are limited by photon availability, the productivity of the páramo must be related to sunlight levels (see Fig. 4.5). Hence, in Figure 4.5a, the total diurnal GPP is correlated with total daily PPFD, and shows a positive correlation with $R^2 = 0.47$ (nonlinear model with 95% confidence band), which demonstrates that GPP proportionally increased as PPFD increased until the GPP reached saturation ($8.5 \text{ gC m}^{-2} \text{ day}^{-1}$, at $96.0 \text{ mol m}^{-2} \text{ day}^{-1}$).

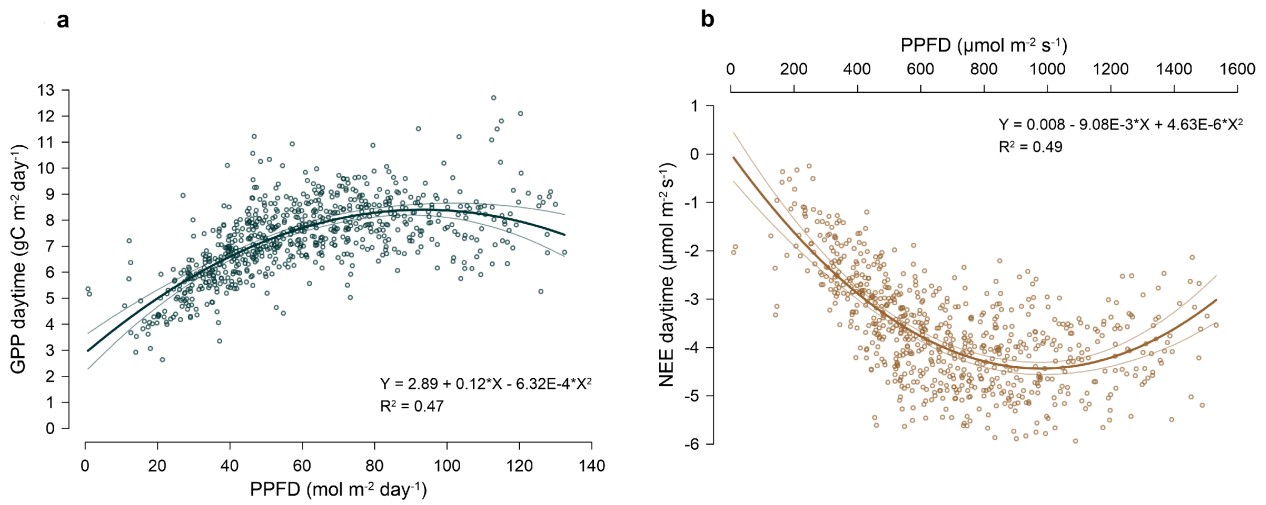


Figure 4.5: Nonlinear fit of diurnal GPP versus PPFD (a) and average diurnal NEE versus PPFD (b) with 95% confidence bands (thin lines).

Furthermore, Figure 4.5b shows the relationship between the average diurnal NEE and the average PPFD (in $\mu\text{mol m}^{-2} \text{ s}^{-1}$, at the 95% confidence level), and depicts a positive correlation ($R^2 = 0.49$) between the C uptake (negative NEE) and the photon flux. NEE was saturated at an emission level of $-4.5 \mu\text{mol m}^{-2} \text{ s}^{-1}$ and at $990 \mu\text{mol m}^{-2} \text{ s}^{-1}$ of PPFD. Our parameterization of C fluxes to light and soil temperature responses for this ecosystem is presented in Equations 4.2 to 4.4 as follows:

$$NEE = GPP_{max} * \left(1 - e^{\frac{0.035 * PPFD}{GPP_{max}}}\right) + 3.192; (R^2 = 0.95, p < 0.05) \quad (4.2)$$

$$GPP = -0.992 * NEE + 3.350; (R^2 = 0.95, p < 0.05) \quad (4.3)$$

$$Reco = 3.207 - 0.209 * T_{soil} + 0.019 * T_{soil}^2; (R^2 = 0.40, p < 0.05) \quad (4.4)$$

In Equation 4.2, the apparent quantum yield coefficient (0.035) and the dark respiration coefficient (3.192) are similar to those reported by Ruimy et al. (1995) for grasslands. These equations are suitable for the empirical estimation of C fluxes in similar páramo locations, where, for instance, PPFD can be inferred from the Rs of conventional AWSs. However, the development of site-specific equations is recommended for more heterogeneous locations.

4.3.4 CO₂ fluxes versus climatic / biophysical controls

Figure 4.6 shows the analyses of the correlations between CO₂ assimilation in the ecosystem (NEP, explained in section 4.2.6), GPP and Reco fluxes and specific climatic / biophysical controls: daily PPFD, soil water content and soil temperature.

For the full period, NEP showed a moderate correlation with GPP and PPFD, a weak or no relationship with soil moisture and soil temperature, and an inverse relationship with Reco. This behavior was undetermined for correlations with $p < 0.05$. On the other hand, GPP cannot be correlated with Reco, given that one is derived from the other (Vickers et al., 2009). Full period GPP was strongly related to PPFD and soil temperature. An inverse correlation between full period GPP and soil water content was found for the three datasets. These findings suggest that limited CO₂ sequestration periods in the páramo (+NEP and GPP) can be promoted by increases in PPFD but are inhibited by increases in soil moisture. Reco also showed a positive correlation with PPFD and soil temperature for the whole period and an especially strong correlation for negative NEP days, as well as an inverse relationship with soil water content. Like those for NEP and GPP, these findings also suggest that C emissions can be promoted through increases in light and soil temperature and through strong reductions in soil water content (a rare occurrence in the páramo). Finally, the relationship between PPFD and the soil water content was inverse and proportional to the soil temperature, and the soil water content was inversely proportional to the soil temperature. Figure 4.15 in the supplementary material illustrates a daily time series for NEP, GPP and Reco versus soil temperature, water content and rain depth for the study period.

4 Net ecosystem exchange and evapotranspiration

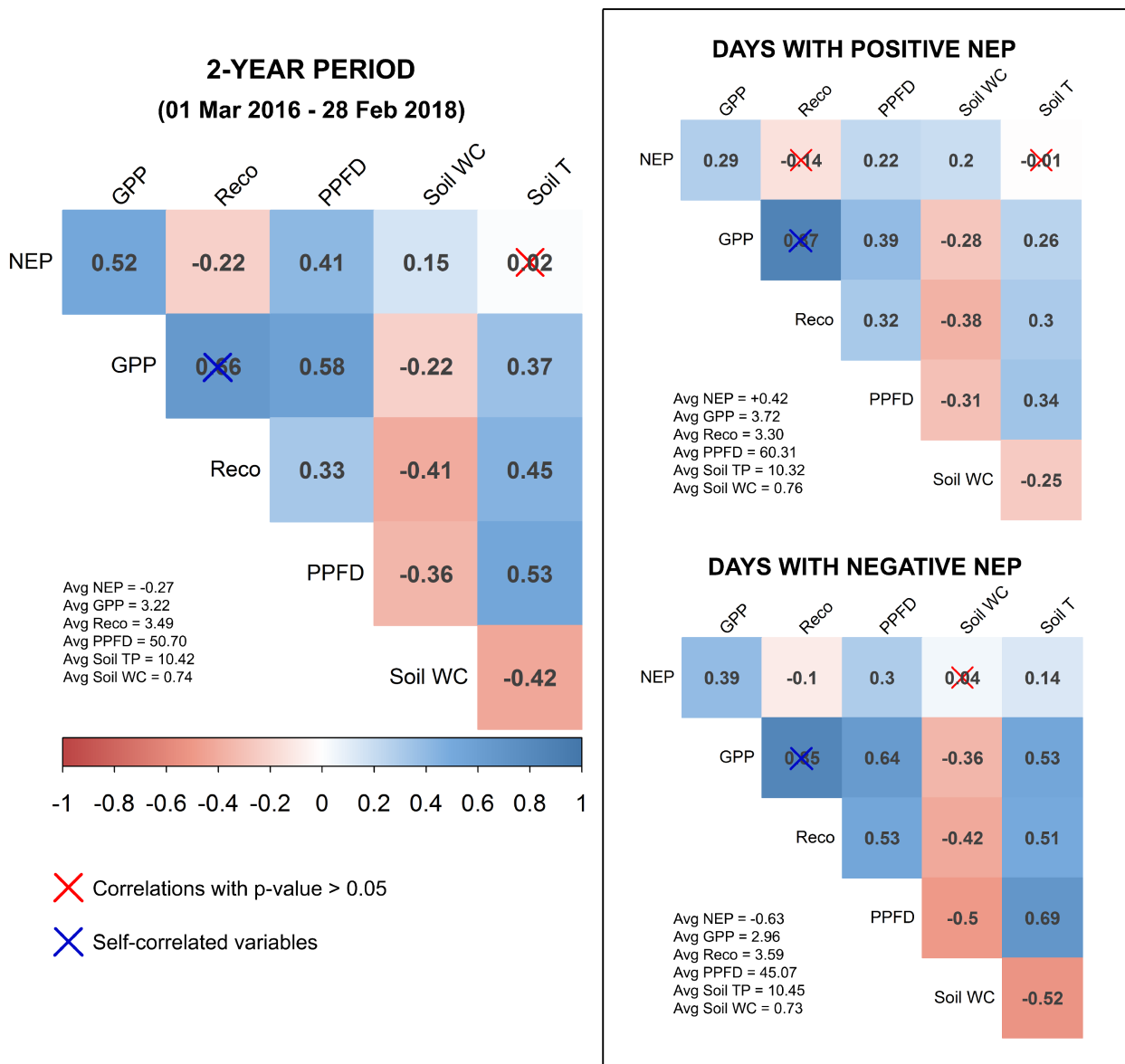


Figure 4.6: Spearman's correlograms for NEP, GPP, Reco, PPFD, soil water content and soil temperature. Days with positive and negative NEP are analyzed independently. Correlations with p-value > 0.05 are cross-marked.

4.3.5 The study period in comparison to longer-term environmental observations

Figure 4.7a depicts (i) the long-term temperature and precipitation series for the El Labrado climate station (INAMHI) as monthly averages with standard deviation, (ii) the 6-year monthly climate data from Zhurucay highlighting the flux measurement periods, and (iii) the NEE, GPP and Reco monthly sums. The overall variability in the long-term temperature and rainfall is consistent with that of the Zhurucay climate series, in spite of the difference in altitudinal temperature at El Labrado. Monthly scale fluxes have an unclear relationship with climatic variables. However, for January and February 2016 and March 2017 the ecosystem exhibits a weak uptake of CO₂ (-0.4, -0.6 and -4.7 gC m² month⁻¹, respectively), which is probably associated with the precedent decline in rainfall and the subsequent radiation increase in the system.

In Fig. 4.7b, the 1-month-based SPEI interestingly shows that the period of EC monitoring can be classified as moderate wet (the beginning of each year) to moderate dry (the 5 intermediate months of each year), according to the categorization of [McKee et al. \(1993\)](#) and the [World Meteorological Organization \(2012\)](#) for meteorological dryness / wetness. Finally, Fig. 4.7c reveals a relative consistency and similar magnitude of the MODIS GPP long-term observations (the daily mean of which is 3.33 ± 0.14 gC m² day⁻¹), when compared to our EC-based GPP estimations (the daily mean of which is 3.21 ± 0.21 gC m² day⁻¹), in spite of the low regression coefficient found.

These results provide an insight to how representative our study period is of the longer-term dynamics of the páramo's climate conditions for the last 54 years and confirm that our flux measurements were acquired in the absence of drought or excess water anomalies.

4.3.6 Evapotranspiration

During the study period, the mean-hourly ET reached 0.13 ± 0.12 mm hour⁻¹ with a mean uncertainty of 0.001 ± 0.004 mm hour⁻¹ for the gap-filled values. Therefore, only 0.9% of the error was introduced to these data as a result of the gap filling process. Additionally, the random error for the water fluxes calculated following the [Finkelstein and Sims \(2001\)](#) method was of 0.13 ± 0.21 μmol m⁻² s⁻¹, which is equivalent to 9.8% of the H₂O half-hourly mean (1.31 ± 1.92 μmol m⁻² s⁻¹). Thus, these biases hardly affected the monthly and annual ET aggregations (as shown in section 4.3.2 for NEE).

Figure 4.8a depicts the hourly dispersion between ET_a and the modeled ET_r from FAO56 ([Allen](#)

4 Net ecosystem exchange and evapotranspiration

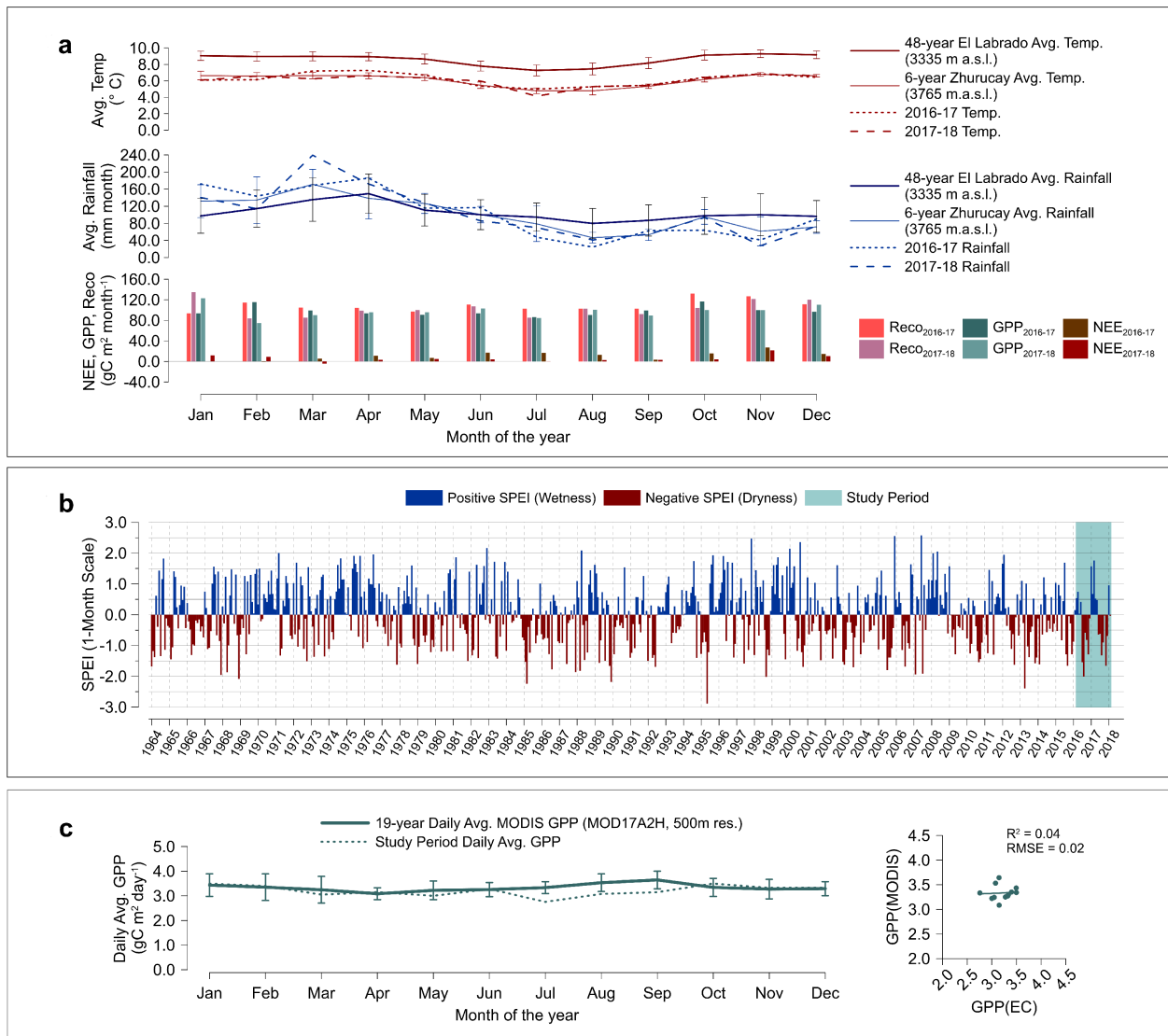


Figure 4.7: Long-term analyses: (a) Temperature and rainfall series for: El Labrado AWS, Zhurucay AWS (including the 2-year EC measurements), NEE, GPP and Reco, (b) Historical monthly SPEI, and (c) MODIS GPP observations versus EC-based GPP estimations.

et al., 1998) and ASCE (ASCE-ERWI, 2001) methods, and Figure 4.8b shows the daily ET values by notched boxplots (95% confidence interval). In Figure 4.8a, we illustrate the daytime course of ET during four days in August 2016 (clear and cloudy conditions). The modeled ETr tended to overestimate the ETa fluctuations, especially for ETr (ASCE). The ETa flux lags during sunshine hours and is suppressed prior to sunset, particularly on sunny days. It is important to note that the general ETr models of FAO56 and ASCE do not account for a surface-normal correction of solar

radiation by default.

The linear fitting of the available half-hourly data exhibits good closure (slope) between ETa and ETr (FAO56) but confirms that ETr (ASCE) is overestimated; however, both show similar regression coefficients.

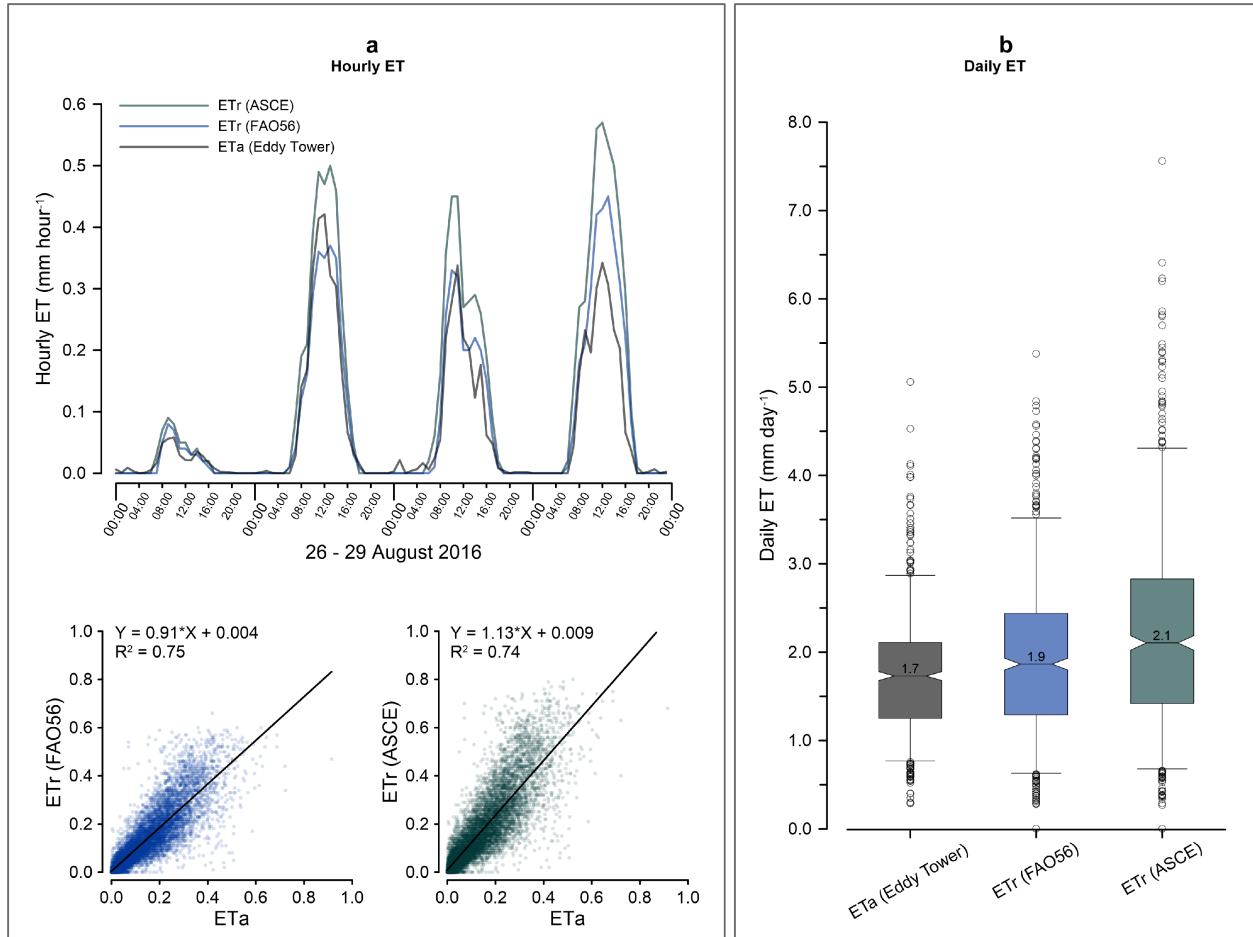


Figure 4.8: Comparison of hourly ETa and ETr based on scatterplots with linear fitting and an example of ET curves for 4 days in August 2016 (a) and of daily ET notched boxplots (95% confidence interval) (b).

Daily means of ET for the 2-year period were measured to be: ETa = 1.74 ± 0.28 mm day⁻¹ (max. = 5.1, min. = 0.3), ETr (FAO56) = 1.93 ± 0.42 mm day⁻¹ (max. = 5.4, min. = 0.0), and ETr (ASCE) = 2.23 ± 0.49 mm day⁻¹ (max. = 7.6, min. = 0.3). Therefore, the values were overestimated by 10.6% and 27.9% for the FAO56 and ASCE ETr methods, respectively. Median values (Fig. 4.8b) are similar to the average values, but the 25th and 75th percentiles and their corresponding upper whiskers (maximum values) and outliers show larger ranges in the ETr outputs. Carrillo-

4 Net ecosystem exchange and evapotranspiration

Rojas et al. (2016) reported average daily ETa values of 1.64 ± 0.47 mm day⁻¹ to 2.27 ± 0.63 mm day⁻¹ (representing the wet period and less humid period, respectively) for remotely sensed ETa maps, calculated using an energy balance based model (with Landsat imagery) of a nearby páramo catchment (Quinoas-Cajas). Córdova et al. (2015) calculated daily estimates of ETr (FAO56) of 1.89 mm day⁻¹ for Quinoas-Cajas and 1.98 mm day⁻¹ for Zhurucay by applying similar meteorological instruments in 2011 to 2013. Table 4.5 shows the ETa and ETr daily averages and aggregated monthly and annual estimates for the full period and for wet and less humid months. The respective Kc coefficients are also shown.

Table 4.5: Daily, monthly and annual ET estimates with standard deviations, and crop coefficients (Kc) for the FAO56 and ASCE ETr models.

	ETa (Eddy Tower)	ETr FAO56	ETr ASCE	Kc FAO56	Kc ASCE
Daily ET Average (mm day ⁻¹)	1.74±0.28	1.93±0.42	2.23±0.49	0.9	0.78
Wet Period Daily Avg. ¹	1.73±0.26	1.86±0.56	2.12±0.37	0.93	0.82
Less humid Period Daily Avg. ²	1.75±0.31	2.01±0.51	2.37±0.59	0.87	0.74
Difference Wet vs. Less humid (%)	1.30%	8.00%	12.10%		
Monthly ET Average (mm month ⁻¹)	52.89±8.48	58.50±12.72	67.67±15.08	0.9	0.78
Wet Period Monthly Avg. ¹	52.41±8.17	56.40±10.26	64.18±11.87	0.93	0.82
Less humid Period Monthly Avg. ²	53.57±8.85	61.45±15.04	72.57±17.53	0.87	0.74
Difference Wet vs. Less humid (%)	2.20%	9.00%	13.10%		
First Year Aggregated ET (mm year ⁻¹)	643.69	709.76	831.8	0.91	0.77
Second Year Aggregated ET (mm year ⁻¹)	625.68	694.23	792.36	0.9	0.79

¹ Wet period considered: January, February, March, April, May, June and October.

² Less humid period considered: July, August, September, November and December.

For the 2-year study period, ETa had a mean of 634.7 ± 9.0 mm per year, a lower value than the ETr sums (ETr (FAO56) mean = 702.0 ± 7.8 mm per year, and ETr (ASCE) mean = 812.1 ± 19.8 mm per year). Compared to the mean annual rain depth (1237.9 ± 3.8 mm per year), ETa accounts for 51% of the precipitation. However, this estimate may not be definitive due to limitations and uncertainties in the tipping bucket technique (TB), as was demonstrated by Padrón et al. (2015) using 3 years (2011-2014) of rainfall observations in Zhurucay. The authors showed that low-resolution techniques, such as the TB (0.1 mm), can underestimate the total rainfall catch by up to

15% compared to a high-resolution optical technique, such as a laser disdrometer (0.01 mm), which detects drizzle contributions with great accuracy. Unfortunately, this instrument was not available for our study period. Mosquera et al. (2015) showed a slightly lower water balance-based ETa result (580 mm year⁻¹) and a ratio over rainfall of 44.6% for the head microcatchment (M2) of Zhurucay (the location of our eddy tower).

The differences between the observed ETa values and the ETr estimates can be mainly attributed to the characteristics of the ETr algorithms. These characteristics include: (i) the sensitivity of ETr to the climatic variables, (ii) the method of estimation of solar energy components (particularly for Rn), and (iii) other factors, such as the crop model characteristics (e.g., canopy height, aerodynamical properties, etc.) or factors related to time-aggregation (Córdova et al., 2013). Therefore, calibrating the ETr models to better fit the tussock grass physiology and páramo environment is necessary. The full period Kc (FAO56) mean = 0.90 is higher than those values reported by (i) Buytaert et al. (2006a) (Kc = 0.42), based on an intra-annual water balance of a small Ecuadorian páramo catchment (Huagrauma) and by (ii) Iñiguez et al. (2016) (Kc = 0.67), based on a model simulation of a nearby páramo grassland area (Calluancay). The full period Kc (ASCE) mean = 0.78 is slightly lower than those reported by Carrillo-Rojas et al. (2016) in the form of the Reference Evapotranspiration Fraction ETrf (ASCE ETr Kc equivalent) for tussock grasslands of the Quinoas-Cajas (ETrf = 0.86 from Landsat-based ET mapping). Therefore, the ETr (FAO56) method and its Kc can be used for the prediction of ETa values in ecosystem analyses and water management applications.

The monthly water balance (the difference between P and ETa), as well as monthly rainfall and ETa, are presented in Figure 4.9.

As expected, during the wet months of January, February, March, April, and May of the complete period of analysis we found a stronger positive balance (i.e., a surplus of water from the precipitation income). Surprisingly, however, for October 2016 (normally a rainy month, 6-year avg. = 95.3 mm month⁻¹), the balance result was negative (-8.8 mm month⁻¹). The latter can be attributed to the presence of short and heavy showers with considerable solar radiation in between, in contrast to other years that had consistent stratiform rainfall and an increment of cloudiness. For the months of August and November, a water deficit is clearly evident. These findings aid our understanding of potential water limitations and their occurrence in the páramo.

Finally, a review of the daily and annual ETa values retrieved from similar high-elevation (alpine) grasslands around the globe is illustrated in Table 4.6.

An analysis of Table 4.6 shows that Tibetan alpine meadows have ETa/Rain ratios of between

4 Net ecosystem exchange and evapotranspiration

Table 4.6: Annual and daily ETa comparisons among alpine grasslands around the globe.

Location (Country)	Elev. m a.s.l.	Lat./ Long.	Type	Rain (mm year ⁻¹)	Annual ET (mm year ⁻¹)	Daily ET (mm day ⁻¹)	ET Method ¹	Reference
Tibetan Kobresia pastures (China)	4410	31.26 N / 92.1 E	Alpine Meadow	430	300	1.90 ³ 4.00 ~ 6.00 ⁴	EC,LYS, MOD	Coners et al. (2016)
Zhurucay Páramo (Ecuador)	3765	3.06 S / 79.24 W	Alpine Tundra	1238	635	1.74	EC	(Present study)
Niwot Ridge (USA)	3500	40.05 N / 105.58 W	Alpine Tundra	1072	631	-	EC	Knowles et al. (2015b)
Qinghai- Tibetan Plateau (China)	3250	37.58 N / 101.33 E	Alpine Meadow	642 ²	391 ²	1.90~2.22 ⁵	EC	Gu et al. (2008)
Swiss Central Alps (Switzerland)	2440	46.56 N / 8.41 E	Alpine Grassland	1900	-	3.70	AT,LYS	van den Bergh et al. (2013)

¹ ET Method: EC = Eddy Covariance, LYS = Lysimeter; AT = Atmometer evaporation, MOD = Model Based.

² Averaged during 2002 to 2004 for the Qinghai-Tibetan Plateau site

^{3,4} Respective values for dry and humid summer in the Tibetan Kobresia pastures

⁵ Values for the growing season in the Qinghai-Tibetan Plateau

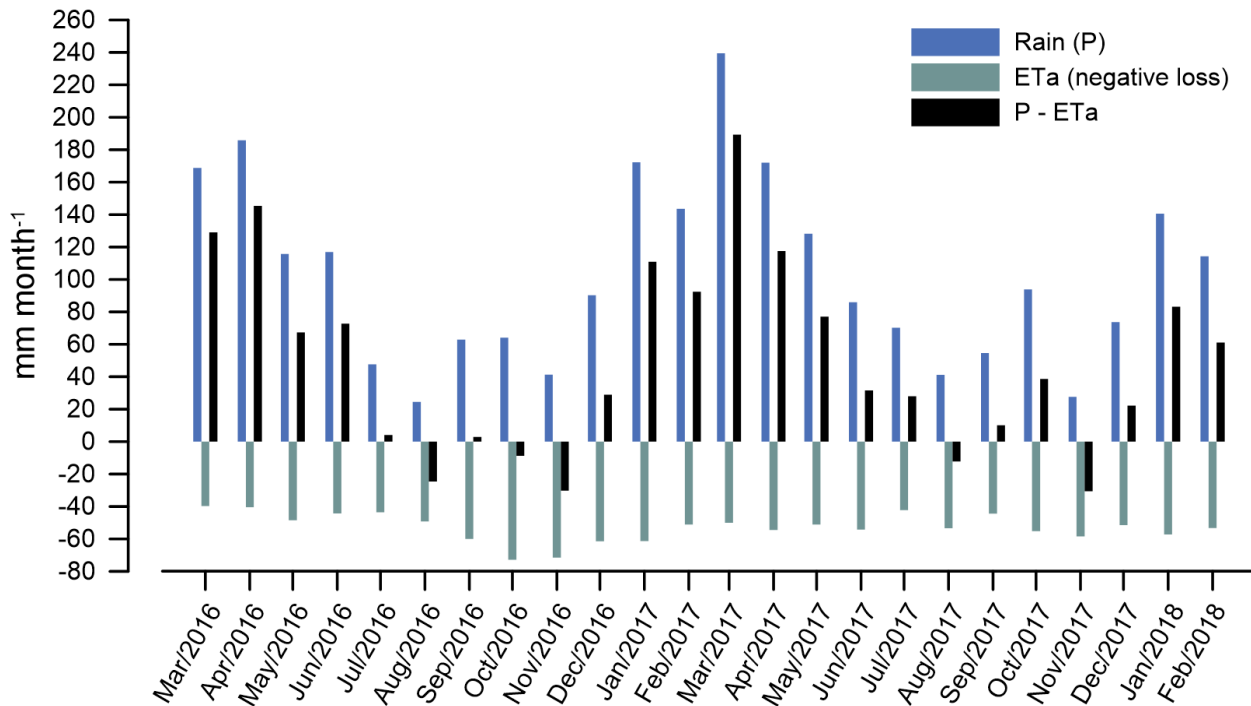


Figure 4.9: Water Balance (P-ETa) at monthly scales.

0.60 and 0.70 and that the North American alpine tundra has a ratio of 0.58, all three of which are higher than that of our study area (0.51). Therefore, the humid páramo experienced a diminished loss of water by evaporative processes. This is corroborated by lower levels of daily ETa loss in our study area relative to those from other locations. Figure 4.16 in the supplementary material depicts ETa, rainfall, VPD and Rn daily time series for the study period.

4.4 Concluding Remarks

Knowledge gaps pertaining to CO₂ exchange, ETa processes and their interactions with microclimates of tropical high mountain grasslands motivated us to install the first EC tower in the highest vegetated frontier of the tropics: the Andean páramo. Our investigation provides insight into carbon / water flux behaviors at different time scales and under different climatic conditions.

The identified CO₂ budget shows that ecosystem respiration levels exceed productivity levels most of the time (66%); this outcome, in an annual balance, doubtlessly renders the Zhurucay páramo a C source. However, a long observational period is needed in future investigations to

4 Net ecosystem exchange and evapotranspiration

confirm the hypothesis that this location (and other páramo sites) mostly act as C sources under current climatic conditions and to understand their intra- and interannual sink / source strength. The C balance found is mainly controlled by low levels of solar energy (which limits the photosynthesis of the available biomass) via climatic controls such as low temperatures and high soil moisture and by the elevated diurnal and nocturnal respiration rates. The CO₂ light and temperature-response equations parameterized in this study will contribute to future studies on páramo EC-ungauged sites. However, the accuracy of these equations would benefit from a parameterization based on long-term data. The páramo showed limitations of C sequestration analogous to those of other high-elevation (alpine grasslands) and high-latitude (tundra) sites. However, some investigations exclusively based on soil or plant-level observations and shorter-term monitoring have suggested that this ecosystem is a CO₂ sink (Bremer et al., 2016; Farley et al., 2013; McKnight et al., 2017; Minaya et al., 2016).

Tonneijck et al. (2010) demonstrated that the C content of the páramo soils is exceptional (87 ± 12 kgC m⁻², up to 200 cm depth), especially in the ectorganic horizon (31 ± 23 kgC m⁻²). If we consider a hypothetical steady loss of 0.099 kgC m⁻² per year (our mean annual NEE), the ectorganic-layer C stock in Zhurucay would be depleted in 313 ± 232 years. Such a hypothetical situation could be worsened in climate change scenarios in which SOM degradation increases due to temperature increases (microorganism-activity acceleration) and rainfall levels diminish (soil drying) (Buytaert et al., 2011), and in which the CO₂ fertilization effect (industrial-era) could be reduced due to extreme weather conditions, as suggested by Obermeier et al. (2017) for temperate C3 grasses. In the páramo, land use / cover-change scenarios can affect the water retention capacities of soil (e.g., increasing ET losses and water transit time) (Crespo et al., 2010; Mosquera et al., 2016b) but can also alter C dynamics and lead to irreversible changes in the hydrophilic characteristics of Andosols (favored by drying effects) (Poulenard et al., 2003). For instance, a detailed examination of the effects of climate change in the northern tropical Andes highlands by Vuille et al. (2018) projected severe shrinkages of glaciers and negative impacts on water supplies for the lowlands. Hence, a deeper understanding of effects of global-warming on large subnival ecosystems such as the páramo is also required.

To our knowledge, we present the first ET_a and crop coefficients for Andean tussock grasslands, retrieved from a reliable H₂O vapor-detection technique and two widely used ETr models. These indicators are highly sought after in research on climate change, ecosystem services and water management in the Inter-Andean valleys (Célleri and Feyen, 2009; Hamel et al., 2017) and will help the scientific community and stakeholders consider near-real losses from evaporative processes in water balances in this fragile ecosystem. Our study introduces novel and relevant data on land-

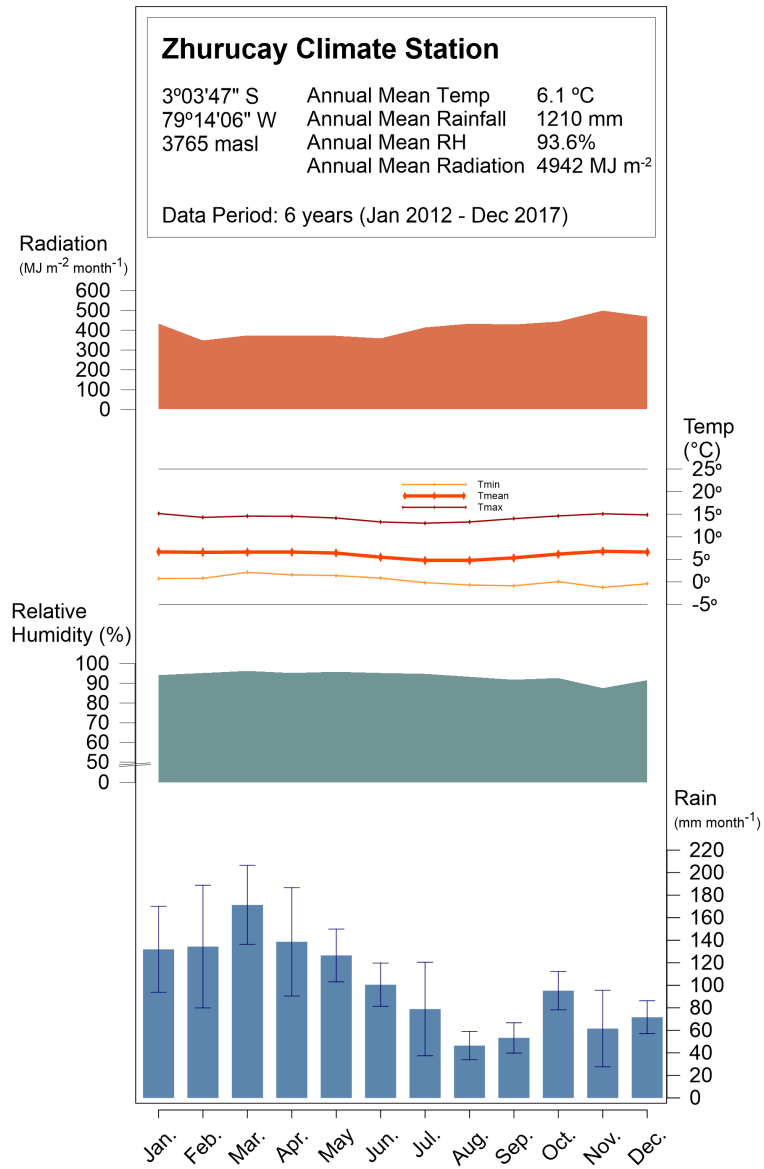
atmosphere exchange processes in the high tropics, similar to other pioneering investigations of torrid-zone mountains (Cullen et al., 2007; Holwerda et al., 2006; Ibrom et al., 2008; Litt et al., 2015). The preservation of the pristine vegetation, soil and hydrology of the Andean páramo is crucial for preventing major losses in C storage and water, which have irreversible consequences for the páramo's ecosystem services.

Future works should pursue (i) the long-term EC monitoring of carbon / water fluxes to analyze interactions between drought and extremely humid periods at interannual time scales; (ii) the evaluation and improved parameterization of C light-response equations and Kc reported here, based on long-term flux datasets, (iii) the prediction of C, energy and water fluxes based on land surface-atmosphere models at landscape and regional scales, with a specific calibration of their soil and vegetation parameters; and (vi) the characterization of the effects of similar greenhouse gases, such as methane, which can be highly abundant in these soils and wetlands.

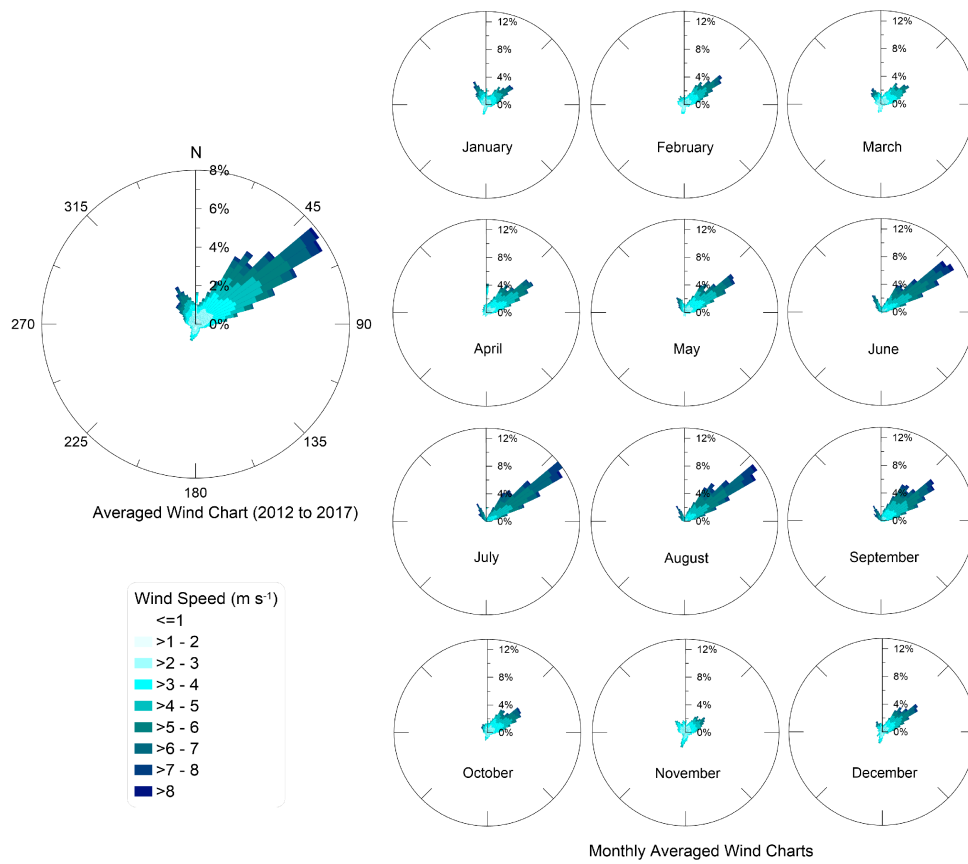
Acknowledgements

This work was funded by the Research Office of the University of Cuenca (DIUC) through the Project XIII-Conc: "Estudio Comparativo de Métodos de Estimación de Evapotranspiración Actual en Suelos Húmedos de una Micro cuenca de Páramo Andino", and by the Ecuadorian Secretary of Higher Education, Science, Technology and Innovation (SENESCYT) through "Programa de Fortalecimiento de las Capacidades en Ciencia, Tecnología, Investigación e Innovación de las Instituciones de Educación Superior Públicas (2013-2014)". We thank these institutions for providing generous funding. The first author especially thanks SENESCYT and the Ecuadorian Government for funding his doctoral scholarship. We thank the German Research Foundation (DFG) and PAK823-825 "Platform for Biodiversity and Ecosystem Monitoring and Research in South Ecuador" Subproject C6 (BE1780/38-1), which supported the study in human and scientific capacities. We also thank Comuna Chumblín Sombredas (Azuay, San Fernando) for providing logistical support, and the National Institute of Meteorology and Hydrology of Ecuador (INAMHI) for providing the El Labrado long-term dataset. We are grateful to Johanna Orellana for her valuable support of the computational implementation; to Mario Córdova, Patricio Crespo, Paúl Muñoz, Olmedo Pauta, Ana Ochoa, Santiago González, Alex Avilés, Lenin Campozano and Wilson Reinoso; and to Juan Pablo Córdova for his professional support in the graphical abstract design. Finally, we thank the editor Prof. Dr. Tim J. Griffis and two anonymous reviewers for their valuable criticism and constructive comments.

Supplementary material



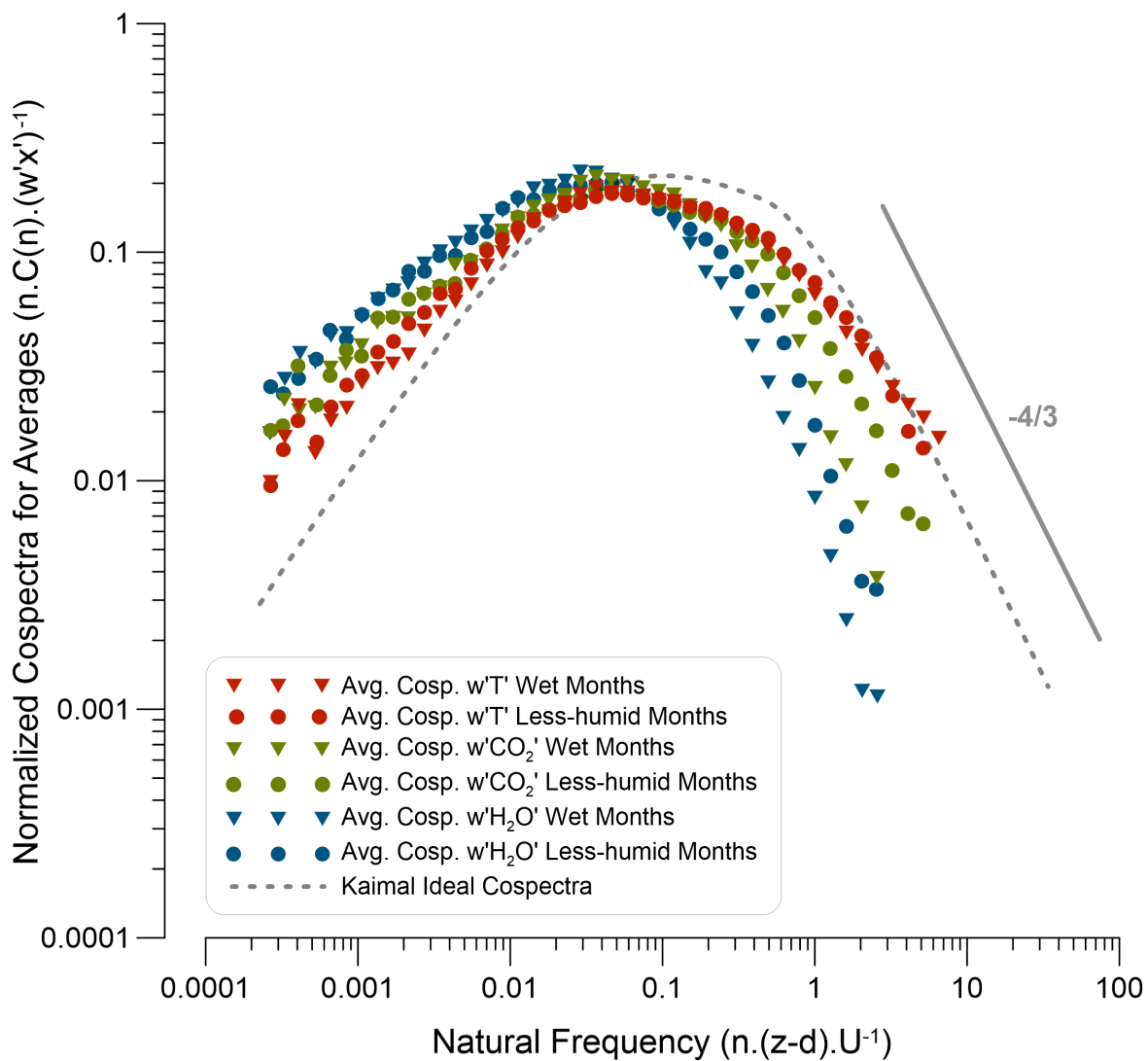
Supplementary Figure 4.10: Monthly climograph for the Zhurucay Ecohydrological Observatory (January 2012 to December 2017)



Supplementary Figure 4.11: 6-year annual and monthly wind charts (2012-2017) for the Zhurucaiy Ecohydrological Observatory.

Annex S1. Normalized ensemble-averaged hourly co-spectra analysis

Using data from a less humid season (JJA 2016) and a wet season (MAM 2016) of the EC experiment period, the normalized ensemble-averaged hourly cospectra binned by frequency for vertical fluxes (sonic temperature (T), CO₂ and H₂O) are plotted in Figure 4.12, wherein the ideal cospectral curve derived from Kaimal et al. (1972) formulae (with a 4/3 exponent) is shown for comparative purposes.



Supplementary Figure 4.12: Cospectra binned by frequency for T, CO₂ and H₂O for wet and less humid months.

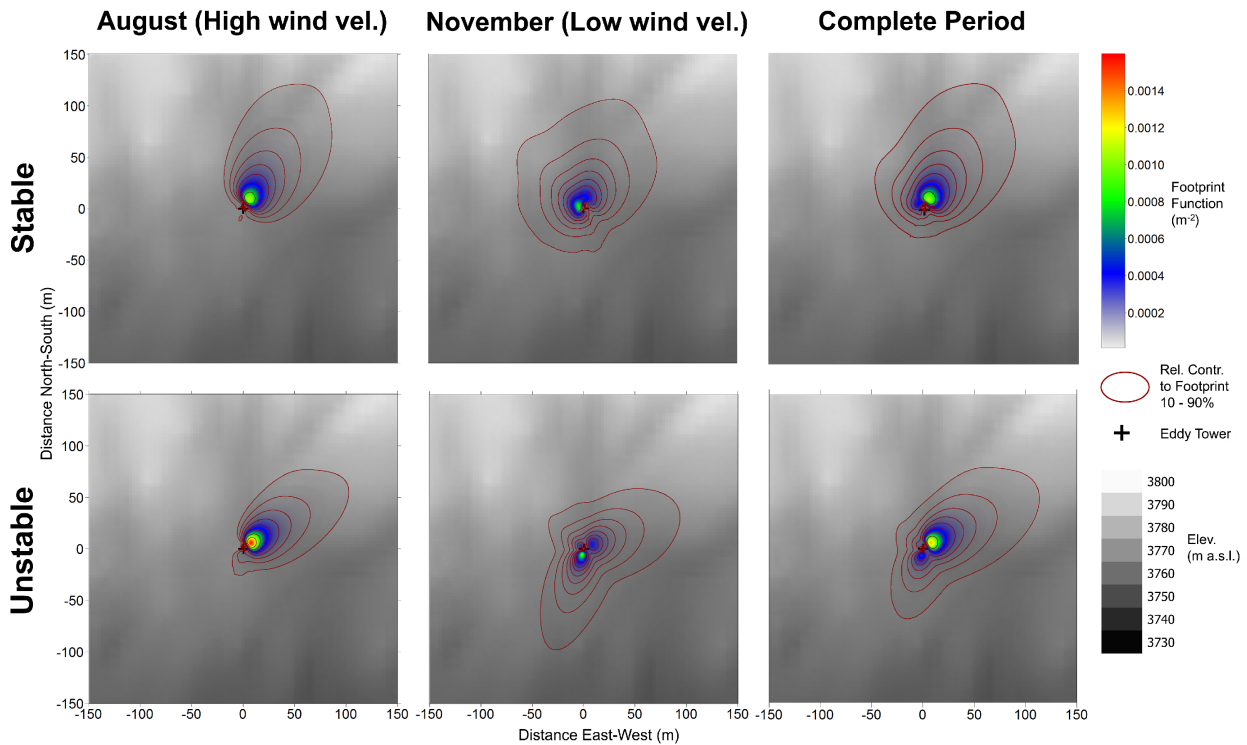
The curves for the CO₂ and H₂O fluxes (for unstable atmospheric conditions in wet and less humid months) fit typical cospectral shapes for a closed-path system (i.e., we did not encounter issues such as insufficient intake flows and noisy frequency signals) following [Burba \(2013\)](#). Hence, the attenuation of water vapor and CO₂ in the inlet components of the EC IRGA (rain cap, filter, tubing and measurement cell) was properly corrected according the method developed by [Fratini et al. \(2012\)](#).

Annex S2. Footprint climatology

A Flux Footprint Prediction (FFP) was conducted following [Kljun et al. \(2015\)](#) to detect and exclude flux sources from the nongrass neighboring vegetation species and to analyze the spatial origins of the flux in relation to patterns of wind seasonality. This tool does not simulate spatiotemporal-explicit flows and scalar source / sink distributions, but it assumes stationarity across the EC measurement integration and the horizontal homogeneity of flows. Previously, atmospheric stratification patterns were analyzed and FFP was limited to stable and unstable conditions. FFP climatological features were analyzed in a selected domain (150 x 150 m), in which Relative Contributions to the Total Footprint Area (Rc) were calculated for each 1x1 m cell and their percentages were visually estimated, with continuous isolines in steps of 10%, from 10 to 90%. The Footprint Function (Fc), which is an expression of the flux density (per unit area), was also given in m⁻². [Figure 4.13](#) illustrates the FFP retrieved from footprint averages (30-min time step) for the period of analysis for a windy month (Aug 2016-17) and for a low-wind month (Nov 2016-17).

Stable and unstable atmospheric stratifications were present, with an occurrence of 40.2% and 59.4%, respectively (neutral < 0.4%). During the windy month, noticeable unidirectional fluxes emerged from the northeast. On the other hand, omni-directional contributions converge within a smaller footprint during the low-wind month. Finally, FFP for the complete period exhibits unidirectional flux (northeast) with minor contributions from the southwest resulting from the average data for low wind speed months. These findings are consistent with the annual and monthly wind variability shown in [Figure 4.11](#). In addition, Fc levels were higher during the windy month than during the low-wind month when the peak turbulence occurred approximately 20 to 30 m from the tower. Generally, 80% of the footprint is found within 100 ~ 130 m of the tower and covers an area of 1.6 ha, which is characterized by homogeneous vegetation and low levels of topographical affectation. Based on our footprint analysis, less than 2.5% of the available data were excluded from the CO₂ and H₂O flux analyses. The missing data were then gap filled.

4 Net ecosystem exchange and evapotranspiration

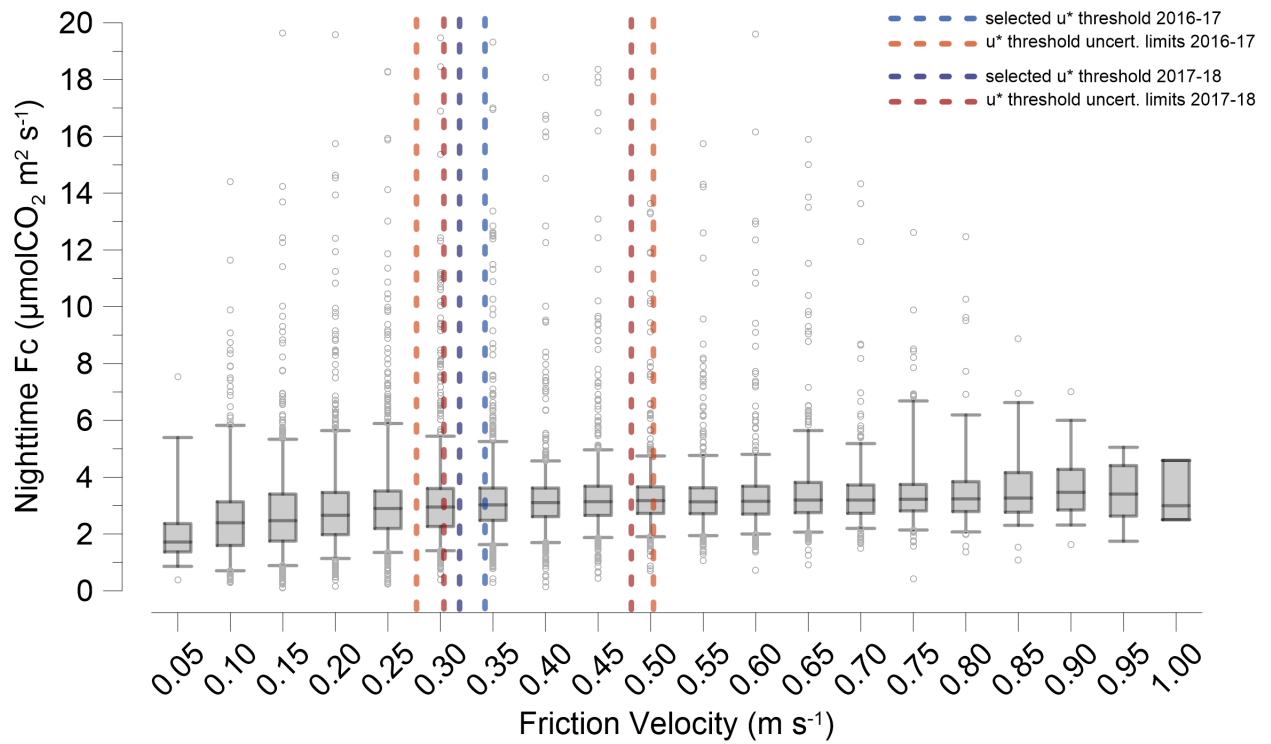


Supplementary Figure 4.13: 2D-Footprint climatology for stable and unstable stratification with wind seasonality. The centered black cross denotes the location of the EC tower. Footprint isolines (in red color) represent the percentage of R_c at intervals of 10% for 10 to 90%. A background DEM (gray area; 3 m resolution) is also shown.

Annex S3. Nighttime turbulence (u^*) and its relationship to nighttime carbon fluxes

In Figure 4.14, the nighttime CO_2 fluxes exhibit a slight increase as u^* increases, especially as u^* increases from 0.0 to 0.30 m s^{-1} . The selected u^* thresholds for the low-turbulence data filtering (0.344 for the first year and 0.321 for the second year; blue dashed lines in Fig. 4.14) and the u^* threshold limits obtained from the uncertainty analysis (0.276 and 0.505 for the first year and 0.306 and 0.467 for the second year; red dashed lines in Fig. 4.14) are also shown.

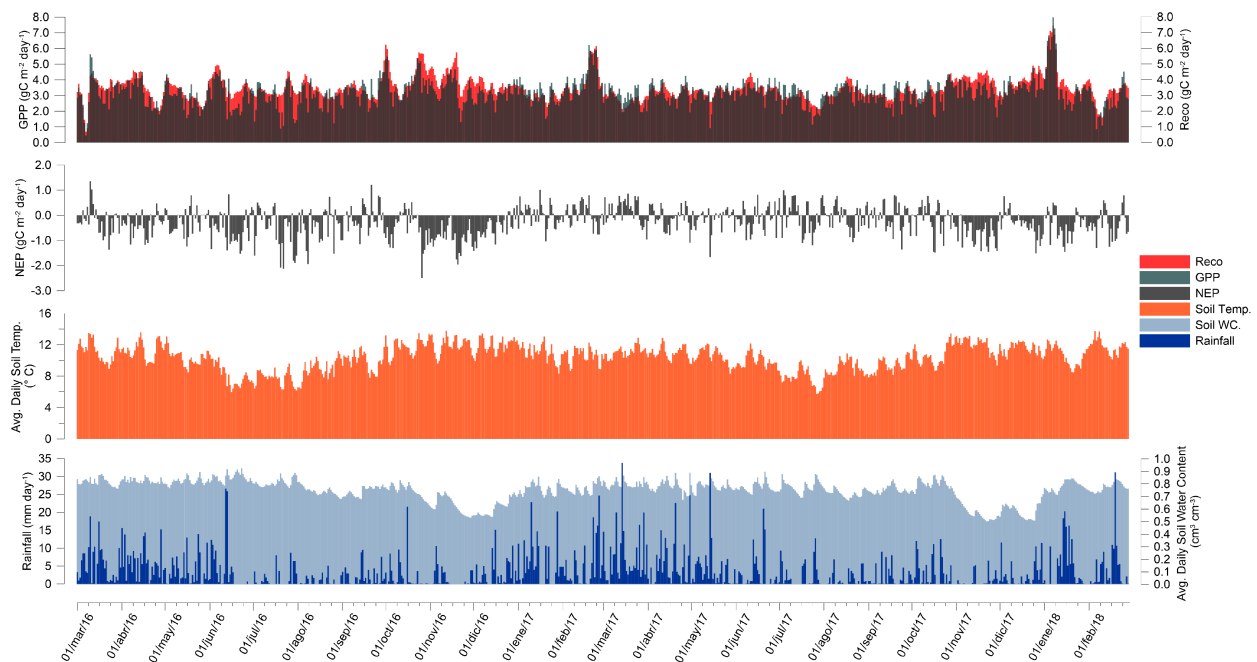
For the complete dataset (without specific temperature normalization) nighttime CO_2 fluxes associated with u^* values $>0.35 \text{ m s}^{-1}$ remain relative constant. Hence, it is unlikely that potential nocturnal advection can lead to a depletion of carbon fluxes in the EC control volume for our site. In summary, by applying the selected annual u^* thresholds for low-turbulent flux filtering, we reduced



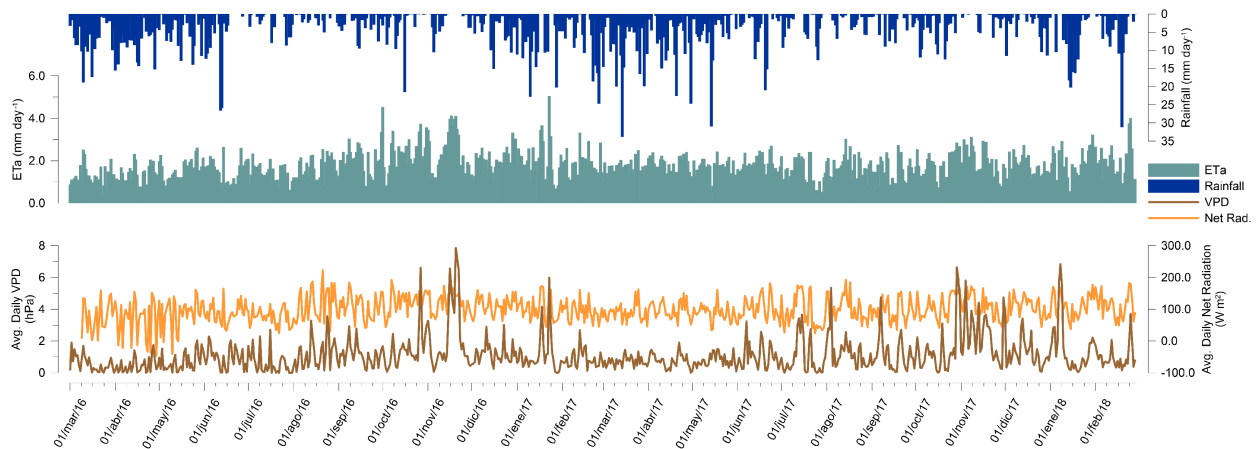
Supplementary Figure 4.14: Nighttime CO₂ fluxes versus friction velocity for the complete period (without normalization of the dataset to a specific temperature).

the possibility of underestimating the Reco in the daily, monthly and annual C balances.

4 Net ecosystem exchange and evapotranspiration



Supplementary Figure 4.15: Daily carbon fluxes (GPP, NEP and Reco) against soil temperature, soil humidity and rainfall for the full period).



Supplementary Figure 4.16: ETa (eddy tower), rainfall, VPD and net radiation for the full period.

References

- Allen, R. G., Pereira, L. S. L., Raes, D., Smith, M., and Others (1998). Crop evapotranspiration-Guidelines for computing crop water requirements-FAO Irrigation and drainage paper 56. *FAO, Rome*, 300(56):D05109.
- Aparecido, L. M. T., Teodoro, G. S., Mosquera, G., Brum, M., Barros, F. d. V., Pompeu, P. V., Rodas, M., Lazo, P.,

- Müller, C. S., Mulligan, M., Asbjornsen, H., Moore, G. W., and Oliveira, R. S. (2018). Ecohydrological drivers of Neotropical vegetation in montane ecosystems. *Ecohydrology*, page e1932.
- ASCE-ERWI (2001). ASCE's Standardized Reference Evapotranspiration Equation. In *Watershed Management and Operations Management 2000*, pages 1–11, Reston, VA. American Society of Civil Engineers.
- Aubinet, M., Vesala, T., and Papale, D. (2012). *Eddy Covariance: A Practical Guide to Measurement and Data Analysis*. Springer Netherlands, Dordrecht.
- Aucapiña, G. and Marín, F. (2014). *Efectos de la posición fisiográfica en las propiedades hidrofísicas de los suelos de páramo de la microcuenca del Río Zhurucay*. Graduate thesis, Universidad de Cuenca, Ecuador.
- Baldocchi, D., Chu, H., and Reichstein, M. (2018). Inter-annual variability of net and gross ecosystem carbon fluxes: A review. *Agricultural and Forest Meteorology*, 249(May):520–533.
- Baldocchi, D., Falge, E., Gu, L., Olson, R., Hollinger, D., Running, S., Anthoni, P., Bernhofer, C., Davis, K., Evans, R., Fuentes, J., Goldstein, A., Katul, G., Law, B., Lee, X., Malhi, Y., Meyers, T., Munger, W., Oechel, W., Paw, K. T., Pilegaard, K., Schmid, H. P., Valentini, R., Verma, S., Vesala, T., Wilson, K., and Wofsy, S. (2001). FLUXNET: A New Tool to Study the Temporal and Spatial Variability of Ecosystem-Scale Carbon Dioxide, Water Vapor, and Energy Flux Densities. *Bulletin of the American Meteorological Society*, 82(11):2415–2434.
- Baldocchi, D. D. (2003). Assessing the eddy covariance technique for evaluating carbon dioxide exchange rates of ecosystems: past, present and future. *Global Change Biology*, 9(4):479–492.
- Beer, C., Reichstein, M., Tomelleri, E., Ciais, P., Jung, M., Carvalhais, N., Rodenbeck, C., Arain, M. A., Baldocchi, D., Bonan, G. B., Bondeau, A., Cescatti, A., Lasslop, G., Lindroth, A., Lomas, M., Luysaert, S., Margolis, H., Oleson, K. W., Rouspard, O., Veenendaal, E., Viovy, N., Williams, C., Woodward, F. I., and Papale, D. (2010). Terrestrial Gross Carbon Dioxide Uptake: Global Distribution and Covariation with Climate. *Science*, 329(5993):834–838.
- Beguiría, S., Vicente-Serrano, S. M., Reig, F., and Latorre, B. (2014). Standardized precipitation evapotranspiration index (SPEI) revisited: parameter fitting, evapotranspiration models, tools, datasets and drought monitoring. *International Journal of Climatology*, 34(10):3001–3023.
- Beltrán, K., Salgado, S., Cuesta, F., León-Yáñez, S., Romoleroux, K., Ortiz, E., Cardenas, A., and Velástegui, A. (2009). Distribución espacial, sistemas ecológicos y caracterización florística de los páramos en el Ecuador. *EcoCiencia*, pages 72–150.
- Bendix, J., Homeier, J., Cueva Ortiz, E., Emck, P., Breckle, S. W., Richter, M., and Beck, E. (2006). Seasonality of weather and tree phenology in a tropical evergreen mountain rain forest. *International Journal of Biometeorology*, 50(6):370–384.
- Bendix, J., Rollenbeck, R., Ritcher, M., Fabian, P., and Emck, P. (2008). Climate. In Beck, E., Bendix, J., Kottke, I., Makeschin, F., Mosandl, R., editor, *Gradients in a Tropical Mountain Ecosystem of Ecuador. Ecological Studies*, volume 198, chapter Climate, pages 63–74. Springer Verlag, Berlin, Germany.
- Beringer, J., Hutley, L. B., McHugh, I., Arndt, S. K., Campbell, D., Cleugh, H. A., Cleverly, J., Resco de Dios, V., Eamus, D., Evans, B., Ewenz, C., Grace, P., Griebel, A., Haverd, V., Hinko-Najera, N., Huete, A., Isaac, P., Kanniah,

4 Net ecosystem exchange and evapotranspiration

- K., Leuning, R., Liddell, M. J., Macfarlane, C., Meyer, W., Moore, C., Pendall, E., Phillips, A., Phillips, R. L., Prober, S. M., Restrepo-Coupe, N., Rutledge, S., Schroder, I., Silberstein, R., Southall, P., Yee, M. S., Tapper, N. J., van Gorsel, E., Vote, C., Walker, J., and Wardlaw, T. (2016). An introduction to the Australian and New Zealand flux tower network - OzFlux. *Biogeosciences*, 13(21):5895–5916.
- Bertzky, M., Ravillous, M., Araujo-Navas, A., Kapos, V., Carrión, D., Chiu, M., and Dickson, B. (2010). Carbon, biodiversity and ecosystem services: Exploring co-benefits. page 20.
- Bremer, L., Farley, K., Chadwick, O., and Harden, C. (2016). Changes in carbon storage with land management promoted by payment for ecosystem services. *Environmental Conservation*, 43(04):397–406.
- Burba, G. (2013). *Eddy Covariance Method-for Scientific, Industrial, Agricultural, and Regulatory Applications*. LI-COR Biosciences, Lincoln, Nebraska, USA.
- Buytaert, W., Célleri, R., De Bièvre, B., Cisneros, F., Wyseure, G., Deckers, J., and Hofstede, R. (2006a). Human impact on the hydrology of the Andean páramos. *Earth-Science Reviews*, 79(1-2):53–72.
- Buytaert, W., Cuesta-Camacho, F., and Tobón, C. (2011). Potential impacts of climate change on the environmental services of humid. *Global Ecology and Biogeography*, 20(1):19–33.
- Buytaert, W., Deckers, J., and Wyseure, G. (2006b). Description and classification of nonallophanic Andosols in south Ecuadorian alpine grasslands (páramo). *Geomorphology*, 73(3-4):207–221.
- Cabral, O. M., da Rocha, H. R., Gash, J. H., Freitas, H. C., and Ligo, M. A. (2015). Water and energy fluxes from a woodland savanna (cerrado) in southeast Brazil. *Journal of Hydrology: Regional Studies*, 4(PB):22–40.
- Cabral, O. M., da Rocha, H. R., Gash, J. H., Ligo, M. A., Freitas, H. C., and Tatsch, J. D. (2010). The energy and water balance of a Eucalyptus plantation in southeast Brazil. *Journal of Hydrology*, 388(3-4):208–216.
- Carrillo-Rojas, G., Silva, B., Córdova, M., Célleri, R., and Bendix, J. (2016). Dynamic Mapping of Evapotranspiration Using an Energy Balance-Based Model over an Andean Páramo Catchment of Southern Ecuador. *Remote Sensing*, 8(2):160.
- Célleri, R. and Feyen, J. (2009). The Hydrology of Tropical Andean Ecosystems: Importance, Knowledge Status, and Perspectives. *Mountain Research and Development*, 29(4):350–355.
- Célleri, R., Willems, P., Buytaert, W., and Feyen, J. (2007). Space-time rainfall variability in the Paute basin, Ecuadorian Andes. *Hydrological Processes*, 21(24):3316–3327.
- Chapin, F. S., Woodwell, G. M., Randerson, J. T., Rastetter, E. B., Lovett, G. M., Baldocchi, D. D., Clark, D. A., Harmon, M. E., Schimel, D. S., Valentini, R., Wirth, C., Aber, J. D., Cole, J. J., Goulden, M. L., Harden, J. W., Heimann, M., Howarth, R. W., Matson, P. A., McGuire, A. D., Melillo, J. M., Mooney, H. A., Neff, J. C., Houghton, R. A., Pace, M. L., Ryan, M. G., Running, S. W., Sala, O. E., Schlesinger, W. H., and Schulze, E.-D. (2006). Reconciling Carbon-cycle Concepts, Terminology, and Methods. *Ecosystems*, 9(7):1041–1050.
- Coners, H., Babel, W., Willinghöfer, S., Biermann, T., Köhler, L., Seeber, E., Foken, T., Ma, Y., Yang, Y., Mieke, G., and Leuschner, C. (2016). Evapotranspiration and water balance of high-elevation grassland on the Tibetan Plateau.

- Journal of Hydrology*, 533:557–566.
- Córdova, M., Carrillo-Rojas, G., and Célleri, R. (2013). Errores en la estimación de la evapotranspiración de referencia de una zona de páramo andino debido al uso de datos mensuales, diarios y horarios. *Aqua-LAC*, 5(2):14–22.
- Córdova, M., Carrillo-Rojas, G., Crespo, P., Wilcox, B., and Célleri, R. (2015). Evaluation of the Penman-Monteith (FAO 56 PM) Method for Calculating Reference Evapotranspiration Using Limited Data. *Mountain Research and Development*, 35(3):230–239.
- Córdova, M., Célleri, R., Shellito, C. J., Orellana-Alvear, J., Abril, A., and Carrillo-Rojas, G. (2016). Near-Surface Air Temperature Lapse Rate Over Complex Terrain in the Southern Ecuadorian Andes: Implications for Temperature Mapping. *Arctic, Antarctic, and Alpine Research*, 48(4):673–684.
- Correa, A., Windhorst, D., Crespo, P., Célleri, R., Feyen, J., and Breuer, L. (2016). Continuous versus event-based sampling: how many samples are required for deriving general hydrological understanding on Ecuador's páramo region? *Hydrological Processes*, 30(22):4059–4073.
- Correa, A., Windhorst, D., Tetzlaff, D., Crespo, P., Célleri, R., Feyen, J., and Breuer, L. (2017). Temporal dynamics in dominant runoff sources and flow paths in the Andean Páramo. *Water Resources Research*, 53(7):5998–6017.
- Crespo, P., Célleri, R., Buytaert, W., Feyen, J., Iñiguez, V., Borja, P., and De Bièvre, B. (2010). Land use change impacts on the hydrology of wet Andean páramo ecosystems. In *Proceedings of the Workshop Status and Perspectives of Hydrology in Small Basins, held at Goslar-Hahnenklee, Germany, 30 March to 2 April 2009*, number APRIL, page 6, Germany. IAHS Publ. 336.
- Cuesta, F. and De Bièvre, B. (2008). Páramo of Northern Andes (Venezuela, Colombia, Ecuador, northern Perú). In *Temperate Grasslands of South America*, pages 3–11, Hohhot, China. The World Temperate Grasslands Conservation Initiative Workshop.
- Cullen, N. J., Mölg, T., Kaser, G., Steffen, K., and Hardy, D. R. (2007). Energy-balance model validation on the top of Kilimanjaro, Tanzania, using eddy covariance data. *Annals of Glaciology*, 46(1):227–233.
- Curiel Yuste, J., Hereñú, A.-M., Ojeda, G., Paz, A., Pizano, C., García-Angulo, D., and Lasso, E. (2017). Soil heterotrophic CO₂ emissions from tropical high-elevation ecosystems (Páramos) and their sensitivity to temperature and moisture fluctuations. *Soil Biology and Biochemistry*, 110:8–11.
- Damm, A., Elbers, J. A., Erler, A., Gioli, B., Hamdi, K., Hutjes, R., Kosvancova, M., Meroni, M., Miglietta, F., Moersch, A., Moreno, J., Schickling, A., Sonnenschein, R., Udelhover, T., Van Der Linden, S., Horstet, P., and Rascher, U. (2010). Remote sensing of sun-induced fluorescence to improve modeling of diurnal courses of gross primary production (GPP). *Global Change Biology*, 16(1):171–186.
- Duffie, J. A. and Beckman, W. A. (2013). *Solar Engineering of Thermal Processes*. Wiley Interscience, New York, second edition.
- Emck, P. (2007). *A Climatology of South Ecuador-With special focus on the Major Andean Ridge as Atlantic-Pacific Climate Divide*. Phd thesis, Friedrich Alexander-Universität, Erlangen-Nürnberg, Germany.

4 Net ecosystem exchange and evapotranspiration

- Euskirchen, E. S., Bret-Harte, M. S., Shaver, G. R., Edgar, C. W., and Romanovsky, V. E. (2017). Long-Term Release of Carbon Dioxide from Arctic Tundra Ecosystems in Alaska. *Ecosystems*, 20(5):960–974.
- Falge, E., Baldocchi, D., Olson, R., Anthoni, P., Aubinet, M., Bernhofer, C., Burba, G., Ceulemans, R., Clement, R., Dolman, H., Granier, A., Gross, P., Grünwald, T., Hollinger, D., Jensen, N.-O., Katul, G., Keronen, P., Kowalski, A., Lai, C. T., Law, B. E., Meyers, T., Moncrieff, J., Moors, E., Munger, J., Pilegaard, K., Rannik, Ü., Rebmann, C., Suyker, A., Tenhunen, J., Tu, K., Verma, S., Vesala, T., Wilson, K., and Wofsy, S. (2001). Gap filling strategies for defensible annual sums of net ecosystem exchange. *Agricultural and Forest Meteorology*, 107(1):43–69.
- Falge, E., Baldocchi, D., Tenhunen, J., Aubinet, M., Bakwin, P., Berbigier, P., Bernhofer, C., Burba, G., Clement, R., Davis, K. J., Elbers, J. A., Goldstein, A. H., Grelle, A., Granier, A., GuÅrmondsson, J., Hollinger, D., Kowalski, A. S., Katul, G., Law, B. E., Malhi, Y., Meyers, T., Monson, R. K., Munger, J., Oechel, W., Paw U, K. T., Pilegaard, K., Rannik, Ü., Rebmann, C., Suyker, A., Valentini, R., Wilson, K., and Wofsy, S. (2002). Seasonality of ecosystem respiration and gross primary production as derived from FLUXNET measurements. *Agricultural and Forest Meteorology*, 113(1-4):53–74.
- Farley, K. A., Bremer, L. L., Harden, C. P., and Hartsig, J. (2013). Changes in carbon storage under alternative land uses in biodiverse Andean grasslands: implications for payment for ecosystem services. *Conservation Letters*, 6(1):21–27.
- Farley, K. A., Kelly, E. F., and Hofstede, R. G. M. (2004). Soil Organic Carbon and Water Retention after Conversion of Grasslands to Pine Plantations in the Ecuadorian Andes. *Ecosystems*, 7(7):729–739.
- Finkelstein, P. L. and Sims, P. F. (2001). Sampling error in eddy correlation flux measurements. *Journal of Geophysical Research: Atmospheres*, 106(D4):3503–3509.
- Fisher, J. B., Malhi, Y., Bonal, D., Da Rocha, H. R., De Araujo, A. C., Gamo, M., Goulden, M. L., Hirano, T., Huete, A. R., Kondo, H., Kumagai, T., Loescher, H. W., Miller, S., Nobre, A. D., Nouvellon, Y., Oberbauer, S. F., Panuthai, S., Rouspard, O., Saleska, S., Tanaka, K., Tanaka, N., Tu, K. P., and Von Randow, C. (2009). The land-atmosphere water flux in the tropics. *Global Change Biology*, 15(11):2694–2714.
- Foken, T. (2008). The energy balance closure problem: An overview. *Ecological Applications*, 18(6):1351–1367.
- Fratini, G., Ibrom, A., Arriga, N., Burba, G., and Papale, D. (2012). Relative humidity effects on water vapour fluxes measured with closed-path eddy-covariance systems with short sampling lines. *Agricultural and Forest Meteorology*, 165:53–63.
- Galvagno, M., Wohlfahrt, G., Cremonese, E., Filippa, G., Migliavacca, M., Mora di Cella, U., and van Gorsel, E. (2017). Contribution of advection to nighttime ecosystem respiration at a mountain grassland in complex terrain. *Agricultural and Forest Meteorology*, 237-238:270–281.
- Grace, J., Jose, J. S., Meir, P., Miranda, H. S., and Montes, R. A. (2006). Productivity and carbon fluxes of tropical savannas. *Journal of Biogeography*, 33(3):387–400.
- Gu, S., Tang, Y., Cui, X., Du, M., Zhao, L., Li, Y., Xu, S., Zhou, H., Kato, T., Qi, P., and Zhao, X. (2008). Characterizing evapotranspiration over a meadow ecosystem on the Qinghai-Tibetan Plateau. *Journal of Geophysical Research*,

- 113(D8):D08118.
- Hamel, P., Riveros-Iregui, D., Ballari, D., Browning, T., Célleri, R., Chandler, D., Chun, K. P., Destouni, G., Jacobs, S., Jasechko, S., Johnson, M., Krishnaswamy, J., Poca, M., Pompeu, P. V., and Rocha, H. (2017). Watershed services in the humid tropics: Opportunities from recent advances in ecohydrology. *Ecohydrology*, page e1921.
- Hammerle, A., Haslwanter, A., Schmitt, M., Bahn, M., Tappeiner, U., Cernusca, A., and Wohlfahrt, G. (2007). Eddy covariance measurements of carbon dioxide, latent and sensible energy fluxes above a meadow on a mountain slope. *Boundary-Layer Meteorology*, 122(2):397–416.
- Harden, C. P., Hartsig, J., Farley, K. A., Lee, J., and Bremer, L. L. (2013). Effects of Land-Use Change on Water in Andean Páramo Grassland Soils. *Annals of the Association of American Geographers*, 103(2):375–384.
- Heinsch, F., Maosheng Zhao, Running, S., Kimball, J., Nemani, R., Davis, K., Bolstad, P., Cook, B., Desai, A., Ricciuto, D., Law, B., Oechel, W., Hyojung Kwon, Hongyan Luo, Wofsy, S., Dunn, A., Munger, J., Baldocchi, D., Liukang Xu, Hollinger, D., Richardson, A., Stoy, P., Siqueira, M., Monson, R., Burns, S., and Flanagan, L. (2006). Evaluation of remote sensing based terrestrial productivity from MODIS using regional tower eddy flux network observations. *IEEE Transactions on Geoscience and Remote Sensing*, 44(7):1908–1925.
- Helfter, C., Campbell, C., Dinsmore, K. J., Drewer, J., Coyle, M., Anderson, M., Skiba, U., Nemitz, E., Billett, M. F., and Sutton, M. A. (2015). Drivers of long-term variability in CO₂ net ecosystem exchange in a temperate peatland. *Biogeosciences*, 12(6):1799–1811.
- Herzog, S. K., Martínez, R., Jørgensen, P. M., and Tiessen, H. (2011). *Climate Change and Biodiversity in the Tropical Andes*. Inter-American Institute for Global Change Research (IAI) and Scientific Committee on Problems of the Environment (SCOPE).
- Hiller, R., Zeeman, M. J., and Eugster, W. (2008). Eddy-Covariance Flux Measurements in the Complex Terrain of an Alpine Valley in Switzerland. *Boundary-Layer Meteorology*, 127(3):449–467.
- Hofstede, R., Calles, J., López, V. V., Polanco, R., Torres, F., Ulloa, J., Vásquez, A., and Cerra, M. (2014). *Los páramos Andinos Qué Sabemos. Estado de conocimiento sobre el impacto del cambio climático en el ecosistema páramo*. UICN, Quito, Ecuador.
- Hofstede, R. G. M., Chilito, E. J. P., and Sandovals, E. M. (1995). Vegetative structure, microclimate, and leaf growth of a páramo tussock grass species, in undisturbed, burned and grazed conditions. *Vegetatio*, 119(1):53–65.
- Holwerda, F., Burkard, R., Eugster, W., Scatena, F. N., Meesters, A. G. C. A., and Bruijnzeel, L. A. (2006). Estimating fog deposition at a Puerto Rican elfin cloud forest site: comparison of the water budget and eddy covariance methods. *Hydrological Processes*, 20(13):2669–2692.
- Hribljan, J. A., Suárez, E., Heckman, K. A., Lilleskov, E. A., and Chimner, R. A. (2016). Peatland carbon stocks and accumulation rates in the Ecuadorian páramo. *Wetlands Ecology and Management*, 24(2):113–127.
- Ibrom, A., Oltchev, A., June, T., Kreilein, H., Rakkibu, G., Ross, T., Panferov, O., and Gravenhorst, G. (2008). Variation in photosynthetic light-use efficiency in a mountainous tropical rain forest in Indonesia. *Tree Physiology*, 28(4):499–508.

4 Net ecosystem exchange and evapotranspiration

- Iñiguez, V., Morales, O., Cisneros, F., Bauwens, W., and Wyseure, G. (2016). Analysis of the drought recovery of Andosols on southern Ecuadorian Andean páramos. *Hydrology and Earth System Sciences*, 20(6):2421–2435.
- Janeau, J. L., Grellier, S., and Podwojewski, P. (2015). Influence of rainfall interception by endemic plants versus short cycle crops on water infiltration in high altitude ecosystems of Ecuador. *Hydrology Research*, 46(6):1008–1018.
- Jantz, N. and Behling, H. (2012). A Holocene environmental record reflecting vegetation, climate, and fire variability at the Páramo of Quimsacocha, southwestern Ecuadorian Andes. *Vegetation History and Archaeobotany*, 21(3):169–185.
- Josse, C., Cuesta, F., Navarro, G., Barrena, V., Cabrera, E., Chacón-Moreno, E., Ferreira, W., Peralvo, M., Saito, J., and Tovar, A. (2009). *Ecosistemas de los Andes del Norte y Centro. Bolivia, Colombia, Ecuador, Perú y Venezuela*.
- Kaimal, J. C., Wyngaard, J. C., Izumi, Y., and Coté, O. R. (1972). Spectral characteristics of surface-layer turbulence. *Quarterly Journal of the Royal Meteorological Society*, 98(417):563–589.
- Kljun, N., Calanca, P., Rotach, M. W., and Schmid, H. P. (2015). A simple two-dimensional parameterisation for Flux Footprint Prediction (FFP). *Geoscientific Model Development*, 8(11):3695–3713.
- Knowles, J. F., Burns, S. P., Blanken, P. D., and Monson, R. K. (2015a). Fluxes of energy, water, and carbon dioxide from mountain ecosystems at Niwot Ridge, Colorado. *Plant Ecology & Diversity*, 8(5-6):663–676.
- Knowles, J. F., Harpold, A. A., Cowie, R., Zeliff, M., Barnard, H. R., Burns, S. P., Blanken, P. D., Morse, J. F., and Williams, M. W. (2015b). The relative contributions of alpine and subalpine ecosystems to the water balance of a mountainous, headwater catchment. *Hydrological Processes*, 29(22):4794–4808.
- Lasslop, G., Reichstein, M., Papale, D., Richardson, A. D., Arneth, A., Barr, A., Stoy, P., and Wohlfahrt, G. (2010). Separation of net ecosystem exchange into assimilation and respiration using a light response curve approach: critical issues and global evaluation. *Global Change Biology*, 16(1):187–208.
- Leuning, R., van Gorsel, E., Massman, W. J., and Isaac, P. R. (2012). Reflections on the surface energy imbalance problem. *Agricultural and Forest Meteorology*, 156:65–74.
- Litt, M., Sicart, J.-E., Helgason, W. D., and Wagnon, P. (2015). Turbulence Characteristics in the Atmospheric Surface Layer for Different Wind Regimes over the Tropical Zongo Glacier (Bolivia, 16°S). *Boundary-Layer Meteorology*, 154(3):471–495.
- Llambí, L. D., Soto-W, A., Célleri, R., Bièvre, B. D., Ochoa, B., and Borja, P. (2012). *Ecología, hidrología y suelos de páramos*. Number 1. CONDENSAN, Ecuador.
- Lloyd, J. and Taylor, J. A. (1994). On the Temperature Dependence of Soil Respiration. *Functional Ecology*, 8(3):315.
- Mauder, M. and Foken, T. (2004). *Documentation and instruction manual of the eddy covariance software package TK2*. Universität Bayreuth, Abt. Mikrometeorologie, Arbeitsergebnisse 26-44, Bayreuth, Germany.
- Mayocchi, C. and Bristow, K. (1995). Soil surface heat flux: some general questions and comments on measurements. *Agricultural and Forest Meteorology*, 75(1-3):43–50.
- McKee, T. B., Doesken, N. J., and Kleist, J. (1993). The relationship of drought frequency and duration to time

- scales. In *Proceedings of the 8th Conference on Applied Climatology*, volume 17, pages 179–183, USA. American Meteorological Society.
- McKnight, J. Y., Harden, C. P., and Schaeffer, S. M. (2017). Soil CO₂ flux trends with differences in soil moisture among four types of land use in an Ecuadorian páramo landscape. *Physical Geography*, 38(1):51–61.
- Meirelles, M. L., Bracho, R., and Ferreira, E. A. B. (2015). Carbon dioxide exchange in a tropical wet grassland. *Wetlands Ecology and Management*, 23(5):817–826.
- Mena-Vásquez, P. and Hofstede, R. (2006). Los páramos ecuatorianos. *Botánica Económica de los Andes Centrales*, pages 91–109.
- Metzger, S., Burba, G., Burns, S. P., Blanken, P. D., Li, J., Luo, H., and Zulueta, R. C. (2016). Optimization of an enclosed gas analyzer sampling system for measuring eddy covariance fluxes of H₂O and CO₂. *Atmospheric Measurement Techniques*, 9(3):1341–1359.
- Minaya, V. (2016). *Ecohydrology of the Andes Páramo Region*. Phd thesis, PhD Thesis, Delft University of Technology, The Netherlands.
- Minaya, V., Corzo, G., van der Kwast, J., and Mynett, A. E. (2016). Simulating Gross Primary Production and Stand Hydrological Processes of páramo Grasslands in the Ecuadorian Andean Region Using the Biome-BGC Model. *Soil Science*, 181(7):335–346.
- Mosquera, G. M., Célleri, R., Lazo, P. X., Vaché, K. B., Perakis, S. S., and Crespo, P. (2016a). Combined use of isotopic and hydrometric data to conceptualize ecohydrological processes in a high-elevation tropical ecosystem. *Hydrological Processes*, 30(17):2930–2947.
- Mosquera, G. M., Lazo, P. X., Célleri, R., Wilcox, B. P., and Crespo, P. (2015). Runoff from tropical alpine grasslands increases with areal extent of wetlands. *CATENA*, 125(FEBRUARY):120–128.
- Mosquera, G. M., Segura, C., Vaché, K. B., Windhorst, D., Breuer, L., and Crespo, P. (2016b). Insights into the water mean transit time in a high-elevation tropical ecosystem. *Hydrology and Earth System Sciences*, 20(7):2987–3004.
- Myers, N., Mittermeier, R. A., Mittermeier, C. G., da Fonseca, G. A. B., and Kent, J. (2000). Biodiversity hotspots for conservation priorities. *Nature*, 403(6772):853–858.
- Nagy, Z., Pintér, K., Pavelka, M., Darenová, E., and Balogh, J. (2011). Carbon fluxes of surfaces vs. ecosystems: advantages of measuring eddy covariance and soil respiration simultaneously in dry grassland ecosystems. *Biogeosciences*, 8(9):2523–2534.
- Novick, K., Brantley, S., Miniati, C. F., Walker, J., and Vose, J. (2014). Inferring the contribution of advection to total ecosystem scalar fluxes over a tall forest in complex terrain. *Agricultural and Forest Meteorology*, 185:1–13.
- Obermeier, W. A., Lehnert, L. W., Kammann, C. I., Müller, C., Grünhage, L., Luterbacher, J., Erbs, M., Moser, G., Seibert, R., Yuan, N., and Bendix, J. (2017). Reduced CO₂ fertilization effect in temperate C₃ grasslands under more extreme weather conditions. *Nature Climate Change*, 7(2):137–141.
- Ochoa-Sánchez, A., Crespo, P., and Célleri, R. (2018). Quantification of rainfall interception in the high Andean tussock

4 Net ecosystem exchange and evapotranspiration

- grasslands. *Ecohydrology*, (October 2017):e1946.
- Oechel, W. C., Laskowski, C. A., Burba, G., Gioli, B., and Kalhori, A. A. M. (2014). Annual patterns and budget of CO₂ flux in an Arctic tussock tundra ecosystem. *Journal of Geophysical Research: Biogeosciences*, 119(3):323–339.
- Olmo, F., Vida, J., Foyo, I., Castro-Diez, Y., and Alados-Arboledas, L. (1999). Prediction of global irradiance on inclined surfaces from horizontal global irradiance. *Energy*, 24(8):689–704.
- Olson, D. M., Dinerstein, E., Wikramanayake, E. D., Burgess, N. D., Powell, G. V. N., Underwood, E. C., D'Amico, J. A., Itoua, I., Strand, H. E., Morrison, J. C., Loucks, C. J., Allnutt, T. F., Ricketts, T. H., Kura, Y., Lamoreux, J. F., Wettengel, W. W., Hedao, P., and Kassem, K. R. (2001). Terrestrial Ecoregions of the World: A New Map of Life on Earth. *BioScience*, 51(11):933.
- Padrón, R. S., Wilcox, B. P., Crespo, P., and Célleri, R. (2015). Rainfall in the Andean Páramo: New Insights from High-Resolution Monitoring in Southern Ecuador. *Journal of Hydrometeorology*, 16(3):985–996.
- Papale, D., Reichstein, M., Aubinet, M., Canfora, E., Bernhofer, C., Kutsch, W., Longdoz, B., Rambal, S., Valentini, R., Vesala, T., and Yakir, D. (2006). Towards a standardized processing of Net Ecosystem Exchange measured with eddy covariance technique: algorithms and uncertainty estimation. *Biogeosciences*, 3(4):571–583.
- Pepin, N., Bradley, R. S., Diaz, H. F., Baraer, M., Caceres, E. B., Forsythe, N., Fowler, H., Greenwood, G., Hashmi, M. Z., Liu, X. D., Miller, J. R., Ning, L., Ohmura, A., Palazzi, E., Rangwala, I., Schöner, W., Severskiy, I., Shahgedanova, M., Wang, M. B., Williamson, S. N., and Yang, D. Q. (2015). Elevation-dependent warming in mountain regions of the world. *Nature Climate Change*, 5(5):424–430.
- Poulenard, J., Podwojewski, P., and Herbillon, A. J. (2003). Characteristics of non-allophanic Andisols with hydric properties from the Ecuadorian páramos. *Geoderma*, 117(3-4):267–281.
- Pullens, J., Sottocornola, M., Kiely, G., Toscano, P., and Gianelle, D. (2016). Carbon fluxes of an alpine peatland in Northern Italy. *Agricultural and Forest Meteorology*, 220:69–82.
- Quichimbo, P., Tenorio, G., Borja, P., Cárdenas, I., Crespo, P., and Célleri, R. (2012). Efectos sobre las propiedades físicas y químicas de los suelos por el cambio de la cobertura vegetal y uso del suelo: Páramo de Quimsacocha al sur del Ecuador. *Suelos Ecuatoriales*, 42(2)(2):138–153.
- Ramsay, P. M. and Oxley, E. R. B. (2001). An Assessment of Aboveground Net Primary Productivity in Andean Grasslands of Central Ecuador. *Mountain Research and Development*, 21(2):161–167.
- Reichstein, M., Falge, E., Baldocchi, D., Papale, D., Aubinet, M., Berbigier, P., Bernhofer, C., Buchmann, N., Gilmanov, T., Granier, A., Grunwald, T., Havrankova, K., Ilvesniemi, H., Janous, D., Knohl, A., Laurila, T., Lohila, A., Loustau, D., Matteucci, G., Meyers, T., Miglietta, F., Ourcival, J.-M., Pumpanen, J., Rambal, S., Rotenberg, E., Sanz, M., Tenhunen, J., Seufert, G., Vaccari, F., Vesala, T., Yakir, D., and Valentini, R. (2005). On the separation of net ecosystem exchange into assimilation and ecosystem respiration: review and improved algorithm. *Global Change Biology*, 11(9):1424–1439.
- Reichstein, M., Migliavacca, M., Wutzler, T., and Moffat, A. (2017). REdDyProc R Package version 1.0.1.

- Rollenbeck, R., Trachte, K., and Bendix, J. (2016). A New Class of Quality Controls for Micrometeorological Data in Complex Tropical Environments. *Journal of Atmospheric and Oceanic Technology*, 33(1):169–183.
- Ruimy, A., Jarvis, P., Baldocchi, D., and Saugier, B. (1995). CO₂ Fluxes over Plant Canopies and Solar Radiation: A Review. In *Advances in Ecological Research*, volume 26, pages 1–68.
- Running, S. W., Nemani, R. R., Heinsch, F. A., Zhao, M., Reeves, M., and Hashimoto, H. (2004). A Continuous Satellite-Derived Measure of Global Terrestrial Primary Production. *BioScience*, 54(6):547.
- Sánchez, M. E., Chimner, R. A., Hribljan, J. A., Lilleskov, E. A., and Suárez, E. (2017). Carbon dioxide and methane fluxes in grazed and undisturbed mountain peatlands in the Ecuadorian Andes. *Mires and Peat*, 19(October):1–18.
- Serrano-Ortiz, P., Sánchez-Cañete, E. P., Olmo, F. J., Metzger, S., Pérez-Priego, O., Carrara, A., Alados-Arboledas, L., and Kowalski, A. S. (2016). Surface-Parallel Sensor Orientation for Assessing Energy Balance Components on Mountain Slopes. *Boundary-Layer Meteorology*, 158(3):489–499.
- Stoy, P. C., Trowbridge, A. M., and Bauerle, W. L. (2014). Controls on seasonal patterns of maximum ecosystem carbon uptake and canopy-scale photosynthetic light response: contributions from both temperature and photoperiod. *Photosynthesis Research*, 119(1-2):49–64.
- Suarez, E. and Medina, G. (2001). Vegetation Structure and Soil Properties in Ecuadorian Paramo Grasslands with Different Histories of Burning and Grazing. *Arctic, Antarctic, and Alpine Research*, 33(2):158.
- Tonneijck, F. H., Jansen, B., Nierop, K. G. J., Verstraten, J. M., Sevink, J., and De Lange, L. (2010). Towards understanding of carbon stocks and stabilization in volcanic ash soils in natural Andean ecosystems of northern Ecuador. *European Journal of Soil Science*, 61(3):392–405.
- Trachte, K., Nauss, T., and Bendix, J. (2010). The Impact of Different Terrain Configurations on the Formation and Dynamics of Katabatic Flows: Idealised Case Studies. *Boundary-Layer Meteorology*, 134(2):307–325.
- UNESCO (2013). Cajas Massif Biosphere Reserve. <http://www.unesco.org/new/en/natural-sciences/environment/ecological-sciences/biosphere-reserves/latin-america-and-the-caribbean/ecuador/macizo-del-cajas/>. Last checked on 2018-11-18.
- van den Bergh, T., Inauen, N., Hiltbrunner, E., and Körner, C. (2013). Climate and plant cover co-determine the elevational reduction in evapotranspiration in the Swiss Alps. *Journal of Hydrology*, 500:75–83.
- Vicente-Serrano, S. M., Beguería, S., and López-Moreno, J. I. (2010). A Multiscalar Drought Index Sensitive to Global Warming: The Standardized Precipitation Evapotranspiration Index. *Journal of Climate*, 23(7):1696–1718.
- Vickers, D. and Mahrt, L. (1997). Quality Control and Flux Sampling Problems for Tower and Aircraft Data. *Journal of Atmospheric and Oceanic Technology*, 14(3):512–526.
- Vickers, D., Thomas, C. K., Martin, J. G., and Law, B. (2009). Self-correlation between assimilation and respiration resulting from flux partitioning of eddy-covariance CO₂ fluxes. *Agricultural and Forest Meteorology*, 149(9):1552–1555.
- Vuille, M., Bradley, R. S., and Keimig, F. (2000). Climate Variability in the Andes of Ecuador and Its Relation to

4 Net ecosystem exchange and evapotranspiration

- Tropical Pacific and Atlantic Sea Surface Temperature Anomalies. *Journal of Climate*, 13(14):2520–2535.
- Vuille, M., Bradley, R. S., Werner, M., and Keimig, F. (2003). 20th century climate change in the tropical Andes: Observations and model results. *Climatic Change*, 59(1/2):75–99.
- Vuille, M., Carey, M., Huggel, C., Buytaert, W., Rabatel, A., Jacobsen, D., Soruco, A., Villacis, M., Yarleque, C., Elison Timm, O., Condom, T., Salzmann, N., and Sicart, J.-E. (2018). Rapid decline of snow and ice in the tropical Andes - Impacts, uncertainties and challenges ahead. *Earth-Science Reviews*, 176(September 2017):195–213.
- Wilczak, J. M., Oncley, S. P., and Stage, S. A. (2001). Sonic Anemometer Tilt Correction Algorithms. *Boundary-Layer Meteorology*, 99(1):127–150.
- Wohlfahrt, G., Hammerle, A., Niedrist, G., Scholz, K., Tomelleri, E., and Zhao, P. (2016). On the energy balance closure and net radiation in complex terrain. *Agricultural and Forest Meteorology*, 226-227:37–49.
- Wolf, S., Eugster, W., Potvin, C., Turner, B. L., and Buchmann, N. (2011). Carbon sequestration potential of tropical pasture compared with afforestation in Panama. *Global Change Biology*, 17(9):2763–2780.
- World Meteorological Organization (2012). Standardized Precipitation Index User Guide (M. Svoboda, M. Hayes and D. Wood), WMO-No. 1090. Technical report, World Meteorological Organization, Geneva, Switzerland.
- WRB-IUSS (2014). World Reference Base for Soil Resources 2014. International soil classification system for naming soils and creating legends for soil maps. Technical report, FAO.
- Zeeman, M., Mauder, M., Steinbrecher, R., Heidbach, K., Eckart, E., and Schmid, H. (2017). Reduced snow cover affects productivity of upland temperate grasslands. *Agricultural and Forest Meteorology*, 232:514–526.
- Zhao, L., Li, J., Xu, S., Zhou, H., Li, Y., Gu, S., and Zhao, X. (2009). Seasonal variations in carbon dioxide exchange in an alpine wetland meadow on the Qinghai-Tibetan Plateau. *Biogeosciences Discussions*, 6(5):9005–9044.

5 Atmosphere-surface fluxes modeling for the highland páramo catchments of Ecuador

This chapter is under review at *Science of the Total Environment (Elsevier)*.

Submitted: 22 January 2019

Atmosphere-surface fluxes modeling for the high Andes: The case of páramo catchments of Ecuador

Galo Carrillo-Rojas^{1,2,3}, Hans Martin Schulz¹, Johanna Orellana-Alvear^{1,2}, Ana Ochoa-Sánchez², Katja Trachte¹, Rolando Célleri² and Jörg Bendix¹

¹ Laboratory for Climatology and Remote Sensing, Faculty of Geography, Philipps-Universität Marburg, Deutschhausstr. 12, Marburg 35032, Germany

² Departamento de Recursos Hídricos y Ciencias Ambientales, Facultad de Ingeniería, Universidad de Cuenca, Campus Balzay, Cuenca 010207, Ecuador

³ Departamento de Química Aplicada y Sistemas de Producción, Facultad de Ciencias Químicas, Universidad de Cuenca, Av. 12 de Abril y A. Cueva, Cuenca 010203, Ecuador

Abstract: Interest on atmosphere-surface flux modeling over the mountainous regions of the globe has increased recently, with a major focus on the prediction of water, carbon and other functional indicators in natural and disturbed conditions. However, insufficient research has been centered on exploring energy fluxes (net radiation; sensible, latent and soil heat) and actual evapotranspiration (ETa) over the Neotropical Andean biome of the páramo. The present study assesses the implementation and parameterization of a state-of-art Land-Surface Model (LSM) for simulation of these fluxes over two representative páramo catchments of southern Ecuador. We evaluated the outputs of the LSM Community Land Model (CLM ver. 4.0) with (i) ground-level

flux observations from the first (and highest) Eddy Covariance (EC) tower of the Northern Andean páramos; (ii) spatial ETa estimates from the energy balance-based model METRIC (based on Landsat imagery); and (iii) derived ETa from the closure of the water balance (WB). CLM's energy predictions revealed a significant underestimation on net radiation, which impacts the sensible and soil heat fluxes (underestimation), and delivers a slight overestimation on latent heat flux. Modeled CLM ETa showed acceptable goodness-of-fit (Pearson $R = 0.82$) comparable to ETa from METRIC ($R = 0.83$). Contrarily, a poor performance of ETa WB was observed ($R = 0.46$). These findings provide a solid evidence on the CLM's plausibility for the ETa (and LE) forecast, and give insights in the selection of ETa methods according to their accuracy. The study contributes to a better understanding of ecosystem functioning in terms of water loss through evaporative processes, and might help in the development of future LSMs' implementations focused on climate / land use change scenarios for the páramo.

Keywords Tropical Andes, Páramo, CLM, METRIC, Evapotranspiration, Eddy covariance.

5.1 Introduction

Evapotranspiration (ET), as the primary water loss in the hydrological cycle (at ground-level) and key-indicator of terrestrial ecosystems functioning, remains little understood for the mountain regions across the globe, especially for the tropical Andes. Likewise, land-surface thermodynamics and energy fluxes (incoming and outgoing radiation balance), which increase ET rates and promote carbon dioxide (CO_2) exchange (through photosynthesis / respiration mechanisms), also persist understudied for this remote region. Main obstacles to estimate actual evapotranspiration (ETa) and energy fluxes in the Andes lie in the scarcity of hydro-meteorological instrumentation (Córdova et al., 2015) and direct measurements of ETa and energy fluxes (by using sophisticated techniques, such as Eddy Covariance (EC), lysimeters or micrometeorological sensors) (Carrillo-Rojas et al., 2016, 2019). Therefore, the adoption of alternative methods such as the simulation of fluxes via Land Surface Models (LSM) (Bonan, 2016) becomes a route for such a purpose. The use of these

5 Atmosphere-surface fluxes modeling

approaches has notably increased in environmental investigations from point to spatially distributed in the last decade, in the search of a better understanding of multi-scale ecosystem dynamics.

Abundant literature exists on the application of LSMs for the prediction of land-atmosphere exchanges for natural and altered scenarios (Fatichi et al., 2016). The most developed LSMs that suit for this purpose include the Community Land Model (CLM) (Lawrence et al., 2011), the Joint UK Land Environment Simulator (JULES) (Best et al., 2011), the Jena Scheme for Biosphere Atmosphere Coupling in Hamburg (JSBACH) - land component of the Max Planck Institute Earth System Model (MPI-ESM) (Giorgetta et al., 2013), the ORganizing Carbon and Hydrology In Dynamic EcosystEms (ORCHIDEE) (Krinner et al., 2005), and the Biome-BGC model (Thornton et al., 2002). Some of these LSMs work coupled to earth-climate models, and can manage several aquatic and terrestrial components using multiple spatial gridding options. These models have been vastly implemented for diverse ecosystems around the planet, especially due to their capability of predicting land-surface exchanges with manipulated biotic / abiotic scenarios. Nevertheless, only very few studies have used LSMs to estimate eco-hydrological processes in the neotropical Andean mountains (Göttlicher et al., 2011; Marthews et al., 2012; Minaya et al., 2016; Silva et al., 2012; van de Weg et al., 2014). To our knowledge, none of them have been specifically used for ETa and energy flux estimations.

Despite the more frequent application of remote-sensing based methods for ETa mapping over croplands and semi-arid locations, their implementation for complex terrain remains limited as well. Fortunately, such an approach has recently been applied to unveil spatial-explicit ETa dynamics in the highland Andes (Carrillo-Rojas et al., 2016) by combination of an energy balance approach with remote-sensing imagery (Allen et al., 2007). The derived ETa maps have proven useful for monitoring the water cycle in high mountain catchments. On the other hand, ground-level surveys of ecosystem fluxes have raised in recent years by the use of sophisticated techniques, such as the EC method (Aubinet et al., 2012), in spite of some limitations of this technique for steeped terrain applications (Baldocchi et al., 2018). At the global scale, EC implementation persists limited for the developing countries and southern-hemisphere regions, mainly due to the high cost of instrumentation and maintenance. Therefore, the use of hydrological methods, such as water balance for ETa estimation, is widely applied nowadays due to the low costs and easiness of implementation and monitoring.

The Northern Andean Ecoregion known as páramo (Olson et al., 2001) has a huge importance in sustaining ecosystem provisioning services such as fresh water for the lowland settlements, agroindustry and the generation of hydro-power (Céleri and Feyen, 2009). The páramo soils

function as a regulation system, due to their massive carbon storage (volcanic-ash origin) which holds and filters the water resource (Hribljan et al., 2016; Tonneijck et al., 2010). Páramos also possess a vast biodiversity which harbors many endemic species (Myers et al., 2000), a fact which has promoted dense recreational tourism in these fragile areas. Similarly to other mountain ecosystems, global warming and land-cover change threatens this biome in several ways: (i) Climate change would lead to a rise of local air temperature and to the alteration of the rainfall regimes (frequency and intensity), with the presence of longer drought events (Vuille, 2013). These effects might cause water retention and carbon sequestration reductions, the migration or extinction of endemic species, and the modification of fire regimes (Anderson et al., 2011). (ii) Páramo land-cover change would lead to similar negative effects, plus the increase of erosion and landslides risks, and environmental harms due to the intensification of grazing, agroindustry and mining (Crespo et al., 2010; Wigmore and Gao, 2014). Here, LSM plays a crucial role in the prediction of effects associated to land cover or climate change scenarios. However, flux estimates derived from non-parameterized LSMs are limited to accurately represent the exchange and functioning of a particular ecosystem in most of the cases. This can be attributed to the use of default forcing inputs (i.e., non-site specific surface or climate parameters), generally embedded in the model packages or linked data repositories. For instance, the use of default coarse grid climate datasets (i.e., reanalysis data from regional climate models), or inaccurate soil properties or plant functional types (PFTs). Such untailored parameters can be inappropriate for mountainous environments, such as the Andean páramo, and thus, this effect has to be evaluated. Therefore, the adjustment and parameterization of a state-of-art LSM, followed by the evaluation of its outputs through ground-based or remote-sensing based observations would allow to simulate fluxes accurately in the páramo. LSM applications would be valuable to analyze and understand surface-exchange processes, particularly for poor or non-monitored páramo areas. In addition, LSMs would allow to foresee potential effects on land-surface exchange associated with land cover / climate change scenarios.

In this investigation, we provide insights about soil-atmosphere thermodynamics and ETa for the Andean páramo, by describing: (i) the parameterization of the state-of-art LSM CLM for ETa and energy fluxes simulation for two representative páramo catchments of southern Ecuador (Zhurucay and Quinoas); and (ii) the assessment of the LSM outputs with ground-level and remote-sensing based fluxes, considering the well (Zhurucay), and a less monitored catchment (Quinoas).

5.2 Materials and methods

5.2.1 Characteristics of the catchments

The Zhurucay and Quinoas ecohydrological observatories are located in the southern cordillera of Ecuador, within the Cajas Massif Reserve - UNESCO World Biosphere (UNESCO, 2013). Zhurucay is exposed to the west and Quinoas to the east mountainside of the Andes, where the Pacific / Amazonian Divortium Aquarum separates the headwater contribution. The catchments raise from 3500 to 3900 m a.s.l. for Zhurucay (area = 7.5 km²) and from 3610 to 4390 m a.s.l. for Quinoas (area = 19.5 km²), and share similar hydrological, edaphic and landscape characteristics which have been comprehensively documented in recent studies (Carrillo-Rojas et al., 2016, 2019; Córdova et al., 2016; Correa et al., 2018, 2017; Mosquera et al., 2016; Muñoz et al., 2016; Ochoa-Sánchez et al., 2018; Orellana-Alvear et al., 2017; Pesántez et al., 2018). Steep topography and valley complexity characteristics are more pronounced for Quinoas than for Zhurucay, however the soil types (Andosols and Histosols, ratio > 4:1) and their properties are quite similar (i.e., a dark Ah horizon depth between 0.20 to 0.70 m with a thin C horizon over solid bedrock, a high organic matter content of 30 ~ 40 %, and a water field capacity of 40 ~ 90 %). Dominant vegetation in both catchments is the alpine C3 tussock grass *Calamagrostis Intermedia* (J. Presl) Steud. (Boom et al., 2001), with > 80% coverage reaching heights of between 0.30 ~ 0.80 m. Other grasses such as *Festuca* sp., cushion plants patches and small *Polylepis* sp. forest patches are part of both landscapes. Small water bodies are found in Quinoas only (< 5% of the area). Figure 5.1 shows the geographical characteristics of the catchments.

Both sites possess a lack of thermal seasonality, with steady low temperatures and convective-orographic clouds (Bendix et al., 2006; Emck, 2007). Precipitation regimes are bimodal (Célleri et al., 2007), with mean annual rainfall of 1210±101 mm year⁻¹ (Zhurucay) and 1076±102 mm year⁻¹ (Quinoas). A time series of 6-year climate observations, for Zhurucay and Quinoas respectively, indicate: mean temperature of 6.1°C (max. = 14.2° C, min. = 0.4° C) and 5.4°C (max. = 13° C, min. = 0.9° C), mean relative humidity (RH) of 93.6% and 90.4%, total incoming solar radiation (Rs) of 4942 MJ m⁻² year⁻¹ and 4629 MJ m⁻² year⁻¹, and mean wind speed of 3.7 m s⁻¹ and 2.3 m s⁻¹. Figure 5.9 of supplementary materials illustrates monthly climographs for each catchment.

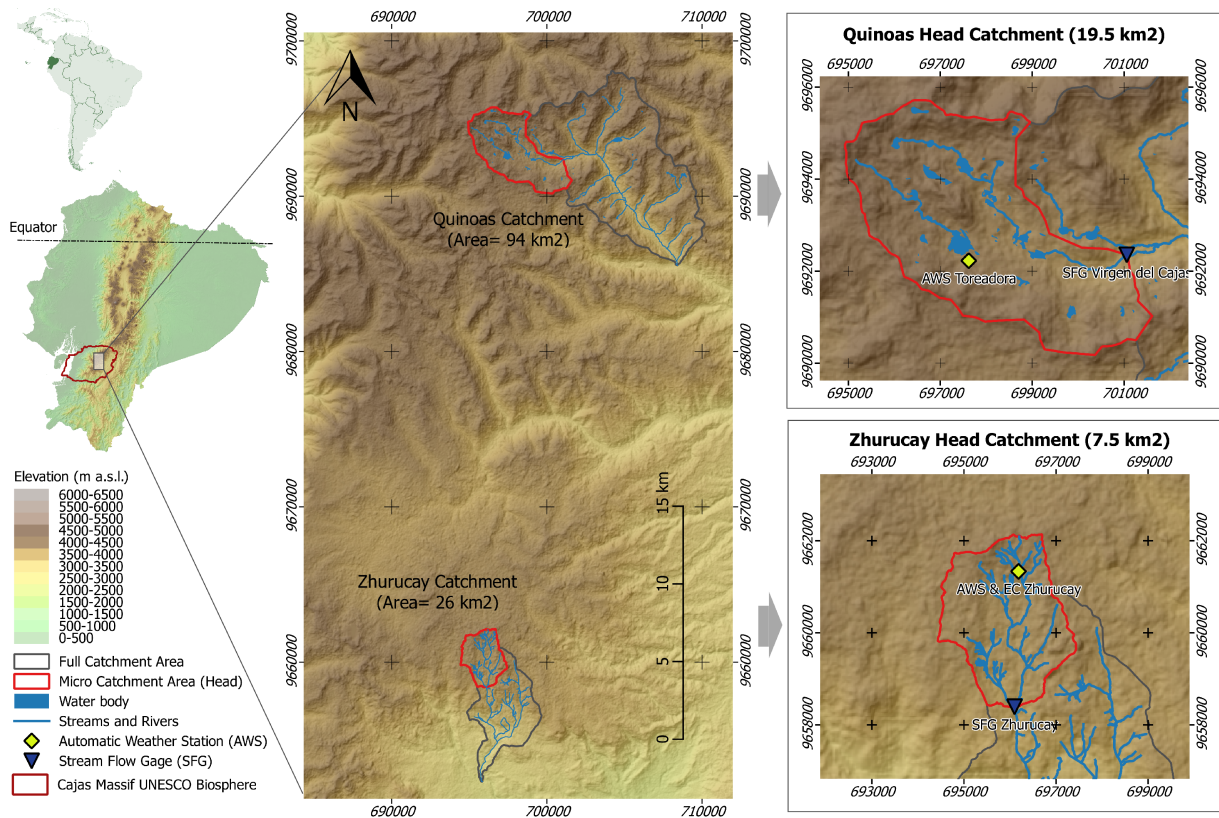


Figure 5.1: Location of the study catchments in Southern Ecuador (páramo-headwater catchments are red lines).

5.2.2 Available data and instrumentation

Sections 5.2.3 to 5.2.6 will give details of the specific application of the following datasets: 6-year climate datasets for each catchment were used for the forcing of the CLM and METRIC models. Site-independent 6-year water discharge, precipitation and soil humidity datasets were used to derive hydrological balances, 22-month (March 2016 ~ December 2017) of energy and ETa fluxes dataset for Zhurucay only, and 4-year of Landsat imagery for each catchment (13 clear-sky valid images). The full hydro-meteorological and flux monitoring instrumentation used in the study are described in Table 5.3 and the information of Landsat Imagery is described in Table 5.4 of the supplementary materials.

5.2.3 CESM-CLM model adjustment for both catchments

The coupled global climate model Community Earth System Model (CESM 1.1.2) (Hurrell et al., 2013) includes the land surface component CLM (version 4.0) in biogeophysics mode (Lawrence et al., 2011; Oleson et al., 2010). We used this process-based model for single-point simulations in order to estimate the net radiation Rn_{CLM} , sensible heat H_{CLM} , latent heat LE_{CLM} , soil heat as well as its storage G_{CLM} , and the $ETa_{(CLM)}$ for each catchment. A 6-year dataset of meteorological information (shortwave solar radiation, air temperature, relative humidity, atmospheric pressure, wind speed and precipitation) measured at 2 m and hourly time step were used for atmospheric forcing of CLM. As a previous step, we spun-up all simulations in Accelerated-Decomposition mode for 800 years, by cycling over the first four years of forcing data. Then, we equilibrated the model for 200 years before running the final simulations for a complete period of 6 years. This spin-up configuration was essential to obtain reliable results. The PFT C3 arctic grass (Oleson et al., 2010) was used for both sites with specific adjustments to the vegetation characteristics for a better representation of the páramo tussock grasslands (i.e., canopy top and bottom heights and Leaf Area Index (LAI)). However, we kept the CLM's internal PFT physio-morphological parameters unchanged, due to the lack of site-specific phenological and biochemical measurements or reliable literature's phenotypic traits for the native species. Furthermore, soil column properties, such as texture (sand, clay, silt) and organic matter density (OMD) at different levels, as well as the soil color and the Maximum Fractional Saturated Area (F_{max}) were adjusted to the soil conditions of the páramo. The páramo soils possess one of the most elevated soil organic carbon contents (SOC) of any mountainous ecosystem in the world (Comas et al., 2017; Tonneijck et al., 2010). Thus, our CLM parameterization for the páramo Andosols required the assumption of OMD level near to the maximum OMD allowed in the model (130 kg m^3). This parameterization fitted to a – pure peatland – land cover scenario in CLM.

The available adjustments made to the model parameters were based on site-observations and a literature survey on traits, which are described in detail in Table 5.1.

CLM follows the principle of energy balance closure described in Equation 5.1, as follows:

$$Rn_{CLM} = H_{CLM} + LE_{CLM} + G_{CLM} \quad (Wm^{-2}) \quad (5.1)$$

where the radiative flux of Rn_{CLM} is calculated as the difference of shortwave and longwave energy fluxes of the system. The numerical solution considers direct radiation, diffuse radiation,

Table 5.1: Modification to CLM parameters for each catchment

	ZHURUCAY		QUINOAS		Source / Reference
	CLM Default Value	Zhurucay CLM Configured Value	CLM Default Value	Quinoas CLM Configured Value	
Percent PFT and other land cover (%)^a	BS (6.0), BETR (10.0), BETM (12.0), BDTR (20.0), C3G (37.0), C4G (6.0), CR1 (9.0)	C3AG (95.0), WT (5.0)	BS (4.1), BETR (3.0), BETM (40.0), BDTR (4.0), BDSB (12.0), C3AG (26.0), C3G (3.0), CR1 (7.0), WT (0.9)	C3AG (95.0), BS (1.0), WT (4.0)	LULC map ^b and experimental setup
LAI monthly average (m² m⁻²)	0.9	1.2	0.9	1.2	Hofstede et al. (1995) and Nagy et al. (2011)
Canopy monthly top height (m)	0.5	0.7	0.5	0.7	Site observation
Canopy monthly bottom height (m)	0.01	0.005	0.01	0.005	Site observation
Soil Color	16	18	16	18	Lawrence and Chase (2007)
Organic matter density (kg m⁻³)^c at different soil depth layers^d	L0 (59.3), L1 (60.4), L2 (51.9), L3 (42.6), L4 (34.1), L5 (27.0), L6 (2.0)	L0 (100.0), L1 (110.0), L2 (120.0), L3 (120.0), L4 (130.0), L5 (130.0), L6 (130.0)	L0 (59.3), L1 (60.4), L2 (51.9), L3 (42.6), L4 (34.1), L5 (27.0), L6 (2.0)	L0 (100.0), L1 (110.0), L2 (120.0), L3 (120.0), L4 (130.0), L5 (130.0), L6 (130.0)	Aucapiña and Marín (2014), Crespo et al. (2011) and Quichimbo et al. (2012)
Clay content (%)[*] at different soil depth layers^d	L0 (17.0), L1 (17.0), L2 (18.0), L3 (19.0), L4 (19.0), L5 (21.0), L6 (10.0)	L0 (20.0), L1 (20.0), L2 (25.0), L3 (25.0), L4 (30.0), L5 (30.0), L6 (50.0)	L0 (17.0), L1 (17.0), L2 (18.0), L3 (19.0), L4 (19.0), L5 (21.0), L6 (10.0)	L0 (20.0), L1 (20.0), L2 (25.0), L3 (25.0), L4 (30.0), L5 (30.0), L6 (50.0)	Aucapiña and Marín (2014), Buytaert et al. (2006b) Crespo et al. (2011)
Sand content (%)[*] at different soil depth layers^d	L0 (45.0), L1 (45.0), L2 (45.0), L3 (45.0), L4 (45.0), L5 (43.0), L6 (15.0)	L0 (70.0), L1 (70.0), L2 (65.0), L3 (65.0), L4 (60.0), L5 (60.0), L6 (15.0)	L0 (45.0), L1 (45.0), L2 (45.0), L3 (45.0), L4 (45.0), L5 (43.0), L6 (15.0)	L0 (70.0), L1 (70.0), L2 (65.0), L3 (65.0), L4 (60.0), L5 (60.0), L6 (15.0)	Aucapiña and Marín (2014), Buytaert et al. (2006b) Crespo et al. (2011)
Fmax	0.3802	0.3628	0.3943	0.3535	Niu et al. (2005) based on local Topographic (Wetness) Index

^a CLM 4.0 PFT are: Bare soil (BS), Broadleaf evergreen tree - tropical (BETR), Broadleaf evergreen tree - temperate (BETM), Broadleaf deciduous tree - tropical (BDTR), Broadleaf deciduous shrub - boreal (BDSB), C3 arctic grass (C3AG), C3 grass (C3G), C4 grass (C4G), Crop 1 (CR1), Wetland (WT).

^b Land use and land use (LULC) map provided by the MAE Geoportal database (Ministerio del Ambiente del Ecuador, 2018).

^c OMD (kg m⁻³) assumed carbon content of 0.58 grams of C per gram of OM. Values are closer to the maximum value allowed in CLM for peatlands (130 kg m⁻³).

^d Soil depths layers (in m) for CLM numerical solution are: L0 (0.0071), L1 (0.0279), L2 (0.0623), L3 (0.1189), L4 (0.2122), L5 (0.3661), L6 (0.6198). Lower layers are considered as impermeable bedrock.

^{*} Silt content is calculated by CLM internally as 100 - Sand content - Clay content.

and longwave radiation (absorbed, transmitted, and reflected) by vegetation and soil. Also, the turbulent fluxes of H_{CLM} and LE_{CLM} are numerically solved in CLM through the Monin-Obukhov similarity theory, considering prescribed aerodynamic properties of the air, temperature, humidity and canopy roughness for vegetated and non-vegetated surfaces. $ETa_{(CLM)}$ is directly inferred from the LE_{CLM} flux. A very detailed description of the CLM's equations and framework is available in Oleson et al. (2010).

5.2.4 Remote-sensing based ETa: METRIC model implementation for both catchments

For the period April 2013 to July 2017, 13 Landsat 7 ETM+ SLC-off scenes (path 10 / row 62, with 30 m resolution and cloud contamination <15%) were gathered from the USGS Earth Explorer server (<http://earthexplorer.usgs.gov>). Landsat 7 SLC-off banding affected less than 2% for both catchment areas, thus missed pixels were gap filled via focal analysis methodology (USGS, 2017). Furthermore, cloud and cloud shadow affected pixels (<15% only in three images) were removed and then gap filled via mosaicking filling process (Kjaersgaard et al., 2012; Zhu and Woodcock, 2012). Each image scene was atmospherically corrected according to Tasumi et al. (2008).

The energy-balance based model Mapping Evapotranspiration at High Resolution with Internalized Calibration (METRIC) was independently implemented for Zhurucay and Quinoas in order to retrieve the spatial $ETa_{(METRIC)}$ estimates, using the aforementioned imagery, a digital elevation model (ASTER GDEM, 30 m res.) and site-specific meteorological data (described in section 5.2.3). The imagery pre-processing and calculations were performed using ERDAS Imagine, R software and QGIS. The METRIC algorithm follows the principle of the equation 5.1. The detailed formulae is provided by Allen et al. (2007), whereas its adaptation for the páramo ecosystem is described by Carrillo-Rojas et al. (2016). The model adjustment for complex terrain demanded corrections regarding roughness length, wind speed, temperature lapse rate and solar radiation. METRIC delivers a crop-coefficient map for each image (known as reference evapotranspiration fraction map, ET_{rf}). These intermediate products are cubic-spline interpolated in time, providing a continuous time series. ETa (at daily frequency) is obtained by multiplying the ET_{rf} maps with daily ASCE standardized reference evapotranspiration (ET_r) maps (obtained from climatological information (ASCE-EWRI, 2005) and spatial interpolation). Finally, the daily $ETa_{(METRIC)}$ maps are aggregated to monthly or annual ETa .

5.2.5 Energy and ETa flux observations: EC and micrometeorological techniques (Zhurucay)

The EC tower and other micrometeorological sensors were located in the head of the Zhurucay catchment (Zhurucay Ecohydrological Observatory) during the period March 2016 to December 2017. The EC instruments were setup at a 3.6 m height surveying a tussock grassland fetch of 100 ~ 150 meters (area = 1.5 ha) in the prevailing upwind direction of fluxes, where the terrain is

characterized by a smooth topography ($< 10^\circ$ of slope). Latent heat (LE_{EC}) and subsequently ET fluxes ($ETa_{(EC)}$) were measured using an enclosed-path infrared gas analyzer (LI-COR, Lincoln, NE, USA) working at 20 Hz sampling rate. Sensible heat flux, H_{EC} , was estimated with a three-dimensional sonic anemometer (Gill New WindMaster, Hampshire, UK). Raw data were processed with the EddyPro software, version 6.2.0 (LI-COR, Lincoln, NE, USA), and high-frequency fluxes were averaged to a half-hour blocks considering diagnostic flags, plausibility limits and removal of spikes. We performed data quality assurance and quality control (QA/QC) along with specific corrections for density fluctuations, time lags, humidity-dependent spectral losses and sector-wise wind planar fit of the fluxes (Mauder et al., 2013). Those corrections proved crucial in the EC experiment (Carrillo-Rojas et al., 2019).

Additional micrometeorological variables were taken with a four-component net radiometer (Kipp & Zonen CNR4, for net radiation Rn_{EC}), and with three soil heat plates (Hukseflux HFP01, for soil heat flux G_{EC}). Rn_{EC} was corrected to a surface-normal energy income due to the slope and aspect characteristics of the site according to Serrano-Ortiz et al. (2016), and we also calculated (and added) the soil heat storage to G_{EC} according to Mayocchi and Bristow (1995). Complementary analyses, such as the identification of the spatial source of ETa fluxes (EC footprint) (Kljun et al., 2015) and EC energy balance closure (Foken, 2008) were performed to confirm the data reliability. The identification and removal of advection-affected fluxes (low-friction velocity values, u^*) were done with the Moving Point Test technique (Papale et al., 2006). Missing $ETa_{(EC)}$ fluxes (due to the u^* filtering, power or instrumental failures, and low quality data) amounted only to 18% of the full dataset. Marginal Distribution Sampling (MDS) methodology was used to fill this data lack (Reichstein et al., 2005). Finally, $ETa_{(EC)}$ fluxes were aggregated at daily, monthly and annual scales. The characteristics of the EC tower and micrometeorological sensors are detailed in Table 5.3 of the supplementary materials, and the full EC experiment are explained in Carrillo-Rojas et al. (2019).

5.2.6 ETa estimated with the water balance for both catchments

The hydrological balance was closed for both, the Zhuruca and Quinoas head catchments. Thus, the actual evapotranspiration $ETa_{(WB)}$ was estimated assuming that subsurface drainage and lateral flow are negligible for these soils (Buytaert et al., 2006a; Crespo et al., 2011) as,

$$ETa_{WB} = P - Q \pm \Delta S \quad (mm \text{ month}^{-1}) \quad (5.2)$$

5 Atmosphere-surface fluxes modeling

where, P is the precipitation; Q is the discharge and ΔS is the change in soil water storage.

At the Zhurucay catchment, P observations were interpolated with Thiessen polygons from five tipping buckets, and for Quinoas the same were performed with three tipping buckets. Q was registered by using V-notch weirs, equipped with water level sensors (stream flow gages, SFG), installed at the outlet of each catchment. The change in Soil Water Content (SWC) at Quinoas was measured with two water content reflectometers located at different locations of the head catchment. ΔS was estimated by the monthly change on the averaged SWC. At Zhurucay, ΔS was estimated from the monthly change of the added storage in organic and mineral soil layers found in the catchment. The soil water storage was measured with ten water content reflectometers located at several depths in the surroundings of the Zhurucay EC tower. QA/QC was applied to the P , Q and ΔS datasets and the $ETa_{(WB)}$ estimates were aggregated at monthly and annual time steps. Table 5.3 of supplementary materials describes the hydrometeorological instrumentation used in this analysis.

5.2.7 Assessment and comparative analyses of CLM derived energy and ETa fluxes

Evaluation of the CLM energy and ETa outputs was performed with hourly and daily EC observations for the catchment of Zhurucay. For this purpose we applied: (i) an analysis of the mean diurnal cycles of heat fluxes (energy flux densities at hourly-time step) for a wet month and a less humid month of the period (with 9 representative clear sky days of each month); and (ii) a linear correlation analysis between the CLM and EC datasets for the full period of EC monitoring (22 months: March 2016 to December 2017). Daily-averaged energy fluxes and daily-aggregated ETa values were calculated for this purpose. Furthermore, catchment-scale $ETa_{(METRIC)}$ areal estimates were evaluated with their correspondent EC footprint-scale $ETa_{(METRIC)}$ areal estimates, and compared with $ETa_{(EC)}$ values. This was done in order to understand the representativeness and limitations of the remote-sensing based ETa method.

The performance of CLM and METRIC models for ETa simulation was evaluated with the best-available ground-based observation for each catchment ($ETa_{(EC)}$ for Zhurucay and $ETa_{(WB)}$ for Quinoas) in the form of Taylor diagrams (Taylor, 2001). Here, the normalized standard deviation (SD), normalized root-mean-square error (RMSE) and Pearson correlation, all illustrated on a two-dimensional plot, provide a goodness-of-fit overview of the predictions for a period of 16-month: March 2016 to June 2017 (where we had a continuous dataset of modeled and observed ETa in both catchments simultaneously). In addition, the 16-month cumulative ETa estimates (all

four methods) and their correspondent hydrological fluxes (P, Q and ΔS) were compared for each catchment. Finally, a statistical evaluation of ETa monthly averages by year for the full period of CLM simulations (6 years) was conducted.

5.3 Results and discussion

5.3.1 Assessment of energy and ETa CLM fluxes for Zhurucay

Modeled (CLM) and observed (EC) energy fluxes for diurnal cycle are compared in Fig. 5.2. Here, we depict aggregated curves of 9 clear sky days (hourly time-step) of the components Rn, H, LE and G from two representative months (less humid month: August 2016, and wet month: January 2017). Climate conditions for the 9-day samples and the specific months are also depicted.

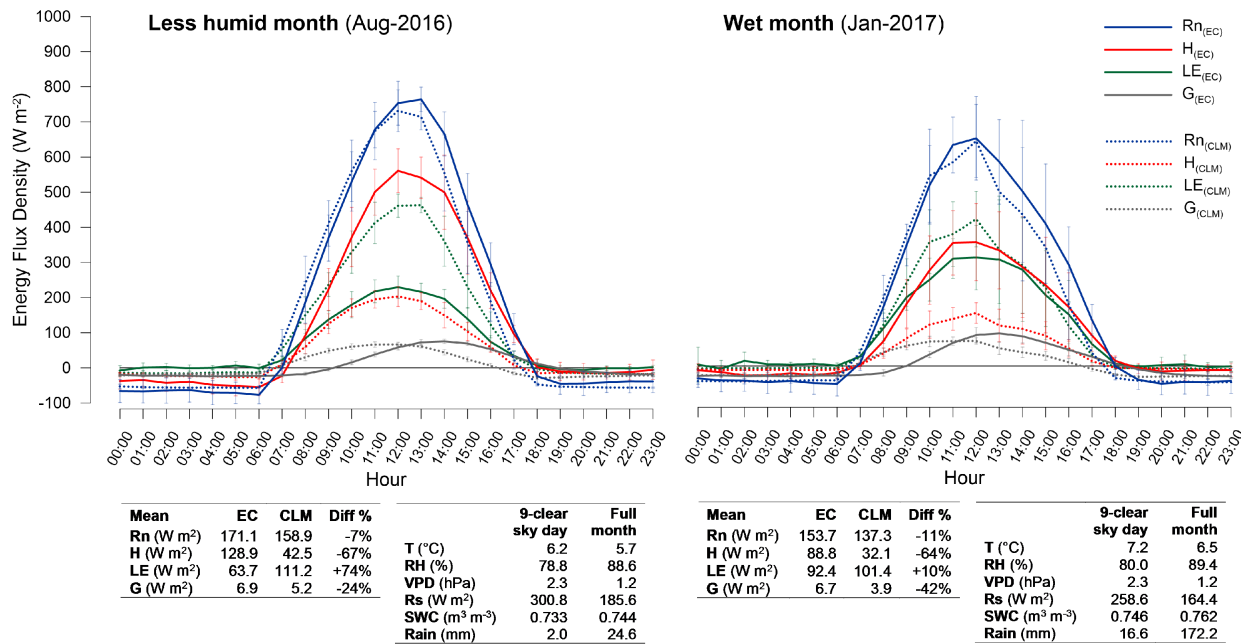


Figure 5.2: CLM and EC diurnal cycle of fluxes for a less humid and a wet month (9-clear sky day sample averaged) with error bars. Mean values of Rn, H, LE and G for the sample and full month are shown along climate variables.

For the less humid month we found a strong underestimation of H_{CLM} (67%), together with a low underestimation of Rn_{CLM} and G_{CLM} (7% and 24%) when compared with EC and micrometeorological observations. In consequence, CLM assigns a significant amount of energy to LE_{CLM}

5 Atmosphere-surface fluxes modeling

to force the energy balance closure (as a rest-term). LE_{CLM} values show an overestimation of 74% when compared to LE_{EC} . For the wet month we observe similar underestimations for H_{CLM} , Rn_{CLM} and G_{CLM} (64%, 11% and 42% respectively). However, in this case the overestimation of LE_{CLM} only is 10%. Additionally, G_{CLM} shows a premature accumulation trend of heat during the diurnal cycle, as well as an early development of its maximum peak when compared to G_{EC} . This can be attributed to an inability of CLM to represent a natural delayed accumulation of soil heat, which is associated to the higher SWC levels and lower air temperatures in this alpine ecosystem. Similar disagreement between CLM model soil heat curves has also been reported by [Chen et al. \(2018\)](#) for sites with high humid and organic soils. Also, the uncertainties in G_{EC} measurements (spatial representativeness) might be a reason for this situation.

In Figure 5.2, the climate and soil conditions related to the wet month are quite similar and representative to those observed in the 22-month period (March 2016 to December 2017) of evaluation ($T = 6.5 \pm 1.1^\circ \text{C}$, $RH = 89.8 \pm 9.7\%$, Vapor Pressure Deficit (VPD) = $1.1 \pm 1.1 \text{ hPa}$, $R_s = 159.6 \pm 69.6 \text{ W m}^2$, $SWC = 0.749 \pm 0.089 \text{ m}^3 \text{ m}^{-3}$, and cumulative rain = 2185 mm). Furthermore, we found that days with higher radiation levels (Rn daily mean $> 250 \text{ W m}^2$) only accounted for 12% of the time in the full period of analysis. In addition, it is clear that during dominant cloudy / rainy episodes, the mismatch is less pronounced. This can be attributed to less developed thermally-driven flows, and thus, less thermally / mechanically induced energy (i.e., Turbulent Kinetic Energy TKE).

Climate conditions play a critical role in the aforementioned findings. The poor performance of CLM in predicting turbulent fluxes (LE and H) for less humid conditions might be attributed to the sensitivity of the model to the moisture conditions of soil, and to the diurnal variation of temperature (and in a lesser degree to other variables, such as wind stress, albedo, etc.). In spite of this situation, the prediction of LE was more accurate for the wet period. CLM was also capable to predict a major water loss (LE) when SWC and rainfall increased (which depends on the incoming energy availability). The simulation of surface heat fluxes is highly sensitive to the hydraulic and soil thermal properties embedded in the CLM algorithms ([Han et al., 2014](#)). Unfortunately, the manipulation of such parameters is restricted because they are hard coded in this model. Therefore, we only adjusted the soil texture, color and F_{max} parameters.

Figure 5.3 illustrates the performance of CLM simulations versus EC / micrometeorological observations (Rn_{EC} , H_{EC} , LE_{EC} , G_{EC} and $ETa_{(EC)}$) based on daily-averaged (energy) and daily-aggregated (ETa) values. The evaluation period was also 22 months.

Rn_{CLM} exhibit an underestimation, especially at low levels (cloudy days) in spite of a good R^2 (0.88) and a low RMSE. H_{CLM} and G_{CLM} estimates also reveal a general underestimation, although

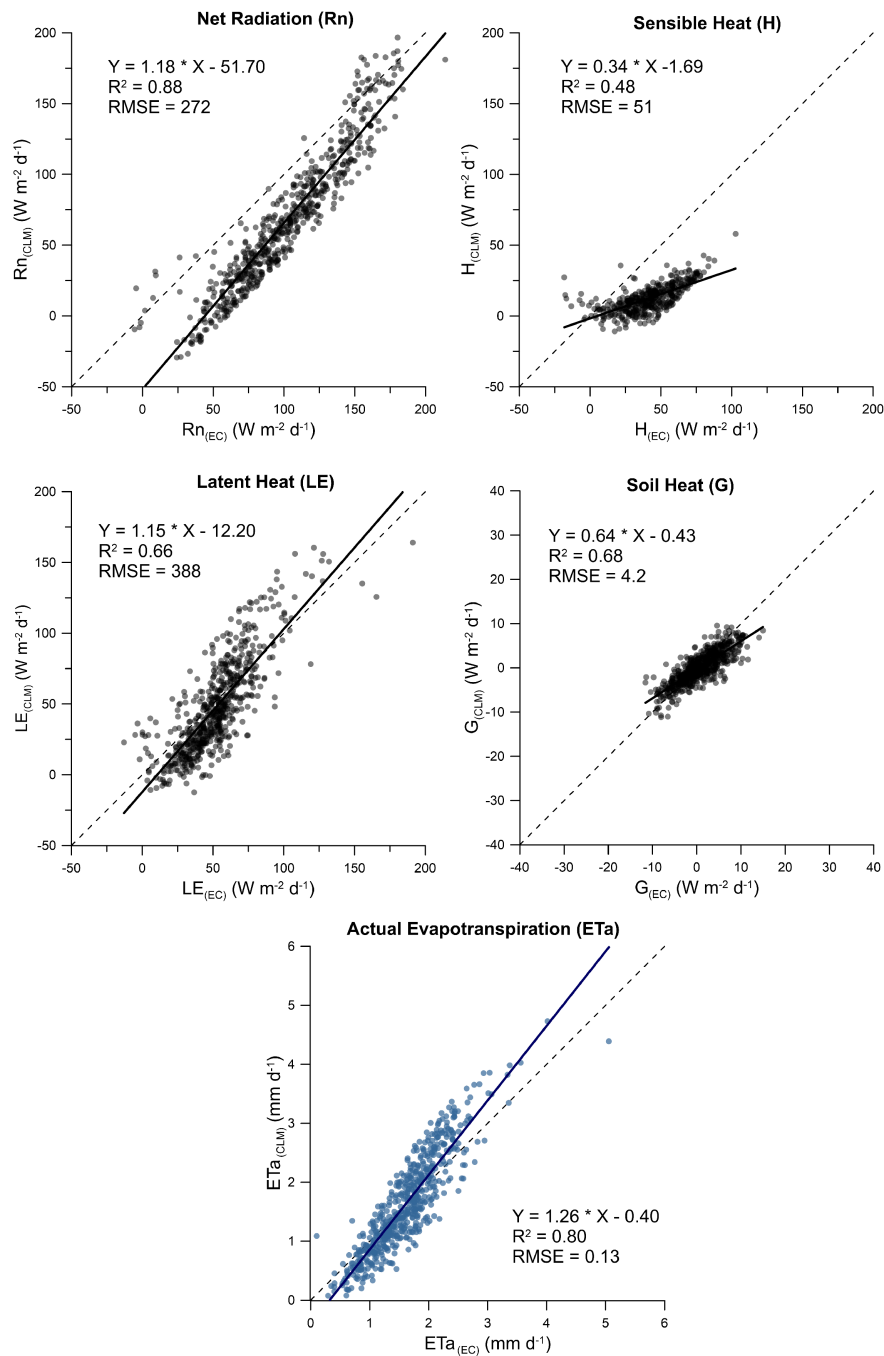


Figure 5.3: Daily-scale CLM modeled and observed energy and ETa fluxes for Zhurucay. The bisector line is depicted as a dotted line.

5 Atmosphere-surface fluxes modeling

they show acceptable correlation coefficients and small errors. On the other hand, simulated LE_{CLM} reveals a low overestimation despite of an acceptable R^2 and low RMSE. Finally, modeled $ETa_{(CLM)}$ shows a small overestimation when contrasted to the EC measurements, and exhibits a good correlation ($R^2 = 0.80$) and a small error. The Fig. 5.2 depicted the diurnal course of representative clear sky days exclusively. However, Fig. 5.3 reveals a complete overview of daily-scale balances of energy fluxes, considering the full environmental conditions of the páramo (cloudy and wet conditions).

Underestimation of the available energy (Rn_{CLM}) can be associated to: (i) The systematic underestimation / overestimation of the incoming longwave radiation (R_{Lin}) / outgoing longwave radiation (R_{Lout}) components, (ii) the CLM vertical numerical solving of longwave radiation fluxes is not able to account for environmental influences (horizontal variability) of the local micro climate (especially true for single-point simulations); and (iii) the insufficient compensation of sensible fluxes to the surface area as a consequence of heat loss of the system to the atmosphere (in the form of R_{Lout}). H and LE are not only affected by the partitioning of energy and the vertical exchange, but also by TKE, which is thermally and mechanically induced in the diurnal cycle due to the steep terrain (anabatic and katabatic flows). Our results expose a higher variability in the measured heat fluxes, a stronger divergence of Rn associated with stronger ground heat fluxes, especially during less cloudy / rainy events. However, strong perturbations are not reflected in a single-point simulation (i.e., small-scale turbulences / windy situations). Taken together, CLM is constrained in the horizontal exchanges and thus, it is limited to adequately reproduce the energy budget in the páramo.

Figure 5.4 illustrates a 4-day time series (where clear and cloudy conditions occur sequentially) for the modeled and observed components of Rn: Incoming shortwave radiation (R_{Sin}), outgoing shortwave radiation (R_{Sout}), R_{Lin} , and R_{Lout} . Respective correlation analyses are depicted through hourly-time scale scatterplots (22-month period).

In Fig. 5.4, CLM was able to reproduce the shortwave (incoming and outgoing) components with a good correlation ($R^2 = 0.93$ and 0.87 respectively). However, the R_{LinCLM} values reveal a strong underestimation for the cloudy days, and consequently a low regression coefficient ($R^2 = 0.17$) is present. On the other hand, $R_{LoutCLM}$ values show relatively consistent with the measurements. This analysis reveals a systematic problem in CLM, attributed to its inability to properly simulate the R_{Lin} in cloudy sky presence (high diffuse radiation conditions) and other site-specific characteristics of the páramo (parameterized in the model). Considering that more than 87% of the period of analysis the páramo exhibits a high cloudiness, the aforementioned underestimation of R_{LinCLM}

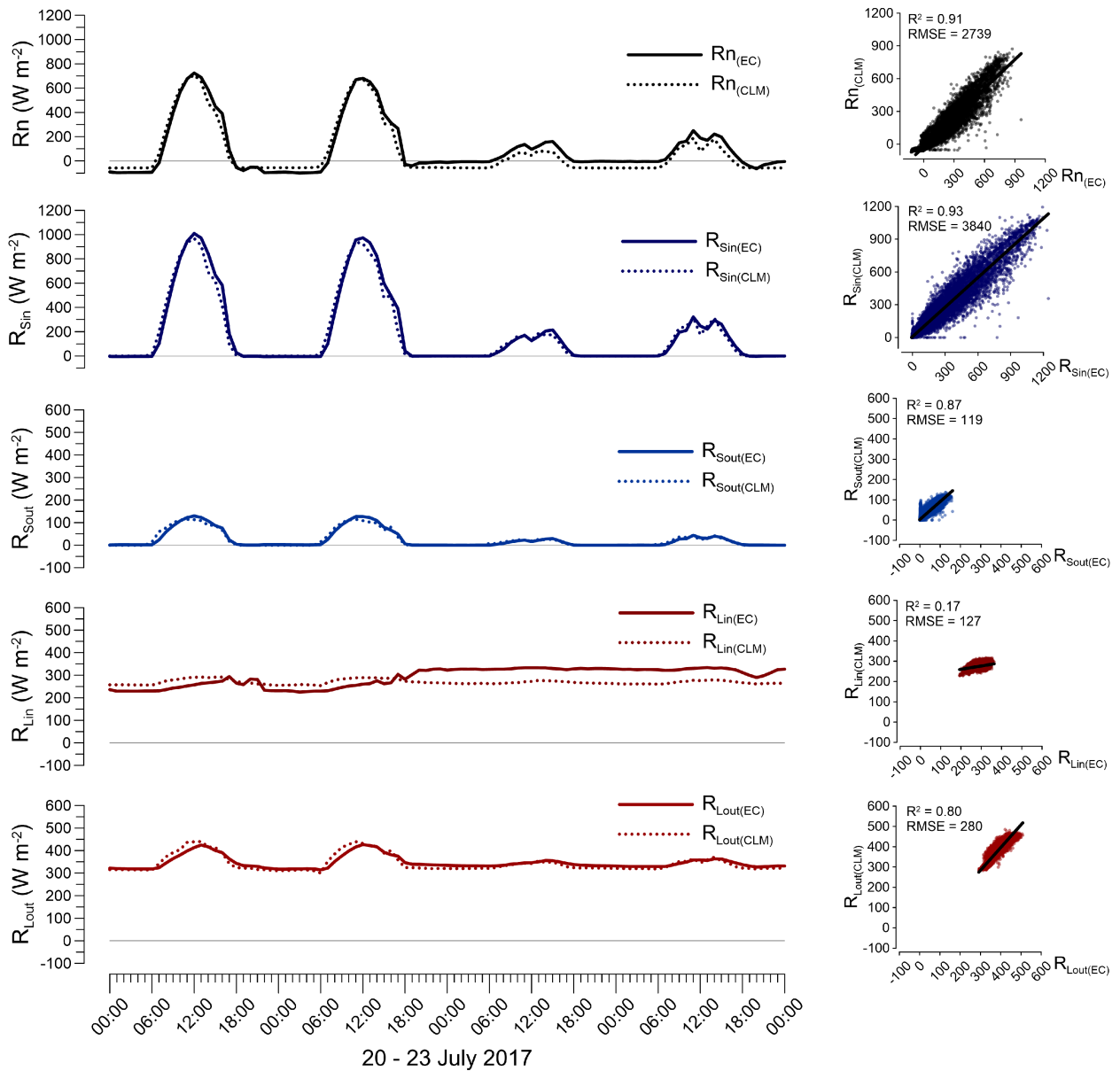


Figure 5.4: Analysis of the four components of R_n : Daily course for R_n , R_{Sin} , R_{Sout} , R_{Lin} and R_{Lout} on two clear sky and two cloudy consecutive days. Hourly-step scatterplots for the 22-month period of CLM-derived and EC-observed values.

5 Atmosphere-surface fluxes modeling

clearly impacts the balance of R_n , and consequently to the turbulent fluxes.

Páramo soils are characterized by a large SOC, which promotes an insulating effect, a reduction in thermal conductivity and an increment in soil heat retention. Sun et al. (2016) demonstrated that the high SOC levels found in cold alpine regions of Tibet severely impact CLM SWC modeled values (underestimation up to 12%). During our evaluation period, Zhurucay showed a measured SWC of $0.75 \pm 0.10 \text{ m}^3 \text{ m}^{-3}$ (10 cm depth) versus the CLM SWC of 0.35 ± 0.07 and $0.37 \pm 0.08 \text{ m}^3 \text{ m}^{-3}$ (6.2 cm and 11.8 cm depth, respectively). For Quinoas, the observed SWC was of $0.68 \pm 0.04 \text{ m}^3 \text{ m}^{-3}$ (10 cm depth) versus the CLM SWC was of 0.35 ± 0.05 and $0.37 \pm 0.06 \text{ m}^3 \text{ m}^{-3}$. Thus, the overall CLM SWC underestimation range between 46 ~ 53% and it can be attributed to a systematic issue in the model. The modeled SWC values are lower than the permanent wilting point for the páramo vegetation of Zhurucay ($0.45 \text{ m}^3 \text{ m}^{-3}$) reported by Aucapiña and Marín (2014). In addition, the aforementioned overestimation in LE_{CLM} can be associated to the wrong SWC estimation in the model. Figure 5.10 of supplementary materials illustrates the temporal variability of measured and modeled SWC for both catchments.

5.3.2 Representativeness of catchment-scale and footprint-scale

$ETa_{(METRIC)}$ areal estimates

In Figure 5.5, catchment-scale areal estimates from $ETa_{(METRIC)}$ are shown next to the areal fraction of $ETa_{(METRIC)}$ within the source footprint of $ETa_{(EC)}$ fluxes. This was done in order to analyze the representativeness of the remote-sensing based ETa estimates for the full catchment area, particularly due to the spatial heterogeneity of the páramo terrain. A 16-month aggregated $ETa_{(METRIC)}$ map was used, where $ETa_{(EC)}$ observations were available. Also, 5-month of wet and less humid sub-periods ETa maps (from the same 16-month time series) were analyzed independently. The EC footprint area was calculated according to Kljun et al. (2015) and represents the area where 80% of the fluxes came from in the respective 16-month, 5-month wet and 5-month less humid periods.

The spatial distribution of the 16-month $ETa_{(METRIC)}$ map is in agreement with the land cover heterogeneity and terrain complexity of the Zhurucay catchment. Areas with a noticeable water vapor loss ($>900 \text{ mm}$) correspond to wetlands, forest patches, shrub lands and bottom-valley evergreen vegetation (with maximum values for water bodies or forest patches, and minimum values for some hilltop peaks with dry bare soils). The full catchment is dominated by tussock grasses and Andosols which evaporate the most of the water ($ETa_{(METRIC)}$ mean of 750 mm for the full period). As expected, the wet period exhibits a lower ETa spatial mean value (224 mm) than the

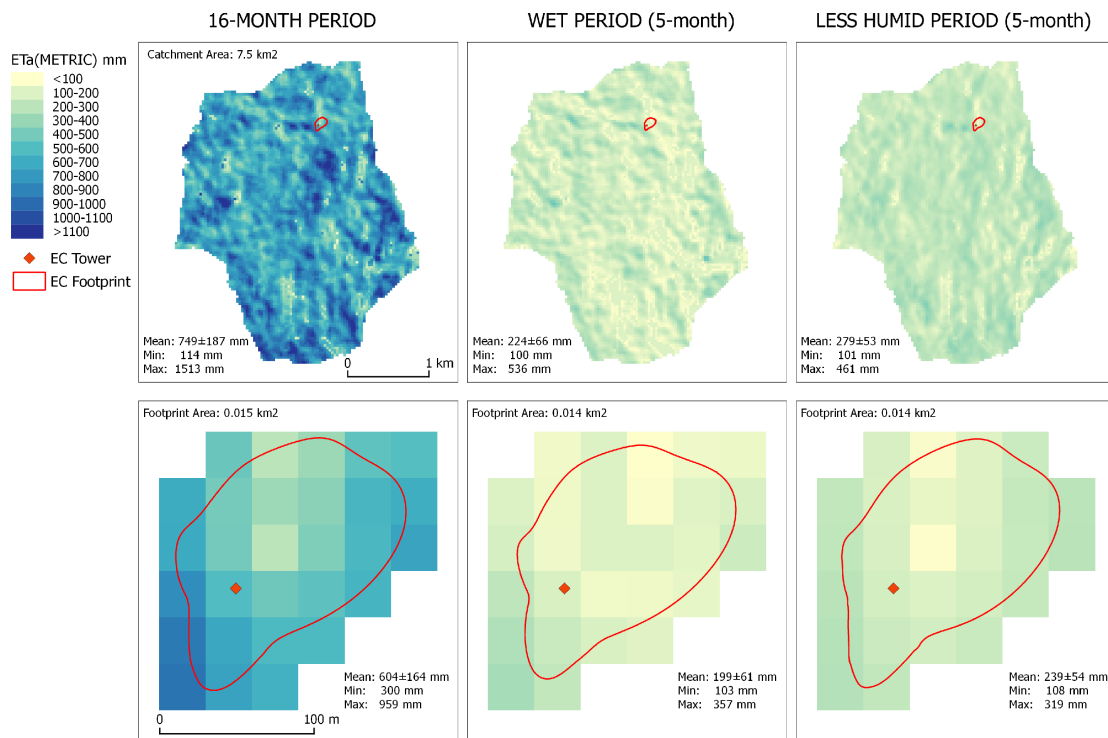


Figure 5.5: Zhurucay $ETa_{(METRIC)}$ maps for a 16-month period (March 2016 to June 2017), wet sub-period (5-month: March, April, May, June and October 2016) and less humid sub-period (5-month: July, August, September, November and December 2016). The EC footprint boundaries (80% of source flux area) for each period are drawn in red lines. Spatial ETa statistics are provided.

5 Atmosphere-surface fluxes modeling

spatial mean of ET_a calculated from the less humid period (279 mm). Such difference is attributed to the higher levels of radiation during the less humid months of August, September, November and December, which increases the VPD and consequently favors a higher evaporation. This behavior was also reported by Carrillo-Rojas et al. (2016) for the Quinoas catchment.

During the 16-month period (as well as the wet and less humid sub-periods), 80% of the source footprint was found within the first 140 meters from the tower, covering an area between 0.014 ~ 0.015 km² (i.e., 0.2% of the catchment extent). This ET_{a(ETC)} source area is characterized by a gentle slope (10°) which has a homogeneous tussock grassland canopy over Andosols. The area corresponds to 29 pixels (30 m of resolution) from the ET_{a(METRIC)} map, where the areal mean value is 604 mm for the 16-month period. ET_{a(METRIC)}-footprint mean value is 19% lower than the ET_{a(METRIC)}-full catchment mean value. Similarly, the ET_{a(METRIC)}-footprint areal mean for the wet and less humid sub-periods are 199 and 239 mm respectively. These values are lower (11% and 14%) than their correspondent ET_{a(METRIC)}-full catchment area mean. The small extent of the footprint in comparison to the catchment area clearly influences on the aforementioned underestimations.

In addition, the ET_{a(ETC)} aggregated values for the 16-month, the wet and less humid periods are 848, 237 and 287 mm respectively, which is 40%, 19% and 20% more evapotranspiration than the corresponding ET_{a(METRIC)}-footprint water losses. Some studies validated LE or ET_a METRIC outputs with EC measurements in different ecosystems or cropland areas. For instance, Liaqat and Choi (2015) found ET_{a(METRIC)} values with overestimations up 48% for an alpine meadow of Qinghai, China; de la Fuente-Sáiz et al. (2017) found LE_{METRIC} values which were overestimated by about 26% for apple orchards in Chile; in contrast Madugundu et al. (2017) reported daily ET_{a(METRIC)} values which were underestimated by 4.2 % for alfalfa croplands of Saudi Arabia.

Based on these findings, we used the full-catchment ET_{a(METRIC)} estimates for the further analyses in this study. This also allows that future catchment-scale ET_a estimations can be easily replicated (and validated) in other mountainous locations with limited or inexistent ground-level ET_a measurements.

5.3.3 Evaluation of CLM modeled ET_a and remote sensing-based ET_a versus ground-level ET_a observations in both catchments

Results of section 5.3.1 demonstrated the suitability of CLM to predict ET_a fluxes at sub-daily and daily time steps, and results of section 5.3.2 revealed the suitability of catchment-scale areal

estimates of ETa derived from METRIC. Thus, we conducted a comparative analysis between $ETa_{(CLM)}$ and $ETa_{(METRIC)}$ outcomes in comparison to water balance-based $ETa_{(WB)}$ and water vapor detection-based $ETa_{(EC)}$ observations. Figure 5.6 illustrates the performance of the models against the best-available observation for each catchment (EC for Zhurucay and WB for Quinoas) in the form of Taylor diagrams (Taylor, 2001) at monthly-scale aggregated ETa. Normalized SD, normalized RMSE and Pearson correlation give a goodness-of-fit overview of how well the models matched the observations. As we mentioned in section 5.2.7, the period used for this assessment was limited to 16 months.

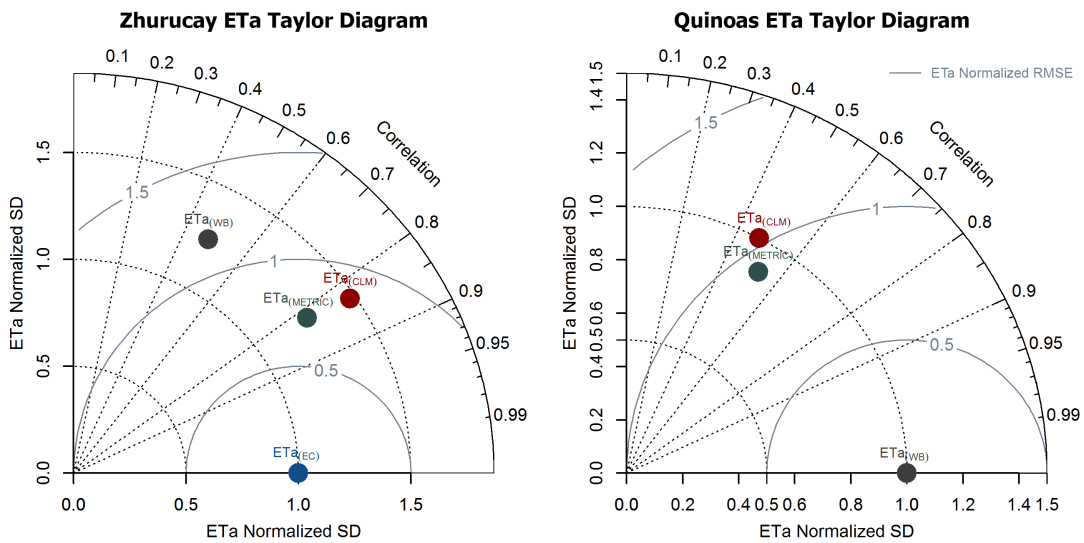


Figure 5.6: Taylor diagrams for $ETa_{(CLM)}$ and $ETa_{(METRIC)}$ vs. the best available ETa observation method for each site. Zhurucay diagram also includes the $ETa_{(WB)}$ estimation for comparison purposes. Statistics of normalized SD (concentric lines from zero), normalized RMSE (concentric lines from the reference method) and Pearson correlation (radial lines) are illustrated.

Zhurucay's Taylor diagram reveals high correlation levels for $ETa_{(CLM)}$ ($R = 0.82$) and $ETa_{(METRIC)}$ ($R = 0.83$). However, both model outputs show higher (>1.0) deviations (SD $ETa_{(CLM)} = 1.26$, and SD $ETa_{(METRIC)} = 1.46$) along lower (<1.0) errors (RMSE $ETa_{(CLM)} = 0.72$, and RMSE $ETa_{(METRIC)} = 0.85$) compared to the direct EC measurements as reference. We found that $ETa_{(WB)}$ has a relatively low correlation compared to our EC-based observations ($R = 0.46$), a similar deviation (SD = 1.25) but with a high error (RMSE = 1.20). This finding suggests that the closure of the water balance method might not suit ideal for an accurate estimation of ETa in the páramo at monthly scale. However, for long-term periods and annual scale the use of $ETa_{(WB)}$

5 Atmosphere-surface fluxes modeling

can be a reliable approach. This is crucial because researchers have shown an increased interest in $ETa_{(WB)}$ (Buytaert et al., 2006c; Carrillo-Rojas et al., 2016; Mosquera et al., 2015) due to the absence of direct measurements of water vapor in this ecosystem.

In spite of this evidence, we used $ETa_{(WB)}$ as the only available (and ground-level) evaluation method for the CLM and METRIC ETa outcomes in Quinoas. The Taylor diagram for this location reveals $ETa_{(CLM)}$ and $ETa_{(METRIC)}$ correlation coefficients of 0.46 and 0.54 respectively. Furthermore, SD as well as RMSE calculated for both models have relatively similar values (SD $ETa_{(CLM)}$ = 1.01 and SD $ETa_{(METRIC)}$ = 0.84; RMSE $ETa_{(CLM)}$ = 1.05 and RMSE $ETa_{(METRIC)}$ = 0.90). These results are similar to those of Zhurucay from a point of view of evaluation, but a large uncertainty clearly exists due to the reference method applied (WB). This consideration must be taken into account in future evaluations of $ETa_{(WB)}$ estimates at similar timescale and locations.

Figure 5.7 depicts the 16-month cumulative balances of $ETa_{(CLM)}$, $ETa_{(METRIC)}$, $ETa_{(WB)}$ and $ETa_{(EC)}$ (the latter for Zhurucay exclusively) along cumulative P, Q and ΔS for each catchment.

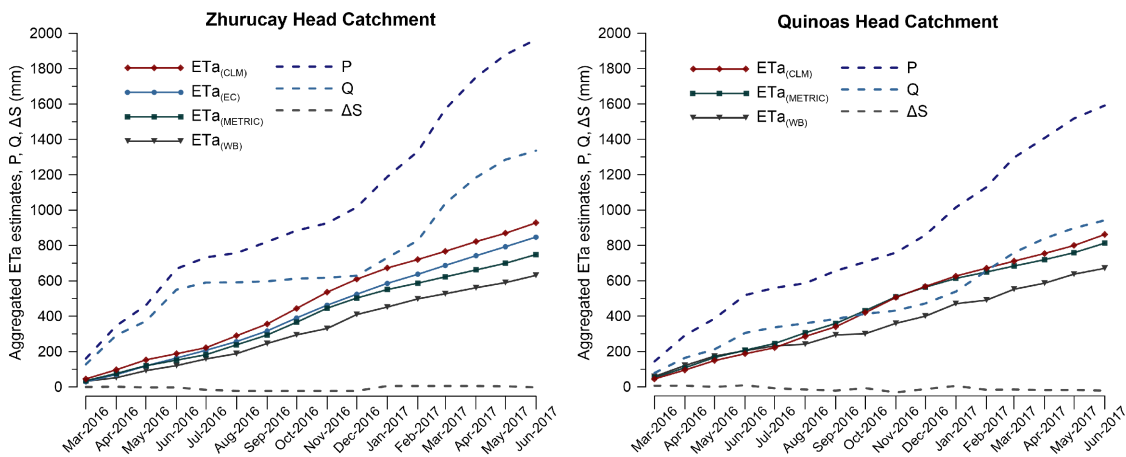


Figure 5.7: Monthly aggregated $ETa_{(CLM)}$, $ETa_{(METRIC)}$, $ETa_{(EC)}$ and $ETa_{(WB)}$ for both catchments. P, Q and ΔS are also included.

Cumulative $ETa_{(CLM)}$ values for Zhurucay exposes the higher slope, followed by $ETa_{(EC)}$ observations, the catchment-level (and spatial-averaged) $ETa_{(METRIC)}$, and the aggregated $ETa_{(WB)}$. P and Q curves show consistent temporal variability. Some ΔS values are closer to zero or become negative in the series. Differences in the cumulative ETa results will be explained further in Table 5.2. The Quinoas ETa curves are closer to each other than their equivalents in Zhurucay. Moreover, $ETa_{(CLM)}$ and $ETa_{(METRIC)}$ in this catchment have at every time step relatively similar values, while $ETa_{(WB)}$ shows slightly lower values. The curves of P, Q and ΔS share similar characteristics

than those of Zhurucay.

ETa differences between Zhurucay and Quinoas can be associated with the extent of the catchments (relation 1 : 2.6) as well as with the spatial representativeness and topography (particularly for $ETa_{(METRIC)}$ and $ETa_{(WB)}$). Uncertainties in ETa derived from WB are mainly related to (i) the spatial interpolation method (Thiessen algorithm and a limited density of points for interpolation), (ii) low density of precipitation sensors, (iii) catchment homogeneity, and (iv) limitations of the tipping bucket technique (underestimation of rainfall). This is especially true for the latter point where the contributions of drizzle (Muñoz et al., 2016; Padrón et al., 2015) and fog (Cárdenas et al., 2017) to the hydrological balance of our sites are unknown. Also, errors associated to the discharge measurements should be considered. In addition, ETa derived from METRIC-Landsat mapping is prone to uncertainties due to (i) the scarcity of cloud free imagery, (ii) gap filling / interpolation effects, (iii) strong changes in soil moisture (due to precedent rainfall events), and (iv) constrained spatial fidelity (Carrillo-Rojas et al., 2016). In summary, we observe that $ETa_{(METRIC)}$ and $ETa_{(CLM)}$ estimates tend to align close to the available reference method on both páramo locations investigated. Table 5.2 shows the ETa and hydrological balances for the cumulative 16-month evaluation period for each catchment.

Table 5.2: Modeled and observed ETa and hydrological balances for the 16-month period.

	ZHURUCAY	% Bias with $ETa_{(EC)}$	% Bias with $ETa_{(WB)}$ *	% ETa/P Ratio	QUINOAS	% Bias with $ETa_{(WB)}$	% ETa/P Ratio
$ETa_{(CLM)}$ (mm)	928.1	+9.5	+47.0	47.2	861.4	+28.5	54.1
$ETa_{(METRIC)}$ (mm)	748.6	-11.7	+18.6	38.1	812.7	+21.3	51.1
$ETa_{(WB)}$ (mm)	631.2	-25.5	-	32.1	670.3	-	42.1
$ETa_{(EC)}$ (mm)	847.7	-	+34.3	43.1	-	-	-
P (mm)	1965.0				1590.9		
Q (mm)	13365.9				941.9		
ΔS (mm)	-2.2				-21.3		
Runoff Coeff.	0.68				0.59		

* WB was not the primary reference method for Zhurucay, only depicted for comparative purposes.

Modeled $ETa_{(CLM)}$ results for Zhurucay indicate an overestimation of $\sim 10\%$ when compared to $ETa_{(EC)}$ and of 47% when compared to $ETa_{(WB)}$. A lower overestimation is observed in Quinoas ($\sim 29\%$) in comparison with $ETa_{(WB)}$. Modeled $ETa_{(METRIC)}$ underestimates the water loss by $\sim 12\%$ when validated with $ETa_{(EC)}$, but the opposite is revealed when compared to $ETa_{(WB)}$ in

5 Atmosphere-surface fluxes modeling

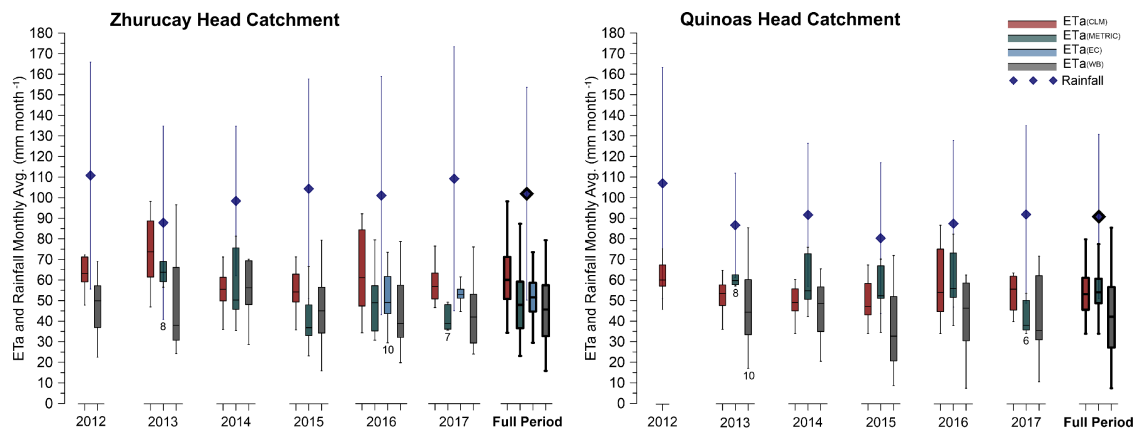


Figure 5.8: Inter-annual $ETa_{(CLM)}$, $ETa_{(METRIC)}$, $ETa_{(EC)}$ and $ETa_{(WB)}$ boxplots (monthly averaged). Monthly mean of precipitation (with SD) is also depicted. Some ETa boxplots with limited monthly coverage include the number of available months below.

Zhurucay (overestimation of $\sim 19\%$). This behavior is also observed in Quinoas since $ETa_{(METRIC)}$ overestimates the $ETa_{(WB)}$ by $\sim 21\%$ for the period. These values are in the same range as those reported by Carrillo-Rojas et al. (2016) for the same upland catchment of Quinoas between 2013-2014, and the annual-scale biases reported by Karimi and Bastiaanssen (2014) for spatial ETa applications on croplands.

A noticeable difference exists between the evaluation methods presented in this study ($ETa_{(WB)}$ underestimates $ETa_{(EC)}$ by $\sim 26\%$). ETa / P ratios show different values for each method and location. Nonetheless, the $ETa_{(EC)} / P$ ratio (43.1%) is very close to the one reported by Mosquera et al. (2015) (44.6%) for a micro-catchment of Zhurucay (contained inside our study area). P , Q and ΔS show strong differences (Zhurucay possesses $\sim 24\%$ more rainfall, $\sim 42\%$ more runoff, and $\sim 90\%$ less water storage than Quinoas), in spite of a small difference (+15%) in the runoff coefficients. Geographic position, topography, edaphic characteristics and the presence of water bodies in Quinoas are key elements involved in such differences.

Finally, a statistical evaluation of monthly ETa averages for each year of the full period of CLM simulations (6 years) was conducted. Figure 5.8 exhibits boxplots of the monthly values for each ETa estimation / observation method (95% confidence interval) at an annual time-step.

For Zhurucay the full period median value for $ETa_{(CLM)}$ shows small differences in relation to $ETa_{(METRIC)}$, $ETa_{(EC)}$ and $ETa_{(WB)}$ of +20%, +14% and +24% respectively. The interannual differences are more distinct if calculated from $ETa_{(WB)}$ than using another method (from -1% up to +48%). ETa sensitivity to rainfall is noticeable for most methods. For Quinoas the full period

5.4 Concluding remarks and future directions

median value for $ETa_{(CLM)}$ shows lower differences to the $ETa_{(METRIC)}$ (underestimation of 2%) and $ETa_{(WB)}$ (overestimation of +21%). As in Zhurucay, the interannual differences are more pronounced for $ETa_{(WB)}$ than for $ETa_{(METRIC)}$. Rainfall also has an impact on ET variability. 25% and 75% percentiles and the upper and lower whiskers (maximum and minimum values) show larger ranges for Zhurucay than for Quinoas, with the exception of $ETa_{(WB)}$ where we have the stronger variation for Quinoas. The latter probably can be attributed to characteristics of the catchment (i.e., extent, topography and the presence of water bodies). Most of the LSM and spatial methods tend to oversimplify thermal and hydrological calculations. This situation reduces the accuracy of the prediction particularly for plot-scale investigations such as the one presented here.

Some studies have assessed the performance of CLM (as standalone component of CESM and coupled with the Weather Research and Forecasting model, WRF-CLM) with the METRIC model for the spatial estimation of ETa in the United States (Ozturk, 2015; Wang et al., 2017). The evidence points out to a general underestimation of ETa by the LSM when compared to remote-sensing ETa , mainly due to the inability to simulate rainfall and soil moisture accurately, and to the generalization of LAI input values. In our case, the use of ground-level climate forcings for the single-point CLM simulations provides an improvement in the final ETa estimation, in spite of the slight overestimation observed. However, the benefits on flux predictions by the use of site-specific LAI on the CLM parameterization remains unknown.

5.4 Concluding remarks and future directions

Very little was known about the plausibility of a LSM for the prescription of energy and ETa fluxes in the Northern Andean páramo, until now. Our research described a successful parameterization of the state-of-art CLM for two representative catchments of this biome. However, the evaluation of model results with ground-level flux measurements revealed some degree of inability of the model to reproduce R_n , H and G accurately. Nonetheless, CLM demonstrated to be suitable for LE and ETa prediction. The comparative analyses of modeled ETa with remote-sensing, water balance and water vapor detection-based methods proved the CLM's effectiveness to simulate this functional indicator at monthly and annual scales. Furthermore, ETa values from CLM exposed the expected variability at inter-annual scale (6-year period) and was consistently related to the precipitation pattern. However, uncertainties induced by the internal structure of CLM, the internal parameters of the PFT selected (C3 arctic grass), the internal mechanism of the $R_{Lin}(CLM)$ modeling, and soil forcing data remain pending to explore. Also, due to the evidence that SOC in cold / alpine regions

5 Atmosphere-surface fluxes modeling

severely impacts SWC (and potentially the thermal exchange) the investigation of these effects in CLM needs further assessment.

METRIC demonstrated its suitability for spatio-temporal ETa estimation on the catchment scale. This fact confirms that the METRIC model performs as a trustworthy tool for the prediction of ET water loss on the harsh environmental conditions of this remote ecosystem (Carrillo-Rojas et al., 2016). Of particular concern is that ETa results obtained as hydrological balance residual (WB) were considerably different from the other approaches, showing strong biases and a higher variability. Main reasons for such discrepancies might be the spatial representativeness of the rainfall measurements (Thiessen method with a limited density of points for interpolation), the limitations of the tipping bucket technique and the uncertainties associated to the water discharge measurements. In hydrological models, the precipitation, discharge and change in soil moisture are the main variables involved. No other variables such as groundwater recharge are key and therefore even conceptual models can be reliable to estimate ETa. The reader has the opportunity to analyze the benefits and limitations of this widely available and cheaper method (WB) in comparison to an expensive, scarce and direct method of water vapor quantification (EC) for ETa survey on this Andean ecosystem. Testing of alternative ETa methods is further needed for the two sites used in this paper, as well as for other Andean sites, for instance: (i) hydrological approaches, such as volumetric / weighing lysimeters or atmometer; (ii) other micrometeorological techniques, such as Bowen ratio, energy budget or scintillometer; and also (iii) the partition of ET components, for transpiration: leaf-level porometry, plant-level chamber or sap flow, and for soil evaporation: soil moisture-depletion (Kool et al., 2014; Rana and Katerji, 2000; Shuttleworth, 2008).

Recent studies provide insights into the potential effects of climate change on precipitation and temperature on the Andean highlands, and particularly on the Ecuadorian cordillera. Herein, the increase in precipitation (frequency and strength) and warming of the atmosphere (Morán-Tejeda et al., 2016; Vuille et al., 2015) are probably expected in the future. Our results suggest that LSMs should be considered as powerful tools for the prediction of ecosystem functional fluxes in land cover or climate change modeled scenarios. Nonetheless, the current available coarse grid of modeled climate change-datasets from regional climate models needs to be downscaled and adjusted to serve as forcing for LSMs, particularly for mountainous locations as the páramo.

Future work could be focused on the determination of physio-morphological characteristics of the native vegetation (leaf and roots) for a better estimation of energy and ET in CLM. Moreover, this will be a crucial requirement if the simulation of carbon fluxes (net ecosystem exchange, primary production and respiration) is pursued, as it was demonstrated for other Andean sites (Göttlicher

et al., 2011; Minaya et al., 2016; Silva et al., 2012). Further studies which take these variables into account, will need to be undertaken.

Acknowledgments

This work was funded by the Research Office of the University of Cuenca (DIUC) through the Project XVI-Conc. "Intercambio suelo-vegetación-atmósfera de flujos de energía y vapor de agua para condiciones de cambio climático, mediante modelamiento con CESM-CLM aplicado al ecosistema de páramo andino". The first author especially thanks SENESCYT and the Ecuadorian Government for funding his doctoral scholarship. We thank the German Research Foundation (DFG) and the Project FOR-2730 "Environmental changes in biodiversity hotspot ecosystems of South Ecuador: RESPonse and feedback effECTs (RESPECT)" - Subproject A1: "Atmospheric fluxes and optical trait diversity under climate and land use changes - observations and LSM modelling", which supported the study in human and scientific capacities. We also thank Comuna Chumblín Sombredas (Azuay, San Fernando) and INV Metals (Canada), Project Loma Larga-Ecuador, for providing logistical support. We are grateful to Patricio Crespo, Gina Berrones, Juan Pesántez and the technical staff of iDRHiCA, and to Maik Dobbermann and Pablo Contreras for their support in the computational implementation of CLM in Germany and Ecuador.

Supplementary material

Supplementary Table 5.3: Instrumentation used in the experiment.

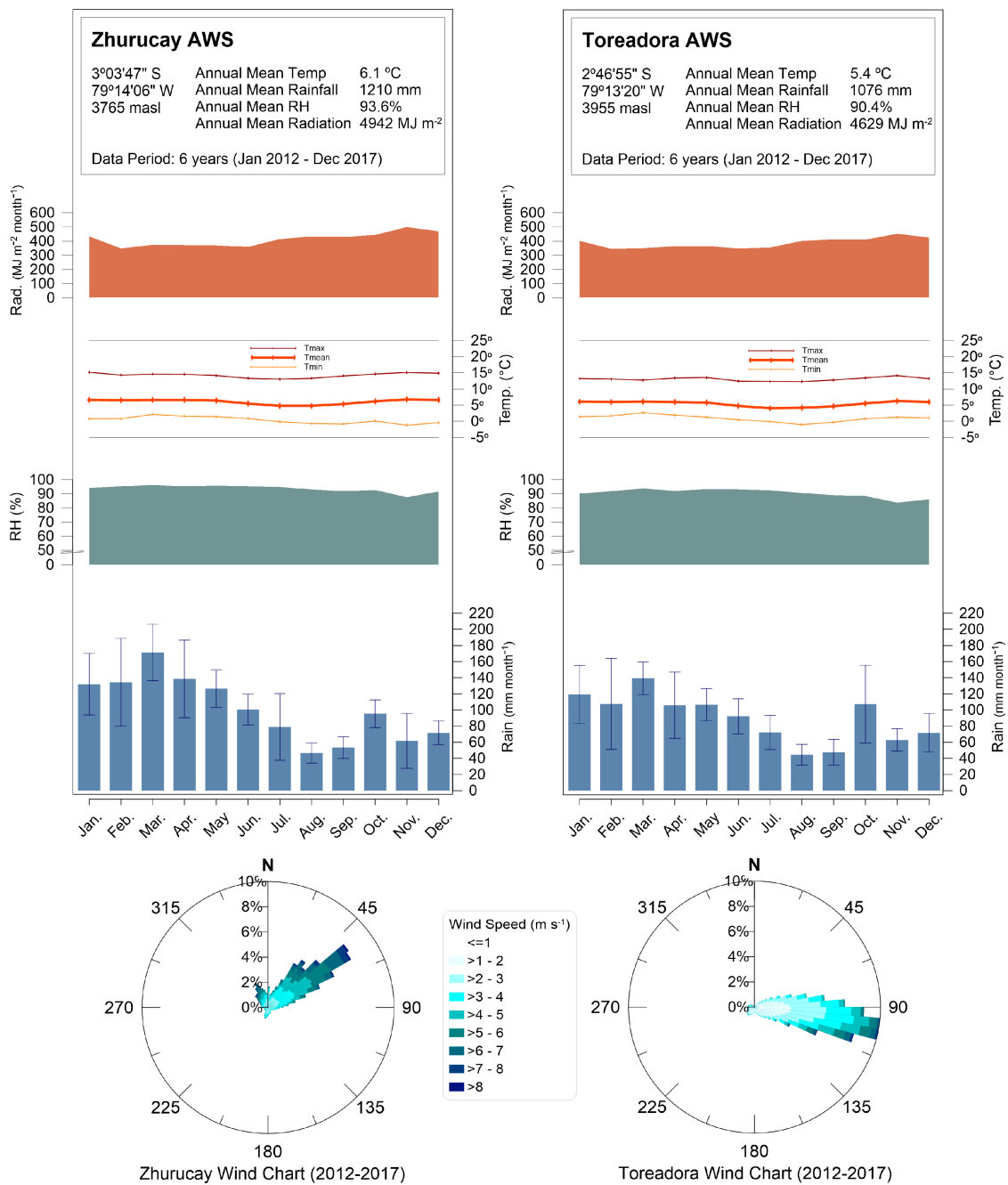
Location	Instrument	Variable	Sensors Type and Setup	Unit / Time Resolution	Accuracy
Zhurucay - Head Micro Catchment	CO₂ and H₂O Gas Fluxes and Sensible Heat (Fast Sensors) With LI-7550 Analyzer Unit	CO ₂ and H ₂ O gas concentration	Enclosed Path IRGA: LI-COR LI-7200 with heated intake tube at 3.6 m height	ppm and mmol mol ⁻¹ / 20 Hz	CO ₂ : Within 1% of reading H ₂ O: Within 2% of reading
		Wind Speed/Direction/ Sonic temperature	3D Sonic Anemometer: GILL-WM Gill New WindMaster at 3.6 m height	m s ⁻¹ / 20 Hz	Wind Speed <1.5%RMS, Direction <2° (at 12 m s ⁻¹) Sonic Temp. < ±0.5% @ 20°C
	Complementary Micrometeorological sensors (Slow sensors) With Sutron 9210B data logger	Net Radiation	4-Component Net Radiometer: Kipp & Zonen CNR4 at 3.6 m height	W m ⁻² / 1 min	<1%
		Soil Heat Flux	Three Soil Heat Flux Plates: Hukseflux HFP01 at 5 cm soil depth	W m ⁻² / 1 min	±0.3%
		Soil Moisture and Temperature	Three Water Content Reflectometers: Stevens Hydra Probe II (each with temperature probes) at 5 cm soil depth	cm ³ cm ⁻³ / 1 min °C / 1 min	Stevens Hydra Probe II (Soil moisture ±2.0% , Soil Temp. ±0.3°C)
		Air temperature and relative humidity PPFD	Thermometer/Hygrometer: Vaisala HMP155 + Radiation Shield at 3 m height Quantum Sensor:LI-COR LI190-R at 3.6 m height	°C and %RH / 1 min $\mu\text{mol s}^{-1}\text{Åm}^{-2}$	±1.7%RH (>90%RH) / ± 0.226 °C <1%
	Automatic Weather Station (AWS) With Campbell CR1000 data logger	Total Solar Radiation	Pyranometer: Campbell CS300 at 2 m height	W m ⁻² / 5 min	±5% daily total
		Air temperature and relative humidity	Thermometer/Hygrometer: Campbell CS-215 + Radiation Shield at 2 m height	°C and %RH / 5 min	±0.3 °C / ±2% RH
		2D Wind Speed/Direction	Anemometer: Met-One 034B Wind Set at 2 m height	m s ⁻¹ / 5 min	±0.11 m s ⁻¹
		Barometric Pressure	Barometer: Vaisala PTB110	hPa/ 5 min	±0.3 hPa
Rainfall		Rain Gage: : Texas TE525MM with wind shield at 1 m height	mm/ 1 min	±1%	
Soil Humidity	Ten Water Content Reflectometers: Campbell CS-616	cm ³ cm ⁻³ / 5 min	Soil moisture ±2.5%		
Stream Flow-gage Station (SF)	Water Level	Campbell SR50A-L Sonic Ranging Sensor	m / 5 min	±0.025 m	
Quinoas - Head Micro Catchment	Automatic Weather Station (AWS) With Campbell CR1000 data logger	Total Solar Radiation	Pyranometer: Campbell CS300 at 2 m height	W m ⁻² / 5 min	±5% daily total
		Air temperature and relative humidity	Thermometer/Hygrometer: Campbell CS-215 + Radiation Shield at 2 m height	°C and %RH / 5 min	±0.3 °C / ±2% RH
		2D Wind Speed/Direction	Anemometer: Met-One 034B Wind Set at 2 m height	m s ⁻¹ / 5 min	±0.11 m s ⁻¹
		Barometric Pressure	Barometer: Vaisala PTB110	hPa/ 5 min	±0.3 hPa
		Rainfall	Rain Gage: : Texas TE525MM with wind shield at 1 m height	mm/ 1 min	±1%
		Soil Humidity	Two Water Content Reflectometers: Campbell CS-616	cm ³ cm ⁻³ / 5 min	Soil moisture ±2.5%
	Stream Flow-gage Station (SF)	Water Level	Campbell SR50A-L Sonic Ranging Sensor	m / 5 min	±0.025 m

Supplementary Table 5.4: Landsat imagery used in ETa mapping (METRIC)

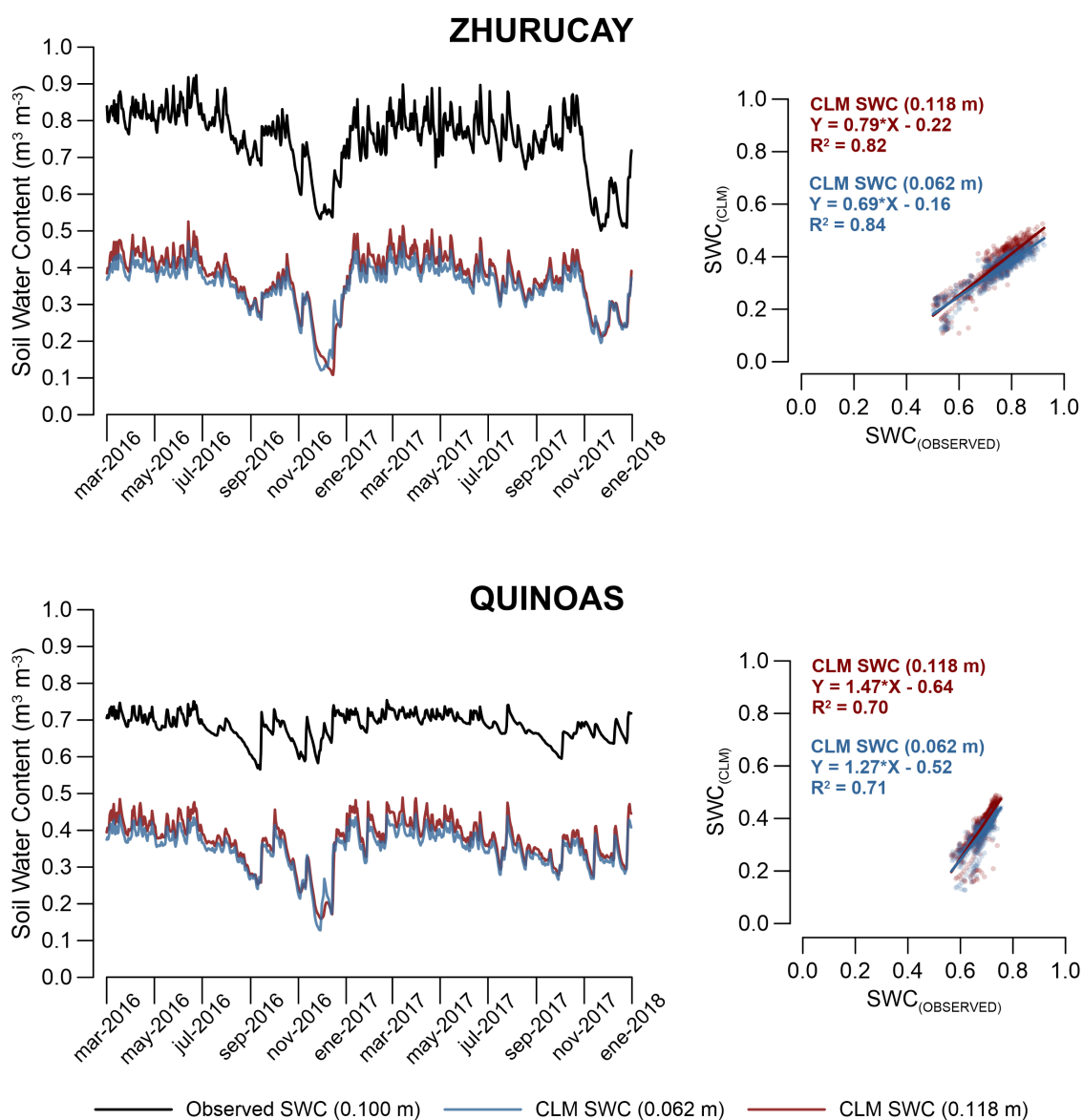
Landsat 7 ETM+ SLC-off scene ID	Date	Path/Row	Cloud and cloud-shadow over the full study area (%) *
LE70100622013116EDC00	2013-Apr-26	10/62	3.0
LE70100622013180EDC00	2013-Jun-29	10/62	1.0
LE70100622013292EDC00	2013-Oct-19	10/62	5.0
LE70100622014087EDC00	2014-Mar-28	10/62	8.0
LE70100622014183EDC00	2014-Jul-02	10/62	2.0
LE70100622014215EDC00	2014-Aug-03	10/62	3.0
LE70100622015122EDC00	2015-May-02	10/62	<12.0
LE70100622015234EDC00	2015-Aug-22	10/62	<30.0
LE70100622016237EDC00	2016-Aug-24	10/62	0.0
LE70100622016301EDC00	2016-Oct-27	10/62	0.0
LE70100622017175EDC00	2017-Jun-24	10/62	4.0
LE70100622017191EDC00	2017-Jul-10	10/62	0.0
LE70100622017223EDC00	2017-Aug-11	10/62	<15.0

* * Identified before the mosaicking procedure.

5 Atmosphere-surface fluxes modeling



Supplementary Figure 5.9: 6-year Zhurucay and Quinoas (Toreadora AWS) Climographs (January 2012 to December 2017).



Supplementary Figure 5.10: Temporal variability of simulated SWC (CLM: 0.062 m and 0.118 m depth) versus Observed SWC (0.100 m depth) at daily frequency for both catchments (16-month period). Scatterplots for the available date are also depicted.

References

- Allen, R. G., Tasumi, M., and Trezza, R. (2007). Satellite-Based Energy Balance for Mapping Evapotranspiration with Internalized Calibration (METRIC)-Model. *Journal of Irrigation and Drainage Engineering*, 133(4):380–394.

5 Atmosphere-surface fluxes modeling

- Anderson, E. P., Marengo, J., Villalba, R., Halloy, S., Young, B., Cordero, D., Gast, F., Jaimes, E., and Ruiz, D. (2011). Consequences of Climate Change for Ecosystems and Ecosystem Services in the Tropical Andes. In Herzog, S. K., Martínez, R., Jørgensen, P. M., and Tiessen, H., editors, *Climate Change and Biodiversity in the Tropical Andes*, pages 1–18. Inter-American Institute for Global Change Research (IAI), São José dos Campos, SP, Brazil, 1st edition.
- ASCE-EWRI (2005). *The ASCE Standardized Reference Evapotranspiration Equation*. ASCE-EWRI Standardization of Reference Evapotranspiration Task Committee Rep., ASCE Reston, Va.
- Aubinet, M., Vesala, T., and Papale, D. (2012). *Eddy Covariance: A Practical Guide to Measurement and Data Analysis*. Springer Netherlands, Dordrecht.
- Aucapiña, G. and Marín, F. (2014). *Efectos de la posición fisiográfica en las propiedades hidrofísicas de los suelos de páramo de la microcuenca del Río Zhuruca*. Graduate thesis, Universidad de Cuenca, Ecuador.
- Baldocchi, D., Chu, H., and Reichstein, M. (2018). Inter-annual variability of net and gross ecosystem carbon fluxes: A review. *Agricultural and Forest Meteorology*, 249(May):520–533.
- Bendix, J., Rollenbeck, R., Göttlischer, D., and Cermak, J. (2006). Cloud occurrence and cloud properties in Ecuador. *Climate Research*, 30(2):133–147.
- Best, M. J., Pryor, M., Clark, D. B., Rooney, G. G., Essery, R., Ménard, C. B., Edwards, J. M., Hendry, M. A., Porson, A., Gedney, N., Mercado, L. M., Sitch, S., Blyth, E., Boucher, O., Cox, P. M., Grimmond, C. S. B., and Harding, R. J. (2011). The Joint UK Land Environment Simulator (JULES), model description - Part 1: Energy and water fluxes. *Geoscientific Model Development*, 4(3):677–699.
- Bonan, G. (2016). Terrestrial Ecosystems and Earth System Models. In *Ecological Climatology*, chapter 25, pages 453–473. Cambridge University Press, New York, US, 3rd edition.
- Boom, A., Mora, G., Cleef, A., and Hooghiemstra, H. (2001). High altitude C4 grasslands in the northern Andes: relicts from glacial conditions? *Review of Palaeobotany and Palynology*, 115(3-4):147–160.
- Buytaert, W., Célleri, R., De Bièvre, B., Cisneros, F., Wyseure, G., Deckers, J., and Hofstede, R. (2006a). Human impact on the hydrology of the Andean páramos. *Earth-Science Reviews*, 79(1-2):53–72.
- Buytaert, W., Deckers, J., and Wyseure, G. (2006b). Description and classification of nonallophanic Andosols in south Ecuadorian alpine grasslands (páramo). *Geomorphology*, 73(3-4):207–221.
- Buytaert, W., Iñiguez, V., Célleri, R., De Bièvre, B., Wyseure, G., and Deckers, J. (2006c). Analysis of the water balance of small páramo catchments in south Ecuador. In *Environmental role of wetlands in headwaters*, pages 271–281. Springer.
- Cárdenas, M. F., Tobón, C., and Buytaert, W. (2017). Contribution of occult precipitation to the water balance of páramo ecosystems in the Colombian Andes. *Hydrological Processes*, 31(24):4440–4449.
- Carrillo-Rojas, G., Silva, B., Córdova, M., Célleri, R., and Bendix, J. (2016). Dynamic Mapping of Evapotranspiration Using an Energy Balance-Based Model over an Andean Páramo Catchment of Southern Ecuador. *Remote Sensing*,

- 8(2):160.
- Carrillo-Rojas, G., Silva, B., Rollenbeck, R., Célleri, R., and Bendix, J. (2019). The breathing of the Andean highlands: Net ecosystem exchange and evapotranspiration over the páramo of southern Ecuador. *Agricultural and Forest Meteorology*, 265:30–47.
- Célleri, R. and Feyen, J. (2009). The Hydrology of Tropical Andean Ecosystems: Importance, Knowledge Status, and Perspectives. *Mountain Research and Development*, 29(4):350–355.
- Célleri, R., Willems, P., Buytaert, W., and Feyen, J. (2007). Space-time rainfall variability in the Paute basin, Ecuadorian Andes. *Hydrological Processes*, 21(24):3316–3327.
- Chen, L., Dirmeyer, P. A., Guo, Z., and Schultz, N. M. (2018). Pairing FLUXNET sites to validate model representations of land-use/land-cover change. *Hydrology and Earth System Sciences*, 22(1):111–125.
- Comas, X., Terry, N., Hribljan, J. A., Lilleskov, E. A., Suarez, E., Chimner, R. A., and Kolka, R. K. (2017). Estimating belowground carbon stocks in peatlands of the Ecuadorian páramo using ground-penetrating radar (GPR). *Journal of Geophysical Research: Biogeosciences*, 122(2):370–386.
- Córdova, M., Carrillo-Rojas, G., Crespo, P., Wilcox, B., and Célleri, R. (2015). Evaluation of the Penman-Monteith (FAO 56 PM) Method for Calculating Reference Evapotranspiration Using Limited Data. *Mountain Research and Development*, 35(3):230–239.
- Córdova, M., Célleri, R., Shellito, C. J., Orellana-Alvear, J., Abril, A., and Carrillo-Rojas, G. (2016). Near-Surface Air Temperature Lapse Rate Over Complex Terrain in the Southern Ecuadorian Andes: Implications for Temperature Mapping. *Arctic, Antarctic, and Alpine Research*, 48(4):673–684.
- Correa, A., Breuer, L., Crespo, P., Célleri, R., Feyen, J., Birkel, C., Silva, C., and Windhorst, D. (2018). Spatially distributed hydro-chemical data with temporally high-resolution is needed to adequately assess the hydrological functioning of headwater catchments. *Science of The Total Environment*, In press.
- Correa, A., Windhorst, D., Tetzlaff, D., Crespo, P., Célleri, R., Feyen, J., and Breuer, L. (2017). Temporal dynamics in dominant runoff sources and flow paths in the Andean Páramo. *Water Resources Research*, 53(7):5998–6017.
- Crespo, P., Célleri, R., Buytaert, W., Feyen, J., Iníiguez, V., Borja, P., and De Bièvre, B. (2010). Land use change impacts on the hydrology of wet Andean páramo ecosystems. In *Proceedings of the Workshop Status and Perspectives of Hydrology in Small Basins, held at Goslar-Hahnenklee, Germany, 30 March to 2 April 2009*, number APRIL, page 6, Germany. IAHS Publ. 336.
- Crespo, P. J., Feyen, J., Buytaert, W., Bücker, A., Breuer, L., Frede, H.-G., and Ramírez, M. (2011). Identifying controls of the rainfall-runoff response of small catchments in the tropical Andes (Ecuador). *Journal of Hydrology*, 407(1-4):164–174.
- de la Fuente-Sáiz, D., Ortega-Farías, S., Fonseca, D., Ortega-Salazar, S., Kilic, A., and Allen, R. (2017). Calibration of METRIC Model to Estimate Energy Balance over a Drip-Irrigated Apple Orchard. *Remote Sensing*, 9(7):670.
- Emck, P. (2007). *A Climatology of South Ecuador-With special focus on the Major Andean Ridge as Atlantic-Pacific*

5 Atmosphere-surface fluxes modeling

Climate Divide. Phd thesis, Friedrich Alexander-Universität, Erlangen-Nürnberg, Germany.

- Fatichi, S., Pappas, C., and Ivanov, V. Y. (2016). Modeling plant-water interactions: an ecohydrological overview from the cell to the global scale. *Wiley Interdisciplinary Reviews: Water*, 3(3):327–368.
- Foken, T. (2008). The energy balance closure problem: An overview. *Ecological Applications*, 18(6):1351–1367.
- Giorgetta, M. A., Jungclaus, J., Reick, C. H., Legutke, S., Bader, J., Böttinger, M., Brovkin, V., Crueger, T., Esch, M., Fieg, K., Glushak, K., Gayler, V., Haak, H., Hollweg, H.-D., Ilyina, T., Kinne, S., Kornbluh, L., Matei, D., Mauritsen, T., Mikolajewicz, U., Mueller, W., Notz, D., Pithan, F., Raddatz, T., Rast, S., Redler, R., Roeckner, E., Schmidt, H., Schnur, R., Segschneider, J., Six, K. D., Stockhause, M., Timmreck, C., Wegner, J., Widmann, H., Wieners, K.-H., Claussen, M., Marotzke, J., and Stevens, B. (2013). Climate and carbon cycle changes from 1850 to 2100 in MPI-ESM simulations for the Coupled Model Intercomparison Project phase 5. *Journal of Advances in Modeling Earth Systems*, 5(3):572–597.
- Göttlicher, D., Albert, J., Nauss, T., and Bendix, J. (2011). Optical properties of selected plants from a tropical mountain ecosystem - Traits for plant functional types to parametrize a land surface model. *Ecological Modelling*, 222(3):493–502.
- Han, X., Franssen, H.-J. H., Montzka, C., and Vereecken, H. (2014). Soil moisture and soil properties estimation in the Community Land Model with synthetic brightness temperature observations. *Water Resources Research*, 50(7):6081–6105.
- Hofstede, R. G. M., Chilito, E. J. P., and Sandovals, E. M. (1995). Vegetative structure, microclimate, and leaf growth of a páramo tussock grass species, in undisturbed, burned and grazed conditions. *Vegetatio*, 119(1):53–65.
- Hribljan, J. A., Suárez, E., Heckman, K. A., Lilleskov, E. A., and Chimner, R. A. (2016). Peatland carbon stocks and accumulation rates in the Ecuadorian páramo. *Wetlands Ecology and Management*, 24(2):113–127.
- Hurrell, J. W., Holland, M. M., Gent, P. R., Ghan, S., Kay, J. E., Kushner, P. J., Lamarque, J.-F., Large, W. G., Lawrence, D., Lindsay, K., Lipscomb, W. H., Long, M. C., Mahowald, N., Marsh, D. R., Neale, R. B., Rasch, P., Vavrus, S., Vertenstein, M., Bader, D., Collins, W. D., Hack, J. J., Kiehl, J., and Marshall, S. (2013). The Community Earth System Model: A Framework for Collaborative Research. *Bulletin of the American Meteorological Society*, 94(9):1339–1360.
- Karimi, P. and Bastiaanssen, W. G. M. (2014). Spatial evapotranspiration, rainfall and land use data in water accounting - Part 1: Review of the accuracy of the remote sensing data. *Hydrology and Earth System Sciences Discussions*, 11(1):1073–1123.
- Kjaersgaard, J., Richard, A., Trezza, R., Robinson, C., Oliveira, A., Dhungel, R., and Kra, E. (2012). Filling satellite image cloud gaps to create complete images of evapotranspiration. *IAHS Publication, Remote Sen(352)*:102–105.
- Kljun, N., Calanca, P., Rotach, M. W., and Schmid, H. P. (2015). A simple two-dimensional parameterisation for Flux Footprint Prediction (FFP). *Geoscientific Model Development*, 8(11):3695–3713.
- Kool, D., Agam, N., Lazarovitch, N., Heitman, J., Sauer, T., and Ben-Gal, A. (2014). A review of approaches for evapotranspiration partitioning. *Agricultural and Forest Meteorology*, 184:56–70.

- Krinner, G., Viovy, N., de Noblet-Ducoudré, N., Ogée, J., Polcher, J., Friedlingstein, P., Ciais, P., Sitch, S., and Prentice, I. C. (2005). A dynamic global vegetation model for studies of the coupled atmosphere-biosphere system. *Global Biogeochemical Cycles*, 19(1).
- Lawrence, D. M., Oleson, K. W., Flanner, M. G., Thornton, P. E., Swenson, S. C., Lawrence, P. J., Zeng, X., Yang, Z.-L., Levis, S., Sakaguchi, K., Bonan, G. B., and Slater, A. G. (2011). Parameterization improvements and functional and structural advances in Version 4 of the Community Land Model. *Journal of Advances in Modeling Earth Systems*, 3(1):1–27.
- Lawrence, P. J. and Chase, T. N. (2007). Representing a new MODIS consistent land surface in the Community Land Model (CLM 3.0). *Journal of Geophysical Research*, 112(G1):G01023.
- Liaquat, U. W. and Choi, M. (2015). Surface energy fluxes in the Northeast Asia ecosystem: SEBS and METRIC models using Landsat satellite images. *Agricultural and Forest Meteorology*, 214-215:60–79.
- Madugundu, R., Al-Gaadi, K. A., Tola, E., Hassaballa, A. A., and Patil, V. C. (2017). Performance of the METRIC model in estimating evapotranspiration fluxes over an irrigated field in Saudi Arabia using Landsat-8 images. *Hydrology and Earth System Sciences*, 21(12):6135–6151.
- Marthews, T. R., Malhi, Y., and Iwata, H. (2012). Calculating downward longwave radiation under clear and cloudy conditions over a tropical lowland forest site: An evaluation of model schemes for hourly data. *Theoretical and Applied Climatology*, 107(3-4):461–477.
- Mauder, M., Cuntz, M., Drüe, C., Graf, A., Rebmann, C., Schmid, H. P., Schmidt, M., and Steinbrecher, R. (2013). A strategy for quality and uncertainty assessment of long-term eddy-covariance measurements. *Agricultural and Forest Meteorology*, 169:122–135.
- Mayocchi, C. and Bristow, K. (1995). Soil surface heat flux: some general questions and comments on measurements. *Agricultural and Forest Meteorology*, 75(1-3):43–50.
- Minaya, V., Corzo, G., van der Kwast, J., and Mynett, A. E. (2016). Simulating Gross Primary Production and Stand Hydrological Processes of páramo Grasslands in the Ecuadorian Andean Region Using the Biome-BGC Model. *Soil Science*, 181(7):335–346.
- Ministerio del Ambiente del Ecuador (2018). Mapa de Ecosistemas del Ecuador Continental. <http://mapainteractivo.ambiente.gob.ec/portal/>. Last checked on 2018-01-02.
- Morán-Tejeda, E., Bazo, J., López-Moreno, J. I., Aguilar, E., Azorín-Molina, C., Sanchez-Lorenzo, A., Martínez, R., Nieto, J. J., Mejía, R., Martín-Hernández, N., and Vicente-Serrano, S. M. (2016). Climate trends and variability in Ecuador (1966-2011). *International Journal of Climatology*, 36(11):3839–3855.
- Mosquera, G. M., Lazo, P. X., Céleri, R., Wilcox, B. P., and Crespo, P. (2015). Runoff from tropical alpine grasslands increases with areal extent of wetlands. *CATENA*, 125(FEBRUARY):120–128.
- Mosquera, G. M., Segura, C., Vaché, K. B., Windhorst, D., Breuer, L., and Crespo, P. (2016). Insights into the water mean transit time in a high-elevation tropical ecosystem. *Hydrology and Earth System Sciences*, 20(7):2987–3004.

5 Atmosphere-surface fluxes modeling

- Muñoz, P., Célleri, R., and Feyen, J. (2016). Effect of the Resolution of Tipping-Bucket Rain Gauge and Calculation Method on Rainfall Intensities in an Andean Mountain Gradient. *Water*, 8(11):534.
- Myers, N., Mittermeier, R. A., Mittermeier, C. G., da Fonseca, G. A. B., and Kent, J. (2000). Biodiversity hotspots for conservation priorities. *Nature*, 403(6772):853–858.
- Nagy, Z., Pintér, K., Pavelka, M., Darenová, E., and Balogh, J. (2011). Carbon fluxes of surfaces vs. ecosystems: advantages of measuring eddy covariance and soil respiration simultaneously in dry grassland ecosystems. *Biogeosciences*, 8(9):2523–2534.
- Niu, G.-Y., Yang, Z.-L., Dickinson, R. E., and Gulden, L. E. (2005). A simple TOPMODEL-based runoff parameterization (SIMTOP) for use in global climate models. *Journal of Geophysical Research*, 110(D21):D21106.
- Ochoa-Sánchez, A., Crespo, P., and Célleri, R. (2018). Quantification of rainfall interception in the high Andean tussock grasslands. *Ecohydrology*, (October 2017):e1946.
- Oleson, K. W., Lawrence, D. M., B, G., Flanner, M. G., Kluzek, E., J, P., Levis, S., Swenson, S. C., Thornton, E., Feddema, J., Heald, C. L., Lamarque, J.-f., Niu, G.-y., Qian, T., Running, S., Sakaguchi, K., Yang, L., Zeng, X., Zeng, X., and Decker, M. (2010). Technical Description of version 4.0 of the Community Land Model (CLM). NCAR/TN-478+STR.
- Olson, D. M., Dinerstein, E., Wikramanayake, E. D., Burgess, N. D., Powell, G. V. N., Underwood, E. C., D'Amico, J. A., Itoua, I., Strand, H. E., Morrison, J. C., Loucks, C. J., Allnutt, T. F., Ricketts, T. H., Kura, Y., Lamoreux, J. F., Wettengel, W. W., Hedao, P., and Kassem, K. R. (2001). Terrestrial Ecoregions of the World: A New Map of Life on Earth. *BioScience*, 51(11):933.
- Orellana-Alvear, J., Célleri, R., Rollenbeck, R., and Bendix, J. (2017). Analysis of Rain Types and Their Z-R Relationships at Different Locations in the High Andes of Southern Ecuador. *Journal of Applied Meteorology and Climatology*, 56(11):3065–3080.
- Ozturk, D. (2015). *Evaluation of Regional Climate Models With Remotely Sensed Evapotranspiration Data*. Master thesis, University of Nebraska, Lincoln, NE, USA.
- Padrón, R. S., Wilcox, B. P., Crespo, P., and Célleri, R. (2015). Rainfall in the Andean Páramo: New Insights from High-Resolution Monitoring in Southern Ecuador. *Journal of Hydrometeorology*, 16(3):985–996.
- Papale, D., Reichstein, M., Aubinet, M., Canfora, E., Bernhofer, C., Kutsch, W., Longdoz, B., Rambal, S., Valentini, R., Vesala, T., and Yakir, D. (2006). Towards a standardized processing of Net Ecosystem Exchange measured with eddy covariance technique: algorithms and uncertainty estimation. *Biogeosciences*, 3(4):571–583.
- Pesántez, J., Mosquera, G. M., Crespo, P., Breuer, L., and Windhorst, D. (2018). Effect of land cover and hydro-meteorological controls on soil water DOC concentrations in a high-elevation tropical environment. *Hydrological Processes*, 32(17):2624–2635.
- Quichimbo, P., Tenorio, G., Borja, P., Cárdenas, I., Crespo, P., and Célleri, R. (2012). Efectos sobre las propiedades físicas y químicas de los suelos por el cambio de la cobertura vegetal y uso del suelo: Páramo de Quimsacocha al sur del Ecuador. *Suelos Ecuatoriales*, 42(2)(2):138–153.

- Rana, G. and Katerji, N. (2000). Measurement and estimation of actual evapotranspiration in the field under Mediterranean climate: a review. *European Journal of Agronomy*, 13(2-3):125–153.
- Reichstein, M., Falge, E., Baldocchi, D., Papale, D., Aubinet, M., Berbigier, P., Bernhofer, C., Buchmann, N., Gilmanov, T., Granier, A., Grunwald, T., Havrankova, K., Ilvesniemi, H., Janous, D., Knohl, A., Laurila, T., Lohila, A., Loustau, D., Matteucci, G., Meyers, T., Miglietta, F., Ourcival, J.-M., Pumpanen, J., Rambal, S., Rotenberg, E., Sanz, M., Tenhunen, J., Seufert, G., Vaccari, F., Vesala, T., Yakir, D., and Valentini, R. (2005). On the separation of net ecosystem exchange into assimilation and ecosystem respiration: review and improved algorithm. *Global Change Biology*, 11(9):1424–1439.
- Serrano-Ortiz, P., Sánchez-Cañete, E. P., Olmo, F. J., Metzger, S., Pérez-Priego, O., Carrara, A., Alados-Arboledas, L., and Kowalski, A. S. (2016). Surface-Parallel Sensor Orientation for Assessing Energy Balance Components on Mountain Slopes. *Boundary-Layer Meteorology*, 158(3):489–499.
- Shuttleworth, J. (2008). Evapotranspiration Measurement Methods. Technical Report 7.1.
- Silva, B., Roos, K., Voss, I., König, N., Rollenbeck, R., Scheibe, R., Beck, E., and Bendix, J. (2012). Simulating canopy photosynthesis for two competing species of an anthropogenic grassland community in the Andes of southern Ecuador. *Ecological Modelling*, 239:14–26.
- Sun, S., Chen, B., Ge, M., Qu, J., Che, T., Zhang, H., Lin, X., Che, M., Zhou, Z., Guo, L., and Wang, B. (2016). Improving soil organic carbon parameterization of land surface model for cold regions in the Northeastern Tibetan Plateau, China. *Ecological Modelling*, 330:1–15.
- Tasumi, M., Allen, R. G., and Trezza, R. (2008). At-Surface Reflectance and Albedo from Satellite for Operational Calculation of Land Surface Energy Balance. *Journal of Hydrologic Engineering*, 13(2):51–63.
- Taylor, K. E. (2001). Summarizing multiple aspects of model performance in a single diagram. *Journal of Geophysical Research: Atmospheres*, 106(D7):7183–7192.
- Thornton, P., Law, B., Gholz, H. L., Clark, K. L., Falge, E., Ellsworth, D., Goldstein, A., Monson, R., Hollinger, D., Falk, M., Chen, J., and Sparks, J. (2002). Modeling and measuring the effects of disturbance history and climate on carbon and water budgets in evergreen needleleaf forests. *Agricultural and Forest Meteorology*, 113(1-4):185–222.
- Tonneijck, F. H., Jansen, B., Nierop, K. G. J., Verstraten, J. M., Sevink, J., and De Lange, L. (2010). Towards understanding of carbon stocks and stabilization in volcanic ash soils in natural Andean ecosystems of northern Ecuador. *European Journal of Soil Science*, 61(3):392–405.
- UNESCO (2013). Cajas Massif Biosphere Reserve. <http://www.unesco.org/new/en/natural-sciences/environment/ecological-sciences/biosphere-reserves/latin-america-and-the-caribbean/ecuador/macizo-del-cajas/>. Last checked on 2018-11-18.
- USGS (2017). Gap-Filling Landsat 7 SLC-off Single Scenes Using ERDAS Imagine 2014. <https://landsat.usgs.gov/gap-filling-landsat-7-slc-single-scenes-using-erdas-imagine-TM>. Last checked on 2017-12-13.
- van de Weg, M. J., Meir, P., Williams, M., Girardin, C., Malhi, Y., Silva-Espejo, J., and Grace, J. (2014). Gross Primary Productivity of a High Elevation Tropical Montane Cloud Forest. *Ecosystems*, 17(5):751–764.

5 Atmosphere-surface fluxes modeling

- Vuille, M. (2013). Climate Change and Water Resources in the Tropical Andes. Technical Report 515, Inter-American Development Bank.
- Vuille, M., Franquist, E., Garreaud, R., Lavado Casimiro, W. S., and Cáceres, B. (2015). Impact of the global warming hiatus on Andean temperature. *Journal of Geophysical Research: Atmospheres*, 120(9):3745–3757.
- Wang, D., Wang, G., Parr, D. T., Liao, W., Xia, Y., and Fu, C. (2017). Incorporating remote sensing ET into Community Land Model version 4.5. *Hydrology and Earth System Sciences Discussions*, pages 1–44.
- Wigmore, O. and Gao, J. (2014). Spatiotemporal dynamics of a páramo ecosystem in the northern Ecuadorian Andes 1988-2007. *Journal of Mountain Science*, 11(3):708–716.
- Zhu, Z. and Woodcock, C. E. (2012). Object-based cloud and cloud shadow detection in Landsat imagery. *Remote Sensing of Environment*, 118:83–94.

6 Conclusions and Outlook

6.1 Conclusions

This investigation constitutes a pioneer work on the knowledge about land-surface mass and energy exchange processes over the Andean páramo region in South America. The selected multi-scale approach allowed to understand the advantages and constrains on the matter and energy flux estimation at ground-level (ecosystem and catchment scales), remote sensing-level (for ETa at catchment scale), and single point LSM simulation-level (particularly for ETa and energy). Such a combination has scarcely been applied in other mountain ecosystems.

For this purpose, the first aim (**A1**) was to determine ETa via remote sensing-based mapping using an energy balance method. This aim required the analysis of the dynamics of modeled ETa at spatial (Landsat and MODIS) and temporal scales (daily, monthly and annual), and the evaluation with a widely used global ETa product (MOD16) and ETa from WB. The aim was assessed through the **WP1** in which the first hypothesis (**H1**) was tested:

H1. The accuracy of spatial-scale ETa estimation depends on: **a)** the site-specific calibration of the model, and **b)** the resolution of the satellite product used in the implementation of energy balance-based algorithms for the ETa calculation.

The results reveal that spatially-explicit ETa can be successfully estimated when (i) specific corrections on the incoming energy for the slope and aspect terrain characteristics, (ii) model adaptations for the wind speed and surface roughness, and (iii) a systematic hot and cold pixel selection for each image, are properly conducted. In addition, for the assessment of METRIC derived ETa with MODIS (500m) the development of a site-specific ETrf vs. NDVI function is mandatory. Such adjustments proven fundamental to improve the accuracy of modeled ETa, and lead to the acceptance of **H1a**. Furthermore, the imagery resolution proven crucial to improve the spatial fidelity of ETa estimates. The use of a mid-high resolution product (Landsat, 30 m res.) revealed monthly and annual overestimations around 30% and 10% respectively, when compared

6 Conclusions and Outlook

with WB at the head catchment area (dominant tussock grassland cover). In contrast to the developed products of thesis, the operationally available MODIS ETa product revealed poor quality with a higher overestimation (> 50% and > 25% respectively) versus WB. Both METRIC outcomes clearly performed better than the coarse VI-based ETa product MOD16 (overestimations >76% and >55% at monthly and annual respectively). This evidence leads to the acceptance of **H1b**. In spite of these results, it was found that the cloud cover variability is not properly captured by the radiation submodel in METRIC and this fact leads to a generalized overestimation of spatial ETa estimates. In addition, the scarcity of clear-sky images for interpolation between dates contributes, in some degree, to an uncertainty on the ETa time series.

The second aim (**A2**) pointed out to the determination of water vapor, CO₂ and energy exchange processes at ground-level via micrometeorological techniques, and to the understanding of the fluxes interactions with biophysical and climatic drivers of the páramo. This aim was completed through the **WP2** in which the second hypothesis (**H2**) was tested:

H2. The CO₂ and ETa flux measurements at ecosystem-scale determine that: **a)** the páramo grasslands act as a CO₂ sink as other studies suggest, and **b)** the modeled reference ETr is approximated to the measured ETa, and this water loss is lower than 60% of the total precipitation amount.

The CO₂ budget detected in the grassland of ZEO indicates that the ecosystem respiration exceed productivity most of the time. Therefore, this representative páramo site behaved as a CO₂ source during the 2-year study period (with an average loss of 99 ± 30 gC m⁻² per year), contrarily to other studies that found some páramo locations (mostly wetlands) as active C sinks. Short-term and spatially-limited studies such as those, do not necessarily show the diurnal-nocturnal changes and ecosystem-level behavior of the páramo's CO₂ exchange. Based on this evidence, **H2a** is rejected. This novel finding can be attributed to some site-specific characteristics: (i) the photosynthesis of the dominant vegetation (with a low biomass / necromass ratio) is strongly affected by sunlight limitations in the cloudy páramo (cloudiness > 70% of the time), and (ii) the upper soil layer of the páramo possess a very elevated SOC (~40%) where CO₂ release is strongly dependent on the SOM decomposition. Here, some environmental factors, such as large soil temperature variations during the diurnal / nocturnal course promote the emission, and the high soil moisture can limit this process. The conditions during the flux measurement period proved representative of the longer-term dynamics of the site's climate (absence of drought or excess water anomalies).

The modeled ETr versus the observed ETa was consistent in magnitude and variability at multiple temporal scales, and rainfall seasonality. Thus, the crop coefficients found are closer to unity

especially for the Kc FAO56 (0.90), and in a lesser degree, for the Kc ASCE-ERWI (0.78). The water loss in the site-specific hydrological cycle due to evaporative processes accounted by 51%, which is lower than the 60% mean value reported by Oki and Kanae (2006) for terrestrial ET at global scale. Consequently, **H2b** was verified. Another key finding is the discovery of specific periods (drier months) which shown a hydric deficit, consistently in the 2-year analysis.

The third aim (**A3**) proposed the prediction of ETa and energy fluxes through the parameterization of CLM model for the ZEO and QEO sites, and the evaluation of these outcomes with METRIC, EC and WB ETa observations and EC energy measurements. This aim was completed through **WP3** in which the third hypothesis (**H3**) was tested:

H3. The LSM CLM 4.0 is suitable for the prediction of ETa and surface energy fluxes in the páramo ecosystem for single-point simulations.

CLM proved suitable for the LE and ETa prediction when compared to the evaluation methods. However the model exhibited a poor performance in the estimation of Rn, H and G, mainly attributed to a systematic problem in the representation of incoming longwave radiation (i.e., the model underestimate R_{Lin} during the dominant cloud-sky conditions of the páramo) and also in the simulation of soil moisture conditions. Solving these issues was not possible due to the cryptic structure of the CLM code (hard-coded algorithms), which unfortunately is limited to the model developers (NCAR). Despite the latter situation, a reliable estimation of ETa was found and it can be attributed to the internal mechanism of CLM to force the EB closure, and also to the applied parameterization and configuration of the LSM. However, this issue should need a deeper investigation further. On the other hand, a comparative analysis between the evaluation methods (METRIC, WB and EC) revealed strong biases and a high uncertainty regarding the WB, which can be attributed to the large spatial variability of rainfall and also to the precipitation and water discharge techniques. Differences in ETa between the ZEO and QEO catchments were observed (attributed to topographical, areal and climatic characteristics). Such findings lead to a partial acceptance of **H3** (CLM was effective for ETa and LE prediction, but showed deficient for Rn, H and G). Furthermore, METRIC demonstrated its suitability for ETa estimation on catchment scale when compared to the EC method (ZEO exclusively).

Finally, the following aspects are the main contributions of the present work:

- The METRIC model proved to be a reliable method for ETa mapping at catchment-scale (and potentially at regional-scale) and longer time scales (monthly, seasonal or annual). The ETa

6 Conclusions and Outlook

dynamics were consistent with the WB-based evaluation. This was especially true for the mid-high resolution satellite product (Landsat). The method also demonstrated the spatial origins of ETa in the catchment area.

- The EC technique was considered the reference (and most accurate) method for ETa, energy and CO₂ quantification at the ecosystem-scale, indistinctly of the time scale (effective from hourly to annual). EC allowed to reveal the –C source– behavior of the ZEO páramo grasslands which is an unprecedented finding, and also to report the first crop coefficients for the tussock grasslands with a direct vapor measurement.
- WB is a plausible (and economical) approach for ETa estimation at catchment-scale and longer time scales (monthly, seasonal or annual), but it demonstrated a lack in accuracy, due to some uncertainties related to instrumental techniques and some neglected components of the WB (storages and subtle ground water contributions) which cannot be totally accounted.
- LSM simulation with CLM is a promising alternative for the forecasting of ETa at single-point (ecosystem)-scale, in spite of some issues exhibited on the prediction of energy fluxes. Therefore the model demands a deeper modification of its internal structure.

6.2 Outlook

The highland páramo regions are potentially exposed to (i) the effects of climate change, such as rising of air / soil temperatures, alteration of rainfall regimes, extended drought periods, the increment of soils' C emission / loss, among others, and to (ii) the negative impact of land cover alterations, such as erosion, landslides and migration / extinction of endemic species due to anthropogenic activities pressure. The present thesis opens the path for future investigations which can assess the aforementioned impacts on the functional indicators here presented (ET, energy and CO₂ fluxes). Herein, LSMs should be tested in forecasting mode to predict these indicators in spatial and point-scale. Moreover, the determination of PFT and other physio-morphological traits of the local vegetation will be essential for a proper simulation of C fluxes. Similarly, the downscaling of coarse regional climate models outcomes to a finer resolution will serve as forcings for LSMs (considering the complex topography of the Andes). This is a door for regional-scale studies which can be developed through refined LSMs or remote sensing-based approaches.

Additionally, the ground level determination of water use efficiency (WUE) for the native vegetation is still unexplored, and it can be a critical variable for the understanding of C and ETa loss. This key-indicator can be assessed through porometry techniques (plant-level / leaf-

level). Furthermore, the knowledge on plant-soil exchange mechanisms can be enriched with the quantification of soil-level gas emissions, and the determination of above / below-ground carbon pools. This is crucially important for the understanding of the autotrophic and heterotrophic Reco mechanisms, which persist unexplored. Last but not least, a longer-term EC monitoring period (e.g., > 5 years) will support the findings of this thesis, and will improve the understanding about the interactions between the ecosystem fluxes and normal (and extreme) biophysical and climate events. This work constitutes a support tool for further research on the páramo and for the development of management policies, which should be focused on the preservation of this pristine region in the tropical Andean cordillera.

Erklärung

Ich erkläre an Eides statt, dass ich meine Dissertation mit dem Titel

”On the multi-scale analysis of land-surface mass and energy exchanges for the tropical Andean páramo of Southern Ecuador“

selbstständig ohne unerlaubte Hilfe angefertigt und mich dabei keinerlei anderen als der von mir ausdrücklich bezeichneten Quellen und Hilfen bedient habe.

Die Dissertation wurde in der jetzigen oder einer ähnlichen Form noch bei keiner anderen Hochschule eingereicht und hat noch keinen sonstigen Prüfungszwecken gedient.

Marburg a. d. Lahn, den 28.01.2019

Galo José Carrillo Rojas

Curriculum vitae



PERSONAL INFORMATION

Name: Galo José Carrillo Rojas
Date of birth: 28-04-1978
Place of birth: Cuenca
Citizenship: Ecuadorian

EDUCATION

2013 - Present PhD candidate, Philipps-Universität Marburg,
Faculty of Geography, Laboratory for Climatology
and Remote Sensing (LCRS), Germany.
From December 17, 2013 to present.
Funding SENESCYT scholarship.

2006 - 2008 Master in Environmental Management for Industries
of Production and Services, University of Cuenca.

2005 Diploma in Formulation and Evaluation of Research
Projects, University of Cuenca.

1997 - 2003 Chemical Engineer, University of Cuenca.

CURRENT POSITION

Associate Professor at Faculty of Chemical Sciences, University of Cuenca, Ecuador. From November 2008 to present. Researcher at Department of Water Resources and Environmental Sciences (iDRHiCA), University of Cuenca, since Jan 2013 to present.

OTHER PEER-REVIEWED PUBLICATIONS

- Córdova, M., Célleri, R., Shellito, C. J., Orellana-Alvear, J., Abril, A. and Carrillo-Rojas, G. (2016). Near-surface air temperature lapse rate over complex terrain in the Southern Ecuadorian Andes: implications for temperature mapping. *Arctic, Antarctic, and Alpine Research*, 48(4), 673-684. <http://doi.org/10.1657/AAAR0015-077>
- Córdova, M., Carrillo-Rojas, G., Crespo, P., Wilcox, B. and Célleri, R. (2015). Evaluation of the Penman-Monteith (FAO 56 PM) Method for Calculating Reference Evapotranspiration Using Limited Data. *Mountain Research and Development*, 35(3), 230-239. <http://doi.org/10.1659/MRD-JOURNAL-D-14-0024.1>
- Córdova, M., Carrillo, G. and Célleri, R. (2014). Errores en la estimación de la evapotranspiración de referencia de una zona de páramo andino debidos al uso de datos mensuales, diarios y horarios. *Aqua-LAC - UNESCO: Programa Hidrológico Internacional para América Latina y el Caribe*, vol. 10 (2): 14-22. <http://unesdoc.unesco.org/images/0022/002281/228115m.pdf>
- Carrillo, G., Andrade, J., Barragán, A. and Astudillo, A. (2014). Impact of electrical energy efficiency programs, case study: Food processing companies in Cuenca, Ecuador. *DYNA*, vol. 80 (184): 41-48. <http://doi.org/10.15446/dyna.v81n184.40821>
- Carrillo G. and Astudillo A., (2011). Evaluación de las emisiones de vapor mercurial en procesos de amalgamado artesanal: Caso Cantón Ponce Enríquez, Provincia del Azuay. *MASKANA*, vol. 2(2): 71-81. [http://dspace.ucuenca.edu.ec/bitstream/123456789/5422/1/MASKANA%20si7285%20\(6\).pdf](http://dspace.ucuenca.edu.ec/bitstream/123456789/5422/1/MASKANA%20si7285%20(6).pdf)

CONTACT DETAILS

Departamento de Recursos Hídricos y Ciencias Ambientales iDRHiCA - Universidad de Cuenca
- Eco-campus Balzaín - Av. Víctor Manuel Albornoz y Cerezos, Cuenca, Ecuador.

Phone +593-74051000 (ext. 4490)
Mobile: +593-998682168
E-mail: galo.carrillo@ucuenca.edu.ec / gcarrillorojas@gmail.com

Marburg, 28th January 2019.

